The University Of Sheffield.

Characterisation and Evaluation of Poly(2-Methacryloyl-oxy) Ethyl Phosphorylcholine - Poly(2-Diisopropyl-amino) Ethyl Methacrylate (PMPC-PDPA) Self-Assembly for Biomedical Applications

Russell Pearson

A thesis submitted in partial fulfilment of the requirements of University of Sheffield for the degree of Doctor of Philosophy

Department of Materials Science and Engineering

November 2015

Acknowledgements

Firstly, I would like to thank my supervisors Dr Gwendolen Reilly and Prof Giuseppe Battaglia for their support. Many thanks to the EPSRC, for funding this project.
Many thanks to the past and present members of the research groups I have worked both in and alongside over the past 4 years. Special thanks to Dr Irene Canton, Dr Nick Warren, Dr Jeppe Madsen, Dr Linge Wang, Dr Katerina LoPresti, Dr Svetomir Tzokov, Mr Chris Hill and Dr Froso.Frosara!!!
Mega thanks to Rich, Faye, Ronan, Rick, Caroline, Celia, Priya, Robin, Gavin, Luca, James, Guy and anyone else who helped to drink away the hard times, the good times, and the times where we didn't need an excuse.
Thanks to my family for their support (both emotional and financial)!
Finally, all the thanks in the world to Jules for being in my life, through the good times and the bad, I love you. Xxx

Publications

- Russell T. Pearson, Nicholas J. Warren, Andrew L. Lewis, Steven P. Armes and Giuseppe Battaglia. Effect of pH and Temperature on PMPC−PDPA Copolymer Self-Assembly. *Macromolecules* 2013 45;**4**:1400-1407
- James Madsen, Irene Canton, Russell Pearson,Andrew L. Lewis, Giuseppe Battaglia and Steven P. Armes. Nile Blue-Based Nanosized pH Sensors for Simultaneous Far-Red and Near-Infrared Live Bioimaging.*JACS* 2013 39;**135**:14863-14870
- Russell T. Pearson, Mila Avila-Olias, Adrian S. Joseph, Sophie Nyberg and Giuseppe Battaglia. Chapter 7:Smart Polymersomes: Foramtion, Characterisation and Applications. From the book: Smart Materials for Drug Delivery: Volume 1.2013 ISBN:978-1-84973-877-4

Conference Presentations

- Poster presentation at 43rd IUPAC World Polymer Congress “MACRO2010” – Glasgow, on 12.07.2010:Characterising PMPC-PDPA polymersomes.
- Oral presentation at TechConnect World Conference and Expo 2011 – “Nanotech 2011” – Boston MA on 15.06.2011:Controlling pH responsive polymersome assembly.'
- Oral presentation at IUPAC World Polymer Congress “MACRO2012”- Blacksburg VA on 29.06.2012:Temperature controlled macromolecular self-assembly of biocompatible pH responsive copolymer PMPC-PDPA.

Contents

Abbreviations

ADE – Area-Difference-Elasticity

ATRP – Atom Transfer Radical Polymerisation

CAC – Critical Aggregation Concentration

CMC – Critical Micelle Concentration

CTA – Chain Transfer Agent

DDS – Drug Delivery System

DLS – Dynamic Light Scattering

DNA – Deoxyribonucleic Acid

DP – Degree of Polymerisation

GPC – Gel Permeation Chromatography

HCl – Hydrochloric Acid

HDF – Human Dermal Fibroblasts

HPLC – High Pressure Liquid Chromatography

IUPAC – International Union of Pure and Applied Chemistry

IV – Intravenous

NaOH – Sodium Hydroxide

NMR – Nuclear Magnetic Resonance

PAA - Poly(Acrylic Acid)

PBD – Poly(Butadiene)

PBO – Poly(Butylene Oxide)

PBS – Phosphate Buffered Saline

PEO/PEG - Poly(ethylene oxide)/Poly (ethylene glycol)

PDPA – Poly(2-Diisopropyl-amino)Ethyl Methacrylate)

PGMA – Poly(Glycerol Monomethacrylate)

PHPMA – Poly(2-hydroxypropyl methacrylate)

PISA – Polymerisation Induced Self-Assembly

PMAA – Poly(Methacrylic Acid)

PMPC – Poly(2-Methacryloyl-oxy)Ethyl Phosphorylcholine)

PPO – Poly(Propylene Oxide)

PS – Poly(Styrene)

PTA – Phosphotungstic Acid

RAFT - Reversible Addition-Fragmentation chain Transfer polymerisation

RNA - Ribonucleic Acid

SEC – Size Exclusion Chromatography

TEM – Transmission Electron Microscopy

Abstract

Drug Delivery Systems (DDS) can be used to improve the effectiveness of therapeutic small molecules by enabling specific targeting, lower doses and reduced side effects. Polymersomes are a fully synthetic, non-toxic DDS capable of entrapping, delivering and releasing a therapeutic cargo inside mammalian cells. Improvements to the production and purification processes for polymersomes may improve their efficiency as a DDS.

The aim of this thesis was to investigate the formation of dispersed pH responsive PMPC-PDPA polymersomes specifically for drug delivery applications. Dynamic Light Scattering (DLS), Transmission Electron Microscopy (TEM), potentiometry and turbidity measurements were used to characterise polymersomes and their formation.

The effects of sample temperature on the formation of polymersomes by pH increase was studied with the aim of controlling polymersome size. Four copolymers were used, each with identical PMPC block lengths and different PDPA block lengths. It was found that the smallest copolymer investigated ($PMPC_{25}$-$PDPA_{47}$) formed micelles, while the remaining three copolymers with varying lengths favoured the formation of polymersomes. Additionally, a shift in the copolymer acid dissociation constant was observed using potentiometry and a trend of smaller particles being formed at higher temperatures (30-50°C) and shorter PDPA block length ($PDPA_{47\text{-}94}$) was also observed. Morphological analysis revealed the formation of polymersomes, micelles and complex structures known as genus particles. Across the four copolymers, micelles were generally formed at the higher temperatures (50°C), while genus structures were formed at low temperatures (<15°C) and polymersomes formed at intermediate temperatures (20-37°C).

Genus particles were then studied further as there are only a handful of publications on experimentally observed genus particles formed from amphiphiles. It was observed via morphological analysis that both the number of genus events (holes) and the size of the particles increased with decreasing temperature. The theory that these structures were formed by the addition of

extra copolymer chains to the outside of already formed polymersomes was tested by mixing dissolved unimers with formed polymersomes at low temperatures. The resulting structures were not full genus particles but there were noticeable differences in the particle topologies compared to polymersome-only samples.

The relationship between temperature and polymersome formation was also explored further by driving the formation via a temperature increase as opposed to a pH increase. This was conducted using a spectrophotometer with an in-built temperature control unit so that formation was measured in situ via an increase in sample turbidity. Formation through temperature change was achieved by maintaining sample pH and increasing the temperature, then TEM was used to confirm the formation of polymersomes.

Finally, an improved calculation of encapsulation efficiency was produced by incorporating the measured size distribution data obtained from DLS into the estimation. An automated Size Exclusion Chromatography (SEC) system was also set up to compare the purification against currently used bench-top systems. Samples processed using the automated system and the improved calculation could be used to more accurately predict the encapsulation of a hydrophilic compound and as a point of reference for encapsulation experiments.

This work demonstrates the high degree of flexibility associated with the formation process of PMPC-PDPA polymersomes and related structures for drug delivery applications. Future work would include further characterisation of genus particles, in vitro delivery studies and experimental validation of the encapsulation model.

Chapter 1.1 – Introduction

1.1.1 Drug delivery systems

For centuries, humans have ingested biologically active substances in order to benefit from particular therapeutic effects. Relatively recent technological advances have also enabled the key active ingredients to be refined and/or synthesised rapidly. There are currently a large range of small molecule and advanced biologic drugs with therapeutic effects, with variations still being discovered. However, the methodologies of introducing biologically active substances into the body have changed very little over the last century, as shown in Figure 1.1. Traditional formulations, such as pills, are designed to survive physiological barriers such as the stomach in order to be absorbed to the blood stream, whilst intravenous (IV) drugs are injected directly into the blood stream, bypassing the acidic environment of the gastrointestinal system.

Figure 1.1: Examples of common drug delivery systems, from left to right – enteral syringes for nasogastric administration, pills for oral administration and an inhaler for pulmonary administration.

In addition to direct medicinal therapies, many substances have diagnostic purposes or are used to manufacture other molecules. For example, drug delivery systems can be utilized to improve the circulation lifetimes or localization of contrast agents for medical imaging.[1] *In vitro* research can involve the use of molecules for imaging or isolating cellular systems: drug delivery systems can also be used to ensure that the molecule has reached its target site within a biological model.[2] Finally, certain therapeutic molecules such as insulin are manufactured using *in vitro* cell cultures; these cells must be "programmed" using biomolecules in order to synthesise the insulin.[3] This is achieved by using a drug delivery system to transport the biomolecule across

the outer cell membrane in order to alter the cell's genetic code. However, some therapeutic molecules will be broken down by the vascular system before reaching the target biological tissue. Therefore, drug delivery systems can be utilized in order to maintain the activity of the drug during transportation to the target tissue or organ. For the purpose of this thesis a drug delivery system (DDS) will be defined as a structure that does not interact with the biologically active substance, or drug, but facilitates transportation of the drug to a target tissue or organ.

Another benefit that can arise from the use of drug delivery systems is the reduction of harmful side effects from the biologically active drug. Health regulatory agencies of the United Kingdom currently assess the therapeutic effects of a particular treatment versus any side effects, as a risk versus benefit calculation.[4] Some side effects are a result of the dose required for therapeutic effect. Additionally, undesirable interactions of the active drug with other biological species can occur, also known as off-target effects. A benefit of drug delivery devices is that targeted delivery could reduce the therapeutic dose required by ensuring that a greater percentage of the total drug reaches the site of therapy, rather than the drug being taken up by all tissues of the body. A reduced dose of drug may also be financially beneficial.

1.1.2 Nanotechnology

Nanotechnology is a field of research that has grown rapidly over the last decade and is focused on the manipulation of matter on the submicron length scale. Moving towards the nanoscale provides certain physical and chemical environments that differ from the macroscale. The higher surface area to volume ratio of smaller structures improves the rate of reaction between two substances,[5] and reducing the size of an object also alters the surrounding interactions available.

A dominant nanoscale force is viscosity, which can be thought of as a fluid's ability to resist flow.[6] This is often described in terms of a solutions' Reynolds number, a dimensionless parameter stating the ratio of inertial to viscous forces. At the nanoscale, viscosity dominates and the particle will experience very low Reynolds numbers. The higher viscosity results from the relative size of the object compared to the medium it is passing through. An example would be two spherical particles of equal density and differing

masses/diameters passing through a solution of water at room temperature, one 100 nm in diameter and the other 100 μm. Each water molecule is constantly moving due to thermal energy. The radius of a single water molecule is around 1 angstrom ($1x10^{-10}$m), which in proportion to the two particles is 1000 times smaller than the 100 nm particle and 1, 000,000 times smaller than the 100 μm particle. The smaller the particle, the greater effect these collisions have on their trajectory. Therefore, when the water molecules collide with nanoscale particles, these collisions cause both particles to move randomly throughout the solution. This effect is known as “Brownian Motion” and creates resistance to directed movement in solution. Brownian motion is random in direction, although the mass of a given particle versus the mass of the bombarding molecules will influence the speed of the particle's movement. This can be useful for measurements on the nanoscale: For example, light scattering techniques indirectly measure the size of sub-micron particles by calculating the brownian motion.

1.1.3 Nanotechnological Applications in Biology

Nanotechnology can have a huge impact on drug delivery and biology. Structurally, many important cellular processes such as deoxyribonucleic acid (DNA) replication, protein formation and hormone signaling occur on a nano length scale;[7] often these interactions involve multiple macromolecules (assemblies of molecules). Figure 1.2 illustrates the relative scale of nano-sized objects. In theory, by using therapies that are also on the nano scale, it is possible to have a more finely tuned interaction with biological processes. Many target molecules for therapeutics reside within the cell, protected by multiple barriers that must be circumvented in order to achieve a therapeutic influence. Nanotechnological agents must reach such intracellular target sites with its active components still therapeutically viable.

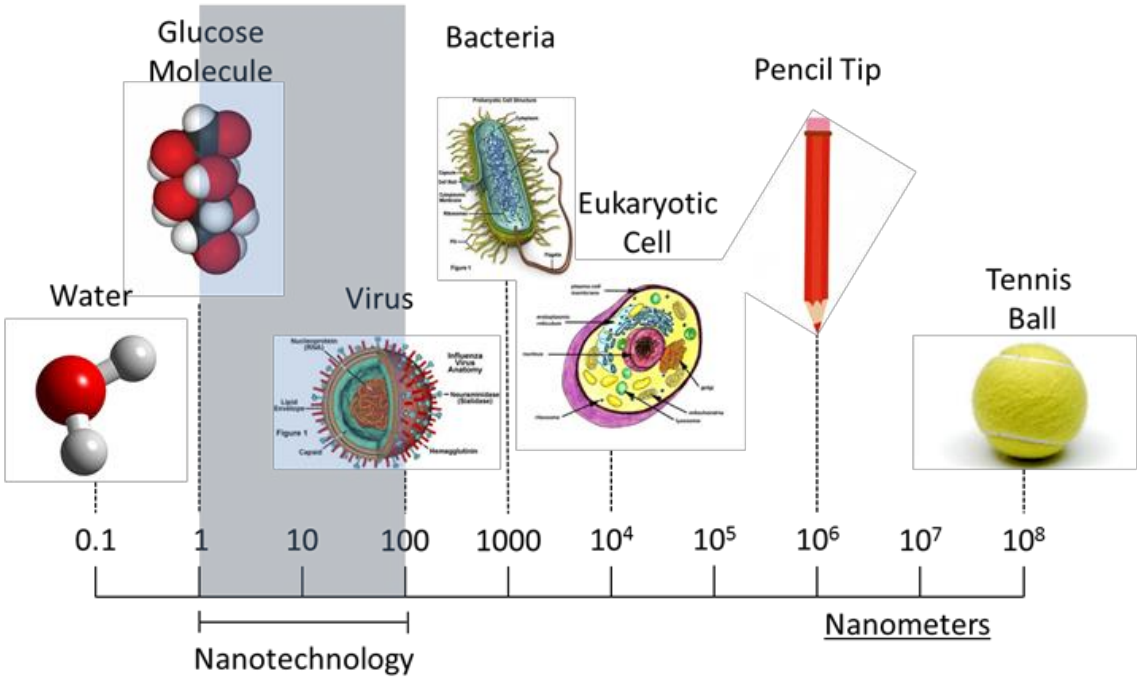

Figure 1.2: An illustration of the size range of nanotechnology.

There are a number of properties and functionalities required from an ideal drug delivery system. Firstly, the drug delivery system (DDS) must be either stable in storage for extended periods or simple to construct with high reproducibility shortly before administration. The storage can have financial implications for the entities funding the treatment, while regulatory agencies may not approve a product with variability outside of pre-determined ranges. Once produced, a route of administration will be chosen based upon the physical properties of the DDS and target site of the therapy. As well as the most common delivery methods of intravenous injection or oral administration, several alternative routes such as intramuscular, mucosal and interosseous can also be used. Once a drug has been administered, dilution of the active molecule by blood (IV administration) or gastric acid (oral administration) may disrupt the therapy if a certain concentration is required to maintain the structure. Additionally, shear forces imparted by blood vessels as well as the highly acidic environment of the stomach need to be considered.

Once within the body, the DDS must avoid detection from the patient's immune system. The innate immune system provides a first line of defense against foreign bodies via complex series of chemical cascade reactions that alert various inflammatory cell types.[7] The DDS must be chemically inactive or unrecognisable to the various components of the innate immune system, such as opsonic and complement proteins as well as phagocyte cells.

Some therapies require a relatively high blood concentration in order to achieve the desired therapeutic effect; this is often due to a lack of specificity and targeting. For example, chemotherapy for solid tumors does not target cancerous cells; it relies on the increased metabolic activity of the tumor cells and the “leaky” blood vessels around the tumor. Ideally, a DDS would be able to single out cancerous cells and target them specifically; this would reduce some of the unwanted side effects related to healthy tissue being exposed to a chemotherapy drug.

Once the DDS has reached the target cell type, it must overcome the external cell membrane to reach the site of therapy. Small molecules can diffuse through membrane pores, whilst larger bodies must be taken into the cell via active uptake. It is beneficial for large DDS to use this uptake process so as not to disrupt the cellular membrane and cause damage to the cell. Studies into the uptake kinetics of nanoparticles have shown that certain parameters are optimal. For example, particles with a diameter < 100nm are typically internalised faster than particles > 100nm,[8,9] with some studies reporting that the optimal size range is 50-60nm in diameter.[10–15] In addition, several studies have concluded that spherical nanoparticles are internalised more efficiently than cylindrical nanoparticles.[12,13,16–18] If the DDS can penetrate the cellular membrane barrier, the cargo must be released from the DDS in order to interact with its target site. Alternatively, the DDS must be designed so that the function of the therapeutic molecule is not affected.

In summary, stability of the ideal intracellular DDS would allow for long-term storage and then dilution. Once administered, the DDS would avoid detection by the immune system and target the required cell type, and subsequently cross the lipid membrane without causing damage in order to release its cargo. The drug delivery system of interest with regards to this study is the vesicle, a biological structure formed from self-assembled amphiphiles.

1.1.4 Amphiphiles

An amphiphile is a molecule that displays discrete regions that interact favourably or unfavourably with a surrounding solvent.[5] Unless stated otherwise, the solvent described in this thesis is water. Typically, amphiphilic molecules contain hydrophilic (*water loving*) and hydrophobic (*water hating*) segments that are connected by a covalent bond. This molecular duality results

in a range of amphiphile applications, including cosmetics, food sciences and medicine. Amphiphiles are largely used as surfactants (contraction of surface active agents) to stabilise mixtures that have both water-miscible and -immiscible phases, by positioning themselves at the interface. As the hydrophobic tails of the amphiphiles integrate with the oil phase while the hydrophilic heads will be present in the water-based phase (Figure 1.3), this reduces the energy at the phase boundary and allows the two phases to form an emulsion. These mixtures would separate into their two phases if the amphiphiles were not present to stabilise the interface.[5]

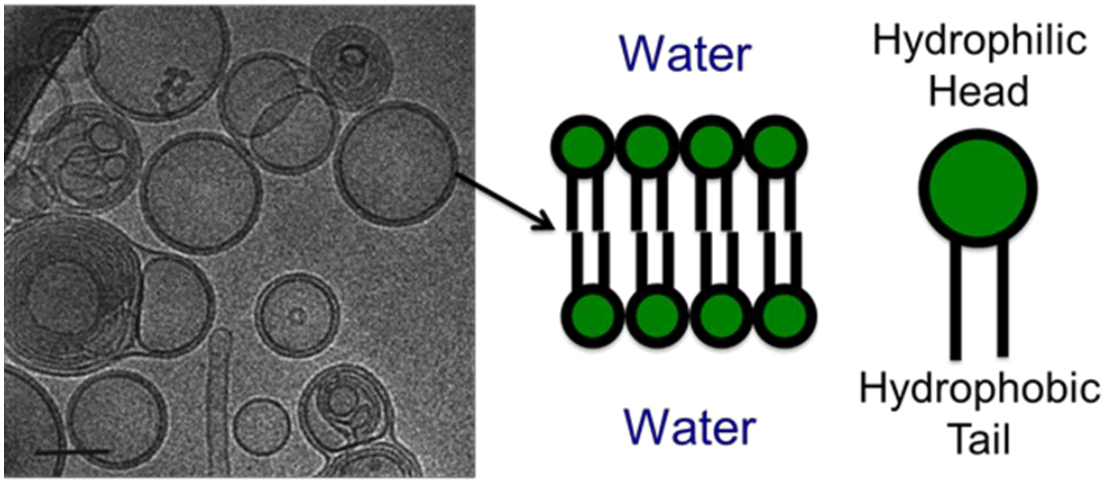

Figure 1.3: Cryogenic electron micrograph showing liposomes formed from milk lipids.[19] The diagram to the right shows how the hydrophobic tail of the lipid molecule is shielded from the surrounding water when in the liposome formation. A range of structures are shown in the micrograph, including multi-lamellar liposomes alongside single membrane liposomes. Scale bar = 100nm. Figure has been reused and adapted with permission from Elsevier.

1.1.5 Lipid Vesicles

Nano-sized applications are of particular interest for human biology because the length scale is on par with many sub-cellular mechanisms such as intracellular trafficking and signalling.[7] One nanoscopic structure of particular interest to this project is the lipid vesicle. First imaged at high resolution by Dr Bangham in 1961 using a transmission electron microscope as shown in Figure 1.3,[19] a vesicle is an enclosed “sack” produced by a bilayer membrane of phospholipids that separates a small volume of liquid from the bulk.[20] The term liposome was coined from the Greek words *lipo* and *soma*, meaning “fat” and “body” respectively. These structures can be produced from lipid-based cell

membranes and exist both inside and outside cells, with a range of uses including compartmentalisation and transport.[21]

The term ‘liposome’ also became the nomenclature used for artificial vesicles produced using extracted natural lipids such as phosphatidylcholine from egg yolks and lecithin.[22] Between the mid-1960s and the 1990s, liposome research advanced our understanding of cellular membrane structures and the events involved with vesicular trafficking (the movement of subcellular components within or between cells using vesicles). Drug delivery systems have also benefitted from liposomal research, which aims to enhance the efficacy or delivery of currently available therapeutic or diagnostic molecules via the addition of a carrier device. Therefore, liposomes have been used *in vitro* and *in vivo* to deliver a range of hydrophilic, hydrophobic and amphiphilic molecules over the last three decades.[23–25] However, liposomes circulate through the blood for a limited time due to opsonisation and eventually degradation. Opsonisation is the marking of an object by blood proteins to indicate clearance by the immune system, resulting from specific interactions between plasma proteins and liposome surface chemistry.[26]

In order to circumvent unwanted protein interactions and subsequent clearance by the immune system, an approach of grafting hydrophilic poly(ethylene oxide) (PEO/PEG) onto liposomes has been explored.[27] The uncharged yet hydrophilic nature of PEO allows for a large amount of water to interact with the vesicle corona. By the addition of a PEO corona onto liposomes, proteins interactions can be reduced and “stealth” liposomes produced.[28] This “stealth” characteristic occurs because a large quantity of water must be removed and the hydrophilic PEO groups forced closer together in order to interact with the liposome, which requires a comparatively large amount of energy. Such a process is energetically unfavourable in most situations leading to minimal interactions with proteins and biomolecules, resulting in “stealth” properties.[29] Several hybrid PEO-lipid vesicles achieved clinical use due to the reduced interactions with blood proteins and immune system, for example PEO-lipid vesicles that carry the chemotherapy drug doxorubicin.[30,31] However, attaching PEO to the outside of the liposomes can disrupt their macromolecular stability and a balance therefore has to be found, which will be covered in a later section.

1.1.6 Polymer Vesicles

During the 1990's, advances in polymer research allowed the production of fully synthetic vesicles with copolymers of various architectures (Figure 1.4).[32,33]

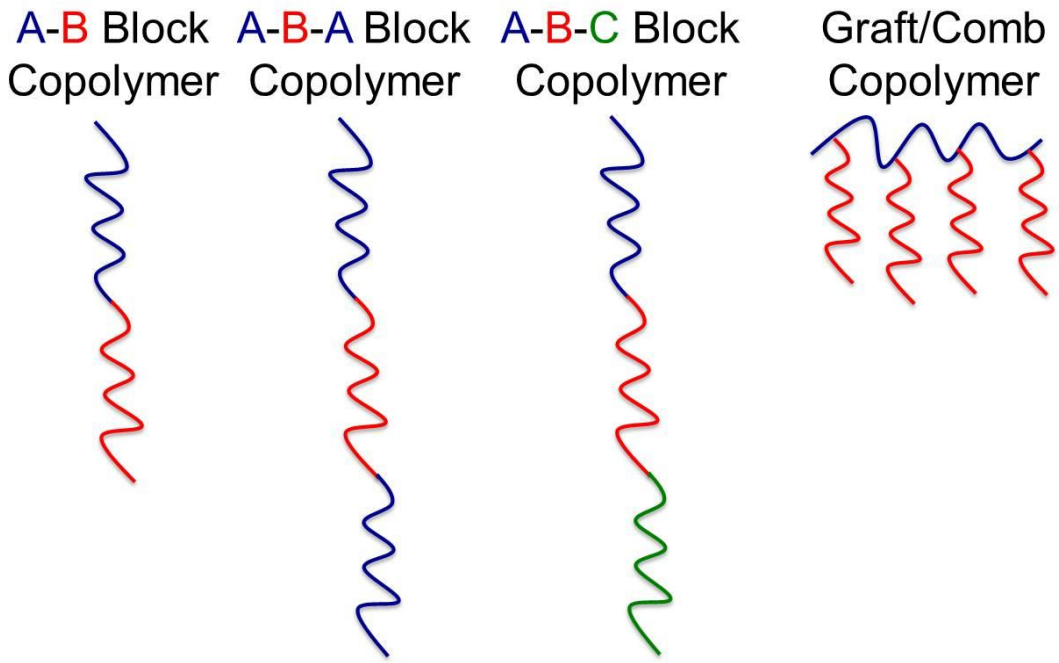

Figure 1.4: Examples of some block copolymer structures. The letters A, B and C denote differing chemistries that have been either polymerized sequentially or grafted onto a preformed backbone. In the case of star copolymers, the sequential polymerisation occurs from a central point and radiates outwards as polymerisation is continued.[32,33]

Advances in synthetic polymer chemistry, specifically living and controlled radical polymerisation, led to increased interest and research into polymer vesicles (polymersomes). Polymerisation is a process whereby monomers (A molecule which can undergo polymerisation, thereby contributing constitutional units to the essential structure of a macromolecule or oligomer molecule[34]) are ionised and react with other monomers or existing polymers, thereby creating or extending polymers. Living polymerisation is defined as "a chain polymerisation from which chain transfer and chain termination are absent" by the International Union of Pure and Applied Chemistry (IUPAC).[35] The polymerisation occurs sequentially, with the reactive species remaining active or "living" after each additional monomer addition.[36] In addition, potential reactions between two polymer living chains in ionic polymerisation are often unfavourable due to electrostatic repulsion, which provides greater control and reductions in cross-polymerisation. The lack of chain termination also allows for control over the

degree of polymerisation and yields low degrees of dispersity (a non-uniform polymer with respect to relative molecular mass or constitution or both[35] compared with the standard radical polymerisation (M_w/M_n lower than 1.2).

However, living polymerisation techniques are often highly sensitive to trace impurities, requiring rigorous purification and a high control over the polymerisation environment.[37] Radical polymerisation of vinyl monomers is comparatively less sensitive to impurities and cost effective on large scales, providing the reactions are conducted in anoxic (oxygen free) environments.[38] Examples of living polymerisation include anionic, cationic and ring-opening polymerisation techniques.[39,40] Two such modern polymerisation techniques are Atom Transfer Radical Polymerisation (ATRP)[41,42] and Reversible Addition-Fragmentation chain Transfer polymerisation (RAFT).[43] The development of these polymerisation processes played a crucial role in the emerging field of polymersomes, as these techniques allowed the preparation of polymer architectures such as multiblock copolymers, which have formed the synthetic building blocks for polymersomes.

By the beginning of the 21st century, bionanotechnology had begun to emerge and interest grew in the use of polymersomes as physical structures.[44] Synthetic polymer membranes displayed intriguing and desirable characteristics when compared to hybrid PEO-liposomes, such as allowing an entirely hydrophilic PEO-based corona[45]. Furthermore, the long polymer chains of vesicles interdigitated and entangled significantly more than the liposome tails, as shown in Figure 1.5. The entangled vesicular “membrane” structure that resulted from the interaction of polymer chains enhanced the mechanical properties of the synthetic carrier vessels compared with liposomes, as shown by micropipette aspiration studies.[46] Polymersomes also displayed a reduced permeability to hydrophilic compounds trapped within the lumen,[47] which resulted from inherent properties generated by the higher molecular weight copolymers and an ability to control membrane thickness via the degree of polymerisation.[48] Alongside these properties, the fully synthetic nature has allowed for different functionalities to be incorporated into the copolymer, either within the membrane or onto the polymersome surface.

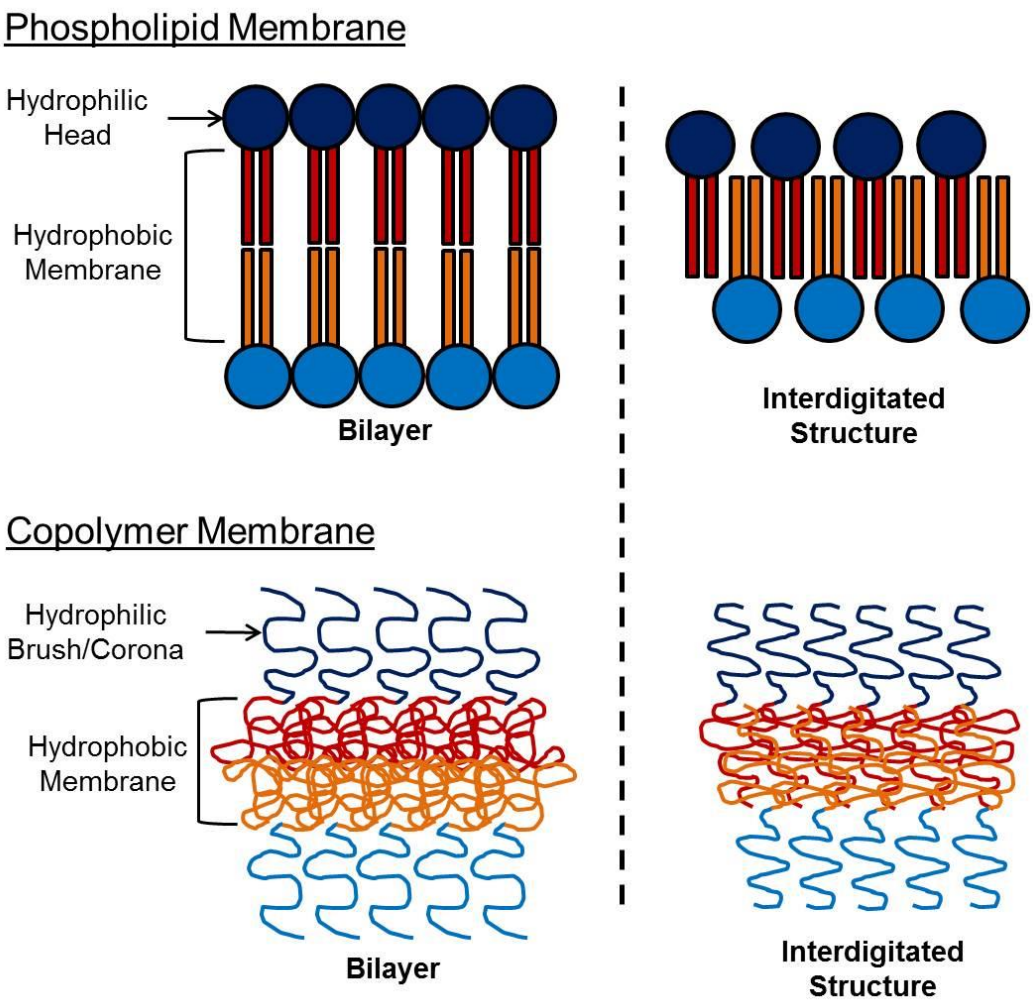

Figure 1.5. The bilayered and interdigitated structures that could be possible with (a) phospholipid membranes and (b) block copolymer membranes. Lipid membranes are documented to adopt either structure; however, it is highly unlikely that a polymer system would achieve a full bilayer conformation as this is entropically unfavorable. Therefore, an interdigitated conformation is believed to be the adopted structure.[48]

By these methods, many molecules have been incorporated into the vesicle structures, including fluorophores,[49–52] proteins or peptides,[53–56] cross-linking agents[57,58] and several other reactive functional groups.[59] Introduction of these additional molecules can be achieved either during the synthesis of the copolymer or by conjugation to the formed polymersomes. Due to the versatility shown from various studies, polymersomes have been used for a range of applications. Fluorophores have been delivered to various cell types *in vitro*[60,61] and *in vivo*,[49] for imaging/diagnostic purposes. Polymersomes have also been used for the encapsulation and delivery of genetic material such as RNA and DNA[62–65] proteins[66–71] and anticancer therapeutics.[72–74] In addition to direct diagnostic or therapeutic biomedical applications, uses for polymersomes as biosensors[75] and nanoreactors[76–78] have also been explored.

To summarise, drug delivery systems aim to improve current small molecule therapies in order to improve their efficiency. This may enable lower healthcare costs and/or a higher quality of life from reduced side effects. Biological vesicles are suitable for synthetic replication as drug delivery systems as the vesicles act as transportation carriers for both inter- and intracellular purposes. Lipid vesicles (or liposomes) have been extensively studied and are currently used to prolong the circulation time of certain drugs. These circulation times have been further improved with the addition of PEO to the outer surface allowing for greater immune system evasion and “stealth-like” properties. More recently, fully synthetic vesicles (polymersomes) made from block copolymers have become available. Polymersomes have advantages over liposomes that include greater control over the chemistries and architecture, tougher mechanical properties and lower permeability. Many of these properties come from the higher molecular weight of the copolymers used to form polymersomes. However, the synthesis process of polymersomes versus liposomes can also be more difficult due to the higher molecular weight, intermolecular forces and complexity of the formation methods.

1.1.7 Intermolecular Forces

Vesicular dispersions are often termed as soft condensed matter with regards to their structure and properties, which describes materials that fall between liquids and crystalline solids.[5] A common example of soft condensed matter would be colloidal dispersions, which are formed from a solid or liquid phase dispersed within a separate liquid phase. There are many everyday examples of such materials, including mayonnaise, paint and household soap. This section describes the intermolecular forces that give rise to the complex physical properties of soft condensed matter.

The forces governing interactions between molecules are of particular interest to the field of soft condensed matter. Any material can be thought of as a balance between attractive and repulsive forces. In a gas, the thermal energy of individual molecules is greater than the attractive forces attempting to condense the molecules to a liquid state. Repulsive forces are due to the Pauli exclusion principle, which dictates that two electrons cannot occupy the same quantum mechanical state or orbital and therefore must organise themselves

into defined electron shells. Attractive interactions can be due to electrostatic interactions but fall into a few different categories based upon magnitude.[5]

The weakest intermolecular interactions are Van der Waals forces. The constant movement of electrons generates small dipole moments at random points around the molecule, this influences neighbouring molecules, creating an opposite dipole. These corresponding dipole moments result in a small attractive force. The potential for Van der Waals forces to occur is proportional to the square of the molecule or atoms' polarisability and the distance between the other species. The strength of a Van der Waals interaction is typically the same order of magnitude as molecular thermal energy at room temperature.[5]

Ionic interactions can occur between two neighbouring oppositely charged species, resulting in the complete transfer of electrons between atoms. They are strong interactions at two orders of magnitude greater than thermal energy at room temperature. Ionic interactions can occur between oppositely charged species in a solid or vacuum, and the interaction strength in a vacuum is dictated by the charges of the two species and distance between the atoms. However, this is heavily affected when the species are in solution due to screening by dissolved free ions. The free ions will orientate around the charged species and form layers of alternatively-charged ions that screen the effective charge interactions of the two original species. This screening (along with solvent polarisation) can lower the strength of the ionic interaction. In solution, the distance over which an ionic species has an electrostatic influence can be measured as the Debye length, which is proportional to the reciprocal of the surrounding solution's ionic strength. For example, many biological experiments are conducted in 0.1M phosphate buffered saline, for which under ambient conditions the approximate Debye length would be 2.3×10^{-9}m[79]. However, if the molarity is increased to 1M phosphate buffered saline the distance drops to 0.7×10^{-9}m, due to the increased shielding from surrounding electrolytes.

Another strong interaction, at least an order of magnitude greater than ambient thermal energy, is covalent bonding. Covalent bonds are formed when the electrons from one atom interact with two or more nuclei, resulting in an overall lower total energy than the individual atoms remaining separate. This bond occurs over a short distance and varies in strength depending on the atoms present in the molecule. A variation of the covalent bond is the metallic

bond, whereby an electron(s) is delocalised from the donor atom and shared with many more atoms than the few neighbouring interactions of the covalent bond.

Hydrogen bonding and the hydrophobic interactions are of particular importance to water-based systems. These forces are essential to amphiphilic self-assembly in water and are responsible for many of the interesting properties of water as a material. Water consists of two hydrogen atoms and an oxygen atom, the bond angle and length of which is illustrated in Figure 1.6. Hydrogen bonding is a specific covalent bonding of a hydrogen atom to a strongly electronegative atom, typically oxygen or nitrogen. Due to hydrogen having only a single electron to use for bonding while the electronegative species (oxygen) will have two electrons available, the atom is left slightly positive upon forming an initial bond. The positive charge then interacts with the electrons of another atom, forming a hydrogen bond that has a strength that falls between van der Waals forces and covalent bonds.

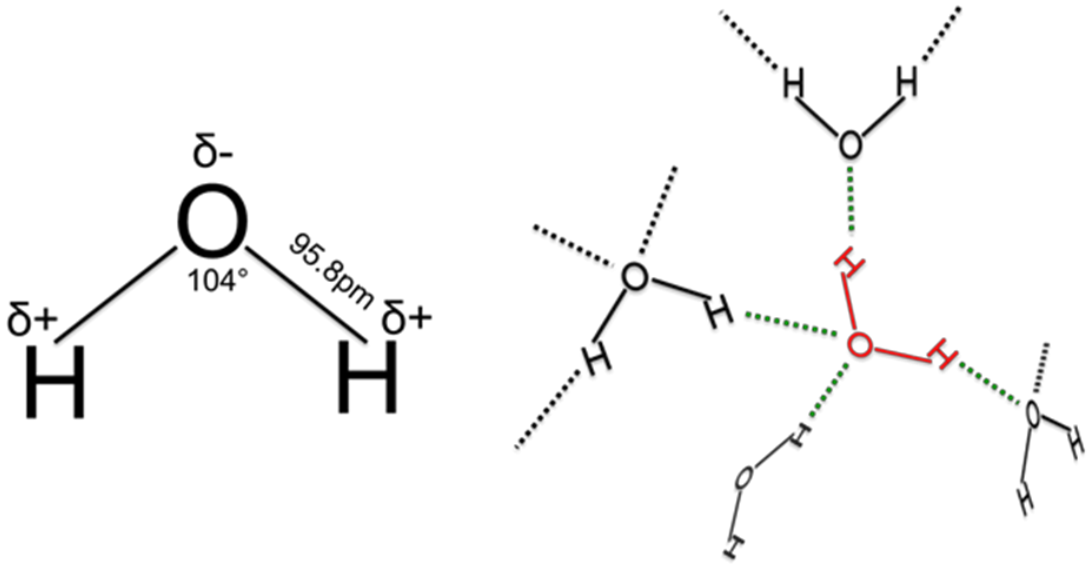

Figure 1.6: The left illustration shows the charges, length of bonds and bond angle of a water molecule. Right: the electronegativity of oxygen attracts electrons from the neighbouring hydrogen atoms, which creates dipoles that bond with neighbouring water molecules to form a tetrahedral arrangement.

Uniquely, each water molecule can form a total of four hydrogen bonds, which would theoretically allow for tetrahedral molecular packing. However, in its liquid state, water is a dynamic system where neighbouring molecules are constantly forming transient short-range tetrahedral ordering but with no long range ordering. This results in a constantly switching system, where each water

molecule moves between a co-ordination number of three and four, with around 10^{13} bond formations per second.[80] The large number of short-range hydrogen bonds gives rise to the high boiling point of water. Structurally similar molecules such as hydrogen sulfide have a higher molecular mass but a much lower boiling point, due to the weaker hydrogen bonding.

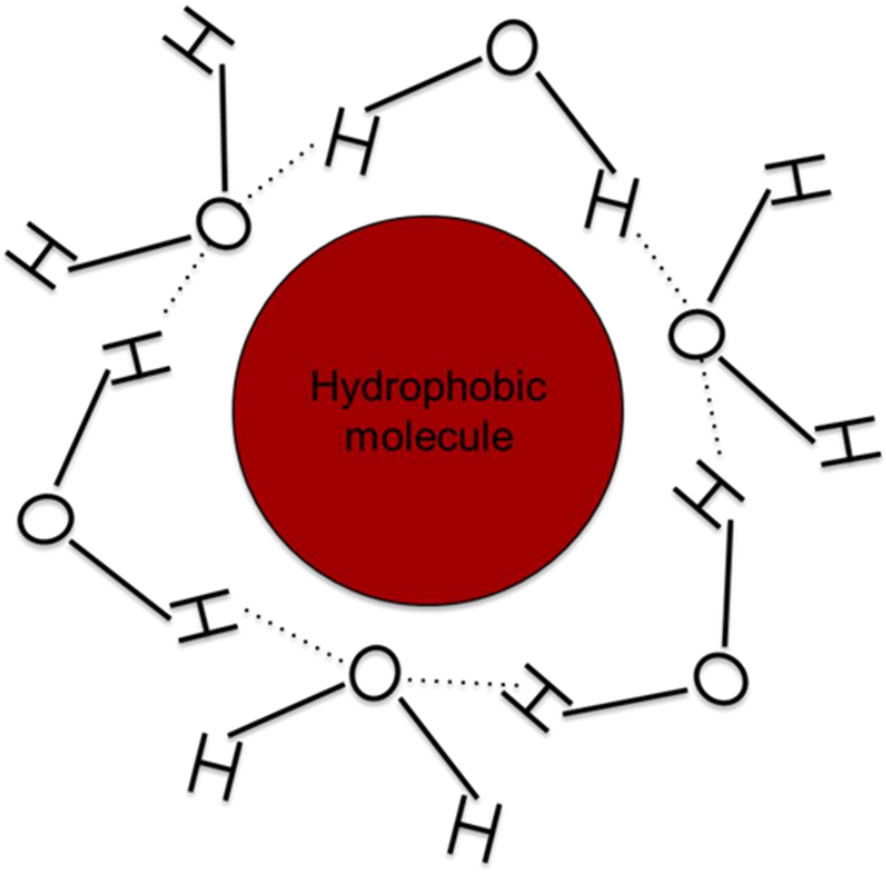

Figure 1.7: In the presence of a hydrophobic molecule, water is forced to bond with neighbouring water molecules in an unfavourable conformation known as a clathrate.

Non-polar molecules or hydrophobes, such as hydrocarbons, have no specific interaction with polar water molecules.[81] When mixed together, the water molecules next to the hydrophobe are unable to undertake their usual dynamic structural conformation.[82] As a result, surrounding water molecules adopt an ordered “lattic” configuration around the hydrophobic (Figure 1.7). As discussed in the next section, this ordering decreases the entropy of the system, a process that is thermodynamically unfavourable.[84] As a consequence, the hydrophobic molecules cluster together, in order to minimise the amount of clathrate formed

by water. This apparent attractive force between the hydrophobic molecules is caused by the entropically-favourable disorganisation of water.[85]

1.1.8 Polymer Solution Thermodynamics

The study of thermodynamics is used to define whether a particular process is energetically "favourable" or not under a given set of parameters. This is measured in terms of a reaction or process change in Gibbs energy *(G)*:[84]

$$\Delta G = \Delta H - T\Delta S$$

The change in Gibbs energy is defined by three parameters: Enthalpy (H), entropy (S) and temperature (T). Enthalpy is the measure of the total energy of a system, which includes the energy required for a system to maintain its current state of being and the required work to be done on the system in order to change it. The change in enthalpy (ΔH) is equivalent to energy transfer in a system, which includes heat transfer, radiation transfer or mechanical work done. Entropy is a measure of the degree of disorder in a system, arising from the number of potential configurations available. A process is deemed energetically favourable when the change in Gibbs free energy *(ΔG)* is negative. Therefore, in order for a polymer and a highly compatible solvent to form a solution, the Gibbs energy of mixing the two materials must be negative.

1.1.9 Entropy of Mixing

Entropically, the most favourable situation for a polymer in solution occurs when the monomers are dispersed throughout, allowing for the maximum number of chain conformations.[79] The entropy of the polymer solution is calculated using the Boltzmann law:

$$S = k_b \ln \Omega$$

Where k_b is the Boltzmann constant and Ω is the number of conformational micro states available to the polymer. All states and positions within a system are treated as having an equal probability. Therefore, the more potential states available to a given polymer will increase the entropy.

Flory-Huggins theory,[86,87] named after Paul Flory and Maurice Huggins, describes the thermodynamics of mixing polymers with differing molecular

weights to their solvents. The theory can be visualised as a two-stage process wherein the polymer first must transfer from a conformationally-confined solid state to a solution, followed by subsequent mixing of the long chains with the solvent molecules. A lattice can be used to demonstrate this concept, as shown in Figure 1.8.[79] The number of potential arrangements that the polymer can take is based upon the length of the polymer containing monomer units. The restriction is that each subsequent monomer unit occupies a place in the lattice adjacent to the previous one. Assuming a large lattice, then the probability of locating an empty site can be calculated for each section of the chain. Therefore, the total number of ways the polymer chain can fit into a lattice is calculated as a product of each possible way. The remaining cells in the lattice can be filled with solvent molecules. As there is only one way in which the solvent can be arranged, there is no impact on the polymer micro-states. The result for higher molecular weight polymers is that at a constant solvent size, the entropy of mixing is much lower than for ideal solutions, where the size of solvent and polymer are assumed equal. The mixing of a polymer with a favourable solvent is largely driven by the entropy of mixing. Furthermore, the magnitude of this entropy is strongly affected by the degree of polymerisation.

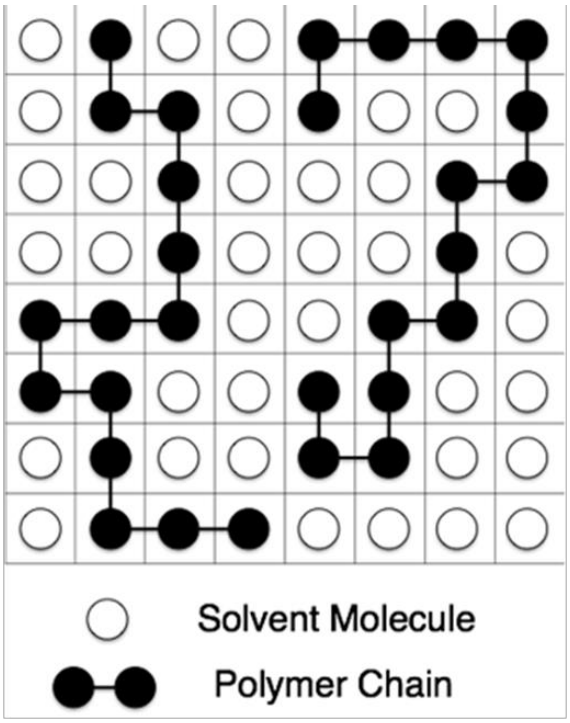

Figure 1.8: A typical Flory-Huggins lattice, depicting the distribution of the polymer (shown as black linked circles) and the solvent (white unlinked circles).

1.2.0 Enthalpy of Mixing

As well as entropic effects, a polymer system will also undergo heat transfer or work done, that can be described as enthalpy. The enthalpy of mixing can also be calculated using the lattice theory. As mentioned, the Flory-Huggins theory interprets mixing as a process where polymer-polymer interactions are broken and new polymer-solvent interactions are created. This may be represented as a chemical process where the formation of new polymer-solvent bonds will result in a change of enthalpy. Assuming no change in volume, the change in energy during polymer-solvent bond formation multiplied by the number of new bonds formed is equal to the change in mixing enthalpy.[79]

In summary, the Flory-Huggins theory of polymers in a favourable solvent is a convenient approach of introducing the concept of solubility. Solubility is governed by both entropic and enthalpic factors. However, as a model for polymer solubility, the Flory-Huggins theory makes several assumptions. In particular, the model fails to accurately describe dilute samples and highly polar solvent molecules, due to their enthalpic contributions. Additionally, the theory only takes into account the combinational entropy of the polymer and the solvent and ignores any contributions to entropy through chain flexibility. Despite these assumptions, the Flory-Huggins theory remains core to the understanding of polymer interactions across a variety of situations.

Further work has since refined the entropic and enthalpic implications of amphiphilic systems, which contain both hydrophilic and hydrophobic sections which are covalently bonded. Amphiphiles must therefore form complex self-assembled structures within water-based systems, in order to minimise the hydrophilic repulsive and hydrophobic attractive forces.

1.2.1 Thermodynamics of Self-Assembly

Self-assembly occurs when the entropic penalty for forming an aggregate is lower than the amphiphiles remaining dispersed. The degree of hydrophobicity present in a molecule alters the energetic penalty of remaining dispersed. The more hydrophobic the molecule is, the higher this entropic penalty will be, meaning such molecules will have a lower entropic penalty of aggregating compared to less hydrophobic but chemically similar amphiphiles. Herein the

theory of amphiphilic self-assembly as described by Israelachvilli *et al.* is summarised.[82,88]

If all amphiphiles are dispersed in solution equally, they will all share the same potential energy. This will alter as individual molecules begin to aggregate. If the average potential energy increases as the aggregate increases in size, so too would the energetic cost of adding another amphiphile. This would make large aggregates unfavourable and would generate a maximum size of aggregate. However, this has not been observed; therefore the average potential energy should decrease as the aggregate grows. However, if this was the case the structure produced would continue to grow indefinitely and any hydrophobic material at the edge of the aggregate would remain exposed to water. This energetic penalty is reduced through end caps of cylindrical monolayers and the formation of spherical structures for bilayers.

At very low amphiphile concentrations, it is possible for the system to withstand the entropic penalty of the hydrophobic effect and favour dispersed molecules over aggregates. If the concentration of molecules increases, the system will experience a drop in entropy and at a defined concentration, self-assembly becomes favourable. This concentration is referred to as the critical aggregation concentration (CAC), also commonly referred to as the critical micelle concentration (CMC) as micelles are often the first structures produced.[89] A micelle is a small spherical particle with a hydrophobic core formed from the hydrophobic sections of the amphiphiles and a corona produce by the hydrophilic sections. The CAC of a system depends on the "hydrophobicity" of the given amphiphile. In general, the CAC will decrease with increasing hydrophobe molecular weight.

For polymeric systems, the CAC is often below the limit of detection for common analysis techniques and therefore difficult to measure.[45,89–91] If more amphiphiles are added to the solution once the CAC is reached then additional aggregates will be formed and any remaining dispersed chains will plateau, as shown in figure 1.9. Aggregates can then form complex structures in order to minimise the attractive hydrophilic and repulsive hydrophobic forces present within water-based systems.

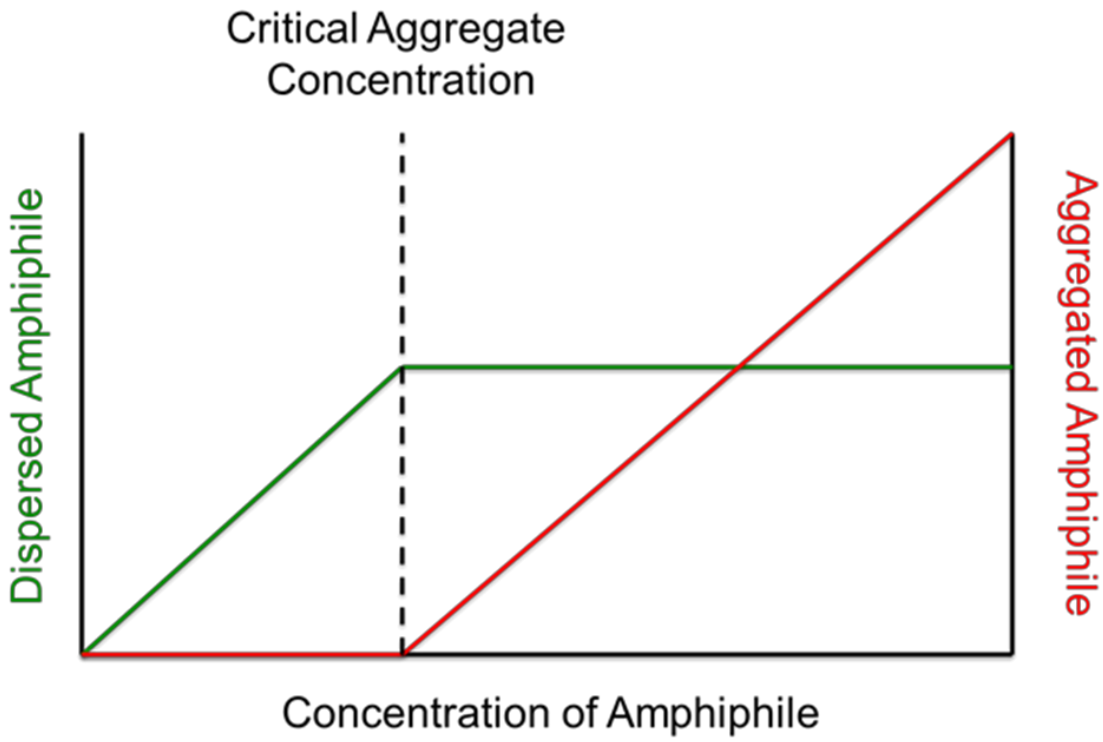

Figure 1.9: Dispersed and aggregated amphiphiles as a function of concentration. Below the critical aggregation concentration, amphiphiles added to the system remain dispersed. Above the critical concentration, additional amphiphiles generate aggregates.[89]

1.2.2 Self-Assembly

Pioneering work by Israelachvili *et al.* conducted on the theory of lipid self-assembly provided the soft matter community with basic thermodynamics of amphiphilic self-assembly.[82,88,92,93] A greater understanding was then gained by studying the intermolecular forces between lipid molecules as a function of hydrophilic/hydrophobic interfacial area. As shown in Figure 1.10, the attractive hydrophobic interactions scale in a linear manner with interfacial area, while the repulsive hydration forces are inversely proportional.[94]

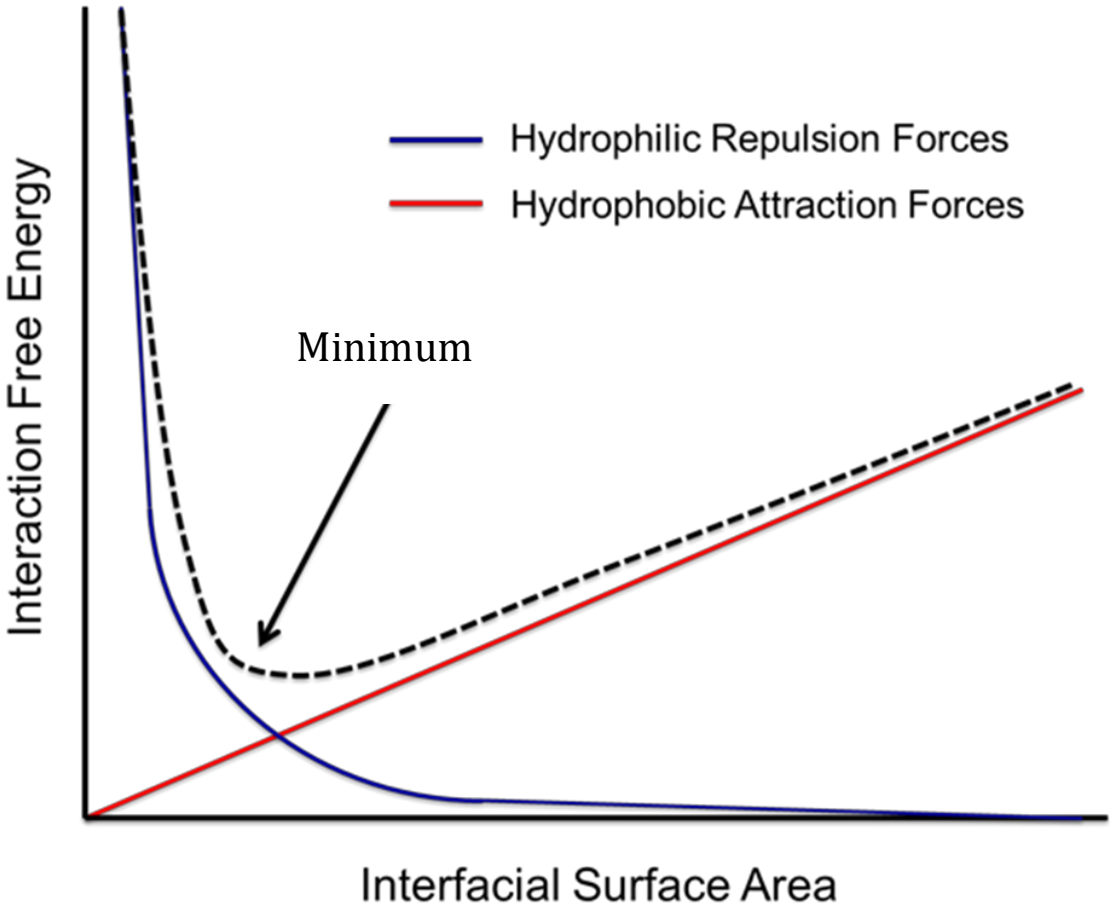

Figure 1.10: Amphiphile self-assembly is governed by the minimum point of the total energy, which has contributions from both repulsive and attractive forces between neighbouring amphiphiles.

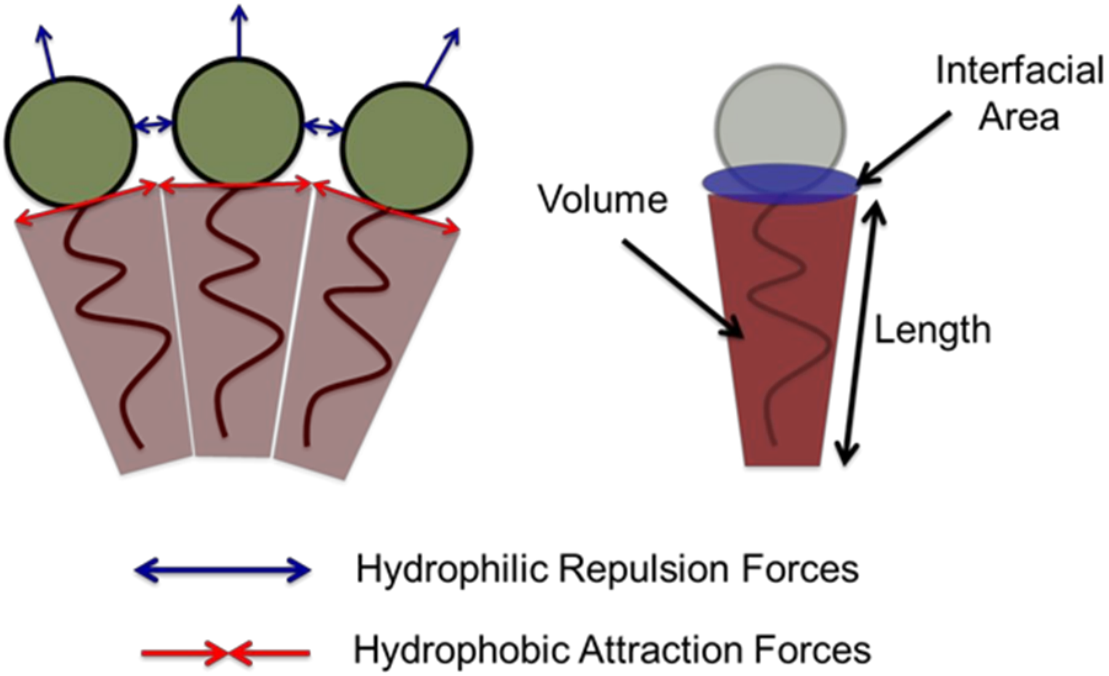

Figure 1.11: Aggregation of amphiphilic molecules due to a balance of attractive and repulsive forces. The magnitude of these forces are related to the molecular dimensions of the hydrophilic and hydrophobic parts.

The total interaction free energy has a minimum at an optimum head group area for a given molecule, which dictates the structure formed by the amphiphiles. In addition, the geometry of the molecule plays a crucial role in the type of the aggregates formed. A particular aggregate can be considered as a discrete number of amphiphilic molecules ($N_{aggregate}$). This is calculated as follows:

$$N_{Aggregate} = \frac{V_{Aggregate}}{V_{Molecule}} = \frac{A_{Aggregate}}{A_{Molecule}}$$

Where V and A are the volume and area of the aggregate and the molecules. Rearranging this formula shows that $N_{aggregate}$ is equal to the volume:area ratio. The allowed volume:area ratios of lipid amphiphiles result in three common structures; spherical micelles, cylindrical micelles and membranes. The ideal molecular geometries of these shapes are illustrated in figure 1.12.

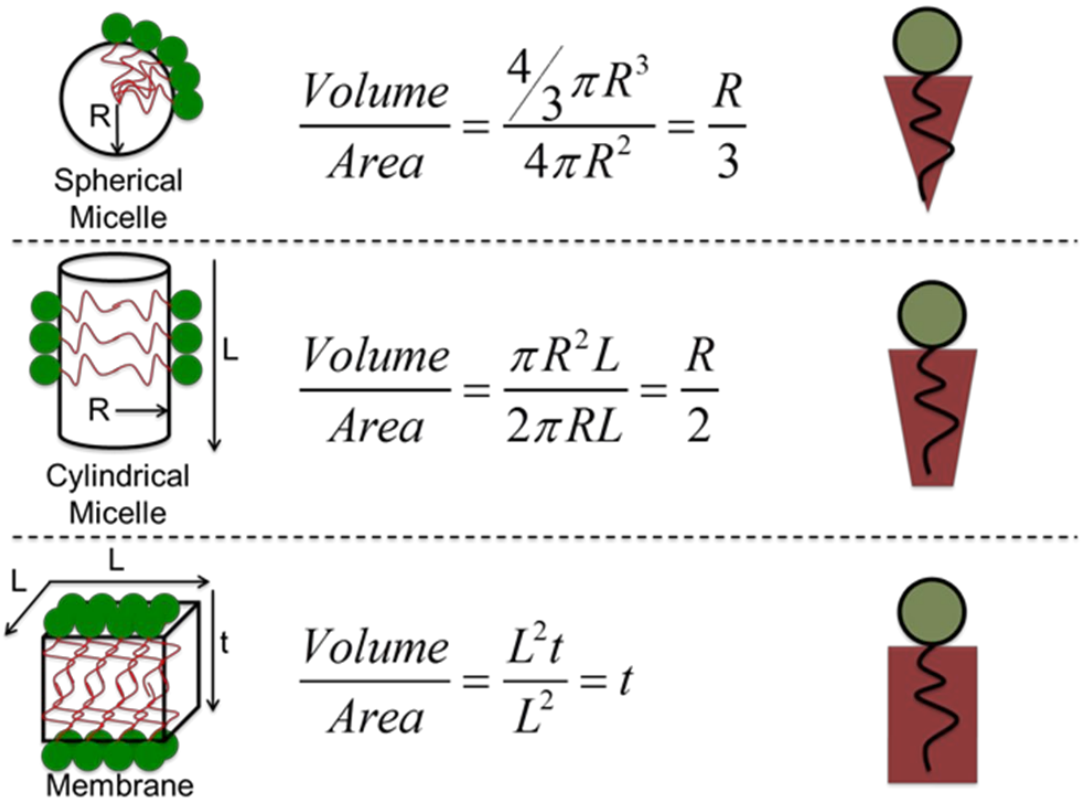

Figure 1.12: The relation between self-assembled structures and molecular geometry, as dictated by the volume-area ratios.

The concept of an optimal head group area (Figure 1.1.0) was combined with the length and volume of the hydrophobic segment to generate a simple formula to predict the aggregate produced by a particular amphiphile: This equation is commonly referred to as the molecular packing parameter (p):[92]

$$p = \frac{v}{a_0 L}$$

where v and L equal the hydrophobic volume and length respectively, while a_0 is the interfacial area between the hydrophilic and hydrophobic sections. This dimensionless value indicates the structures that are formed, as illustrated in figure 1.12. When $p < 1/3$ spherical micelles are favoured, which are often the first structures produced in amphiphilic lipid or polymer systems. A molecular packing parameter between $1/3 < p < 1/2$ is associated with cylindrical micelles, while membranes are optimal conformations for molecular packing parameters of $1/2 < p \leq 1$. A molecular packing parameter of 1 will mostly result in planar membranes, whereas a $p < 1$ will drive amphiphile formation towards curved membranes.[93]

However, even when the packing factor is preferable for membrane formation as per vesicular systems, micelles will also be formed as the structures require fewer molecules than a vesicle. In this situation, the amphiphile is kinetically trapped as a micelle despite the packing factor being preferable to forming a membrane. Therefore, during vesicle production for a drug delivery system, undesired micelle structures should be removed during purification. Many drug delivery systems are based upon lipid or polymer micelles and they have their own advantages such as improved size control, increased circulation time within biological systems and entrapment of compounds. However, micelles are limited in the range of compounds that can be entrapped due to the hydrophobic environment of the core and they have been shown to exhibit surfactant-like toxicity at higher concentrations [95]. Therefore, the amphiphile self-assembly process needs to be well understood and controlled in order to successfully manufacture drug delivery systems.

To summarise, self-assembly of amphiphiles occurs as a compromise of the typical solution behaviours of hydrophilic and hydrophobic molecules. Due to being covalently bonded, the amphiphile cannot phase separate and as a result can aggregate to form macromolecular structures. Above a certain concentration the formation of these ordered aggregates is energetically

favourable; this concentration is known as the critical aggregate concentration. The structures formed are related to the geometry of the amphiphile as described by the packing parameter. This is based on calculations and observations of lipid systems, and predicts the ideal structures produced (or average molecular curvature) based on the hydrophilic/hydrophobic volume ratios. For membrane-forming systems, kinetically trapped precursor structures such as micelles may also be present due to the reduced amount of material required for formation. As single-layered micelle structures have a hydrophobic lumen, these can be used as hydrophobic drug delivery systems. However for more complex biological therapies such as large hydrophilic proteins or antibodies, the bilayered vesicle structures with hydrophilic lumens that are created within the membrane-forming systems are required. The next section therefore focuses on the experimental observations of producing vesicles through both liposomal and polymer systems, and the current understanding of the formation process.

1.2.3 Comparison of Vesicle Formation by Lipids and Polymers

Lipid vesicles can be described as particles generated by one or more closed lipid bilayers, where the space between the bilayers and the internal cavity of the vesicle is filled with aqueous solvent and the bilayer is in a liquid crystalline state. Synthetic vesicles can also be produced using diblock co-polymers, which are termed polymersomes. For low molecular weight lipid amphiphiles, the process of producing vesicles is relatively simple. Often the addition of an aqueous buffer to a small quantity of pure lipid followed by gentle aggravation is sufficient to yield liposomes. On the other hand, polymeric amphiphiles typically have higher molecular weights and much slower hydration kinetics, which can require additional energy input or alternative formation processes. Furthermore, it can be difficult to achieve a polymer solution with homogenous structures (ie. only vesicles), as a variety of micelles, vesicles and multi-layered complex structures can often result. These differences are thought to be due to a combination of factors. Typically, diblock copolymers have higher molecular weights compared with lipids, often by an order of magnitude. Synthetic polymers also show polydispersity due to their production process. In addition, the interface between the hydrophilic section and the hydrophobic one may not

be as defined as with lipids, where it is head group and a hydrocarbon tail. Alongside these variations in molecular consistency, copolymers of a higher molecular weight will also have slower kinetics at ambient temperatures.

Despite these potential processing problems, polymer membranes offer several advantages over their lipid counterparts. Firstly, the interdigitated structure leads to greatly improved mechanical properties. For example poly(ethylene oxide)-block-poly(ethyl ethylene) (PEO-PEE) membranes have been shown to be 5-50 times tougher than phosphatidylcholine (PC) membranes, as measured by micropipette aspiration.[45] This leads to an enhanced ability to withstand *in vivo* forces. The use of high molecular weight copolymers also provides the advantages of very low critical aggregation concentrations [96]. This reduces problems such as disassembly into dispersed chains by dilution when creating an optimal *in vivo* dose. This work therefore covers the experimental observations of polymersome formation through the various processes, which include dry film hydration, pH/temperature/solvent switch formation and polymerisation-induced self-assembly.

1.2.4 Polymersome Formation Methods

Self-assembling systems are characterised by the spontaneous organisation of basic building blocks into ordered structures of greater length scales. As described in section 1.2.2, the shape of the self-assembled structure is dependent on the equilibrium of opposing intermolecular forces. The molecular packing parameter describes this balance and relates the thermodynamic equilibrium to the molecular architecture. However, the kinetics of reaching such an end point are typically very slow for polymeric amphiphiles. An example is the formation of polymersomes by the hydration of a copolymer film. The polymer is initially dissolved in a suitable organic solvent, which is evaporated to form a uniform film. Then, water or aqueous buffer is added to the dry polymer film and the mixture is agitated for a specified amount of time. During this time, water diffuses into the polymer film, causing it to swell. As water moves into the film, the copolymer begins to form ordered conformations based on the hydrophobic effect and molecular packing parameter. Over time, the concentration of water in the film increases and a multitude of structures evolve via highly ordered lytropic phases and increasingly dispersed mesophases,

ending with isotropically-dispersed polymersomes. This hydration process has been well-documented for numerous block copolymer systems[91,97–99] largely using X-ray scattering[100] and electron microscopy approaches.[101,102] Typically, initial diffusion of water into the polymer causes molecular orientation into an ordered structure, the organisation of which is mainly determined by the following factors:

a) Molecular Weight

Polymersome-forming copolymers produce bi-continuous sponge phases at high molecular weights, which then transform into polymersomes grouped together in a hexagonally close packed arrangement as summarised in Figure 1.13. Polymersomes then begin to disperse into individual aggregates at a concentration of around 1 weight (wt) % copolymer. Low-molecular weight films (typically <4kDa for poly [ethylene oxide]- poly- [butylene oxide] [PEO-PBO] polymersome-forming copolymers tested) will generally form cubic-packed multilamellar vesicles, which will eventually transform into an interconnected phase with tubular membranes.[97,103] These connections are then lost and the polymersomes disperse as single aggregates.

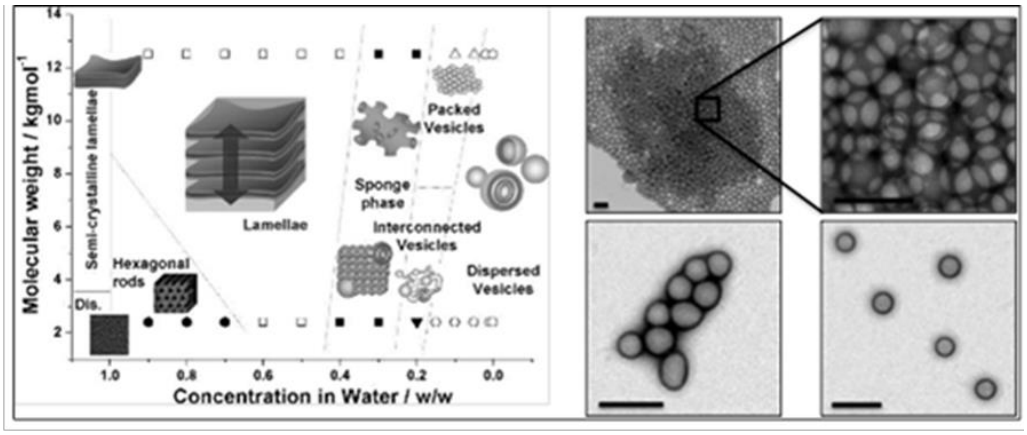

Figure 1.13: Left: A phase diagram showing the structural transitions of copolymer amphiphiles, from solid films through to dispersed polymersomes. The process of hydrating a dry film of copolymer causes movement through these phases before reaching dispersed vesicles, or polymersomes. Right: transmission electron micrographs of Poly([2-methacryloyl-oxy]ethyl phosphorylcholine)-block-poly(2-[diisopropyl-amino]ethyl methacrylate) (PMPC-PDPA) polymersomes showing the interconnected "sponge" phase (above) with packed and dispersed polymersomes shown below. Scale bars equal 200nm. Reproduced and adapted with permission from the American Chemical Society (ACS).[104]

b) Water Content

Within a low-water environment (≈80 wt% polymer), copolymer films with a higher molecular weight will hydrate and form lamellar structures, whereas hydrated films of low molecular weight copolymers (typically < 4kDa) adopt a hexagonal cylinder structure. The lamellar phase will swell with increasing water concentration, which is observed as an increase in lamellar spacing (d). At around 50 wt.% – 30 wt.% polymer, swollen films form new phases known as "spongy" or gel phases that still display some long range order.[91] As the water content increases further (20wt% – 10wt% polymer), the polymer undergoes a transition from lyotropic gel phases to isotropically-dispersed phases.

c) Block Composition

The effects of block composition on hydrated structures can be illustrated using the well-characterised PEO-PBO diblock copolymer. If the PBO content is increased, formation of polymersomes is favoured. Conversely, a higher ratio of PEO will result in more micelles and the percentage of polymersome structures will therefore decrease.[98,100]

d) Temperature

Micelle-forming PEO-PBO polymers form a series of close packed gels with optical and mechanical properties that vary with temperature.[97–100]

e) Co-Solvents

The formation of polymersomes can also be conducted using dissolved monomers in a solvent suitable for both blocks. Self-assembly can then be achieved by changing the solvent quality through parameters such as pH, temperature or co-solvent, so that one of the polymer blocks comes out of solution and polymersome formation is forced.[105–114]

A common model used to describe polymersome formation by changing the solvent quality is a two-step process of nucleation and growth.[113] Initially, coalescence of copolymer chains occur through the hydrophobic effect, forming spherical micelle aggregates. Aggregates then

grow into a range of architectures of decreasing curvature, until spherical polymersomes form as shown in Figure 1.14.

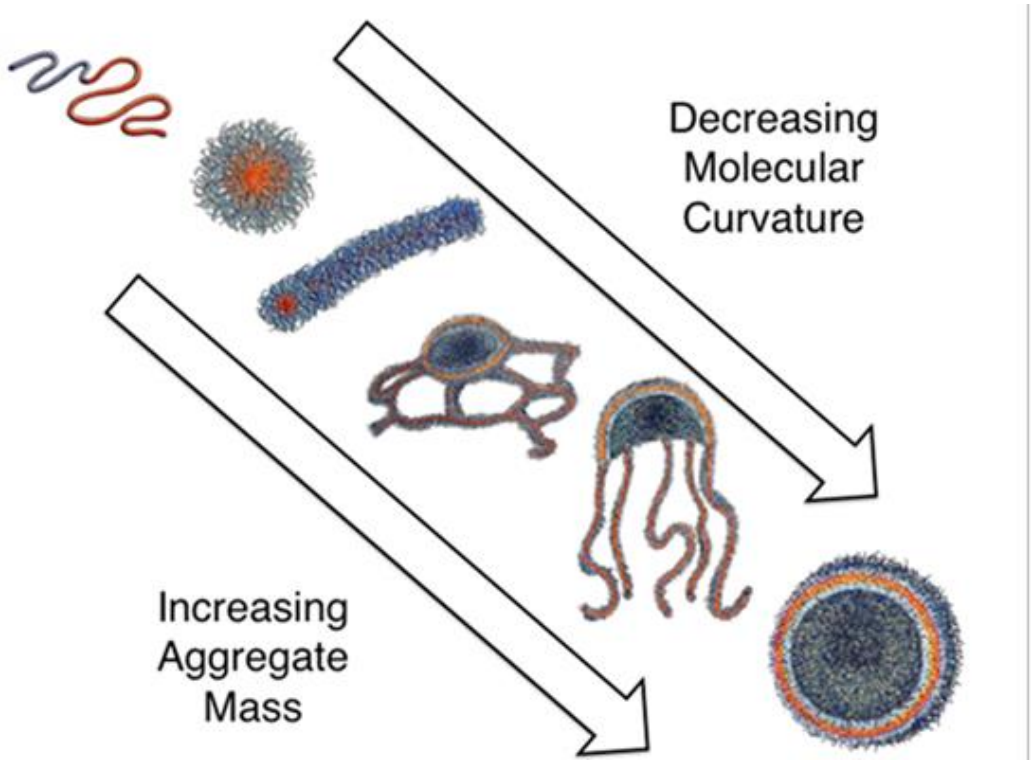

Figure 1.14: The formation of polymersomes from dispersed chains forms a series of aggregates of decreasing average molecular curvature and increasing aggregate mass.

Detailed investigations into these intermediate structures have been conducted across various polymer systems.[108,113,115–117] Eisenberg *et al.* studied the micelle-to-vesicle transition of polystyrene-block-poly(acrylic acid) (PS-PAA) as a function of the water:dioxane ratio.[117] At low water content (11 wt% water), formation of short cylindrical micelles was observed. Increasing the water content (11–14 wt%) increased the length of the cylindrical micelles. Eventually, small vesicles were observed at 28 wt% water. The vesicle size was found to increase with water content. The whole process was reversible if dioxane was added, summarised in Figure 1.15.

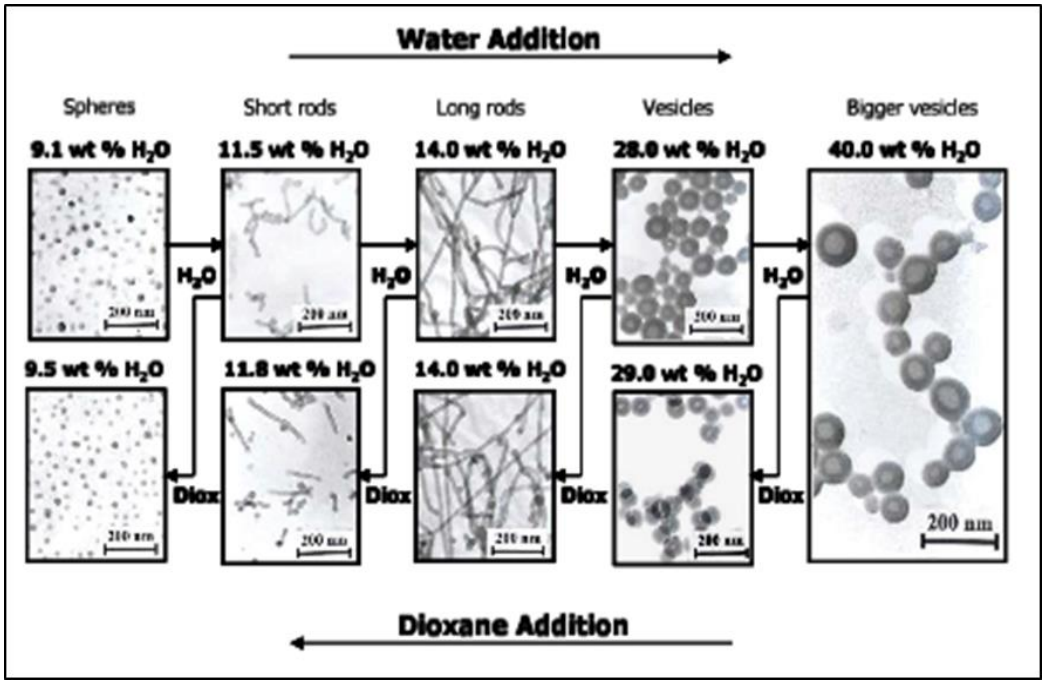

Figure 1.15: Evolution of self-assembled morphologies formed from PS-PAA polymer in a solution of dioxane and water, imaged by cryogenic electron microscopy. The increased water content swells the hydrophilic PAA brush and changes the packing factor of the polymer, resulting in a changed from spherical micelles via cylindrical micelles to polymersomes. This process is reversible upon the reduction of water content. Figure is reproduced with permission from the American Chemical Society (ACS).

By studying the transition kinetics and quenching samples at various time points, the same transition of micelles to vesicles via cylindrical micelles was observed.[32] The presence of “paddle” shaped structures comprising lamellae and cylindrical micelle sections were observed between the pure cylinders and pure polymersome time points. The same group then investigated the effect of changing PS-PAA block lengths on the transition boundaries between the structures observed.[29] The results correlated with the packing factor theory, which states that a longer core-forming block favours the production of polymersomes.[93]

pH-responsive poly(butadiene) - block - poly(methacrylic acid) (PBD-PMAA) has since been used to study the vesicle-to-micelle transition and the intermediate structures produced as a function of the PMAA degree of ionisation.[107] Transmission electron microscopy (TEM) images taken across the pH range studied (pH 4 – 11) shows the production of further intermediate species between polymersomes, including cylindrical micelles and spherical micelles. Specifically, these structures include a

mixture of bilayers and monolayers that are between polymersomes and cylinders, including the striking “jellyfish” aggregate (Figure 1.16).

Figure 1.16: A TEM micrograph showing a “Jellyfish” structure, composed of the copolymer Poly([2-methacryloyl-oxy]ethyl phosphorylcholine)-block-poly(2-[diisopropyl- amino]ethyl methacrylate) (PMPC-PDPA). These structures are rarely trapped by the process routes used in this thesis, however other formation processes such as polymerisation-induced self-assembly allow for the study of such structures in greater detail. Scale bar = 200 nm.

Polymerisation-Induced Self-Assembly

More recently, a study of the self-assembly process was conducted using an *in situ* controlled radical polymerisation of poly(glycerol monomethacrylate)-block-poly (2-hydroxypropyl methacrylate) (PGMA-PHPMA), known as polymerisation induced self-assembly (PISA).[118] The HPMA monomer is water soluble up to 13 w/v% at room temperature but forms an insoluble polymer. Therefore, the evolution of micelles to vesicles could be studied in detail by observing the structures produced at different HPMA conversion when polymerised in water. TEM micrographs show the transition from spherical micelles, to shorter cylindrical micelles and then to longer cylindrical micelles. This approach yielded significantly more information on the transitions between cylindrical micelles to complete vesicles due to the high degree of control and frequent sampling in this study that allowed the intermediate steps between cylindrical micelles and polymersomes to be visualised in greater detail (Figure 1.17).[119]

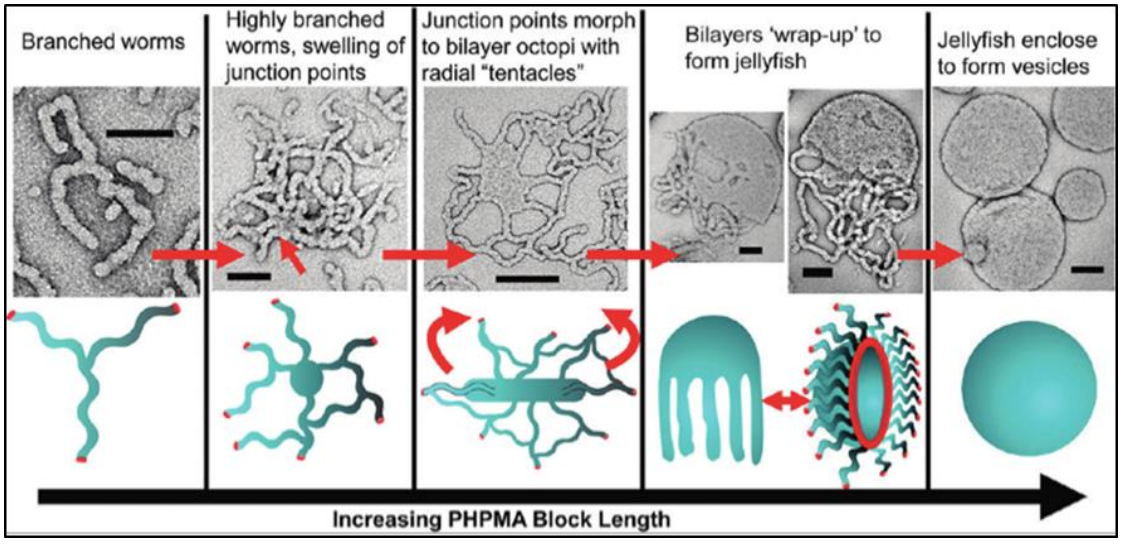

Figure 1.17: Electron micrographs depicting the morphological evolution of PGMA-PHPMA structures the degree of polymerisation of the hydrophobic PHPMA block increases. These structures follow the packing factor theory that greater amounts of the amphiphile must adopt a bilayer conformation as the block length increases in order to satisfy the self-assembly. This is shown in the cartoons. The scale bar equals 200nm. Figure is reproduced with permission from the American Chemical Society (ACS).[119]

The octopus structures illustrated in Figure 1.17 form when PHPMA polymerisation is allowed to continue, causing the cylindrical micelles to branch. These branching points then swell until they eventually contain enough material to form a bilayer surrounded with cylindrical micelles attached. Similar octopus structures have also been reported in a PEO-PBD system by Jain and Bates.[108] At higher PHPMA degrees of polymerisation, i.e. when the hydrophobic block increases, bilayers curve to produce the "jellyfish" morphology. Finally, the bilayer segment of the jellyfish closes to form polymersomes. These experimental approaches have reported the evolution of spherical micelles to polymersomes as the copolymer aggregate curvature reduces.

High molecular weight polymeric amphiphiles display reduced molecular kinetics due to their increased hydrophobicity and weakly segregating interdigitated membranes,[48,120,121] thereby diminishing the likelihood of bilayer "flip flopping"[122] or monomer insertion/expulsion events that occur during the transition from one structure to another.[119] A reduction in the number of chain exchange events leads to kinetically frozen structures in many cases. In these cases, polymers can produce a range of non-ergodic structures that are "frustrated" with regards to their ideal curvature, but are unable to fuse or exchange with surrounding aggregates and thus remain in a thermodynamically

unfavourable conformation. Larger structures or packed vesicles (vesicles full of more polymer vesicles, similar to a Russian doll) can also occur due to the differing shear forces or variance in the rate of diffusion experienced across the polymer solution during the hydration process. The presence of packed vesicles, or contaminants, therefore requires stringent purification and post processing if well-defined polymersomes are required.

For pharmaceutical or industrial use, the appropriate hydration method and degree of sample “contamination” allowed is dictated by the application and polymer system used. For biomedical applications, the use of organic solvents is highly detrimental to cell viability. In addition, the formation method employed is often determined by the Log P (partition coefficient) of the therapeutic or diagnostic compound to be encapsulated. Poly([2-methacryloyl-oxy]ethyl phosphorylcholine)-block-poly(2-[diisopropyl- amino]ethyl methacrylate) (PMPC-PDPA) therefore lends itself to biomedical applications as the formation step to produce polymersomes can occur without organic solvents and the chemical properties of the polymersomes also result in enhanced cellular uptake[61]

1.2.5 Comparison of Polymersome-Formation Methods

The oldest mechanism of polymersome formation originally developed with liposome systems is the hydration of dry bulk polymer films with water, resulting in the progression through complex, highly concentrated amphiphile phases as water diffuses into the film until dispersed particles are produced. This approach often requires days to weeks in order to achieve dispersed polymersomes and is more likely to be contaminated with packed aggregates and large particles. Alternatively, if the chemistry allows, polymersomes can be produced from dispersed chains and a change in system parameters that drive self-assembly such as solvent, temperature, pH or water concentration. These approaches result in aggregates that progress through various structures, as predicted by the molecular packing parameter. There are also several intermediate structures observed at the boundaries between phases such as the “octopus” and “jellyfish” structures. This approach is often faster than film hydration, typically hours to days. However, samples are more likely to be contaminated with smaller structures from the formation process. PMPC-PDPA polymersomes

are commonly generated by exploiting the pH responsive behaviour of the PDPA block. As the biological drug delivery applications for polymersomes require reproducibility and control over the size of polymersomes produced, the formation method and chemical properties of PMPC-PDPA have been investigated.

1.2.6 Chemical Characterisation of PMPC-PDPA

PMPC-PDPA is a pH responsive, biocompatible block copolymer, as shown in Figure 1.18. Hydrophilic zwitterionic polymer PMPC has been investigated for around two decades. It is a polymer analogue of the lipid phosphatidylcholine and is frequently used as a non-fouling coating for medical devices.[123–127]

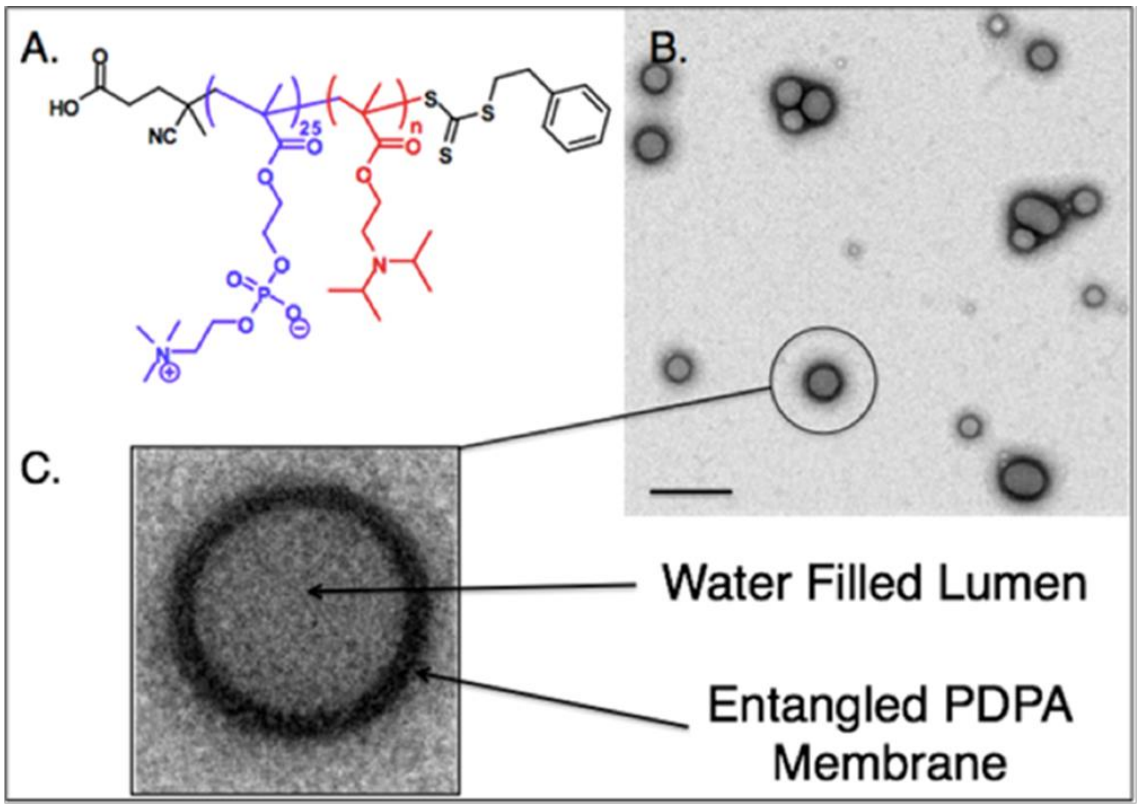

Figure 1.18: A) The chemical structure of the PMPC-PDPA diblock copolymer used for the studies discussed in this thesis. B) An electron micrograph showing dried PMPC-PDPA polymersomes. Contrast is achieved using staining with phospotungstic acid (PTA). C) A magnified image of a single polymersome. The copolymer membrane and the lumen of the collapsed polymersome is clearly visible in the stained samples Scale bar = 200 nm.

The resistance of the PMPC polymer to protein and cell adhesion is believed to be due to its' "super" hydrophilic nature,[128] which results in a large amount of water being bound to the polymer. Therefore, in order for a protein to interact with the substrate material, the water occupying the PMPC coating layer must be removed. This process is highly unfavourable, generating a large energy barrier that has to be overcome before any interactions with the copolymer occur.

PDPA is a pH-sensitive polymer that becomes hydrophilic at mildly acidic conditions, which can be classified using the acid dissociation constant, pK_a. The pK_a can provide the extent of ionisation that occurs for a substance within water. PDPA has a pK_a of 6.4 under ambient conditions.[106] The formation of PMPC-PDPA vesicles can therefore be achieved through a pH switch mechanism, as the tertiary amine groups within the hydrophobic PDPA block cause the section to become hydrophilic or hydrophobic as a function of solution pH.[106] However, the PMPC remains hydrophilic irrespective of the pH. This allows the diblock copolymer to switch from hydrophilic to amphiphilic as a function of pH and therefore dispersed monomers aggregate into polymersomes and micelles. Whilst the film hydration method is frequently used, the pH switch method is much more rapid. This means that the probability of losing sample sterility is reduced and any degradation of the cargo molecules are reduced. The pH responsive region of PDPA is particularly convenient for intracellular drug delivery into mammalian cells.[129] Due to the pH-responsiveness of PDPA, the copolymer PMPC-PDPA forms vesicles at neutral pH, allowing for the encapsulation of various species. PMPC-PDPA vesicles can therefore mimic liposomal vesicles in order to act as biological DDS.[61] However, as described in the next section, a defined range of vesicle sizes are required for optimal cellular uptake. Therefore, it is important to control the formation of polymersomes for size or implement effective post-formation purification steps.

As polymersomes decrease in size, the ratio of polymer forming the inner and outer leaflets of the membrane move rapidly away from unity, and the leaflets experience unfavourable degrees of curvature. Therefore, structures smaller than 50 nm have a reduced probability of polymersome formation due to the high curvature. Thus with the $PMPC_{25}$-$PDPA_{77\text{-}147}$ it is estimated that

structures less than 40nm are (mono-layered) spheres or micelles, which is roughly estimated by taking a membrane thickness of 7–10 nm from TEM measurements and estimating a brush thickness of around 3.5 nm from simple carbon-carbon bond lengths (140 pm x 25). Previous studies have shown that $PMPC_x$-$PDPA_y$ with block lengths of 25-30 for x and 70-160 for y result in polymersomes, whereas shorter DPA block lengths (y = 30-60) produce micelles.[106,130,131]

Studies into PMPC-PDPA blended polymersomes have been conducted by Lo Presti *et al.*, wherein the formation of domains was analysed on a micro and nanoscale with two different chemistries.[132] Micrometre-sized polymersomes created from a blend of PMPC-PDPA and PEO-PBO were produced by electroformation. Electroformation is a method where the hydration of a polymer film is conducted under a potential difference, which can result in micrometre “giant” polymersomes. The two copolymers were tagged with different fluorophores so the separate domains could be imaged under a confocal microscope. Micrographs showed the two polymers phase separating over a period of 12 hours and then remained stable over the 36-hour timescale observed. In a separate experiment, bulk fluorescence measurements of a 50:50 molar ratio of PMPC-PDPA and PEO-PBO labelled with diethylaminocoumarin carbonyl azide (DEAC) in the PBO block were taken. DEAC exhibits a blue shift in its emission spectra when its surrounding polarity is reduced.[53,54,132] PDPA is a less polar environment for DEAC than PBO, therefore, for the blended formulation, an emission wavelength of 439nm is blue shifted from the 450 nm emission wavelength of the pure PEO-PBO sample. Furthermore, this 11 nm shift then reduced over the 30 days of analysis, indicating an increase of polarity surrounding DEAC. The authors stated the results were due to the creation and coarsening of PBO domains within the blended membrane. Furthermore, electron microscopy studies were conducted on samples containing varying molar ratios of PMPC-PDPA:PEO-PBO (10:90, 25:75, 50:50, 75:25 and 90:10) over 30 days. Domains appeared to coarsen over the course of the experiment, resulting in both the 90:10 and 10:90 samples completely phase separating into asymmetrical “Janus” particles.[132]

Lo Presti *et al.* repeated these studies for PMPC-PDPA:PEO-PDPA and PEO-PBO:PEO-PDPA copolymer blends, i.e. blends with the same hydrophobic

or hydrophilic block. Phase separation appeared to be more advanced after 14 days for the PMPC-PDPA:PEO-PDPA system, indicating that the hydrophobic block has a greater influence over phase separation. However, the authors noted that differences in chain length and hydrophilicity may also strongly contribute to the rate of phase separation. As discussed in the next section, blended polymersomes have also been used for biological studies due to the successful cellular uptake of PMPC-PDPA polymersomes, which has led to the evaluation of both PMPC-PDPA and various blended copolymer PMPC-PDPA systems as drug delivery vehicles for biological systems.[61,133]

1.2.7 Cellular uptake of PMPC-PDPA

Biological studies of PMPC-PDPA have demonstrated its suitability as a DDS, due to the intracellular uptake of PMPC-PDPA and the low levels of cytotoxicity that result.[61] Studies into PMPC-PDPA indicate that the uptake mechanism used by mammalian cells to transport PMPC-PDPA into the intracellular space is most likely endocytosis, an active process that uses endosomal vesicles within the cell.[7] Endocytosis involves the deformation and budding-off of cell membrane sections into intracellular lipid vesicles called endosomes.[129] As the trafficking vesicle progresses into a late endosome once within the intracellular space (Figure 1.19), the organelle moves towards the nucleus and proton pumps gradually increase the H^+ concentration within the lumen of the endosomal compartments. This pushes the pH from neutral at the start of the process to mildly acidic pH values as the process continues.

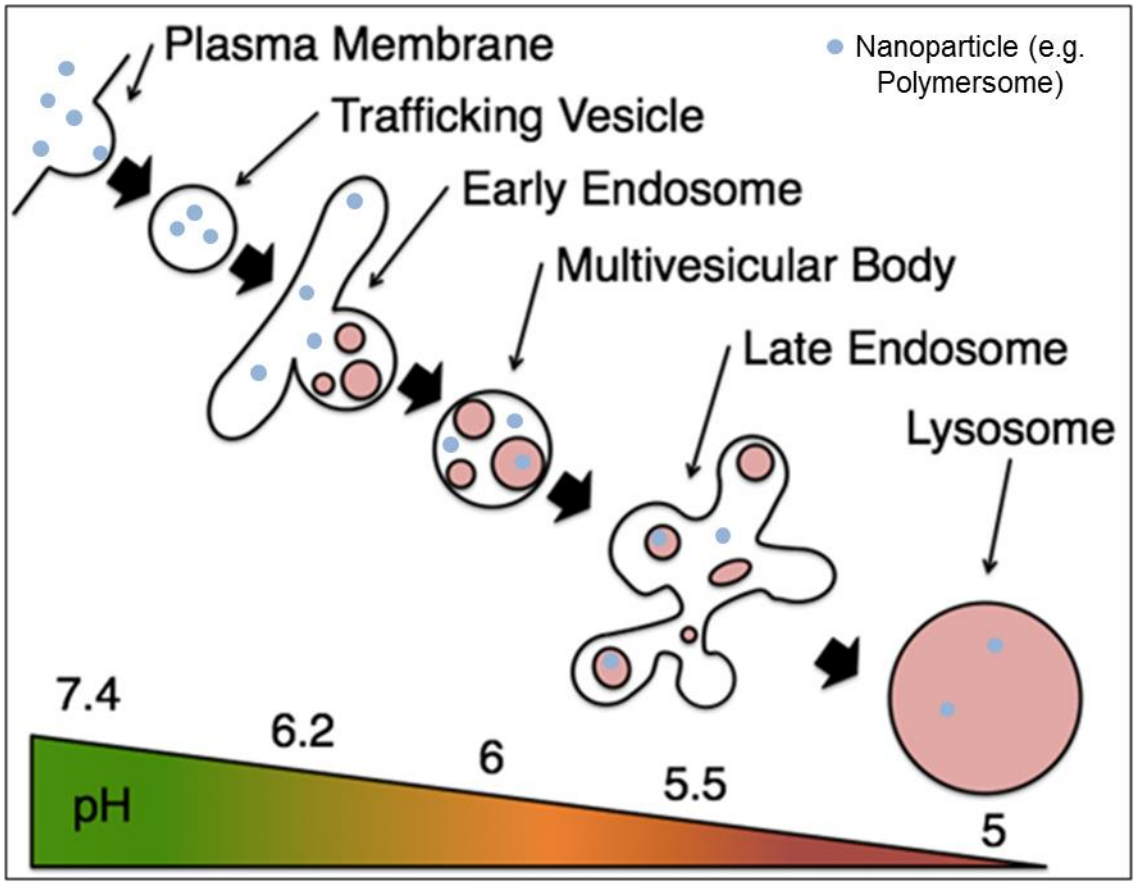

Figure 1.19: A diagram depicting the change in pH during the early stages of intracellular transport by endocytosis.

It has been suggested that PMPC-PDPA polymersomes are taken up through endocytosis and subsequently disassemble when the lumen environment becomes sufficiently acidic, which in turn would cause an increase in the osmotic pressure due to the newly-dispersed hydrophilic polymer chains.[129]The efficiency of cellular uptake and internalisation can be affected by polymersome diameter and surface chemistry. Generally, polymersomes 50-100nm in diameter show optimal uptake kinetics.[129] Polymersomes greater than 100nm often show reduced cellular uptake, which is thought to be due to the amount of disruption to the cell membrane required in order to engulf the particle. Due to these limitations it is important to control the size of the polymersomes in order to maximise their efficiency of uptake.[8,9]

The use of a PMPC block as the hydrophilic section of the amphiphile rather than PEO has been found to improve cellular uptake, with very low toxicity or inflammatory response shown across many cell types. [61] Vesicle compositions containing pH-responsive PDPA as the membrane-forming

component have been found to release their contents throughout the cell cytoplasm, while PBO-based vesicles remain within the endosomes.[60] This indicates that the pH responsive vesicles must escape the endosomes upon disassembly. The current hypothesis is that dissolution of the polymer chains creates an increase in osmotic pressure, which in turn perforates the endosome, allowing contents to escape. This disruption is assumed not to be catastrophic due to the lack of inflammatory response to PMPC-PDPA polymersome. [61] The correlation between vesicle size and uptake kinetics also supports the endocytosis theory. The "best" size for particle uptake by endocytosis question is a complex one; factors such as chemistry, shape and mechanical properties are closely related to outcomes, making it very hard to isolate the effects of size. A detailed review of endocytosis and nanoparticles has been written by Canton and Battaglia.[129] A rough figure of 50-60nm seems to be an optimal range for uptake many nanoparticle systems.[10] In addition, the different topologies produced by blending PMPC and PEO-based copolymers add additional factors to consider for uptake studies. The "patches" of different chemistries seem to facilitate a more rapid uptake of larger particles when compared to single chemistry polymersomes of the same size.[132]

Blanazs *et al.* also studied the effects of surface chemistry and vesicle diameter on the uptake kinetics.[134] From previous studies it had been shown that PMPC based polymersomes interact strongly with cell membranes, whilst PEO-based polymersomes had much slower uptake kinetics[132]. Uptake studies were therefore conducted with molar blends of two copolymer compositions, PMPC-PDPA and PEO-PDPA. Blends were produced by mixing molar ratios of the copolymer (100:0, 75:25, 50:50, 25:75 and 0:100) and forming polymersomes via film rehydration to produce vesicles. Transmission electron microscopy images stained with phosphotungstic acid (PTA) were taken; PTA interacts strongly with PMPC but not PEO, therefore allowing composition specific staining. Images show the formation of domains in the blended compositions, with the lesser fraction generating these domains. In addition, polymersomes from each sample were extruded through polycarbonate membranes to produce vesicles of three difference average diameters, 100nm, 200nm and 400nm. The uptake studies showed that for the single copolymer compositions, total uptake was reduced with increasing vesicle diameter and

PMPC-based polymersomes showed greater uptake overall than PEO-based ones for 100nm and 200nm samples, whilst uptake was comparable for the 400nm samples. For the blended samples, vesicle diameter appears less dominating on controlling the uptake. The authors present the hypothesis that the uptake is more regulated by the presence and the size of domains upon the vesicle surface. This relates to theoretical calculations that the optimum diameter for initiating endocytosis is approximately 50-60 nm.[10]

In conclusion, current theory describes how the increase in osmotic pressure disrupts the early endosome, causing pores to form and the contents are therefore released into the cell cytosol.[62] Any drugs originally entrapped within the polymersomes are also released into the intracellular space, enabling the therapeutic effect of the drugs to occur. The intracellular transport process thereby results in PMPC-PDPA polymersomes having a highly efficient, non-cytotoxic release mechanism for delivering compounds.[61] Cellular uptake and the rapidity of internalisation can also be affected by the composition of copolymer blends, polymersome domains and vesicle size. The ability to tailor these systems for intracellular drug delivery has therefore been an extensive area of research for the PMPC-PDPA system over the past decade.

1.2.8 Evaluation of PMPC-PDPA as a drug delivery system for diagnostic, research and medicinal purposes

One of the most exciting and challenging applications realised for polymeric vesicles is the delivery of compounds across external cellular barriers to the intracellular space of the cell for diagnostic, research and medicinal reasons. This field of intracellular delivery for both drugs and genetic materials through the use of polymersomes has been a major focus of research by the Battaglia group over the past 10 years.

Previous studies into the transportation of genetic material have investigated the use of polymers to transport DNA. However, these methods typically show low levels of transfection due to a combination of toxicity and lack of a release mechanism. Liposomal delivery of DNA is currently seen as the gold standard of synthetic delivery systems, despite relatively low yields of transfection, typically <50%.[135] Calcium-phosphate complexes can also be used due to the electrostatic interactions with DNA, however the precipitates that

form can only be used within a very narrow range of physio-chemical conditions.[136]

In 2007, Battaglia and Lomas published a paper illustrating the successful encapsulation and delivery of a DNA plasmid to living cells.[62] Using non-fouling hydrophilic polymers PEO and PMPC and pH-responsive PDPA, polymersomes were demonstrated to encapsulate and deliver fluorescent DNA without causing cellular toxicity. The reversible protonation of the tertiary amine groups present on the PDPA chains creates a hydrophilic molecularly dissolved polymer under mildly acidic (pH 5-6) conditions and a hydrophobic, charge neutral polymer under neutral pH conditions. As previously stated, when chemically bonded to a hydrophilic polymer this process of changing the solution pH from acidic to neutral generates the formation of polymersomes.

Lomas et al. used the pH-switch method to produce polymersomes in the presence of plasmid DNA, which is strongly negatively charged throughout the pH range used for the formation method.[62] At pH 6, the copolymer exists as dissolved monomers with a net positive charge and the negatively charged DNA plasmids were therefore electrostatically attracted to the copolymer. Once PMPC-PDPA and the plasmid DNA were mixed, the pH was raised to 7.4 and polymersomes were formed. During the process, the DNA was unbound from the PDPA due to the change in charge of the PDPA block. Quantification of the DNA plasmid was conducted by measuring the absorbance of samples before and after purification by gel permeation chromatography (GPC) which showed that approximately 20% of the original plasmid was trapped within the polymersomes. Retention of 20% of the total DNA demonstrated highly efficient encapsulation, and the rationale was that electrostatic interactions just prior to formation result in high concentrations of DNA in the immediate vicinity of the polymer, which are subsequently entrapped by the formation of polymer vesicles. Transmission electron microscopy images were taken of samples at pH 6 and pH 7.4 to show the morphology of structures produced. Micrographs showed the condensation of polymer to DNA at pH 6 and larger macromolecular assemblies of polymersomes at pH 7.4.[62]

Images of the DNA/copolymer interactions were also reported by Stolnik *et al.*, in similar experiments with the copolymer 2-(dimethylamino)ethyl methacrylate-block-2-(methacryloyloxyethyl phosphorylcholine).[137] The DNA-

loaded polymersomes were exposed to Chinese Hamster Ovary (CHO) and Human Dermal Fibroblast (HDF) cells for uptake efficiency and toxicity testing. When compared with commercially available liposome delivery system Lipofectamine® TD131 and calcium phosphate-complex delivery methods, the polymersome samples showed higher delivery efficiency and no cytotoxicity.

The cytotoxicity, uptake and disassembly of PMPC-PDPA polymersomes were also investigated by Lomas et al. through the production of micrometre-sized fluorescently-tagged polymersomes with the electroformation technique.[61] The pH was then reduced to below the copolymer pKa and the giant polymersomes were observed to disassemble. Time lapse images showed the formation of a pore that grew in size until the polymersome collapsed fully. In addition, the paper investigated the cytotoxicity of nanoscopic PMPC-PDPA by analysing the response of HDF cells to PMPC-PDPA polymersomes through transcription factor NF-κB. Activation of NF-κB triggers an inflammatory response, which has been shown to occur by exposure to endotoxins, viruses, UV irradiation and auto-immune activation.[138] When inactive, NF-κB resides in the cell cytoplasm. Upon activation, the molecules transpose to the nucleus of the cells where it binds to DNA and activates the transcription of inflammatory proteins. By using cells with a fluorescently tagged NF-κB molecule, the location can be tracked within the cell after exposure to external stimuli. PMPC-PDPA polymersomes showed very low levels of NF-κB translocation, that were comparable to the negative control, indicating a lack of inflammatory response by HDFs to treatment by these polymersomes.[61]

These promising results for intracellular delivery using PMPC-PDPA polymersomes led to studies on the uptake kinetics of the polymersomes, which would relate strongly to the dose-response of any therapeutic or diagnostic molecules[132]. The fluorophore rhodamine was encapsulated within PMPC-PDPA and PEO-PBO polymersomes, and then the uptake by HDF cells was measured using flow cytometry to give the percentage of cells containing rhodamine. PMPC-PDPA uptake was seen in cells as fast as 1 minute after exposure, with 95% of cells showing uptake after 1 hour of exposure. In contrast, PEO-PBO polymersomes took 5 hours exposure before any uptake was detected and after 24 hours, a transfection rate of 80% by the HDF cells

was reported. This indicates a stronger interaction between PMPC and the cell surface than for PEO.

These studies were taken further by Blanazs *et al.*, where an understanding of the uptake mechanism and the relationships between polymersome size and surface chemistry were investigated further [132]. HDF cells were again treated with rhodamine labelled, pH-responsive PMPC-PDPA polymersomes and non-pH responsive PEO-PBO. In addition, cells were treated with LysoTracker®, a commercially available fluorescent lysosome marker. High resolution confocal images showed fluorophore propidium iodide present throughout the cell cytoplasm in the PMPC-PDPA samples, whilst the PEO-PBO polymersomes were restricted to the endosomes as indicated by co localisation of the two fluorophores. These results indicated that the main internalisation mechanism for the polymersomes was an active cellular process known as endocytosis. To confirm this observation, delivery was attempted in the presence of compounds known to block endocytosis. Chloroquine and Nocodazole block membrane functions as does cooling the cells to 4°C. Subsequent delivery by either PMPC-PDPA or PEO-PBO was significantly reduced under each of these conditions when compared to standard delivery at 37°C. Uptake of PMPC-PDPA polymersomes was also measured in 23 different cell types including cell lines, primary cells and stem cells. The only cells to show no uptake were erythrocytes, which do not undergo endocytosis.[132]

As well as delivery of plasmid DNA and other species through endocytosis, PMPC-PDPA polymersomes have also been used to deliver siRNA, as reported by Nisa Patikarnmonthon.[139] Canton *et al.* also showed the successful delivery of antibodies into living cells using PMPC-PDPA polymersomes.[69] The antibodies were intact and functional, and the study reported binding to specific epitopes within the cell and control over subcellular events. Several therapeutic compounds have also been delivered to date. Wayakanon *et al.* treated intracellular porphyromonas gingivalis infected epithelial cells by delivering antibiotics[140] and Colley *et al.* have explored the effectiveness of delivering various anticancer drugs, both independently and in combination, for treating head and neck cancer.[141–143] For diagnostic applications, PMPC-PDPA polymersomes have been used to deliver a range of fluorescent probes. These range from non-specific rhodamine dyes to the cell

cytoplasm,[60] to specific binding complexes such as DNA[144–146], the cytoskeleton,[147] and pH specific probes for mapping the internal pH values in living cells.[148]

A major area of interest for PMPC-PDPA polymersomes is in their use as an intracellular delivery vector. Due to this ability to deliver compounds whilst retaining the cellular viability, the Battaglia group and colleagues have successfully delivered many compounds for therapeutic or diagnostic applications. With so many promising applications of intracellular delivery emerging for PMPC-PDPA polymersomes; it is crucial to ensure consistency during production, with the future aims of scalability for any manufacturing process employed. This thesis therefore focuses on further characterising the encapsulation and purification of polymersomes, with the aim of optimising the formation process to maximise the yield of polymersomes. The next chapter describes experimental methods used, and Chapter 3 then investigates the effect of temperature on the self-assembly of PMPC-PDPA polymersomes, with the aim to control nanoparticle size for biological drug delivery applications.

1.2.9 Aims and Objectives

The aim of this work is to evaluate and improve the formation of pH responsive PMPC-PDPA polymersomes for biomedical applications, primarily as a drug delivery system (DDS). This builds on a large body of previous work that shows PMPC-PDPA to be a biocompatible DDS, capable of delivering a range of molecules to living cells in a functional and unperturbed state: [60,62,69,130,140,141,147,148]

1. Investigate the effects of sample temperature on polymersome formation. Characterisation was performed using dynamic light scattering, potentiometry and transmission electron microscopy.
2. Assess whether an increase in sample temperature can be used to drive the formation of polymersomes at a constant starting pH. Formation was measured using a spectrophotometer to conduct turbidometry at temperature intervals and transmission electron microscopy was conducted to evaluate particle morphology.
3. Evaluate the formation of genus particles at low temperatures. A literature review was also conducted in order to understand the formation of genus structures. Formation validation was attempted via the addition of dissolved copolymer to preformed polymersomes at 1°C.
4. Investigate an automated size exclusion chromatography (SEC) method for purifying polymersome samples to remove unwanted micelles. The automated set-up was compared to a manual SEC column that is typically used. Absorbance measurements were then conducted to assess the separation distribution. Dynamic light scattering and transmission electron microscopy were also used to evaluate the discrete fractions of polymersome samples.
5. Expand upon a previously used model to predict the number of polymersomes in a sample and the theoretical encapsulation efficiency. This was achieved through the addition of sample-specific distribution data as obtained by dynamic light scattering to calculate the total internal polymersome volume and estimate the optimal hydrophilic loading. The optimal loading value can then be compared to the actual value as a point of reference to measure the efficiency of the system.

1.3.0 References

1. Torchilin, V. P. PEG-based micelles as carriers of contrast agents for different imaging modalities. *Adv. Drug Deliv. Rev.* **54,** 235–252 (2002).
2. Cecchelli, R. *et al.* In vitro model for evaluating drug transport across the blood–brain barrier. *Adv. Drug Deliv. Rev.* **36,** 165–178 (1999).
3. Baeshen, N. A. *et al.* Cell factories for insulin production. *Microb. Cell Factories* **13,** 141 (2014).
4. Published | Guidance | NICE. www.nice.org.uk/guidance/published. Accessed May 2015.
5. Jones, R. A. L. *Soft Condensed Matter*. (2002).
6. Callister, W. . and R., D. .. *Materials Science and Engineering*. (John Wiley & Sons, 2010).
7. Alberts, B. J., A. Lewis, J. Raff, M. Roberts, K. Walter, P. *Molecular Biology of the Cell*. (2007).
8. Prabha, S., Zhou, W. Z., Panyam, J. & Labhasetwar, V. Size-dependency of nanoparticle-mediated gene transfection: studies with fractionated nanoparticles. *Int. J. Pharm.* **244,** 105–115 (2002).
9. Desai, M. P., Labhasetwar, V., Walter, E., Levy, R. J. & Amidon, G. L. The mechanism of uptake of biodegradable microparticles in Caco-2 cells is size dependent. *Pharm. Res.* **14,** 1568–1573 (1997).
10. Zhang, S. L., Li, J., Lykotrafitis, G., Bao, G. & Suresh, S. Size-Dependent Endocytosis of Nanoparticles. *Adv. Mater.* **21,** 419–+ (2009).
11. Gao, H., Shi, W. & Freund, L. B. Mechanics of receptor-mediated endocytosis. *Proc. Natl. Acad. Sci. U. S. A.* **102,** 9469–74 (2005).
12. Chithrani, B. D., Ghazani, A. A. & Chan, W. C. W. Determining the size and shape dependence of gold nanoparticle uptake into mammalian cells. *Nano Lett.* **6,** 662–668 (2006).
13. Chithrani, B. D. & Chan, W. C. W. Elucidating the mechanism of cellular uptake and removal of protein-coated gold nanoparticles of different sizes and shapes. *Nano Lett.* **7,** 1542–1550 (2007).
14. Yuan, H. & Zhang, S. Effects of particle size and ligand density on the kinetics of receptor-mediated endocytosis of nanoparticles. *Appl. Phys. Lett.* **96,** 033704 (2010).
15. Jiang, W., Kim, B. Y. S., Rutka, J. T. & Chan, W. C. W. Nanoparticle-mediated cellular response is size-dependent. *Nat. Nanotechnol.* **3,** 145–150 (2008).
16. Decuzzi, P. & Ferrari, M. The receptor-mediated endocytosis of nonspherical particles. *Biophys. J.* **94,** 3790–3797 (2008).
17. Champion, J. A. & Mitragotri, S. Shape Induced Inhibition of Phagocytosis of Polymer Particles. *Pharm. Res.* **26,** 244–249 (2009).
18. Geng, Y. *et al.* Shape effects of filaments versus spherical particles in flow and drug delivery. *Nat. Nanotechnol.* **2,** 249–255 (2007).
19. Bangham, A. D. Liposomes - the Babraham Connection. *Chem. Phys. Lipids* **64,** 275–285 (1993).
20. Waninge, R., Nylander, T., Paulsson, M. & Bergenstahl, B. Milk membrane lipid vesicle structures studied with Cryo-TEM. *Colloids Surf. B-Biointerfaces* **31,** 257–264 (2003).
21. Le Roy, C. & Wrana, J. L. Clathrin- and non-clathrin-mediated endocytic regulation of cell signalling. *Nat. Rev. Mol. Cell Biol.* **6,** 112–126 (2005).

22. Kunitake, T., Okahata, Y., Shimomura, M., Yasunami, S. I. & Takarabe, K. Formation of Stable Bilayer Assemblies in Water from Single-Chain Amphiphiles - Relationship between the Amphiphile Structure and the Aggregate Morphology. *J. Am. Chem. Soc.* **103,** 5401–5413 (1981).
23. Gabizon, A. *et al.* Long-circulating liposomes for drug delivery in cancer therapy: A review of biodistribution studies in tumor-bearing animals. *Adv. Drug Deliv. Rev.* **24,** 337–344 (1997).
24. Patil, S. D., Rhodes, D. G. & Burgess, D. J. DNA-based therapeutics and DNA delivery systems: A comprehensive review. *Aaps J.* **7,** E61–E77 (2005).
25. Magin, R. L., Wright, S. M., Niesman, M. R., Chan, H. C. & Swartz, H. M. Liposome Delivery of NMR Contrast Agents for Improved Tissue Imaging. *Magn. Reson. Med.* **3,** 440–447 (1986).
26. Yan, X. D., Scherphof, G. L. & Kamps, J. A. A. M. Liposome opsonization. *J. Liposome Res.* **15,** 109–139 (2005).
27. Moghimi, S. M. & Szebeni, J. Stealth liposomes and long circulating nanoparticles: critical issues in pharmacokinetics, opsonization and protein-binding properties. *Prog. Lipid Res.* **42,** 463–478 (2003).
28. Needham, D. H., K. McIntosh, T.J. Dewhirst, M. Wu, N. Lasic, D.D. Polymer-Grafted Liposomes: Physical Basis for the 'Stealth' Property. *J. Liposome Res.* **2,** 411–430 (1992).
29. Harris, J. M. & Chess, R. B. Effect of pegylation on pharmaceuticals. *Nat. Rev. Drug Discov.* **2,** 214–221 (2003).
30. Goebel, F. D., Goldstein, D., Goos, M., Jablonowski, H. & Stewart, J. S. Efficacy and safety of stealth liposomal doxorubicin in AIDS-related Kaposi's sarcoma. *Br. J. Cancer* **73,** 989–994 (1996).
31. Lasic, D. D. Doxorubicin in sterically stabilized liposomes (vol 380, pg 562, 1996). *Nature* **381,** 630–630 (1996).
32. Stals, P. J. *et al.* How far can we push polymer architectures? *J. Am. Chem. Soc.* **135,** 11421–4 (2013).
33. Kataoka, K., Harada, A. & Nagasaki, Y. Block copolymer micelles for drug delivery: Design, characterization and biological significance. *Adv. Drug Deliv. Rev.* **64,** 37–48 (2012).
34. Jenkins, A. D., Kratochvíl, P., Stepto, R. F. T. & Suter, U. W. Glossary of basic terms in polymer science (IUPAC Recommendations 1996). *Pure Appl. Chem.* **68,** (1996).
35. GoldBook, I. IUPAC Compendium of Chemical Terminology Gold Book v2.3.3. at <http://goldbook.iupac.org/PDF/goldbook.pdf>
36. Odian, G. *Principles of Polymerization*. (2004).
37. Sawamoto, M. & Higashimura, T. Principles and Design of Living Cationic Polymerization of Vinyl Monomers - the Nature of the Growing Species Based on In situ H-1-NMR Analysis. *Makromol. Chem.-Macromol. Symp.* **67,** 299–309 (1993).
38. Ahmad, N. M. *et al.* Chain Transfer to Polymer and Branching in Controlled Radical Polymerizations of n-Butyl Acrylate. *Macromol. Rapid Commun.* **30,** 2002–21 (2009).
39. Matyjaszewski, K., Gnanou, Y., Leibler, L. *Macromolecular Engineering: Precise Synthesis, Materials Properties, Applications*. (2007).
40. Szwarc, M., Levy, M. & Milkovich, R. Polymerization Initiated by Electron Transfer to Monomer - a New Method of Formation of Block Polymers. *J. Am. Chem. Soc.* **78,** 2656–2657 (1956).

41. Siegwart, D. J., Oh, J. K. & Matyjaszewski, K. ATRP in the design of functional materials for biomedical applications. *Prog. Polym. Sci.* **37,** 18–37 (2012).
42. Wang, J. S. & Matyjaszewski, K. Transition-Metal-Catalyzed Atom-Transfer Radical Polymerization (Atrp) - Principle and Mechanism. *Abstr. Pap. Am. Chem. Soc.* **210,** 226–PMSE (1995).
43. Chiefari, J. *et al.* Living free-radical polymerization by reversible addition-fragmentation chain transfer: The RAFT process. *Macromolecules* **31,** 5559–5562 (1998).
44. Discher, D. E. & Ahmed, F. Polymersomes. *Annu. Rev. Biomed. Eng.* **8,** 323–341 (2006).
45. Discher, B. M. *et al.* Polymersomes: Tough vesicles made from diblock copolymers. *Science* **284,** 1143–1146 (1999).
46. Battaglia, G. & Ryan, A. J. Bilayers and interdigitation in block copolymer vesicles. *J. Am. Chem. Soc.* **127,** 8757–8764 (2005).
47. Bermudez, H., Brannan, A. K., Hammer, D. A., Bates, F. S. & Discher, D. E. Molecular weight dependence of polymersome membrane structure, elasticity, and stability. *Macromolecules* **35,** 8203–8208 (2002).
48. Battaglia, G., Ryan, A. J. & Tomas, S. Polymeric vesicle permeability: A facile chemical assay. *Langmuir* **22,** 4910–4913 (2006).
49. Ghoroghchian, P. P. *et al.* Near-infrared-emissive polymersomes: Self-assembled soft matter for in vivo optical imaging. *Proc. Natl. Acad. Sci. U. S. A.* **102,** 2922–2927 (2005).
50. Zhang, Y. *et al.* Improving the visualization of fluorescently tagged nanoparticles and fluorophore-labeled molecular probes by treatment with CuSO4 to quench autofluorescence in the rat inner ear. *Hear. Res.* **269,** 1–11 (2010).
51. Katz, J. S. *et al.* Modular Synthesis of Biodegradable Diblock Copolymers for Designing Functional Polymersomes. *J. Am. Chem. Soc.* **132,** 3654–+ (2010).
52. Madsen, J., Warren, N. J., Armes, S. P. & Lewis, A. L. Synthesis of Rhodamine 6G-Based Compounds for the ATRP Synthesis of Fluorescently Labeled Biocompatible Polymers. *Biomacromolecules* **12,** 2225–2234 (2011).
53. Christian, N. A. *et al.* Tat-functionalized near-infrared emissive polymersomes for dendritic cell labeling. *Bioconjug. Chem.* **18,** 31–40 (2007).
54. Hammer, D. A. *et al.* Leuko-polymersomes. *Faraday Discuss.* **139,** 129–141 (2008).
55. Licciardi, M., Tang, Y., Billingham, N. C. & Armes, S. P. Synthesis of novel folic acid-functionalized biocompatible block copolymers by atom transfer radical polymerization for gene delivery and encapsulation of hydrophobic drugs. *Biomacromolecules* **6,** 1085–1096 (2005).
56. Battaglia, G. *et al.* Wet Nanoscale Imaging and Testing of Polymersomes. *Small* **7,** 2010–2015 (2011).
57. Discher, B. M. *et al.* Cross-linked polymersome membranes: Vesicles with broadly adjustable properties. *J. Phys. Chem. B* **106,** 2848–2854 (2002).
58. Gaitzsch, J., Appelhans, D., Grafe, D., Schwille, P. & Voit, B. Photo-crosslinked and pH sensitive polymersomes for triggering the loading and release of cargo. *Chem. Commun.* **47,** 3466–3468 (2011).

59. Rosselgong, J. *et al.* Thiol-Functionalized Block Copolymer Vesicles. *Acs Macro Lett.* **1,** 1041–1045 (2012).
60. Massignani, M. *et al.* Enhanced Fluorescence Imaging of Live Cells by Effective Cytosolic Delivery of Probes. *Plos One* **5,** (2010).
61. Lomas, H. *et al.* Non-cytotoxic polymer vesicles for rapid and efficient intracellular delivery. *Faraday Discuss.* **139,** 143–159 (2008).
62. Lomas, H. *et al.* Biomimetic pH sensitive polymersomes for efficient DNA encapsulation and delivery. *Adv. Mater.* **19,** 4238–4243 (2007).
63. Kim, Y. *et al.* Polymersome delivery of siRNA and antisense oligonucleotides (vol 134, pg 132, 2009). *J. Controlled Release* **137,** 256–256 (2009).
64. Korobko, A. V., Backendorf, C. & van der Maarel, J. R. C. Plasmid DNA encapsulation within cationic diblock copolymer vesicles for gene delivery. *J. Phys. Chem. B* **110,** 14550–14556 (2006).
65. Korobko, A. V., Jesse, W. & van der Maarel, J. R. C. Encapsulation of DNA by cationic diblock copolymer vesicles. *Langmuir* **21,** 34–42 (2005).
66. Meier, W., Nardin, C. & Winterhalter, M. Reconstitution of channel proteins in (polymerized) ABA triblock copolymer membranes. *Angew. Chem.-Int. Ed.* **39,** 4599 (2000).
67. Wittemann, A., Azzam, T. & Eisenberg, A. Biocompatible polymer vesicles from biamphiphilic triblock copolymers and their interaction with bovine serum albumin. *Langmuir* **23,** 2224–2230 (2007).
68. Napoli, A. *et al.* Glucose-oxidase based self-destructing polymeric vesicles. *Langmuir* **20,** 3487–3491 (2004).
69. Canton, I. *et al.* Fully synthetic polymer vesicles for intracellular delivery of antibodies in live cells. *Faseb J.* **27,** 98–108 (2013).
70. Arifin, D. R. & Palmer, A. F. Polymersome encapsulated hemoglobin: a novel type of oxygen carrier. *Biomacromolecules* **6,** 2172–81 (2005).
71. Kishimura, A., Koide, A., Osada, K., Yamasaki, Y. & Kataoka, K. Encapsulation of myoglobin in PEGylated polyion complex vesicles made from a pair of oppositely charged block lonomers: A physiologically available oxygen carrier. *Angew. Chem.-Int. Ed.* **46,** 6085–6088 (2007).
72. Choucair, A., Soo, P. L. & Eisenberg, A. Active loading and tunable release of doxorubicin from block copolymer vesicles. *Langmuir* **21,** 9308–9313 (2005).
73. Ahmed, F. *et al.* Biodegradable polymersomes loaded with both paclitaxel and doxorubicin permeate and shrink tumors, inducing apoptosis in proportion to accumulated drug. *J. Controlled Release* **116,** 150–158 (2006).
74. Li, S. L., Byrne, B., Welsh, J. & Palmer, A. F. Self-assembled poly(butadiene)-b-poly(ethylene oxide) polymersomes as paclitaxel carriers. *Biotechnol. Prog.* **23,** 278–285 (2007).
75. Wong, D., Jeon, T. J. & Schmidt, J. Single molecule measurements of channel proteins incorporated into biomimetic polymer membranes. *Nanotechnology* **17,** 3710–3717 (2006).
76. Gaitzsch, J., Appelhans, D., Wang, L. G., Battaglia, G. & Voit, B. Synthetic Bio-nanoreactor: Mechanical and Chemical Control of Polymersome Membrane Permeability. *Angew. Chem.-Int. Ed.* **51,** 4448–4451 (2012).
77. Nardin, C., Thoeni, S., Widmer, J., Winterhalter, M. & Meier, W. Nanoreactors based on (polymerized) ABA-triblock copolymer vesicles. *Chem. Commun.* 1433–1434 (2000). doi:10.1039/B004280n

78. Vriezema, D. M. *et al.* Positional assembly of enzymes in polymersome nanoreactors for cascade reactions. *Angew. Chem .Int .Ed.* **46,** 7378 (2007).
79. Cowie, J.M.G. *Polymers: Chemistry and Physics of Modern Materials*. (1991).
80. Smith, J. D. *et al.* Unified description of temperature-dependent hydrogen-bond rearrangements in liquid water. *Proc. Natl. Acad. Sci. U. S. A.* **102,** 14171–14174 (2005).
81. Southall, N. T., Dill, K. A. & Haymet, A. D. J. A view of the hydrophobic effect. *J. Phys. Chem. B* **106,** 521–533 (2002).
82. Israelachvili, J. N., Mitchell, D. J. & Ninham, B. W. Theory of Self-Assembly of Lipid Bilayers and Vesicles. *Biochim. Biophys. Acta* **470,** 185–201 (1977).
83. Ide, M., Maeda, Y. & Kitano, H. Effect of hydrophobicity of amino acids on the structure of water. *J. Phys. Chem. B* **101,** 7022–7026 (1997).
84. Atkins, P. D. P., J. *Atkins' Physical Chemistry*. (Oxford).
85. Tanford, C. Hydrophobic Effect and Organization of Living Matter. *Science* **200,** 1012–1018 (1978).
86. Flory, P. J. Thermodynamics of High Polymer Solutions. *J. Chem. Phys.* **10,** 51–61 (1942).
87. Huggins, M. L. Solutions of Long Chain Compounds. *J. Chem. Phys.* **9,** 440–440 (1941).
88. Israelachvili, J. N., Mitchell, D. J. & Ninham, B. W. Theory of Self-Assembly of Hydrocarbon Amphiphiles into Micelles and Bilayers. *J. Chem. Soc.-Faraday Trans.* **72,** 1525–1568 (1976).
89. Leibler, L., Orland, H. & Wheeler, J. C. Theory of Critical Micelle Concentration for Solutions of Block Co-Polymers. *J. Chem. Phys.* **79,** 3550–3557 (1983).
90. Wilhelm, M. *et al.* Polymer Micelle Formation .3. Poly(Styrene-Ethylene Oxide) Block Copolymer Micelle Formation in Water - a Fluorescence Probe Study. *Macromolecules* **24,** 1033–1040 (1991).
91. Battaglia, G. & Ryan, A. J. The evolution of vesicles from bulk lamellar gels. *Nat. Mater.* **4,** 869–876 (2005).
92. Israelachvili, J. N. & Mitchell, D. J. Model for Packing of Lipids in Bilayer Membranes. *Biochim. Biophys. Acta* **389,** 13–19 (1975).
93. Israelachvili, J. N., Marcelja, S. & Horn, R. G. Physical Principles of Membrane Organization. *Q. Rev. Biophys.* **13,** 121–200 (1980).
94. Israelachvili, J. & Wennerstrom, H. Role of hydration and water structure in biological and colloidal interactions. *Nature* **379,** 219–25 (1996).
95. Schreier, S., Malheiros, S. V. P. & de Paula, E. Surface active drugs: self-association and interaction with membranes and surfactants. Physicochemical and biological aspects. *Biochim. Biophys. Acta BBA - Biomembr.* **1508,** 210–234 (2000).
96. Jain, N. *et al.* Critical Aggregation Concentration in Mixed Solutions of Anionic Polyelectrolytes and Cationic Surfactants. *Langmuir* **20,** 8496–8503 (2004).
97. Battaglia, G. & Ryan, A. J. Effect of amphiphile size on the transformation from a lyotropic gel to a vesicular dispersion. *Macromolecules* **39,** 798–805 (2006).
98. Battaglia, G. & Ryan, A. J. Pathways of polymeric vesicle formation. *J. Phys. Chem. B* **110,** 10272–10279 (2006).

99. Hamley, I. W., Mai, S. M., Ryan, A. J., Fairclough, J. P. A. & Booth, C. Aqueous mesophases of block copolymers of ethylene oxide and 1,2-butylene oxide. *Phys. Chem. Chem. Phys.* **3,** 2972–2980 (2001).
100. Pople, J. A. *et al.* Ordered phases in aqueous solutions of diblock oxyethylene/oxybutylene copolymers investigated by simultaneous small-angle X-ray scattering and rheology. *Macromolecules* **30,** 5721–5728 (1997).
101. Wanka, G., Hoffmann, H. & Ulbricht, W. Phase-Diagrams and Aggregation Behavior of Poly(Oxyethylene)-Poly(Oxypropylene)-Poly(Oxyethylene) Triblock Copolymers in Aqueous-Solutions. *Macromolecules* **27,** 4145–4159 (1994).
102. Jain, S. & Bates, F. S. On the origins of morphological complexity in block copolymer surfactants. *Science* **300,** 460–464 (2003).
103. Battaglia, G. & Ryan, A. J. Neuron-like tubular membranes made of diblock copolymer amphiphiles. *Angew. Chem.-Int. Ed.* **45,** 2052 (2006).
104. Agut, W., Brulet, A., Schatz, C., Taton, D. & Lecommandoux, S. pH and Temperature Responsive Polymeric Micelles and Polymersomes by Self-Assembly of Poly[2-(dimethylamino)ethyl methacrylate]-b-Poly(glutamic acid) Double Hydrophilic Block Copolymers. *Langmuir* **26,** 10546 (2010).
105. Du, J. Z., Tang, Y. P., Lewis, A. L. & Armes, S. P. pH-sensitive vesicles based on a biocompatible zwitterionic diblock copolymer. *J. Am. Chem. Soc.* **127,** 17982–17983 (2005).
106. Fernyhough, C., Ryan, A. J. & Battaglia, G. pH controlled assembly of a polybutadiene-poly(methacrylic acid) copolymer in water: packing considerations and kinetic limitations. *Soft Matter* **5,** 1674–1682 (2009).
107. Jain, S. & Bates, F. S. Consequences of nonergodicity in aqueous binary PEO-PB micellar dispersions. *Macromolecules* **37,** 1511–1523 (2004).
108. Marsden, H. R., Gabrielli, L. & Kros, A. Rapid preparation of polymersomes by a water addition/solvent evaporation method. *Polym. Chem.* **1,** 1512–1518 (2010).
109. Qin, S. H., Geng, Y., Discher, D. E. & Yang, S. Temperature-controlled assembly and release from polymer vesicles of poly(ethylene oxide)-block-poly(N-isopropylacrylamide). *Adv. Mater.* **18,** 2905 (2006).
110. Sanson, C., Le Meins, J. F., Schatz, C., Soum, A. & Lecommandoux, S. Temperature responsive poly(trimethylene carbonate)-block-poly(L-glutamic acid) copolymer: polymersomes fusion and fission. *Soft Matter* **6,** 1722–1730 (2010).
111. Shen, H. W. & Eisenberg, A. Block length dependence of morphological phase diagrams of the ternary system of PS-b-PAA/dioxane/H2O. *Macromolecules* **33,** 2561–2572 (2000).
112. Shen, L., Du, J. Z., Armes, S. P. & Liu, S. Y. Kinetics of pH-induced formation and dissociation of polymeric vesicles assembled from a water-soluble zwitterionic diblock copolymer. *Langmuir* **24,** 10019–10025 (2008).
113. Yildiz, M. E., Prud'homme, R. K., Robb, I. & Adamson, D. H. Formation and characterization of polymersomes made by a solvent injection method. *Polym. Adv. Technol.* **18,** 427–432 (2007).
114. Chen, L., Shen, H. W. & Eisenberg, A. Kinetics and mechanism of the rod-to-vesicle transition of block copolymer aggregates in dilute solution. *J. Phys. Chem. B* **103,** 9488–9497 (1999).

115. Geng, Y., Ahmed, F., Bhasin, N. & Discher, D. E. Visualizing worm micelle dynamics and phase transitions of a charged diblock copolymer in water. *J. Phys. Chem. B* **109,** 3772–3779 (2005).
116. Shen, H. W. & Eisenberg, A. Morphological phase diagram for a ternary system of block copolymer PS310-b-PAA(52)/dioxane/H2O. *J. Phys. Chem. B* **103,** 9473–9487 (1999).
117. Blanazs, A., Madsen, J., Battaglia, G., Ryan, A. J. & Armes, S. P. Mechanistic insights for block copolymer morphologies: how do worms form vesicles? *J Am Chem Soc* **133,** 16581–7 (2011).
118. Creutz, S., van Stam, J., De Schryver, F. C. & Jerome, R. Dynamics of poly((dimethylamino)alkyl methacrylate-block-sodium methacrylate) micelles. Influence of hydrophobicity and molecular architecture on the exchange rate of copolymer molecules. *Macromolecules* **31,** 681 (1998).
119. Creutz, S., vanStam, J., Antoun, S., DeSchryver, F. C. & Jerome, R. Exchange of polymer molecules between block copolymer micelles studied by emission spectroscopy. A method for the quantification of unimer exchange rates. *Macromolecules* **30,** 4078–4083 (1997).
120. Won, Y. Y., Davis, H. T. & Bates, F. S. Molecular exchange in PEO-PB micelles in water. *Macromolecules* **36,** 953–955 (2003).
121. Anglin, T. C. & Conboy, J. C. Kinetics and Thermodynamics of Flip-Flop in Binary Phospholipid Membranes Measured by Sum-Frequency Vibrational Spectroscopy. *Biochemistry (Mosc.)* **48,** 10220–10234 (2009).
122. Wang, C., Javadi, A., Ghaffari, M. & Gong, S. A pH-sensitive molecularly imprinted nanospheres/hydrogel composite as a coating for implantable biosensors. *Biomaterials* **31,** 4944–51 (2010).
123. Lewis, A., Tang, Y., Brocchini, S., Choi, J. W. & Godwin, A. Poly(2-methacryloyloxyethyl phosphorylcholine) for protein conjugation. *Bioconjug. Chem.* **19,** 2144–55 (2008).
124. Tateishi, T., Kyomoto, M., Kakinoki, S., Yamaoka, T. & Ishihara, K. Reduced platelets and bacteria adhesion on poly(ether ether ketone) by photoinduced and self-initiated graft polymerization of 2-methacryloyloxyethyl phosphorylcholine. *J. Biomed. Mater. Res. A* (2013). doi:10.1002/jbm.a.34809
125. Seo, J. H., Matsuno, R., Takai, M. & Ishihara, K. Cell adhesion on phase-separated surface of block copolymer composed of poly(2-methacryloyloxyethyl phosphorylcholine) and poly(dimethylsiloxane). *Biomaterials* **30,** 5330–40 (2009).
126. Yoneyama, T., Ishihara, K., Nakabayashi, N., Ito, M. & Mishima, Y. Short-term in vivo evaluation of small-diameter vascular prosthesis composed of segmented poly(etherurethane)/2-methacryloyloxyethyl phosphorylcholine polymer blend. *J. Biomed. Mater. Res.* **43,** 15–20 (1998).
127. Ishihara, K. *et al.* Why do phospholipid polymers reduce protein adsorption? *J. Biomed. Mater. Res.* **39,** 323–330 (1998).
128. Canton, I. & Battaglia, G. Endocytosis at the nanoscale. *Chem. Soc. Rev.* **41,** 2718–2739 (2012).
129. Lomas, H. *et al.* Efficient Encapsulation of Plasmid DNA in pH-Sensitive PMPC-PDPA Polymersomes: Study of the Effect of PDPA Block Length on Copolymer-DNA Binding Affinity. *Macromol. Biosci.* **10,** 513–530 (2010).
130. Giacomelli, C. *et al.* Phosphorylcholine-based pH-responsive diblock copolymer micelles as drug delivery vehicles: Light scattering, electron

microscopy, and fluorescence experiments. *Biomacromolecules* **7,** 817–828 (2006).
131. LoPresti, C. *et al.* Controlling Polymersome Surface Topology at the Nanoscale by Membrane Confined Polymer/Polymer Phase Separation. *Acs Nano* **5,** 1775–1784 (2011).
132. Blanazs, A., Armes, S. P. & Ryan, A. J. Self-Assembled Block Copolymer Aggregates: From Micelles to Vesicles and their Biological Applications. *Macromol Rapid Commun* **30,** 267–77 (2009).
133. Blanazs, A., Massignani, M., Battaglia, G., Armes, S. P. & Ryan, A. J. Synthesis of pH-responsive amphiphilic ABC block copolymers: The generation of asymmetric vesicle membranes and their cell uptake kinetics. *Abstr. Pap. Am. Chem. Soc.* **236,** 393–POLY (2008).
134. Felgner, P.L. *et al.* Lipofection - a Highly Efficient, Lipid-Mediated DNA-Transfection Procedure. *Proc. Natl. Acad. Sci. U.S.A.* **84,** 7413 (1987).
135. Jordan, M., Schallhorn, A. & Wurm, F. M. Transfecting mammalian cells: optimization of critical parameters affecting calcium-phosphate precipitate formation. *Nucleic Acids Res.* **24,** 596–601 (1996).
136. Lam, J. K. W. *et al.* Phosphorylcholine–polycation diblock copolymers as synthetic vectors for gene delivery. *J. Controlled Release* **100,** 293 (2004).
137. Schreck, R., Albermann, K. & Baeuerle, P. A. Nuclear Factor Kb: An Oxidative Stress-Responsive Transcription Factor of Eukaryotic Cells (A Review). *Free Radic. Res.* **17,** 221–237 (1992).
138. Patikarnmonthon, N. PMPC-PDPA polymersomes-mediated siRNA delivery. (2014). at http://etheses.whiterose.ac.uk/5476
139. Wayakanon, K. *et al.* Polymersome-mediated intracellular delivery of antibiotics to treat Porphyromonas gingivalis-infected oral epithelial cells. *FASEB J. Off. Publ. Fed. Am. Soc. Exp. Biol.* **27,** 4455–4465 (2013).
140. Colley, H. E. *et al.* Using polymersomes to deliver chemotherapeutic agents to oral cancer cells. *Oral Dis.* **16,** 527–527 (2010).
141. Murdoch, C. *et al.* Internalization and biodistribution of polymersomes into oral squamous cell carcinoma cells in vitro and in vivo. *Nanomed.* **5,** 1025–1036 (2010).
142. Colley, H. E. *et al.* Polymersome-Mediated Delivery of Combination Anticancer Therapy to Head and Neck Cancer Cells: 2D and 3D in Vitro Evaluation. *Mol. Pharm.* **11,** 1176–1188 (2014).
143. Gill, M. R. & Thomas, J. A. Ruthenium(II) polypyridyl complexes and DNA—from structural probes to cellular imaging and therapeutics. *Chem. Soc. Rev.* **41,** 3179–3192 (2012).
144. Gill, M. R. *et al.* A ruthenium(II) polypyridyl complex for direct imaging of DNA structure in living cells. *Nat. Chem.* **1,** 662–667 (2009).
145. Gill, M. R., Derrat, H., Smythe, C. G. W., Battaglia, G. & Thomas, J. A. Ruthenium(II) Metallo-intercalators: DNA Imaging and Cytotoxicity. *Chembiochem* **12,** 877–880 (2011).
146. Chierico, L., Joseph, A.S., Lewis, A.L. & Battaglia, G. Live cell imaging of membrane / cytoskeleton interactions. *Sci. Rep.* **4,** (2014).
147. Madsen, J. *et al.* Nile Blue-Based Nanosized pH Sensors for Simultaneous Far-Red and Near-Infrared Live Bioimaging. *J. Am. Chem. Soc.* **135,** 14863–14870 (2013).
148. Pearson, R. T., Avila-Olias, M., Joseph, A. S., Nyberg, S. & Battaglia, G. in *Ch 7* (2013). at http://pubs.rsc.org/en/content/chapter/bk9781849738774-00179/978-1-84973-877-4.

Chapter 2.1 – Materials and Methods

2.1.1 Experimental Materials

Unless otherwise stated, all materials were purchased from Sigma Aldrich (UK) at the highest purity grade and used without further purification. 4-Cyano-4-(2-phenylethane sulfanylthiocarbonyl)sulfanylpentanoic acid chain transfer agent (PETTC) was synthesised according to a previously reported method.[1] Deuterated methanol (CD3OD, 99.96 atom %) was purchased from Goss Scientific (UK). Solvents were obtained from Fisher Scientific (Loughborough, UK) and were used as received. Hydrochloric acid (HCl, 32%, general purpose grade) was purchased from Fisher Scientific (Loughborough, UK) and was used as received. 2-(Methacryloyloxy)ethyl phosphorylcholine monomer (MPC, 99.9% purity) was donated by Biocompatibles UK Ltd (Farnham, UK) and was used as received. 2-(Diisopropylamino)ethyl methacrylate was purchased from Scientific Polymer Products, Inc. (Ontario, USA) and passed through a basic alumina column to remove the inhibitor prior to use. Phosphate-buffered saline (PBS) was prepared from tablets obtained from Oxoid (Basingstoke, UK). Regenerated cellulose dialysis membrane (1,000 molecular weight cut-off) was purchased from Spectra/Por. Polymer synthesis was conducted by Dr Nick Warren in the Chemistry Department of the University of Sheffield.

2.1.2 Synthesis of PMPC Macro-Chain Transfer Agents

The monomer (2-methacryloyl-oxy) ethyl phosphorylcholine (MPC, 10.32 g, 34.92 mmol, target DP 25) and PETTC (0.474 g, 1.40 mmol) were dissolved in ethanol (9.0 mL). After purging with nitrogen for 20 minutes in an ice bath, 4,4'-Azobis(4-cyanovaleric acid) (ACVA) (V501) initiator (0.098 g, 0.35 mmol, 0.25 eq.) was added and the mixture was purged for a further 5 minutes. At this point the flask was immersed in an oil bath at 75 °C. After 1 h, the reduction in the vinyl proton signal in the 1H nuclear magnetic resonance (NMR) spectrum indicated 97 % monomer conversion. The reaction flask was removed from the oil bath, opened to the air and the reaction solution was diluted with ethanol. The PMPC macro-CTA was precipitated into tetrahydrofuran (THF) to remove any unreacted PETTC and subsequently dialysed against methanol for 24 h, changing the methanol every 2 h for the first 8 h. After solvent removal via rotary evaporation, a glassy yellow solid was obtained, which was placed in a

vacuum oven overnight at 50 °C to remove residual methanol. The final PMPC macro-CTA was characterised by both 1H NMR spectroscopy (CD3OD) and aqueous GPC using a series of near-monodisperse poly (ethylene oxide) calibration standards.

Final composition: $PMPC_{25}$ Mn = 9,800Da Mw/Mn = 1.19.

2.1.3 Alcoholic Solution Synthesis of PMPC-PDPA by RAFT Using a PMPC Macro-CTA

As a representative example, $PMPC_{25}$-$PDPA_{147}$ diblock copolymer was prepared by placing $PMPC_{25}$ macro-CTA (0.50 g, 0.068 mmol, 1 eq.) and DPA (2.02 g, 4.74 mmol, target DP for PDPA block = 140) into a 25 mL round-bottomed flask containing a magnetic stirrer bar. Dissolution in ethanol was achieved with the aid of sonication, followed by stirring and purging with nitrogen for 20 minutes in an ice bath. ACVA initiator was added (4.6 mg, 0.017 mmol, 0.25 eq.) and the mixture was purged for a further 5 minutes. At this point, the flask was immersed in an oil bath at 75 °C. After 18 h, 1H NMR indicated 95% DPA conversion. The reaction was removed from the oil bath, opened to the air and diluted with ethanol. Purification was achieved by dialysis against ethanol overnight followed by one week against water with twice-daily water changes. After freeze-drying from water overnight, the pure product was isolated as a light yellow powder. The final polymer was characterised by both 1H NMR spectroscopy in CD^3OD and GPC (3:1 chloroform/methanol eluent).

Final composition: $PMPC_{25}$-$PDPA_{147}$ Mn = 31,400Da; Mw/Mn = 1.27.

2.1.4 Polymersome Self-Assembly Using the pH Switch Method

Copolymer self-assembly was conducted by increasing the solution pH from mildly acidic to approximately neutral pH; this was achieved by the addition of base. Copolymer solutions in phosphate-buffered saline (100 mM PBS) were made up at a concentration of 5 mg/mL (0.05 wt. %) and adjusted to pH 5. This ensured that the copolymer chains were molecularly dissolved, generating a homogeneous initial solution. Equal volumes of copolymer solution and various aqueous NaOH solutions were mixed and stirred for 15 minutes prior to measuring the solution pH. This process was repeated until the concentration required to induce a pH jump from pH 5.0 to pH 7.5 was obtained for all four copolymers used in this study. For temperature-controlled pH adjustments, 500

µL of copolymer solution was immersed in a water bath set at the desired temperature and allowed to equilibrate for 15 minutes. In the same water bath, the required NaOH solution was also allowed to reach the same temperature. Then 500 µL of NaOH was added to the copolymer solution before stirring for 1 hour at constant temperature. Samples were then removed from the water bath and allowed to reach room temperature, prior to sonication and subsequent analysis by dynamic light scattering (DLS) and TEM.

2.1.5 Polymersome Self-Assembly from Film Hydration

Typically, 20 mg of freeze dried copolymer powder was added to a clean 30 ml glass vial. A total of 9 mL of solvent, comprising of a 2:1 v/v ratio of chloroform:methanol, was added to the copolymer powder, producing a transparent solution within 5 minutes of addition. The glass vial was then placed in a vacuum oven, where the solvent was driven off at 45°C and $1x10^{-3}$ bar for a minimum of 6 h. This process resulted in a thin layer of copolymer film coating the inside of the glass vial, the exposure to organic solvents also had the added effect of reducing biological contamination. After preparing the film, filtered PBS (100 mM) was added to the vial. The volume added was dependent on the final concentration required, typically a final copolymer concentration of between 1mg/mL and 5mg/mL was achieved. Therefore, between 20–4 mL of PBS was added. After the addition of PBS the sealed vial was left to stir under moderate agitation for between 2–6 weeks. Samples were tested throughout this period by DLS and TEM analysis to mark their progress towards polymersomes. Typically, lower concentration samples progressed to a usable standard faster than higher concentration ones.

2.1.6 Dynamic Light Scattering

Dynamic light scattering (DLS) studies were performed using a Zetasizer Nano ZS instrument (Malvern) at a copolymer concentration of 0.25 mg/mL. Measurements consisted of 12–14 sub-runs of ten seconds duration each; a total of three measurements were conducted for intensity-average particle size distributions. Samples were analysed at 25°C at a scattering angle of 173° using a 633 nm HeNe laser. DLS measurements are non-destructive and produce a scatter pattern upon the detector from the reflected laser light. Traditionally, light scattering measurements are conducted at 90° to the incident

laser light. This is to reduce the non-linear discrepancies experienced at most other angles. The changing scatter pattern is then examined over a range of timescales to produce a decaying correlation function. The correlation function is then modelled, often using CONTIN or NNLS (nearest neighbour least squared) methods, in order to estimate the mean particle diameter and population size dispersity. This process makes two assumptions; firstly, that all particles are undergoing movement by Brownian motion (the random walk motion due to bombardment from surrounding molecules, water, air etc). Secondly, it is assumed that all particles are spherical, and therefore, the diffusion coefficient values as measured can be converted into diameter using the Stokes-Einstein equation:

$$D = \frac{K_B T}{6\pi\eta a}$$

Where D equals the diffusion coefficient, K_B and T are the Boltzmann constant and T in kelvin respectively, η equals the sample viscosity and a is the hydrodynamic radius. The hydrodynamic radius includes a few layers of water bound to the particles' surface due to hydrophilic interactions and therefore is slightly larger than the actual radius of the particle. The Zetasizer nano ZS DLS has a detector angle of 173° that allows for backscattered measurements to be taken. The software corrects for the non-linear relationship with scattering intensity and diameter at this angle, whilst the back scattered measurements allow for the interaction volume to be adjusted. This allows for a much wider range of concentrations to be measured, allowing for more appropriate data collection by not having to greatly dilute samples.

2.1.7 Transmission Electron Microscopy

Phosphotungstic acid (PTA) powder was dissolved in boiling distilled water to produce a 0.75 wt. % solution. 5 M NaOH was added dropwise while stirring, until the solution pH reached pH 7.5. After allowing to cool, the staining solution was passed through a 0.20 µm sterile filter and kept at 3–4°C prior to use. A small volume (5 µL) of the copolymer solution was added to a freshly glow-discharged, carbon-coated copper/palladium square mesh grid (Agar Scientific) and allowed to adsorb for 1 minute. The grid was then blotted dry, before

immersing it in a droplet of PTA stain for 5 seconds; afterwards, the grid was blotted dry for a second time and any excess liquid was removed under vacuum. This resulted in positively-stained samples suspended on a thin carbon film. Imaging was conducted using a FEI Tecnai G2 Spirit electron microscope. Micrographs were recorded at 120 keV with a spot size of 3 and analysed using Gatan Digital Micrograph and Image J64 software (http://rsb.info.nih.gov/ij) packages.

2.1.8 Potentiometric Titration

Potentiometric titration involves taking a solution containing a pH-responsive material across a wide range of pH values. This is conducted either by starting under acidic conditions and adding base, or by starting at basic pH values and adding acid. Here, titrations were conducted by adding sodium hydroxide (NaOH) to acid solutions containing copolymer, the change in the solution pH was then measured as base was added. Titrations were conducted using a custom-built rig (shown below), consisting of a heated water bath, a magnetic stirrer, a syringe driver and pH meter. Firstly, 500 µL of copolymer solution at a concentration of 2.0 mg/mL was allowed to equilibrate at the required temperature for 30 minutes. Then 2.0 mL of 5×10^{-3} M NaOH was added to the copolymer solution at a flow rate of 0.17 mL/min, under constant sample agitation. Microprobe pH measurements were taken at 5 second intervals and exported to a computer automatically. When required, an external probe connected to the fluorimeter (Cary Eclipse, Agilent Technologies) was also added to the sample in order to conduct fluorescence measurements online. For these measurements, a minimum sample volume of 10 mL was required, the concentration of copolymer was kept at 2.0 mg/mL.

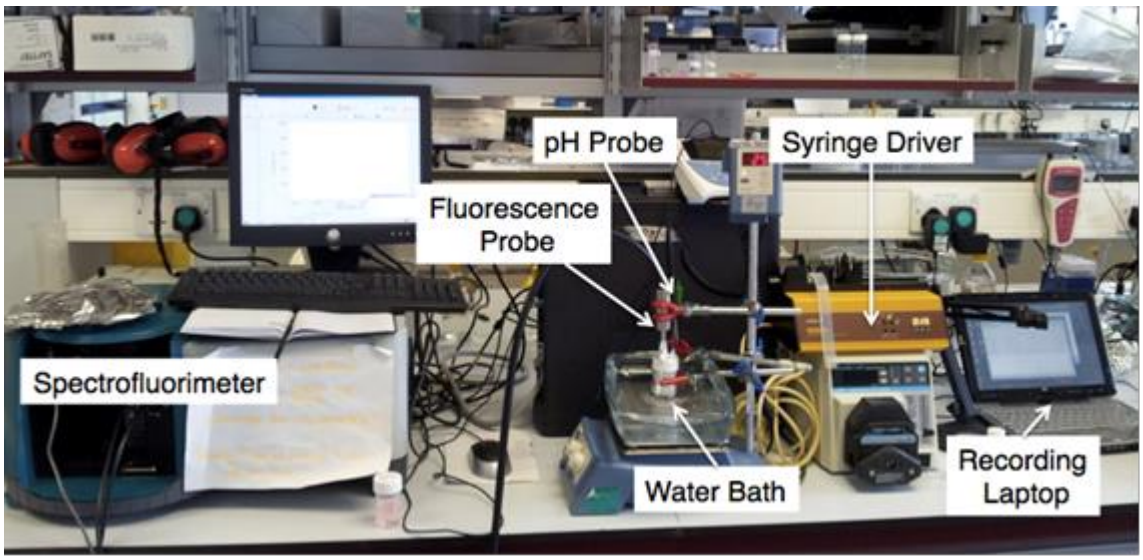

Figure 2.1: Experimental setup of potentiometric titration

2.1.9 Ultraviolet/Visual Spectrophotometry

When electromagnetic radiation interacts with a material, the radiation can either be scattered or absorbed. Scattering can occur either elastically or inelastically, which will be covered elsewhere. Ultraviolet/visual (UV/Vis) spectrophotometry works by quantifying the electromagnetic radiation between ultraviolet and visual wavelengths that is absorbed by the material. This visual range of wavelengths from the electromagnetic spectrum is more commonly referred to as light, as these wavelengths/energies are roughly those that we are able to perceive without the aid of instrumentation. At smaller wavelengths/higher energy (< 400 nm) than the visual light spectrum is ultraviolet (UV) light, and at longer wavelengths/lower energies (> 800 nm) is infrared (IR) light. The use of electromagnetic energy from this range (roughly 100 – 2000 nm) is common place in most scientific laboratories, due to the large amounts of information that can be gained from the interactions between light and materials. As mentioned, UV/Vis spectrophotometry is used to analyse light absorption from a material across the UV/Vis spectrum. Regarding experiments that used UV/Vis spectrophotometry within this thesis, all materials were liquid samples suspended in aqueous buffer, unless stated otherwise.

Absorbance is measured as the logarithmic scale of the ratio of the amount of light that passes through the sample and hits the detector against the amount of light that initially hit the sample. Mathematically this is shown as follows:

$$A_\lambda = -\log_{10}\left[\frac{I_T}{I_0}\right]$$

Where A_λ is the absorbance at a given wavelength, I_T is the quantity of light of the given wavelength that reaches the detector and I_0 is the quantity of light of a given wavelength before reaching the sample. This interaction is useful experimentally, due to the absorbance of a sample having a linear relationship with concentration at lower absorbance values, typically 0.05–1.50 Absorbance Units (A.U.). This relationship between absorbance and concentration is described by the Beer-Lambert law:

$$A_\lambda = \varepsilon BC$$

This linear equation states that the absorbance at a given wavelength (A_λ) is equal to the molar absorptivity (ε in $Lmol^{-1}cm^{-1}$), the path length (B in cm) and the sample concentration (C $molL^{-1}$). In a typical measurement, ε is a material constant under ambient conditions and B is an experimental constant dictated by the cuvette dimensions, usually 1 cm. Therefore, absorbance measurements are used to determine the concentration of unknown samples by comparing the absorbance measurements against a pre-made standard curve of known concentrations.

Ultraviolet/Visual spectrophotometry was conducted using a Jasco V-650 spectrophotometer (Jasco UK) within a wavelength range of 190–800 nm. Three different quartz glass cuvettes were used depending on available sample volume, 100 µL, 1 mL and 3 mL. The quartz glass ensured a smooth baseline with no cuvette absorbance or scattering across the wavelength range used. Prior to use, each cuvette was washed three times with distilled water and twice with solvent of the sample, typically phosphate buffered saline (PBS 100 mM), before drying with an air-line. After leaving the spectrophotometer on for 15 minutes to warm up, baseline measurements were taken using a fresh filtered sample of the solvent phase at a scan speed of 1 nm/sec. Typically, three measurements were taken to ensure a flat baseline. If there was large variation between baselines (> 0.05 A.U.), the spectrophotometer was left for a further five minutes before repeating the baseline measurements. After a successful baseline measurement was achieved, the value was later subtracted from subsequent measurements, which were taken under the same parameters as

the baseline. For temperature controlled spectrophotometry measurements, a single cuvette Peltier device (Jasco PTC-423) was used to maintain temperature within a range of -10°C to 110°C at an accuracy of 0.1°C. Samples measured at a constant temperature were left to equilibrate for a minimum of 15 minutes before measurement, as well as separate baseline measurements for each temperature used. For samples measured with a temperature trend, baseline PBS measurements were made separately for each temperature point and subtracted afterwards. Temperature trend measurements were conducted using the Jasco UV/Vis software, a scan was taken at the start temperature using the same parameters as the static samples. Once the measurement was taken, the temperature was taken to the next programmed point and left for 5 minutes to equilibrate before measuring. All data was exported as .txt files and processed using Microsoft Excel before producing graphs using pro Fit software (Version 6.1.14).

2.2.0 Fluorescence Spectroscopy

Fluorescence is a powerful measurement and can be used as an alternative method of detection and quantification compared with absorbance spectroscopy. It is often more sensitive and can be used at much lower concentrations of material. Fluorescence can also reveal information on molecular interactions and structural conformations, relationships with solvent environments and distances between sections of molecules or between molecules themselves. Fluorescence is a multi-stage process, the first stage is absorbance of incoming electromagnetic radiation and entering an excited state. In order for this to occur, the incoming energy must match one of the quantised energy levels for an atom or the molecule to enter a higher energy state or vibrational energy level. The energy of a single package of light (quantum) is related to the wavelength of the light:

$$E = h\nu = \frac{hc}{\lambda}$$

Where ν and λ are the frequency and the wavelength respectively, h equals Planck's constant (6.624×10^{-34} m^2 kg s^{-1}) and c is the speed of light (3×10^8 ms^{-1}). Each molecule capable of fluorescence, also known as a fluorophore, has defined energy levels capable of absorbing light and entering an excited

state. In practical terms, fluorophores can be “excited” by exposure to the required wavelengths of light. A molecule before energy absorption is said to be in its ground state (S0), which is a series of energy levels dictated by the electron shell distributions of the molecule. With the intake of energy, the molecule experiences some energy increase and is elevated to a higher level (S1). Examples of this are shown using a Jablonski diagram (Figure 2.2). Once the molecule is “excited” but before fluorescence occurs, some of the energy is dissipated through molecular interactions such as collisions and intersystem crossing. Fluorescence then occurs when the molecule undergoes radiative decay from the lowest S1 level to one of the S0 levels. Part of the energy released is emitted as photons, and most of the emitted photons are of lower energy than the original radiation absorbed.

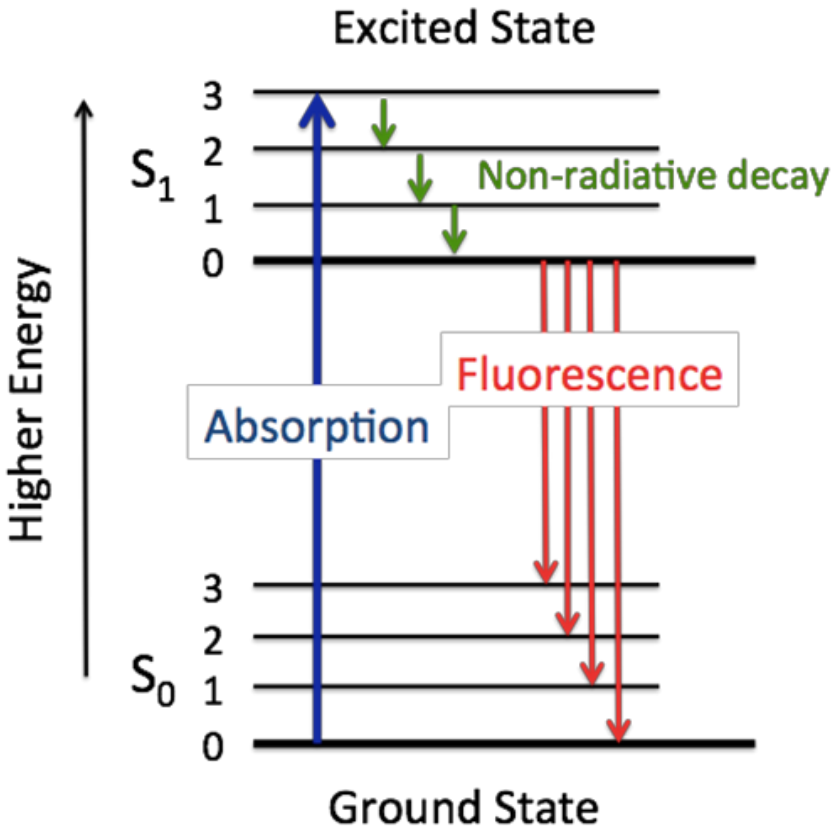

Figure 2.2: A Jablonski diagram showing the excitation and relaxation of an electron.

Fluorescence measurements were conducted using a Cary Eclipse spectrofluorimeter and three measurement set-ups were used. For single sample measurements, a 1 cm path length quartz cuvette with a sample volume of 3 mL was used and fluorescence measurements were conducted at 90° to

the incident light. For large sample numbers, measurements were conducted using a 96 well plate, samples varied in volume from 100–300 µL per well, however, comparable sample volumes were maintained for accurate measurements. The detector and incident light were both positioned above the well plate and measurements were conducted in a raster scan pattern. The third experimental set-up was for temperature controlled fluorescent measurements, an external probe was immersed in a sample located in a temperature controlled water bath. The probe and the sample were shielded from stray light in order to reduce background noise.

2.2.1 Gel Permeation Chromatography / Size Exclusion Chromatography

Size exclusion chromatography (SEC) is the process of separating molecules based upon their molecular weight. A chromatography column is filled with a stationary phase, whilst a continuous phase is passed through. For polymersomes the stationary phase used was Sepharose 4B (Sigma) a gel made from agarose beads, where each bead contains pores with a diameter of 30 nm. SEC works by providing two different path lengths for molecules/aggregates/particles to traverse, therefore particles greater than 30 nm in diameter may only pass through the column in the spaces between the beads. However, particles less than 30 nm may enter the pores of the beads as well as the space between and entering the pores results in a much greater path length experienced on averaged. Smaller particles will therefore take a comparatively longer time to reach the end of the SEC versus larger particles > 30 nm in diameter. Unlike many other forms of chromatography, this process assumes a minimal interaction between the stationary phase and the particles being separated. For bench-top SEC experiments a 25 cm long column with an internal diameter of 1 cm and a bed volume of 16 mL was used to separate 500 µL of polymersomes at 1 mg/mL polymer concentration. Before use, ethanol was removed by centrifuging the gel to the base of a tube and tipping off the liquid. The gel was then re-suspended in filtered PBS. This process was repeated 5 times to ensure that the ethanol was removed. To pack the column in preparation for use, Sepharose was then added to the open column to allow for the PBS to exit and the gel to pack. Once 20 cm of Sepharose was added, the column was washed with three times the bed volume (equalling the volume of Sepharose used) to ensure packing and remove any bubbles that may form

due to residual ethanol. For a high-performance liquid chromatography (HPLC) SEC column, a cross-linked Sepharose 4B with 30 nm pores was used, as the cross-linked stationary phase allows the Sepharose to be packed under pressure and withstand greater flow rates. A 30 cm long column with an internal diameter of 1 cm and a bed volume of 24 mL was used. The column was packed with cleaned Sepharose under a flow rate of 26 cm/hr (0.339 mL/min) and PBS was passed through the column overnight to ensure equilibrium. The set-up was tested using polystyrene latex particles of 100 nm, 300 nm and 460 nm in diameter and fluorescent dextran, fluorescein isothiocyanate (FITC) dextran at 2,000,000 Da and 500,000 Da and Texas Red Dextran at 3000 Da. Slower flow rates showed little difference in separation improvement, therefore, the maximum flow rate of 26 cm/hr was used throughout. When not in use, columns containing Sepharose were stored in the fridge for up to 1 month before fresh Sepharose was used.

2.2.2 References

1. Semsarilar, M., Ladmiral, V., Blanazs, A. & Armes, S. P. Anionic Polyelectrolyte-Stabilized Nanoparticles via RAFT Aqueous Dispersion Polymerization. *Langmuir* **28,** 914–922 (2011).

Chapter 3.1: The effect of temperature on PMPC-PDPA polymersome formation

Introduction

3.1.1 The Effect of Temperature on Chemical Reactions

Possibly the most universally controlled variable in any process is temperature, due to it often being the simplest method of manipulating energy transfer. Temperature is a fundamental component of both thermodynamics and kinetics, therefore, intrinsically affecting every reaction.[1] As discussed in Chapter 1, thermodynamics dictates whether a process is energetically favourable via the Gibbs equation:

$$\Delta G = \Delta H - T\Delta S$$

From this equation it can be seen that temperature has a fundamental influence on whether a reaction is favourable. Furthermore, the first term, enthalpy (ΔH), encompasses the internal energy, the sum of a system's potential and kinetic energies. For simplicity, the change in enthalpy (ΔH) of a system describes the heat absorbed or released at a constant pressure and volume. This allows for reactions to be classified in terms of their enthalpic contribution: reactions that release heat have a negative ΔH and are referred to as exothermic, while a process that absorbs energy has a positive ΔH and is designated endothermic. As shown in the above equation, temperature directly influences the entropy of the system. Entropy is an abstract concept and describes the degree of "disorder" in a system. Simply, the greater number of configurations that a substance can exist in, the lower is its ordering and the higher its entropy. Higher entropy contributes to a lower Gibbs energy.

Importantly in the context of this chapter, temperature also influences the kinetics of reactions. As mentioned, temperature is one of the easiest conditions to experimentally control. A simple relationship between temperature and reaction rate is the Arrhenius equation:

$$k = Ae^{-E_a/(k_B T)}$$

This relates the reaction rate constant (k) to the temperature (T), where E_a and k_B are the activation energy and the Boltzmann constant respectively, whilst A is

usually experimentally determined. Using this equation it becomes apparent that either increasing the temperature or decreasing the activation energy, for example through a catalyst, results in a higher reaction rate.

As described in Chapter 1, polymersome formation from homogeneously dispersed unimer chains is a complex process. It relies on the coalescence or nucleation of unimers and the subsequent formation of polymersomes by molecular exchange and rearrangement. Also, the increase in mass of the structures due to the transition from micelles to vesicles necessitates an exchange of materials. This chapter hypothesises that temperature alters the formation of PMPC-PDPA polymersomes and that by controlling the temperature, a degree of control over the polymersome size can be achieved.

Results

3.1.2 PMPC-PDPA

The pH responsive nature of PDPA causes the chain to exist as a random coil in its "good" aqueous solvent at mildly acidic conditions, and inversely, to collapse towards a hard sphere configuration in its "bad" aqueous solvent around neutral pH values.[2] Therefore, in order to study the effect of temperature across a range of block ratios, 4 diblock copolymers were synthesised by reversible addition-fragmentation chain transfer (RAFT) polymerisation. This was achieved using a single batch of $PMPC_{25}$ macro-CTA, which was used to synthesise a series of four copolymers with identical PMPC blocks and varying PDPA block lengths in form of $PMPC_{25}$-b-$PDPA_n$. Characterisation of the resulting four copolymers by ^1H NMR spectroscopy (not shown, data not accessible) indicated PDPA degrees of polymerisation (DP) of 47, 77, 94 and 147 units. GPC studies (Figure 2.1) indicated that the M_n values obtained increase systematically with target DP, as expected from controlled polymerisation. Moreover, narrow molecular weight distributions were achieved for all the block copolymers (M_w/M_n = 1.24 – 1.27).

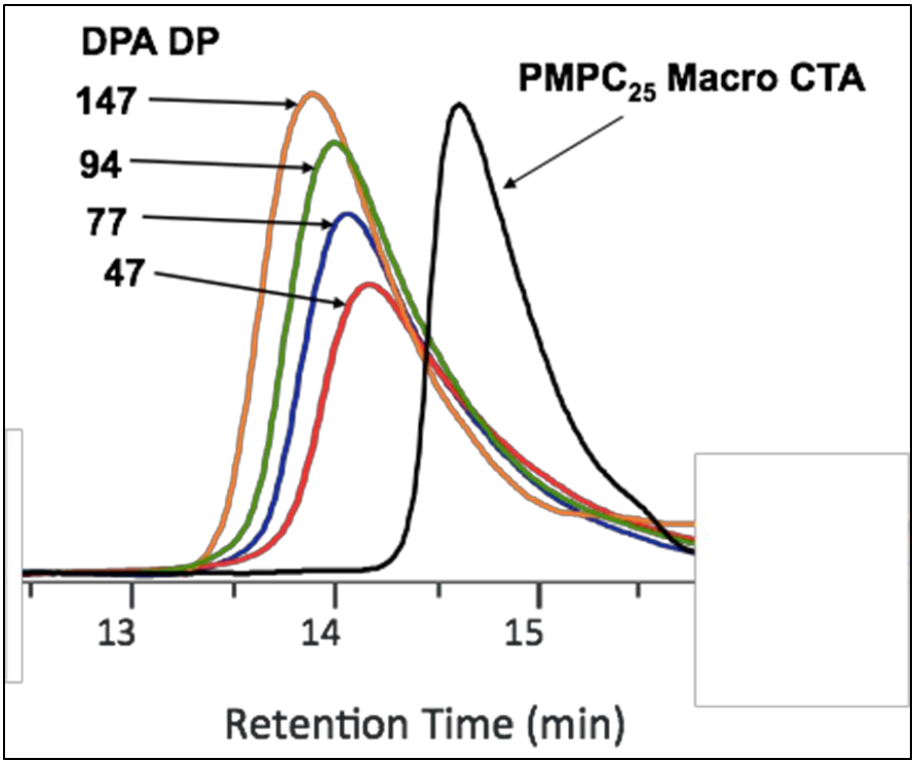

Figure 3.1. Gel permeation chromatography of the $PMPC_{25}$ Macro chain transfer agent and the subsequent copolymers produced. All traces show a mono model population distribution.

3.1.3 Potentiometric Titration of PMPC-PDPA block copolymers

One way to assess the effects of temperature on the pH responsive behaviour of the copolymers is through potentiometric titration.[3,4] Acid dissociation constants (pK_a) are measured as the midpoint of the plateau region for each curve generated. Figure 3.2 shows a shift in copolymer pK_a as the sample temperature changes. Specifically, the pK_a is close to neutral pH below room temperature. Above room temperature, the pK_a decreases. Plotting the measured pK_a values (Figure 3.3) against sample temperature shows a linear relationship for all block lengths with minimum and maximum values of 5.74 ± 0.01 and 7.59 ± 0.03 at 50°C and 5°C respectively. There appears to be no difference in pK_a values observed for the four different block lengths, suggesting that the degree of PDPA polymerisation has no effect on pK_a above the minimum degree of polymerisation of 47 used in this study.

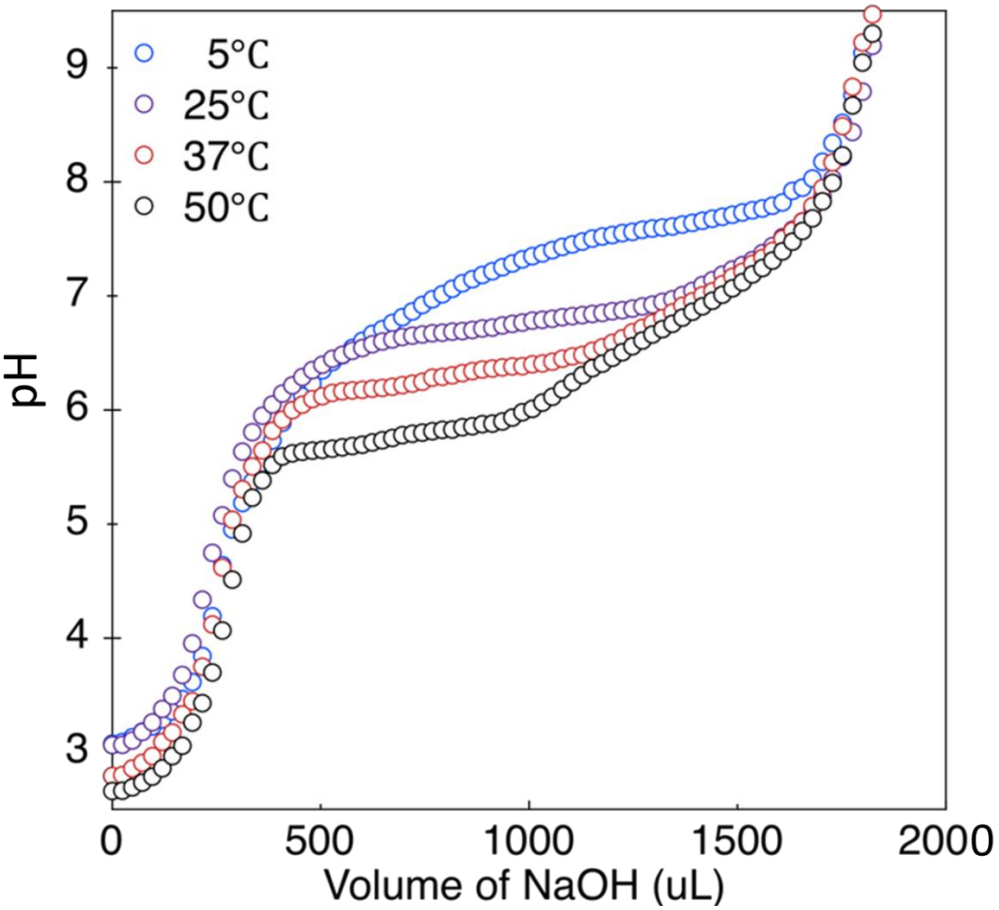

Figure 3.2: Potentiometric titration traces for PMPC-PDPA copolymer conducted at 4 different solution temperatures. Measurements were conducted at a copolymer concentration of 2 mg/mL, NaOH was added at 0.17 mL/min at a concentration of 5 x 10^{-3} M. This experiment was conducted in the presence of a buffer; therefore equivalence points have been estimated.

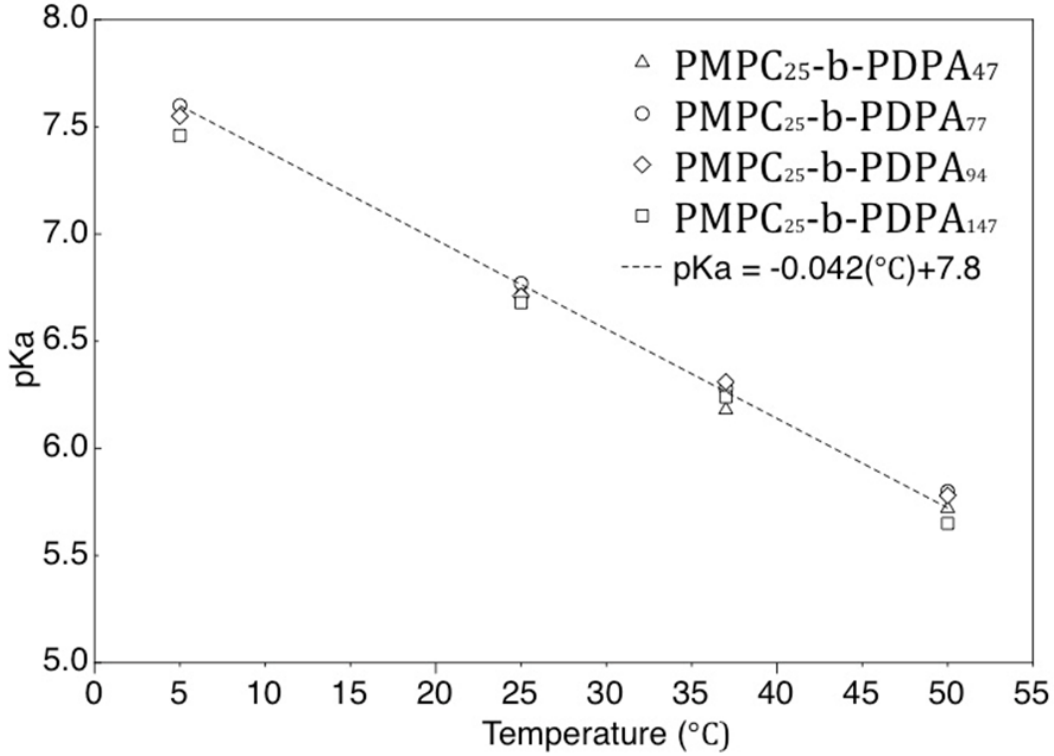

Figure 3.3: pKa as a function of temperature obtained from potentiometric titration curves for four different PMPC-PDPA block copolymer at four different temperatures. Reprinted with permission from Pearson RT et al. *Macromolecules* 2013;46(4):1400–1407. Copyright (2015) American Chemical Society.

This linear relationship between the sample temperature and pK_a allows the estimation of the degree of copolymer ionisation at a given pH and temperature by using the simple Henderson-Hasselbach equation:[5]

$$pH = pK_a + \log\left(\frac{[A^-]}{[HA]}\right)$$

This relates the ratio between deprotonated groups and protonated groups ($[A^-]/[HA]$) to the pK_a at a given pH. The degree of copolymer ionisation as a function of pH and temperature can be calculated as follows:

Let:

$$x = \left(\frac{[A^-]}{[HA]}\right)$$

Therefore,

$$pH = pK_a + \log x$$

Rearranging the formula gives:

$$x = 10^{(pH - pK_a)}$$

From this equation we can calculate the fraction of ionised (α) copolymer:

$$\alpha = \frac{1}{(1 + x)}$$

The use of this approach to estimate how the degree of ionisation is modulated as a function of both pH and temperature demonstrates a dependence on both quantities, (Figure 3.4). This calculation allows us to visualise the PDPA's solubility behaviour and therefore the self-assembly characteristics in terms of α.

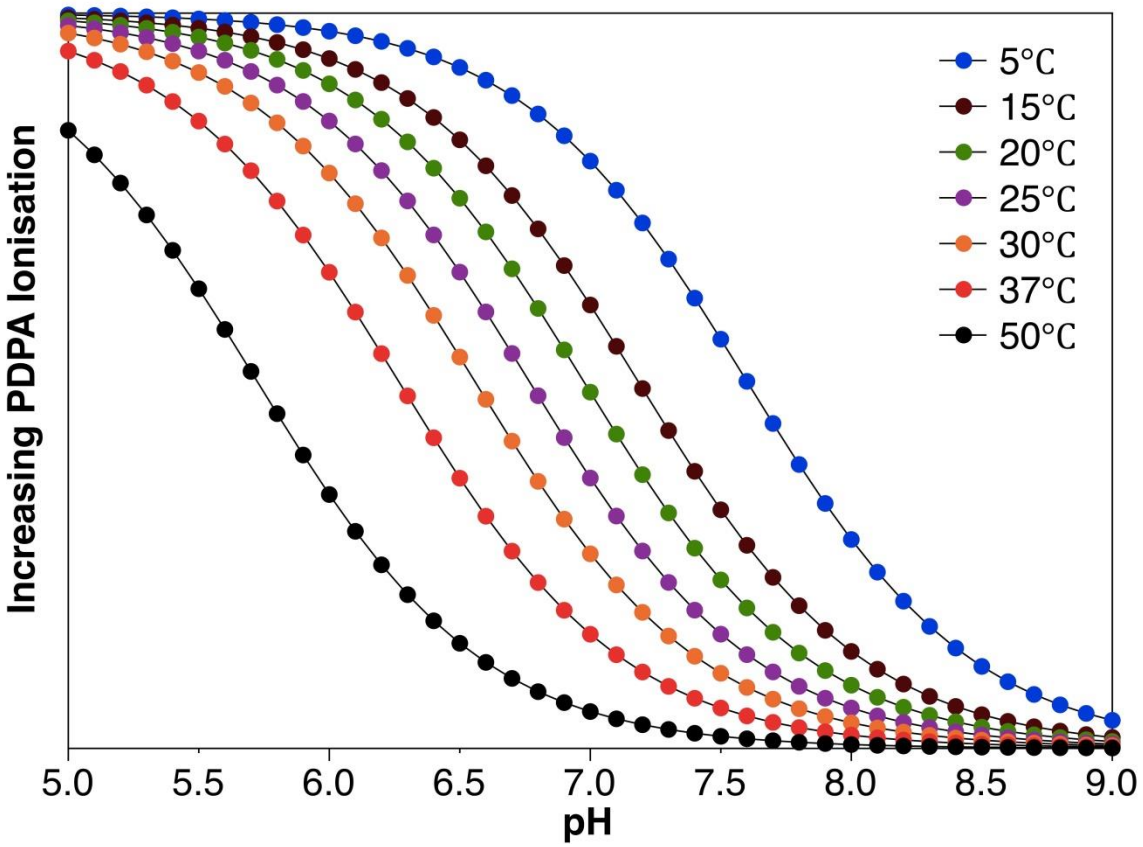

Figure 3.4: The degree of copolymer ionisation shown as a function of pH and temperature. Values were calculated using the pK_a values from potentiometric titrations. Reprinted with permission from Pearson RT et al. *Macromolecules* 2013;46(4):1400–1407. Copyright (2015) American Chemical Society.

The fraction of ionised copolymer is beneficial if one is able to define boundary conditions for α. For example, the balance between the hydrophobic forces driving self-assembly and the hydrophilic charge interactions counteracting self-assembly can be defined in terms of α. At α = 1, all amine functional groups are protonated and the hydrophobic forces are minimal. Inversely, at α = 0, PDPA is entirely deprotonated and displays the maximum possible hydrophobicity. Using a combination of values predicted using the Henderson-Hasselbach equation on the potentiometric titrations and experimental observations on self-assembly, it is possible to determine boundaries such as the maximum value of α obtainable prior to the onset of self-assembly, which is covered in Chapter 5. However, it is worth noting that the Henderson-Hasselbach equation is a simplified approach to modelling α.Therefore, Figure 3.4 shows a rough trend in the way PDPA ionisation changes with sample temperature and pH. Predicting the exact pH behaviour of large molecular weight polyelectrolytes is often difficult due to electrostatic

shielding and double layer effects.[6] As mentioned in Chapter 1, the focus of this thesis was to improve the formation and control of polymersomes for biomedical applications. Due to these applications, all experiments were conducted in 100 mM phosphate buffered saline, which complicates the measurement of the pK_a and use of the Henderson-Hasselbach equation for large polyelectrolytes. However, the use of more complex mathematical models to account for electrostatic shielding and high molecular weight effects falls outside the remit of this thesis, which focuses on the processing and formation of polymersomes in order to generate an improved and consistent drug delivery system.

3.1.4 Polymersome Size

Having established that temperature has an effect on pH responsive behaviour, investigations into how this effect alters the self-assembly process could be pertinent. In order to assess the effects of temperature on the size of aggregates formed, samples were analysed by dynamic light scattering to give decaying correlation functions and intensity averaged size distributions.[7,8] Figure 3.5 displays the distribution of particle hydrodynamic diameters formed by the four copolymers at different production temperatures. Interestingly, for $PMPC_{25}$-$PDPA_{47}$ there is no more than a 5% variation in particle diameter for samples formed at 30°C, 37°C and 50°C, with a value of around 37 nm. At 25°C the average diameter of particles formed increases from 37 nm to 48 nm, which equates to particles becoming 30% larger on average. A further size increase is observed as the production temperature decreases, with samples produced at 5°C having an average diameter of 160 nm. This is equal to a 4.5 fold increase in particle size between 50°C and 5°C.

Size distributions for $PMPC_{25}$-$PDPA_{77}$ and $PMPC_{25}$-$PDPA_{94}$ show the same trend. Namely, larger particles are being formed at 37°C, 30°C and 25°C with respect to 50°C samples. For samples prepared at 20°C and 15°C there is little difference in size distributions. Similarly, $PMPC_{25}$-$PDPA_{147}$ particle sizes increase in accordance to smaller copolymers between sample preparation temperatures of 50°C and 30°C. Below 30°C there is little variation in the distribution of hydrodynamic diameters. These lower temperature samples also display an increase in sample polydispersity, suggesting that the range of particle sizes produced are beyond those for which dynamic light scattering is capable of making a reliable measurement. This occurs because the intensity of

scattered light rapidly increases with larger particles, with a scaling of particle diameter to the power of six.[9] As a result of this, a sample with high polydispersity will have scattering information from smaller particles masked by large ones due to saturation of the detector. In addition, the larger particles will cause intensity spikes in measurements, making the formation of a flat baseline correlation function difficult as without a correct baseline, the function cannot be accurately modelled to give an average size and distribution. Interestingly, samples of $PMPC_{25}$-$PDPA_{94}$ and $PMPC_{25}$-$PDPA_{147}$ prepared at 5°C display smaller sizes than samples made at higher temperatures. However, these samples contain large amounts of sedimented polymer, indicating the formation of very large aggregates that are unable to remain suspended long enough for a light scattering measurement due to gravitational sedimentation. Therefore, the measurements represent the smaller proportion of the aggregates formed that remain in solution for the duration of the measurement. Figure 3.5 also displays the decaying correlation functions for the samples discussed above, clearly showing a shift towards longer decay times with decreasing temperature, indicative of larger particles.

In Figure 3.6, Z-average hydrodynamic diameters are taken from DLS intensity distributions and plotted as a function of temperature for the four copolymers used. At 50°C all of the copolymers produced their smallest aggregates with hydrodynamic diameters of 37.4nm ±6.3nm, 34.9nm ±2.9nm, 36.9nm ±4.1nm and 47.8nm ±2.5nm for PDPA blocks lengths of 47, 77, 94 and 147 respectively. Measurements taken between 50°C and 20°C show an increase in average hydrodynamic diameter with values of 53.1nm ±5.9nm, 116.4nm ±6.9nm, 184.7nm ±10.5nm and 294.5nm ±33.7 at 20°C for PDPA blocks lengths of 47,77,94 and 147 respectively. Measurements conducted on samples prepared at 15°C and 5°C exhibit the same trend; an increase in particle diameter for $PMPC_{25}$-$PDPA_{47}$ and $PMPC_{25}$-$PDPA_{77}$ (85.8nm ±7.2nm to 166.6nm ±9.2nm for $PMPC_{25}$-$PDPA_{47}$ and 138.5nm ±13.7 to 251.1nm ±58.3nm for $PMPC_{25}$-$PDPA_{77}$). For $PMPC_{25}$-$PDPA_{94}$ and $PMPC_{25}$-$PDPA_{147}$, samples produced at 5°C and 15°C display high polydispersities and exhibit inconsistent average diameters, suggesting that large aggregate sedimentation affected the light scattering measurements. As mentioned in chapter 1, increasing the DPA volume fraction creates a higher packing factor which favours the formation of membrane assemblies such as polymersomes. This is consistent with light

scattering measurements, where longer DPA block length polymers consistently form larger aggregates.

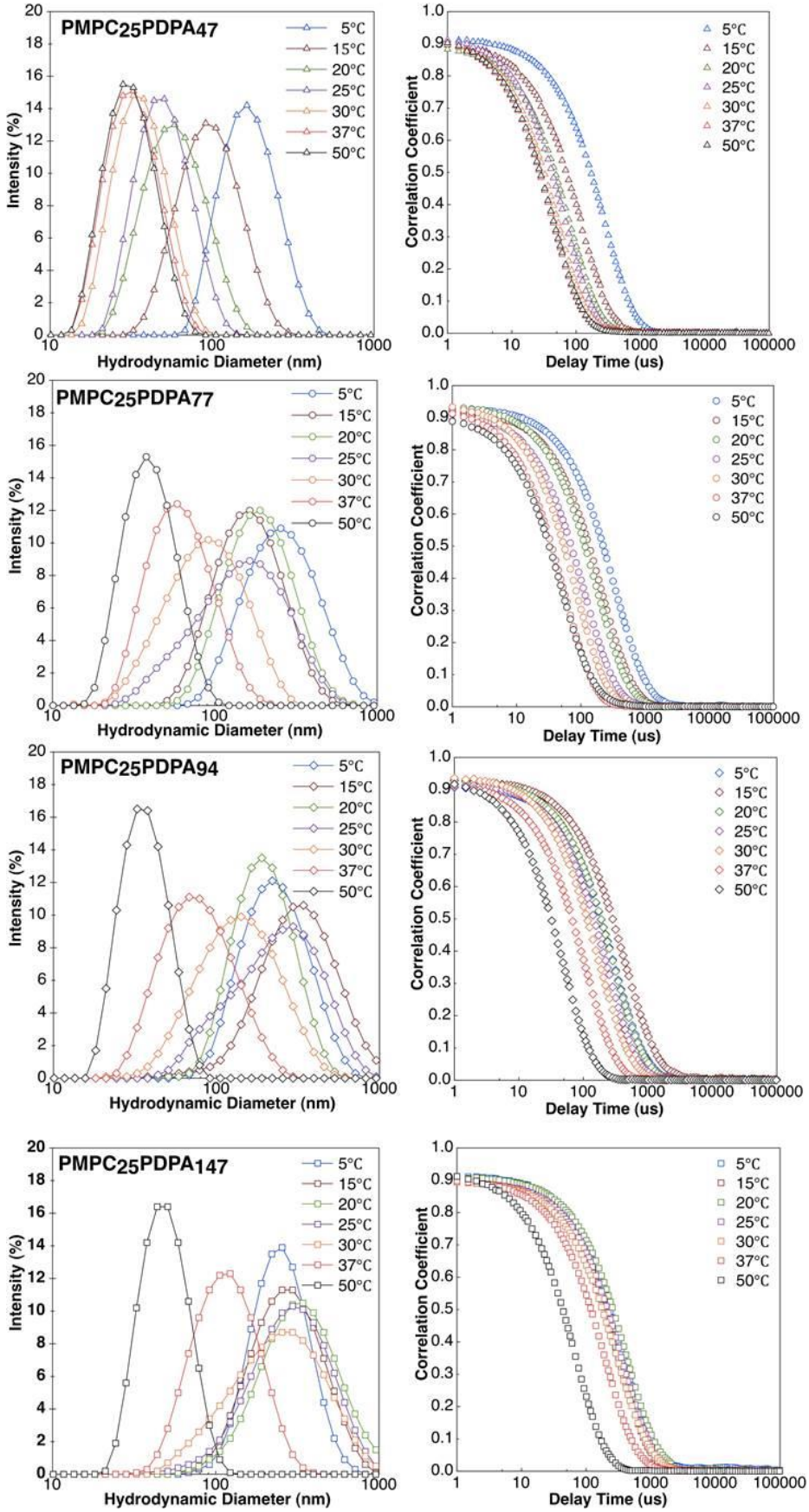

Figure 3.5: Decaying correlation functions generated and dynamic light scattering intensity distribution functions. Data shows a shift in the initial decay time to longer delay times for lower

temperature samples, indicating the formation of larger particles. A smooth baseline and a single exponential decay confirms an accurate measurement has been achieved. Modified with permission from Pearson RT et al. *Macromolecules* 2013;46(4):1400–1407. Copyright (2015) American Chemical Society.

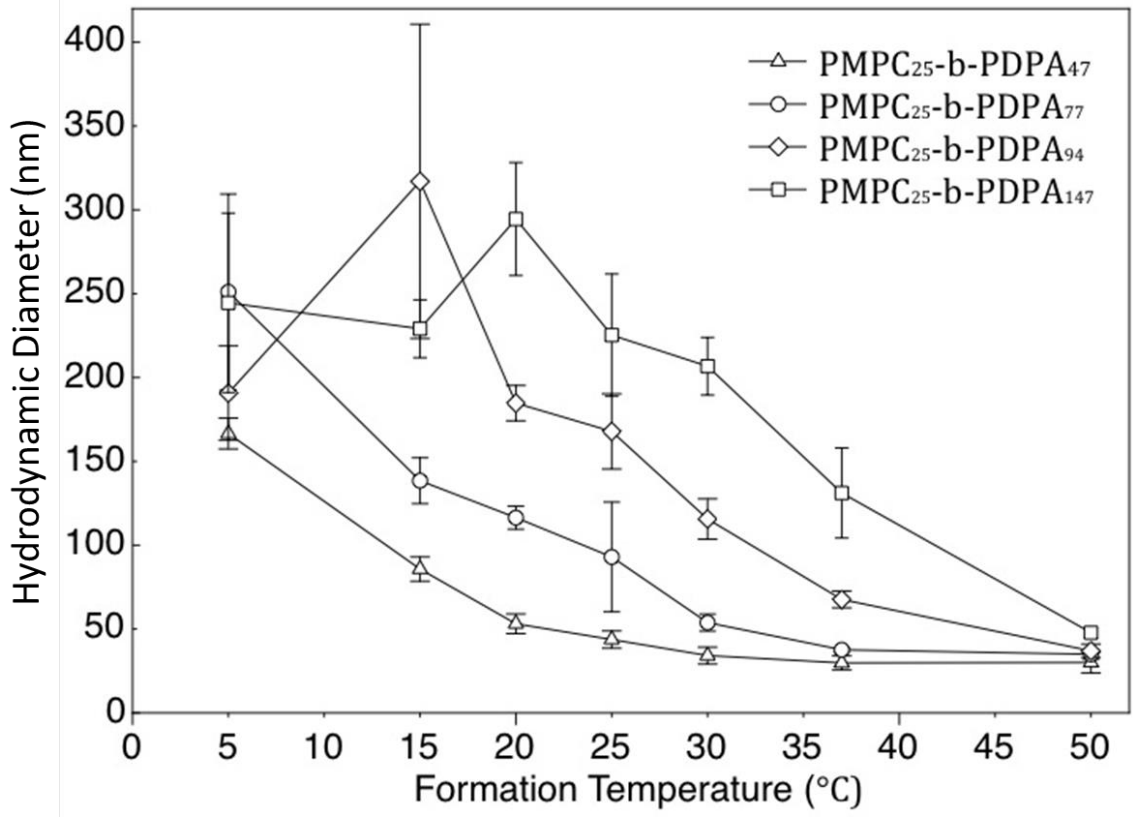

Figure 3.6: The z-averaged hydrodynamic diameters of three samples were combined to generate the average particle diameter for each copolymer at the 7 sample temperatures. Samples were measured at a copolymer concentration of 1 mg/mL. Error bars represent the standard deviation for n=3. Reprinted with permission from Pearson RT et al. *Macromolecules* 2013;46(4):1400–1407. Copyright (2015) American Chemical Society.

3.1.5 Aggregate Morphology

Figure 3.7 displays the typical macromolecular aggregate morphologies formed by the copolymer across a range of temperatures and molecular weights studied. At 50°C all four copolymers produce the smallest aggregates. TEM images of samples for $PMPC_{25}$-$PDPA_{47}$, $PMPC_{25}$-$PDPA_{77}$ and $PMPC_{25}$-$PDPA_{94}$ indicate the formation of micelles, as is expected for structures in this size range. Samples from $PMPC_{25}$-$PDPA_{147}$ at 50°C show a combination of micelles and small vesicles. Measurements of particle diameter from the TEM images show that the average micelle and vesicle sizes for $PMPC_{25}$-$PDPA_{147}$ at 50°C are 31.7 nm ± 3.8 nm and 52.3 nm ± 13.8 nm respectively. At 37°C, $PMPC_{25}$-$PDPA_{47}$ and $PMPC_{25}$-$PDPA_{77}$ continue to produce spherical micelles with narrow size distributions. However, at this temperature both $PMPC_{25}$-$PDPA_{94}$ and $PMPC_{25}$-$PDPA_{147}$ produce a combination of polymersomes and micelles. Reducing the sample temperature further to 30°C, maintains the formation of

micelles for $PMPC_{25}$-$PDPA_{47}$. A combination of polymersomes and micelles can be seen in samples from $PMPC_{25}$-$PDPA_{77}$ and $PMPC_{25}$-$PDPA_{94}$.

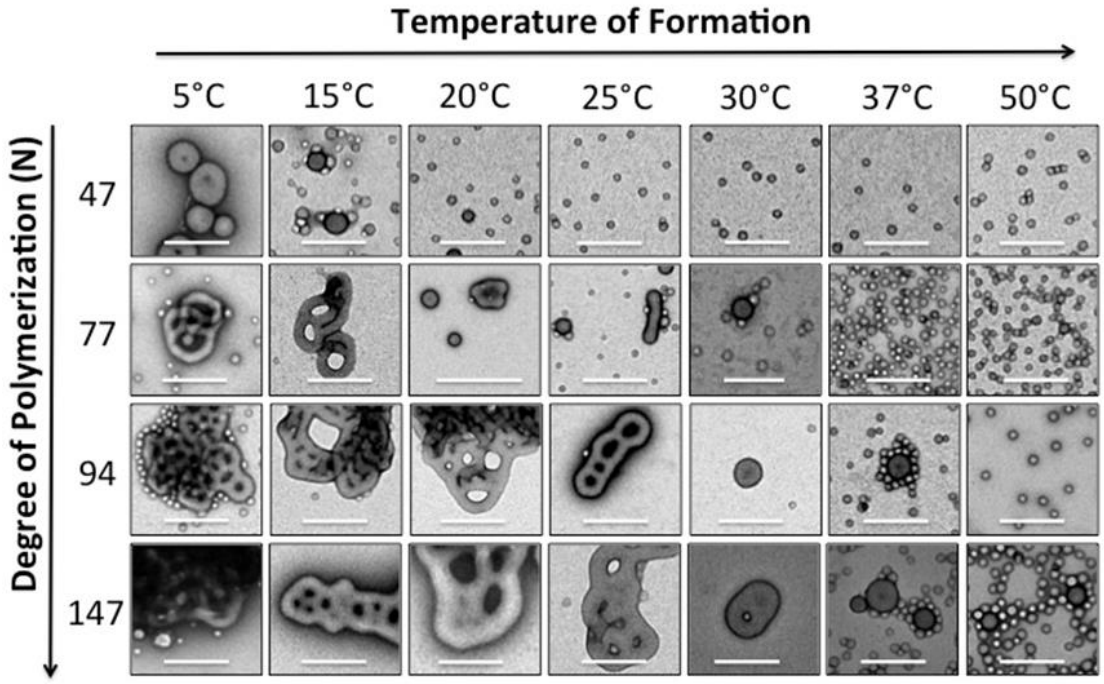

Figure 3.7: Typical macromolecular assemblies formed by each copolymer across the temperature range as shown by transmission electron microscopy. Contrast was gained by positive staining with phosphotungstic acid. Samples were analysed at a copolymer concentration of 0.5mg/mL. Scale bar equals 200 nm. Reprinted with permission from Pearson RT et al. *Macromolecules* 2013;46(4):1400–1407. Copyright (2015) American Chemical Society.

However, $PMPC_{25}$-$PDPA_{147}$ can form particles with genus "events". These structures are of particular interest and are discussed in more detail in Chapter 4. At 25°C $PMPC_{25}$-$PDPA_{47}$ forms micelles, while $PMPC_{25}$-$PDPA_{77}$ produces micelles and polymersomes. Alongside this, there are non-spherical particles with diameters greater than 50 nm, suggesting the presence of two membrane formations and indicating tubular polymersomes. Cylindrical micelles would exhibit diameters consistent with spherical micelles (due to being monolayers), while diameters less than 40 nm were estimated for $PMPC_{25}$-$PDPA_{77}$ from membrane-width measurements. For $PMPC_{25}$-$PDPA_{94}$ and $PMPC_{25}$-$PDPA_{147}$ genus particles were produced at 25°C, with larger and more complex genus assemblies being produced from $PMPC_{25}$-$PDPA_{147}$. Samples prepared at 20°C from $PMPC_{25}$-$PDPA_{47}$ show a combination of micelles and polymersomes, which is in contrast to the higher temperature samples. For $PMPC_{25}$-$PDPA_{77}$, the TEM images show the presence of polymersomes and larger non-spherical structures, indicating the onset of genus assemblies.

$PMPC_{25}$-$PDPA_{94}$ and $PMPC_{25}$-$PDPA_{147}$ continue to produce larger and more complex genus particles at 20°C. The three longer block length copolymers also produce genus structures at both 15°C and 5°C. In addition, DLS data correlates with this observation, indicating formation of larger particles. Interestingly, $PMPC_{25}$-$PDPA_{47}$ continues to produce polymersomes at 15°C and 5°C, which is unexpected from the short DPA block length.

3.1.6 Membrane Scaling

Good correlation has been shown between membrane thickness measurements taken from ambient TEM micrographs obtained on dried samples, and those taken from cryogenic TEM pictures and x-ray scattering techniques, where the latter techniques investigate the structures in their native state.[10] Therefore, average polymersome membrane thickness and micelle diameters based on TEM micrographs are used for all polymers studied. Figure 3.8 shows the average membrane thickness plotted against degree of polymerisation.

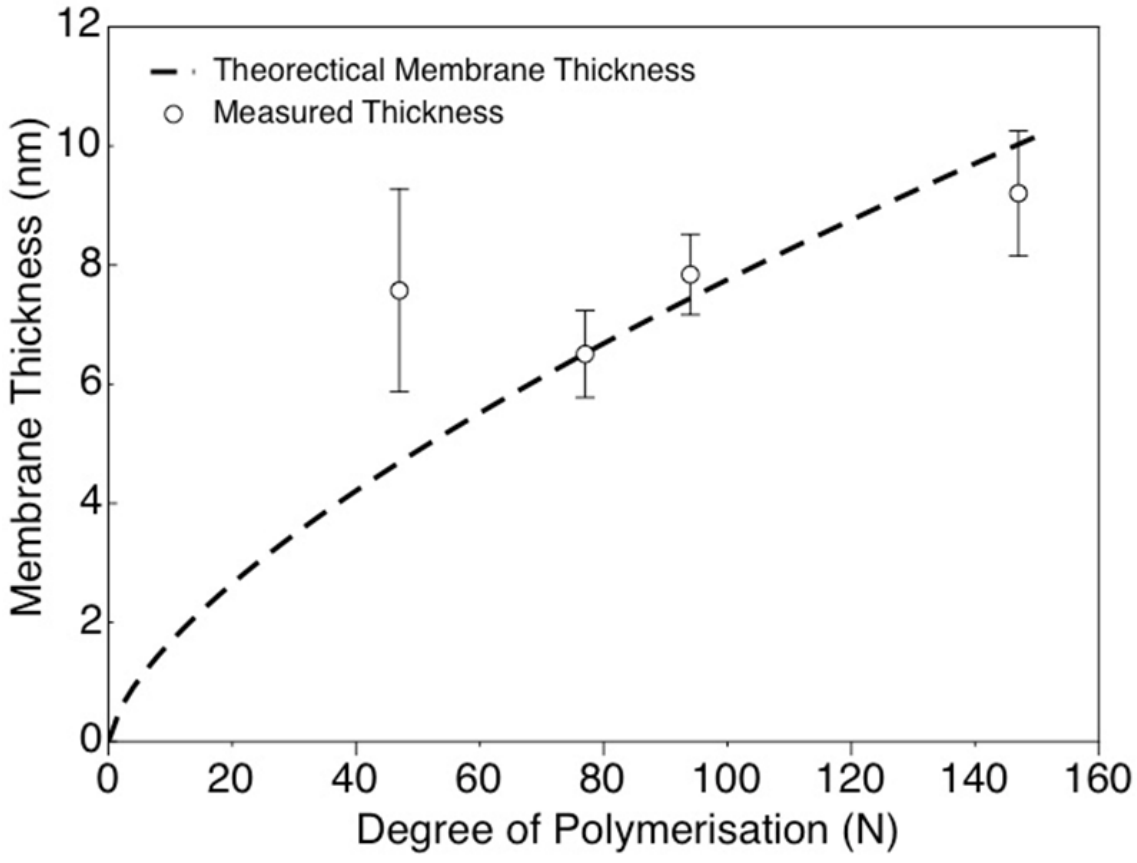

Figure 3.8: Membrane thickness measurements taken from transmission electron micrographs and plotted as the degree of copolymer polymerisation. The dotted line shows the expected membrane scaling as $N^{2/3}$. Reprinted with permission from Pearson RT et al. *Macromolecules* 2013;46(4):1400–1407. Copyright (2015) American Chemical Society.

For the three longest block lengths the membrane thickness scales with $N^{2/3}$, which is expected for interdigitated polymeric membranes and micelles.[10,11] However, the polymersomes formed by $PMPC_{25}$-$PDPA_{47}$ display membranes that are 7.6 nm in thickness, which is 2.9 nm larger than expected. As previously stated, the short block length of 47 is predicted to form micelles rather than polymersomes, due to its shorter block length. Despite this, the lower temperatures of 5°C and 15°C produce polymersome morphologies (Figure 3.8) with membranes comparable to a DPA block length twice as long. This indicates that the polymer formed a more uncoiled conformation within the membrane.

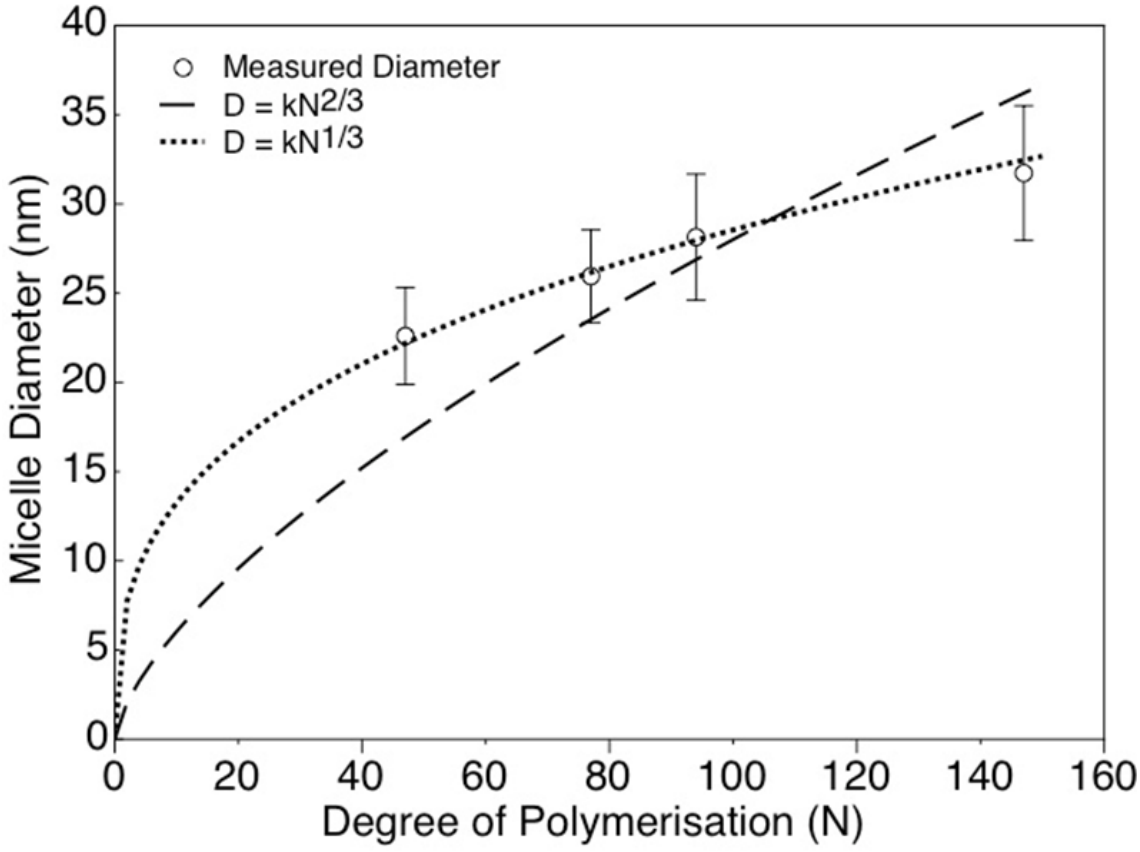

Figure 3.9: Micelle diameter measurements taken from transmission electron micrographs of 50°C samples and plotted as the degree of copolymer polymerisation. Results scale with N1/3, indicating a highly coiled conformation. Reprinted with permission from Pearson RT et al. *Macromolecules* 2013;46(4):1400–1407. Copyright (2015) American Chemical Society.

Such behaviour is most likely due to the sample pH being close to the pK_a, where a significant fraction of the amino groups are protonated. This results in a stretched PDPA block due to repulsive charge effects. However, micelle diameters scale with $N^{1/3}$ better than $N^{2/3}$ as shown in Figure 3.9. This would

suggest that these micelles are formed from more coiled amphiphiles than predicted from the interdigitated conformation. The entropic penalty for taking this conformation indicates that the micelles are kinetically trapped structures rather than formed simply due to packing factor constraints.

As predicted by the molecular packing parameter, increasing the relative hydrophobic volume fraction is sufficient to cause the assembly of structures with lower curvatures. Traditionally, this can be achieved by extending the degree of polymerisation of the hydrophobic block until vesicular aggregates are observed after assembly. However, as demonstrated above, the pH responsive nature of PDPA adds another dimension of control. Working on the assumption that a more ionised PDPA occupies a greater volume due to repulsive forces, the effective volume and therefore packing factor of PMPC-PDPA can be controlled via α. At pH 7.5 and 50°C the polymer is 1.7 pH units above its pK_a (Figure 3.3) and is more than 99% deprotonated on average (Figure 3.4). In this state, the PDPA block collapses to reduce its effective volume due to water becoming an unfavourable solvent environment.

For polymers in poor solvents the radius of gyration (R_g) scales to the inverse cubic root of the degree of polymerisation ($R_g \alpha N^{1/3}$).[2] As a result of the relationship between polymer pK_a and temperature, the degree of DPA protonation increases as the sample temperature decreases. As the amount of protonation increases, water becomes an overall more favourable environment for the polymer, thus increasing its effective volume in solution. The limit is where the polymer is fully protonated, at this point the chain is extended to its maximum volume and can be modelled as a random coil where $R_g \alpha N^{1/2}$.[2] However, under these conditions the PDPA is fully water-soluble and the PMPC-PDPA has no driving force for self-assembly. Therefore, at a specific value of deprotonation (and therefore hydrophobicity), self-assembly is expected to occur into structures as dictated by the molecular packing factor of PMPD-PDPA at this point. Between these boundaries of a critical value of deprotonation, where the PDPA block is sufficiently hydrophobic to allow self-assembly and a fully deprotonated state, the effective volume fraction of the DPA block alters. This in turn, generates a range of potential molecular packing parameters in addition to those theorised by the degree of polymerisation.

3.1.7 Particle Stability

Once these assemblies are produced they appear to be stable within the temperature range tested for at least 133 days at room temperature. Figure 3.11 shows the hydrodynamic diameters as measured by DLS for $PMPC_{25}$-$PDPA_{147}$ samples produced at 50°C and stored at room temperature. This storage stability is beneficial for applications of polymersomes which require longer shelf lives or processing time scales. However, these structures are kinetically trapped and would in theory tend towards their ideal structures as defined by their packing factor. Yet the energy barrier presented by exposing the hydrophobic sections to water is sufficient to maintain these structures under ambient conditions for at least four months.

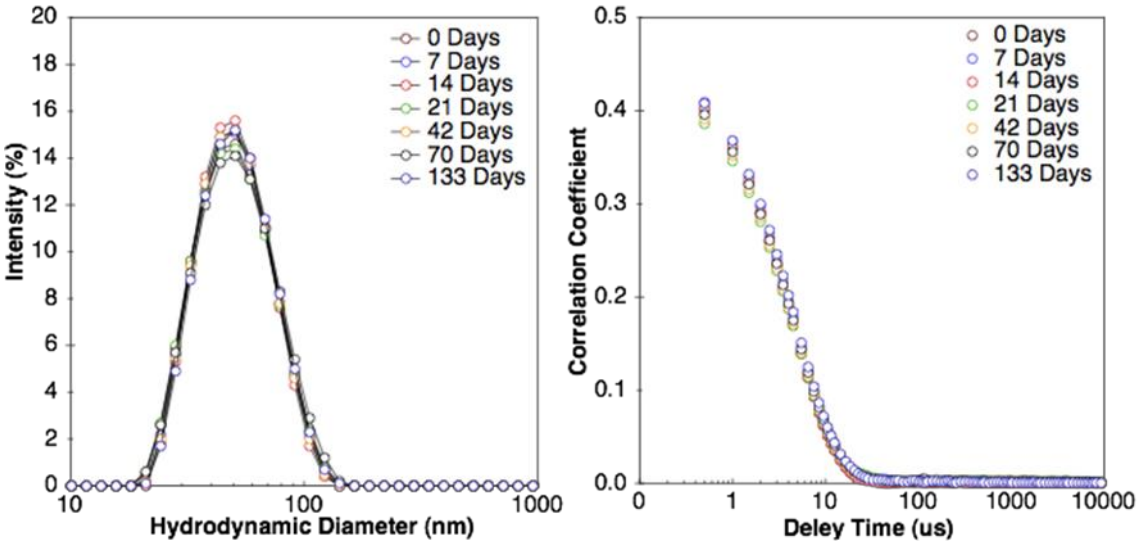

Figure 3.11: Dynamic light scattering measurements confirm no change in particle diameter over 133 days of storage under ambient conditions.

3.1.8 Discussion

The observations in this Chapter show that altering the temperature of $PMPC_{25}$-$PDPA_n$ self-assembly dramatically changes the morphology of the resulting macromolecular aggregates. By modulating the sample temperature, the polymer pK_a changes, causing the polymer to exhibit different degrees of protonation at a constant pH value. This in turn changes the volume of the responsive PDPA block due to swelling and collapse induced by protonation of the hydrophobic block, which changes the molecular packing parameter. The packing parameter dictates the ideal curvature formed between two or more amphiphiles, and in turn, the structures formed. However, alongside the packing parameters' dictated curvature, a molecular transition from hydrophile to

amphiphile occurs as a function of pH increase. This causes the spontaneous nucleation of polymer chains, which is driven by the hydrophobic effect. Once sufficient mass of polymer has aggregated, the process of assembling into the most energetically favourable structure begins. The structures formed undergo a well characterised structural transformation ending on the formation based upon the molecular packing factor.[11,12]

However, at higher temperatures, the formation of micellar aggregates exclusively is seen for all but the largest molecular weight copolymer. In addition, micelle diameter measurements show that the hydrophobic block of the assembled copolymer adopts a more coiled and frustrated conformation. This indicates that the micelles generated in the system are kinetically trapped structures resulting from a combination of faster nucleation kinetics and reduced unimer exchange. Inversely, the formation of vesicular aggregates with thicker membranes by the smallest block copolymer at low temperatures indicates an alteration in the copolymer packing factor.

An increase in copolymer ionisation at lower temperatures is thought to increase the degree of unimer exchange during the assembly process. This results in the formation of genus structures, which are explored in more detail in later Chapters. However, an increase in unimer exchange fails to explain the formation of vesicular aggregates by $PMPC_{25}$-$PDPA_{47}$, which has previously been shown to produce micelles. The formation of membranes was approximately twice as thick as predicted, which indicates that the polymer is in a highly stretched conformation. This would suggest that the PDPA volume increase due to ionisation is sufficiently larger than the area and length increases to produce a more planar packing factor. The larger PDPA volume pushes the copolymer dimensions into the membrane forming region. The formation of genus structures is due to the spontaneous curvature by the copolymer membrane. This spontaneous curvature is caused by the reduced probability of the copolymer membrane to undergo molecular reorganisation mechanisms such as “flip-flopping”. The increased entropic penalty of exposing the hydrophobic section to water and the hydrophilic block to the non-polar membrane results in high molecular weight copolymer membrane flipping being energetically unfavourable.[13–17] Similarly, unimer exchange is more unfavourable in copolymer systems. However, an increase in hydrophilicity of the membrane forming block decreases the energetic penalty.[18,19]

In summary, a strong temperature dependence on the formation process of PMPC-PDPA polymersomes via pH increase was observed. Increasing the temperature appears to have the effect of trapping self-assembly at the earlier stages or micelle formation. However, a strong shift in the pH responsive behaviour of PMPC-PDPA with temperature was observed, specifically a change in pK_a. This finding, in conjunction with the presence of vesicular aggregates being formed by a copolymer expected to form only micelles (from previous studies), has led to the hypothesis that the degree of copolymer ionisation and molecular volume are interlinked, which can be used to control the formation of polymersomes. In addition, the formation of genus particles under conditions of higher PDPA ionisation opens the polymer system up to the study of these interesting and complex structures which is covered in the next chapter.

3.1.9 Permissions

Part of this work has been published in Pearson RT et al. *Macromolecules* 2013;46(4)1400–1407, for which permission was received by American Chemical Society (2015).

3.2.0 References

1. Connors, K. A. *Chemical Kinetics: The Study of Reaction Rates in Solution*. (John Wiley & Sons, 1990).
2. Nagasawa, M., Murase, T. & Kondo, K. Potentiometric Titration of Stereoregular Polyelectrolytes. *J. Phys. Chem.* **69,** 4005–& (1965).
3. Katchalsky, A. & Gillis, J. Theory of the Potentiometric Titration of Polymeric Acids. *Recl. Trav. Chim. Pays-Bas-J. R. Neth. Chem. Soc.* **68,** 879–897 (1949).
4. Po, H. N. & Senozan, N. M. The Henderson-Hasselbalch equation: Its history and limitations. *J. Chem. Educ.* **78,** 1499–1503 (2001).
5. LoPresti, C., Lomas, H., Massignani, M., Smart, T. & Battaglia, G. Polymersomes: nature inspired nanometer sized compartments. *J. Mater. Chem.* **19,** 3576–3590 (2009).
6. Goldburg, W. I. Dynamic light scattering. *Am. J. Phys.* **67,** 1152–1160 (1999).
7. Pecora, R. Dynamic Light-Scattering from Macromolecules. *Proc. Static Dyn. Light Scatt. Med. Biol.* **1884,** 2–15 (1993).
8. Malvern Instruments Ltd. *Dynamic Light Scattering an Introduction in 30 minutes*. (Malvern Instruments Ltd). at <http://www.malvern.com/en/support/resource-center/technical-notes/TN101104DynamicLightScatteringIntroduction.aspx>
9. Letchford, K. & Burt, H. A review of the formation and classification of amphiphilic block copolymer nanoparticulate structures: micelles, nanospheres, nanocapsules and polymersomes. *Eur. J. Pharm. Biopharm.* **65,** 259–269 (2007).
10. Bermudez, H., Brannan, A. K., Hammer, D. A., Bates, F. S. & Discher, D. E. Molecular weight dependence of polymersome membrane structure, elasticity, and stability. *Macromolecules* **35,** 8203–8208 (2002).
11. Cowie, J. M. G. *Polymers: Chemistry and Physics of Modern Materials*. (1991).
12. Israelachvili, J. N., Mitchell, D. J. & Ninham, B. W. Theory of Self-Assembly of Lipid Bilayers and Vesicles. *Biochim. Biophys. Acta* **470,** 185–201 (1977).
13. Battaglia, G., Ryan, A. J. & Tomas, S. Polymeric vesicle permeability: A facile chemical assay. *Langmuir* **22,** 4910–4913 (2006).
14. Discher, B. M. *et al.* Polymersomes: Tough vesicles made from diblock copolymers. *Science* **284,** 1143–1146 (1999).
15. Anglin, T. C. & Conboy, J. C. Kinetics and Thermodynamics of Flip-Flop in Binary Phospholipid Membranes Measured by Sum-Frequency Vibrational Spectroscopy. *Biochemistry (Mosc.)* **48,** 10220–10234 (2009).
16. Bermudez, H., Hammer, D. A. & Discher, D. E. Effect of bilayer thickness on membrane bending rigidity. *Langmuir* **20,** 540–543 (2004).
17. Nakano, M. *et al.* Flip-Flop of Phospholipids in Vesicles: Kinetic Analysis with Time-Resolved Small-Angle Neutron Scattering. *J. Phys. Chem. B* **113,** 6745–6748 (2009).
18. Creutz, S., vanStam, J., Antoun, S., DeSchryver, F. C. & Jerome, R. Exchange of polymer molecules between block copolymer micelles studied by emission spectroscopy. A method for the quantification of unimer exchange rates. *Macromolecules* **30,** 4078–4083 (1997).
19. Van Stam, J., Creutz, S., De Schryver, F. C. & Jerome, R. Tuning of the exchange dynamics of unimers between block copolymer micelles with temperature, cosolvents, and cosurfactants. *Macromolecules* **33,** 6388–6395 (2000).

Chapter 4.1: Genus polymersomes

Introduction

4.1.1 PMPC-PDPA structures

Chapter 3 reported that the average size of structures produced by PMPC-PDPA can be affected by sample temperature, when measured by dynamic light scattering. However, when using electron microscopy to view the particle morphologies, there were some unexpected structures at lower temperatures (higher degrees of protonation). Specifically, structures where the surface of the particle appeared to curve inwards and form a dimple, recess or hole, were shown. Three-dimensional shapes with connected, orientable surfaces that contain holes can be termed genus structures, which can also be defined as an integer representing the maximum number of cuttings along non-intersecting closed simple curves without rendering the resultant manifold disconnected.[1] To the author's knowledge, these formations had not been seen with PMPC-PDPA samples before and the driving force for generating such structures is not well understood. This Chapter therefore covers the current understanding of structures that contain dimples, recesses or holes and explores the potential driving forces for their formation in PMPC-PDPA.

4.1.2 Homeomorphism

Topology is a branch of mathematics concerned with the study of objects or space and their unbroken transformations. It is used to describe the transition from one shape to another only via deformation, not by cutting or removing any part of the shape. This process is known as homeomorphism. In three dimensions a toroid or donut shape can be deformed to produce the shape of a single handled mug without breaking its surface. In the case of polymersomes, this could be a fitting approach to explain the formation of such structures. In simple terms, the process of moving between macromolecular assemblies (from micelle to polymersome, then polymersome to toroid) involves structural rearrangement and in many cases an increase in particle mass. Due to the high entropic penalty of exposing the hydrophobic core of these structures, it was hypothesised that the evolution of structures during formation is driven by a combination of unimer (single polymer chains) exchange and topological transformations.

The homeomorphism approach has been used in cell biology to understand the various shape transformations undertaken by the cell membrane. As mentioned, the energetic penalty of exposing the hydrophobic core means that these movements rarely break the membrane. Such structures range from long planar protrusions to highly curved mitochondrial membranes. Current understanding of cell membrane shape transformations is that a combination of supporting cellular structures such as proteins or filaments and intrinsic curvature generated by membrane composition are the main driving forces.[2] The desire to understand how such complex structures are formed by lipid amphiphiles has led to vast amounts of research into membrane physics and their surface topologies. For example, Deuling H.J. and Helfrich W. studied the topology and curvature of erythrocytes (red blood cells).[3] The authors were particularly interested in explaining how the thin lipid membrane forms and then maintains the biconcave disc conformation of a standard erythrocyte when submitted to shear forces. In order to achieve this, mathematical models have been produced to explain and predict the various structures that can be formed from thin lipid membranes. However, in the area of polymer membranes there have been fewer published works.

4.1.3 Curvature and Topology

In order to discuss the topologies seen be amphiphilic systems, the various components involved in defining and calculating a surface should be confirmed. Any surface can be defined by its fundamental curvatures; these are calculated from its principal curvatures. A surface's principal curvatures (C_1 and C_2) are defined as the reciprocal of the radius of curvature. Where a surface that curves towards the normal direction (convex) is defined as positive and away from the normal (concave) as negative. Through these principal curvatures, the mean curvature (the average curvature) and Gaussian curvatures (the product of the curvatures) can be defined.

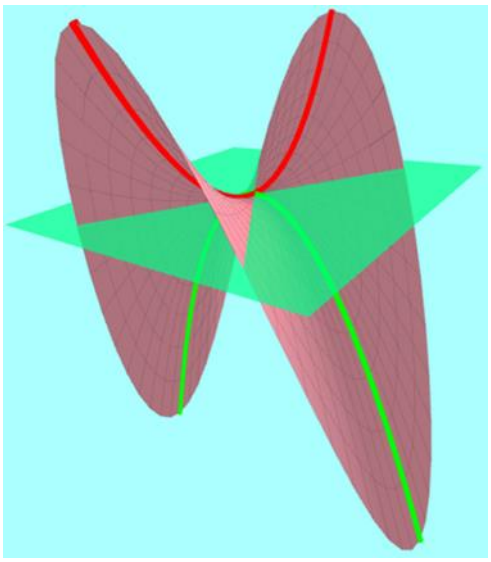

Figure 4.1: Any surface can be defined in terms of its principle curvatures. Here, a saddle point is shown, having both negative curvature (red line) and positive curvature, whereas a sphere has constant positive curvature. Image taken from http://profs.scienze.univr.it/~baldo/tjs/principal_curvatures.html under General Public License.[4]

Defining shapes in terms of their Mean and Gaussian curvatures is often a useful perspective. Taking a sphere as an example, all points across the surface have positive principal curvatures. Therefore, a sphere has a constant positive mean curvature and a positive gaussian curvature. Comparatively, a saddle point (Figure 4.1) has equally positive and negative principal curvatures, i.e. $C_1 + C_2 = 0$. This shape results in a mean curvature of 0 and a negative gaussian curvature. A shape of particular interest is the catenoid (Figure 4.2), in which the mean curvatures at all points cancel out, producing a shape with overall minimal curvature. In relation to polymer and lipid membranes it is useful to view the curvature as related to the energy required to bend the membrane.

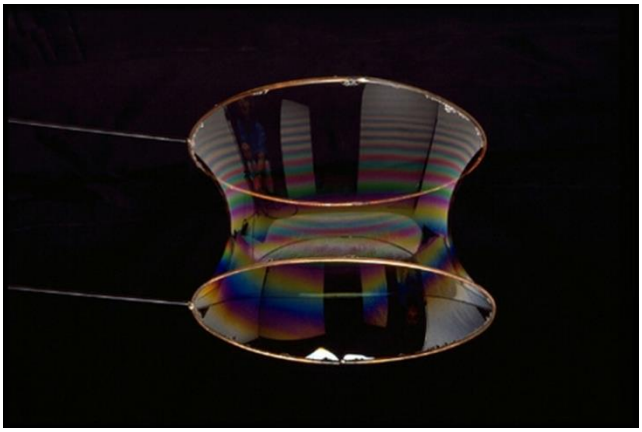

Figure 4.2: A catanoid produced by soap bubbles between two circles. At each point of the surface, the external and internal curvatures are equally opposite. This results in an overall mean curvature of 0. This photograph is reproduced under the Creative Commons license for non-commercial purposes and was not modified prior to use.[5]

In order to reduce the energy required to form and maintain a structure, a membrane will adopt the lowest energy state and therefore the lowest possible curvature. However, consideration of the hydrophobic sections of the

membrane needs to be taken into account. Figure 4.3 gives an example of the compromise between minimising the curvature by shielding the hydrophobic membrane core. It should also be reiterated that this approach assumes that the amphiphile packing factor is in the membrane forming region ($1/2 < p < 1$) and does not consider kinetically-trapped structures.

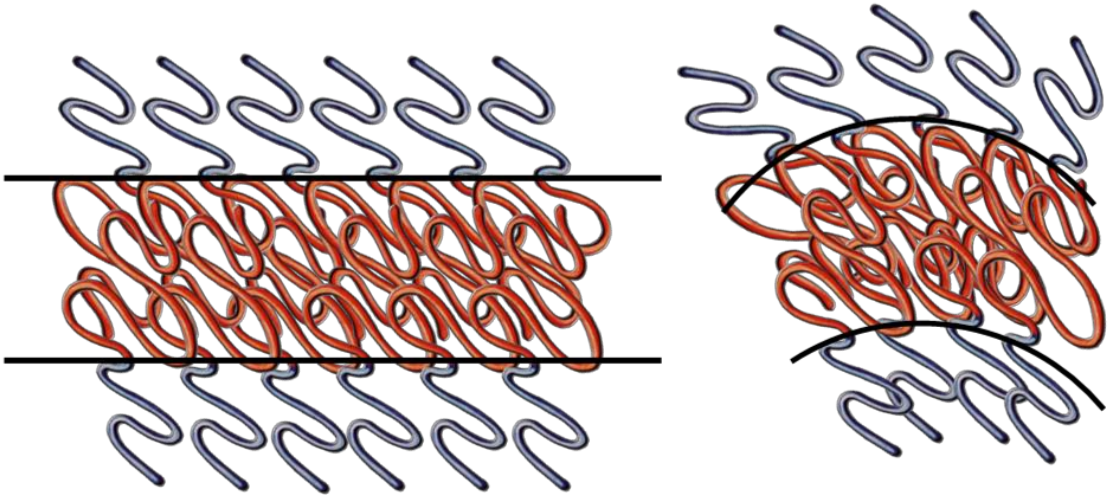

Figure 4.3: Illustration of the possible configurations by amphiphilic copolymer systems when present in an aqueous, hydrophilic environment. Blue sections are hydrophilic, whereas the red sections are hydrophobic. Through this configuration, contact with water by the hydrophobic sections is minimised. Membrane structures may also show curvature (right), in order to seal the ends of the membrane through adopting a spherical shape.

The final variable is spontaneous curvature (C_0), which is used to relate changes in curvature due to differences that can occur between the membrane leaflets. These differences can be changes in mass, chemistry or molecular geometry that arises from inconsistencies between the inner and outer surfaces of the membrane. This can be important, as the inner leaflet of a vesicle membrane experiences a higher curvature than the outer leaflet and typically is formed from fewer or different amphiphiles depending on the system. By combining these curvature variables and treating the mechanical properties of the membrane as elastic, a mathematical model of membrane curvature has been generated.[6] This is known as the “Helfrich” or spontaneous curvature model, and is used to predict the structures formed for minimal energy values. As this field of mathematics expanded, additional terms were added in and new models have been produced that help to explain other observed structures. For example, the Area-Difference –Elasticity (ADE) model expands on the idea that differences in the surface area/total mass of the leaflets drives shape transformations.[7–10] Figure 4.4 illustrates some of the structures produced,

including the biconcave disc of erythrocytes, there are many more predicted structures.[3,8,11–15]

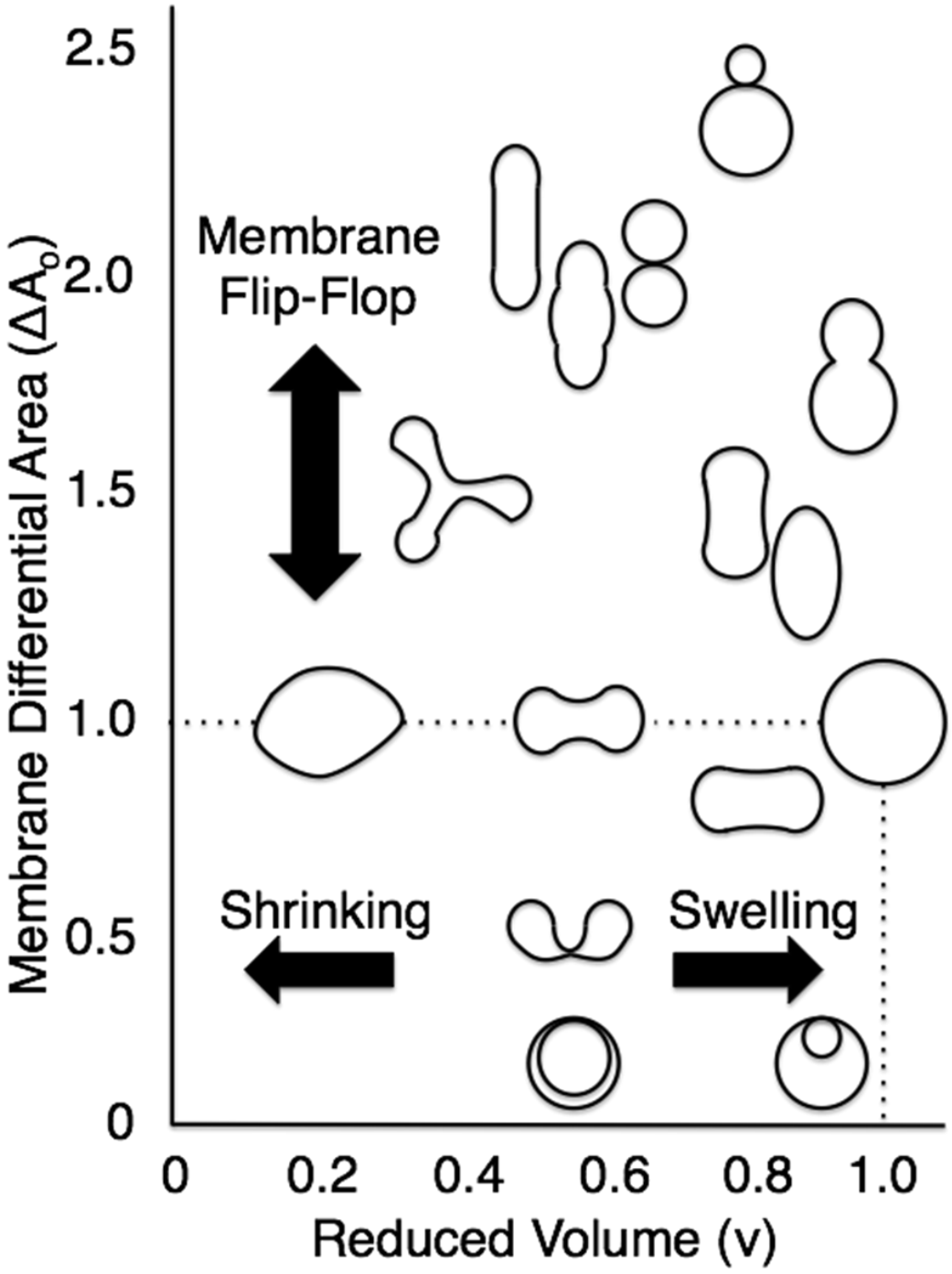

Figure 4.4 A phase diagram of the predicted shapes formed from vesicles when using the ADE model. The changes in morphology are obtained by either reducing the lumen volume and maintaining a constant membrane volume (x-axis), or by altering the bilayer mass ratio via transmembrane mass transfer but maintaining a constant internal volume (y-axis).

Many of the structures described by the ADE model have been seen in the PMPC-PDPA system, it is not uncommon to see slightly elongated polymersomes in samples. However, the main structure of interest for this

Chapter is the “donut like” vesicle and other structures with hole formations. For the purposes of topology, these “hole” structures are referred to as genus events and they contribute a specific amount of curvature to a surface. Therefore, a constant energy contribution term (equal to the number of genus events, or holes, present in a structure) can be added to the ADE model and solved to find the minimal energy states of genus structures. [16] It has also been shown mathematically that a torus (donut) with a genus of 1 is the minimal energy conformation of a sphere, which was hypothesised by Willmore in the 1960’s, [17] and a complete proof was recently published on arxiv.org. [18] Specifically, a particular type of torus known as a Clifford torus was the preferable morphology. A Clifford torus is a donut shaped structure where the radius ratio between the internal and external ring edges is measured as 1:1/√2. Furthermore, the calculation has been extended to show that structures of higher genus have an energy minima close to that of a torus. [19,20]

Theoretical models have shown that genus vesicles are a minimal energy conformation that membranes can adopt when a sphere cannot be produced or is no longer the minimal energy conformation. However, it is not well understood which of the variables is the dominating factor that drives the morphological change. Using the Helfrich model it has been shown that a torus is favoured when the model is solved for reduced membrane volume and area. However, this model only applies when the spontaneous curvature is taken to zero. [16] This would indicate that the effects of bilayer mass asymmetry or chemical differences are not required for toroid formation. However, calculations by Ou-Yang Zhong-can showed that negative spontaneous curvature stabilises the formation of torus vesicles. [21] The next section will look at the experimental formation of genus vesicles in lipid and polymer systems.

4.1.4 Lipid Genus Vesicles

The above studies investigated the production of torus vesicles and higher genus structures from a theoretical perspective. Alternatively, many publications have shown the experimental formation of genus structures, produced by a variety of methods. M.Mutz and D.Bensimon managed to produce “giant” (>4 μm) torus vesicles using a polymerisable lipid, 1,2-bis(10,12-tricosadiynoyl)-*sn*-glycero-3-phosphocholine.[22] The giant vesicles were formed via solid film hydration; the liposomes were then cooled to below their melting temperature,

whereupon a winding tubular bilayer conformation was observed.[23] At this point the lipids were partially polymerised with UV radiation for 1-10 minutes. Without polymerisation, the tubular vesicles returned to their spherical morphology upon heating back to a fluid temperature. However, with partial polymerisation, a large number of toroidal vesicles were observed upon reheating. Additionally, most of these torus vesicles displayed the radius ratio of $1/\sqrt{2}$ that is expected for a Clifford Torus. In this study, the authors hypothesise that the partial polymerisation process produces areas of spontaneous curvature, which drives the toroidal morphology. In a follow-up study, Fourcade *et al.* observed the formation of genus 1 and 2 vesicles using the same polymerisable lipid.[24] They also observed toroidal vesicles from the un-polymerised samples, however, these occurred at comparatively much lower numbers. Interestingly, a range of genus 1 particles in the un-polymerised samples were observed that are in good agreement with theoretical predictions, such as sickle-shaped vesicles. However, with the partially polymerised samples, some Clifford torus shapes as well as a few conformational variations were reported, i.e. torus shape where the hole is slightly off-centre. As a result, the authors speculated that the formation of the torus occurs during a “re-inflating” and curving process. In the partially polymerised samples, reheating of the lipid to drive the re-inflation resulted in an increase in lipid volume and the first conformation reached through increasing the molecular volume is the Clifford torus, as shown by solving the Helfrich model for reduced volume.[16]

4.1.5 Polymer Genus Vesicles

As discussed in Chapter 1, polymer amphiphiles have received a large amount of attention over the past 15 years, with some examples of torus particles formed from polymeric systems. However, many of the structures produced exist as toroidal micelles, formed by the enclosure of cylindrical micelles, [25,26] or by the controlled nucleation and growth of plate-shaped micelles.[27,28] These structures are interesting in their own right, but they are not comparable to membrane-forming genus structures. An observation of genus structures using copolymers include the striking genus that was composed of over 100 particles formed using polybutadiene-polyethylenoxide (PBD-PEO) by Haluska *et al.* [29] Through this study it was concluded that the high genus structures were produced through the generation of spontaneous curvature. This non-zero C_0 is

thought to be produced by a combination of two factors; sugar asymmetry either side of the membrane and a difference in the number of polymer molecules that make up each side of the membrane.[9]

Results

4.1.6 PMPC-PDPA Genus Vesicles

Currently, there is limited published work on polymeric genus structures and no apparent driving force behind their formation. However, a few research groups have reported the generation of spontaneous curvature as a key factor of genus structures. Previous work with PMPC-PDPA by Battaglia *et al* (see chapter 3). has not shown the formation of high genus structures. The presence of genus structures in the samples produced at low temperatures (5-15°C) rather than those produced at higher temperatures indicates that low temperature affects a variable that leads to a greater likelihood of forming genus vesicles.

As discussed in Chapter 3, PMPC-PDPA has an acid dissociation constant (pK_a) of approximately 6.5 at 25°C (Figure 4.5).[30,31] In addition to this, temperature has been shown to have an effect on the copolymer pK_a and therefore the degree of PDPA ionisation. [32] The DPA block protonation may be modulated as a function of pH and temperature. This in turn allows the overall amphiphilic nature of the copolymer to be altered based on the relative hydrophobicity of the DPA block. When fully protonated, the copolymer is hydrophilic and there is no driving force for self-assembly. Above a critical value of deprotonation the copolymer becomes sufficiently amphiphilic to begin nucleating into aggregates. Beyond this point, the degree of ionisation will decrease as the copolymer is taken further above its pKa. This shifts the copolymer to a more hydrophobic conformation, thus reducing the potential for unimer exchange.

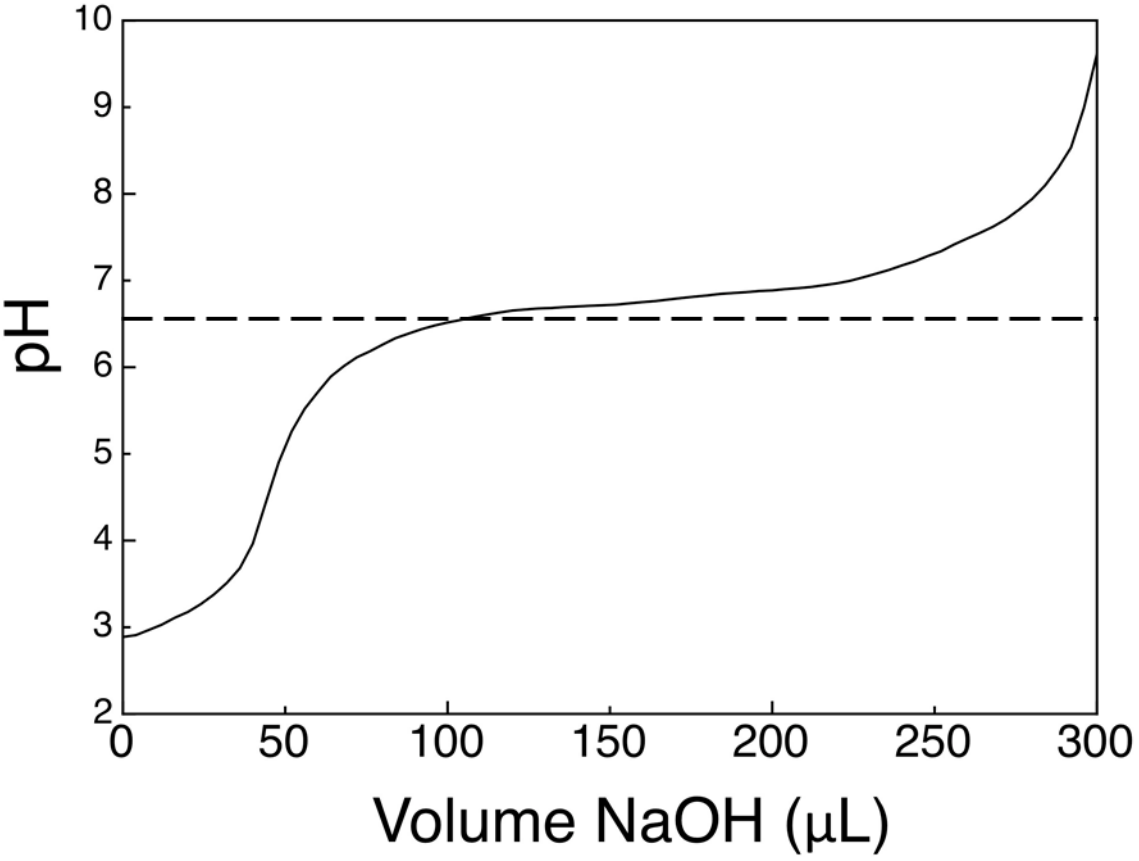

Figure 4.5: A potentiometric acid/base titration curve produced by $PMPC_{25}$-$PDPA_{94}$ at 25°C. The pK_a has been estimated to be roughly 6.5 under these conditions as indicated by the dotted line. Due to the presence of a buffer the true equivalence point is difficult to determine accurately.

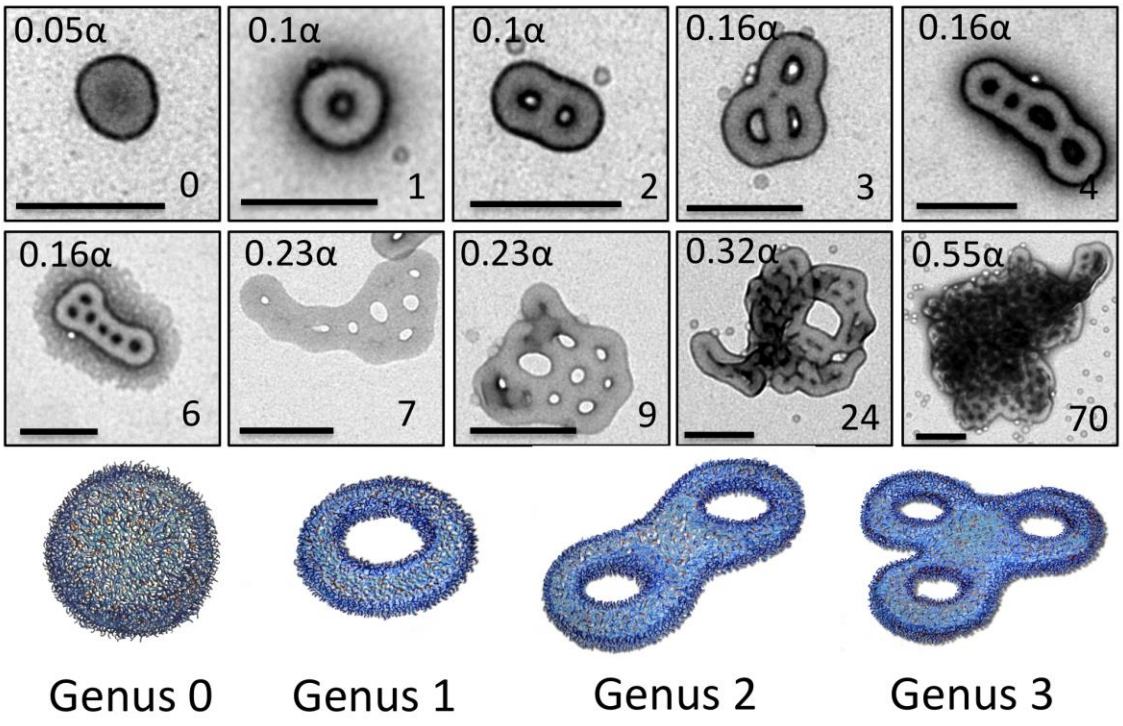

Figure 4.6: TEM micrographs showing a correlation between increasing copolymer ionisation and the genus characteristic of the polymersomes. The number at the bottom right of each

image corresponds to the number of Genus events seen. Scale bar equals 200 nm.

Through this, an increase in the size and number of genus events was observed by modulating the copolymer ionisation. Figure 4.6 shows how a range of genus assemblies and polymersomes were produced as a function of copolymer ionisation. Transmission electron microscopy (TEM) revealed a mix of spherical aggregates, easily identified as polymersomes and micelles. As the degree of ionisation was increased, larger particles were formed as seen by the increase in sample hydrodynamic diameter. This is in agreement with electron microscopy images taken, where a progression from polymersomes to larger particles was seen, displaying an increasing number of genus events.

The progression from micelles to polymersomes (Figure 4.7) is characterised by a steady increase in the amount of mass per aggregate and an overall decrease in intermolecular curvature [33]. Therefore, a degree of mass exchange and molecular reorganisation is required for this process to occur.

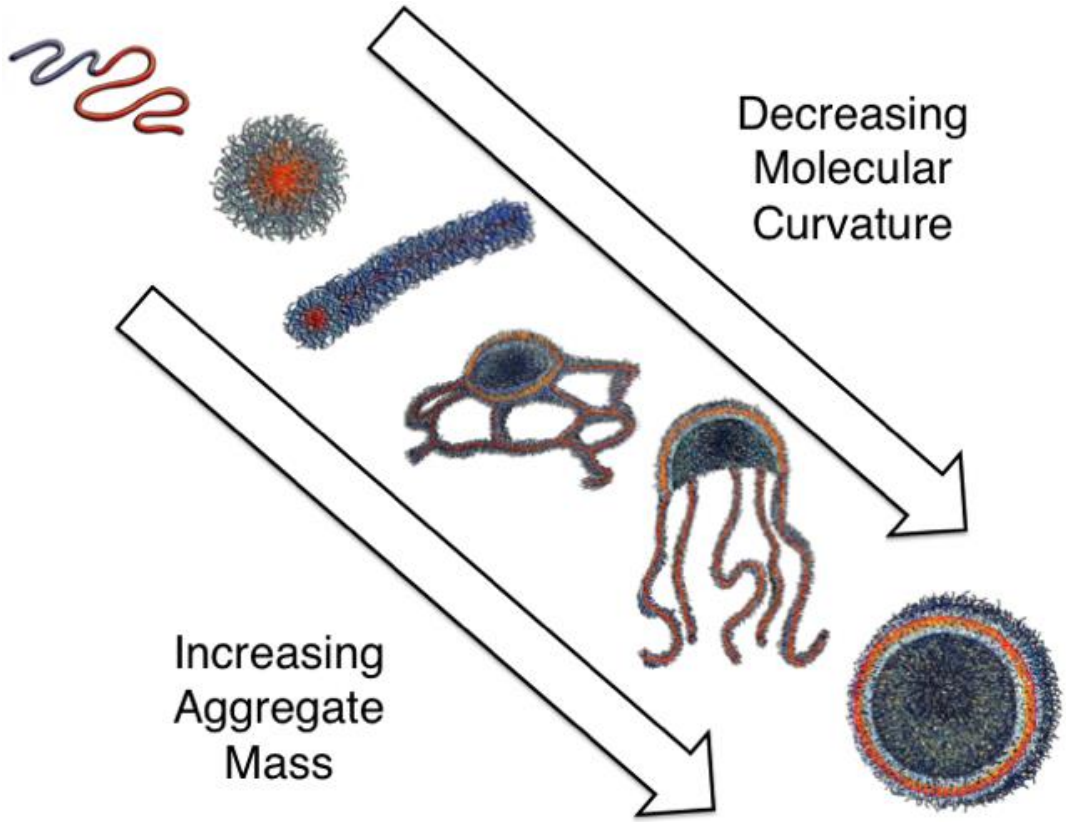

Figure 4.7: The formation of polymersomes from dispersed unimers occurs through a series of aggregates of decreasing average molecular curvature and increasing aggregate mass.

The molecular reorganisation methods adopted by membrane forming amphiphiles fall into two approaches; the first is molecular “flip-flop”, wherein amphiphiles are transferred through the membrane core and integrate into the

opposing membrane leaflet. This causes a transfer of mass from the inner to the outer surface, or visa versa. The second method is interaggregate molecular exchange. For this to occur a single amphiphile must break free from an aggregate and insert itself into the outer membrane of a neighbouring aggregate. For polymeric systems, the weakly segregated, interdigitated membrane [34] increases the entropic penalty of either process occurring, with respect to small molecular amphiphiles such as lipids or surfactants. [35–38] This penalty for releasing a unimer from a self-assembled aggregate arises by exposing the hydrophobic segments of the copolymer to the aqueous solvent. Theoretical modelling of strongly segregating diblock copolymers has shown to generate a three stage process for unimer expulsion from a micellar aggregate.[39,40]

Firstly, the copolymer must untangle and remove its hydrophobic contribution to the core. The condensed hydrophobic block must then form an interface with the aqueous solvent and finally, it must diffuse through the hydrophilic corona. The rate determining step in this process is the cost of forming an interface with the aqueous solvent, which has been calculated to equal the interfacial tension between the hydrophilic and hydrophobic block when assembled. [41] In addition, this energy barrier is increased for longer degrees of polymerisation and is highly dependent on solvent composition.[41–46] Longer hydrophobic blocks increase the surface area and the degree of entanglement, and both of these processes contribute to the energy barrier.

However, a more favourable solvent for the core forming block reduces this barrier by lowering the interfacial tension between the blocks. At higher levels of DPA protonation, water becomes a more favourable solvent. Stopped flow absorbance measurements (Figure 4.8) were used to elucidate the initial stages of aggregate assembly. Solutions of acidified copolymer unimers and sufficient NaOH to reach pH 7.5 were rapidly mixed at varying solution temperatures, which has been shown to alter PMPC-PDPA copolymer pK_a. [32]

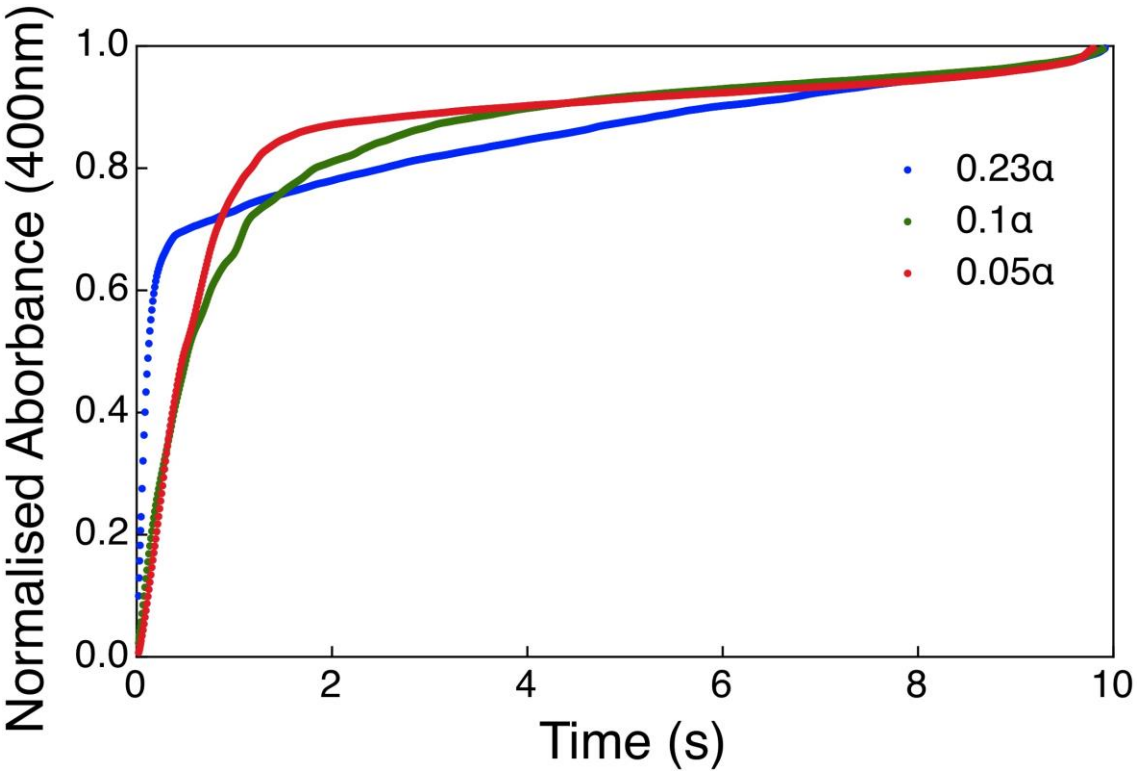

Figure 4.8: Stopped Flow Absorbance Measurements show a difference in formation kinetics at higher degrees of copolymer ionisation taken from an average of 5 measurements.

The self-assembly process resulted in the rapid aggregation of copolymer unimers, which can be characterised by a reduction in transmitted light due to elastic scattering. Samples formed at 0.23α showed distinctly different formation kinetics compared with samples produced at 0.1α and 0.05α. TEM micrographs showed that samples at 0.23α contained large numbers of genus particles, whereas for lower values of α, very few genus particles were observed. This indicates an alternate pathway for the production of genus structures, where formation occurs over slower timescales, perhaps allowing time for sufficient unimer exchange or molecular reorganisation to satisfy this non-spherical vesicular conformation. Figure 4.9 shows TEM micrographs and light scattering results of particles produced at higher degrees of copolymer ionisation. The results show that for higher degrees of PDPA ionisation, larger particles were formed with increasing genus events. Therefore, there appears to be a connection between the ionisation caused by self-assembly at reduced temperatures and the preference of producing torus vesicles or higher genus particles. As mentioned previously, one driver for the formation of torus particles is thought to be the generation of spontaneous curvature due to membrane asymmetry.

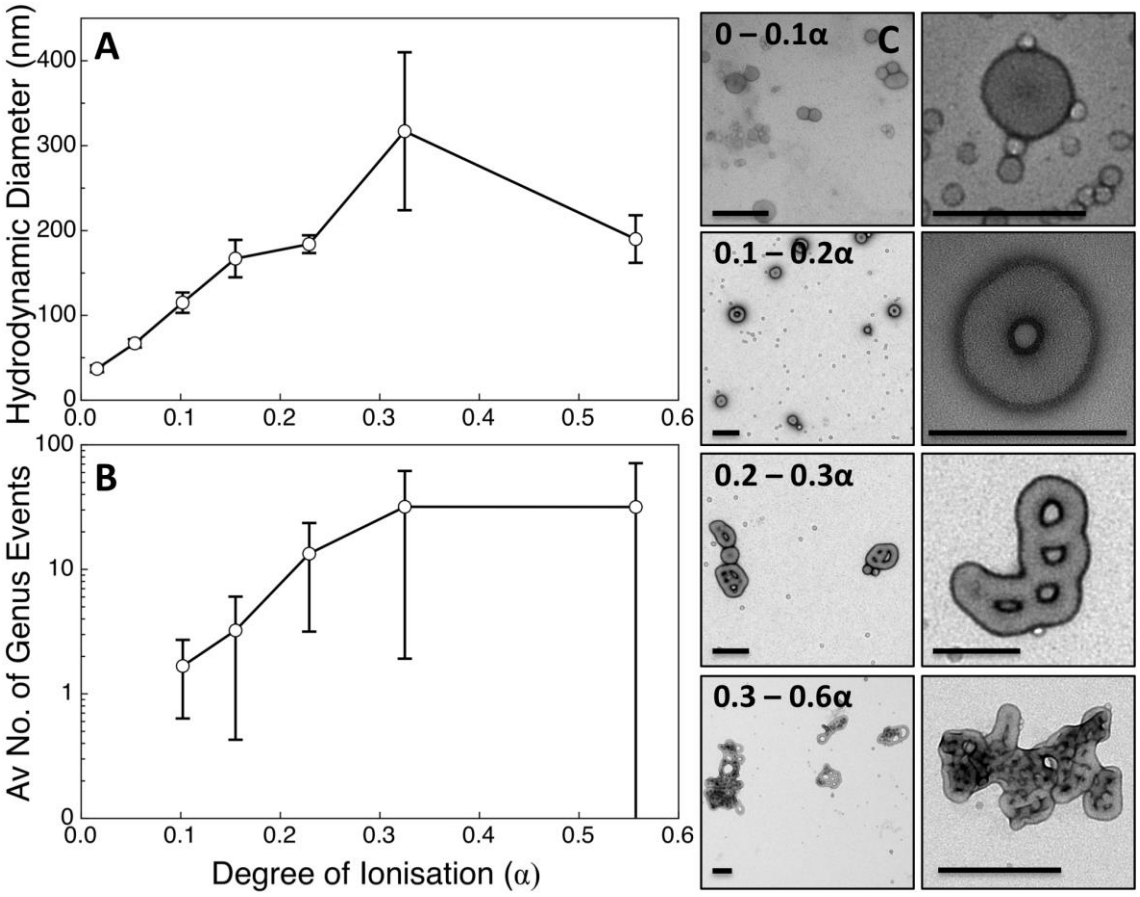

Figure 4.9: A) Average hydrodynamic diameters for $PMPC_{25}$-$PDPA_{94}$ aggregates formed at increasing degrees of copolymer ionisation. Larger aggregates are seen at greater degrees of copolymer ionisation, the polydispersity of the samples increases in a similar manner. Aggregates formed above 0.5α appear smaller than those formed 0.32α, this is due to larger aggregates sedimenting. B) Image analysis shows a rough trend of increasing average genus events per aggregate with increasing copolymer ionisation. C) Medium (left) and high (right) resolution images micrographs of samples formed at increasing degrees of copolymer ionisation. Aggregates appear to become larger, less spherical and exhibit more genus events as the degree of ionisation increases.Scale bar equals 200nm.

4.1.7 The Driving Force of Genus Formation

With the information seen thus far, a hypothesis is presented herein that the formation of genus structures is due to unimer insertion events to the outside of self-assembled structures. Insertion events create a mismatch in the mass of copolymer contained within the external surface with respect to the internal layer. An imbalance in copolymer mass between the leaflets generates spontaneous curvature and leads to the formation of genus assemblies. The greater number of unimers present at the latter stages of assembly is due to the higher degrees of copolymer ionisation at lower solution temperatures. Inherent differences can be observed between genus assemblies and spherical polymersomes, by calculating the inner and outer surface areas for each structure.

The most simple genus particle to be modelled thus is the torus. Therefore, the total mass of copolymer required to form a polymersome or a torus for a range of particle diameters has been calculated. Also, the outer and inner leaflet surface area ratio and how this scales with diameter was calculated. This was conducted as follows:

$$N_{Agg}^{Polymersome} = \frac{4\pi(r_1 + r_2)^2}{A_{Mol}}$$

Where r_1 and r_2 are the external and internal radii respectively assuming a constant torus ring thickness, A_{Mol} is the area per copolymer chain. The area ratio of the internal and external membrane surfaces can be calculated as follows:

$$MembraneAreaRatio^{Polymersome} = \sqrt{\frac{r_1}{r_2}}$$

The total surface area of a torus can also be calculated by treating it as two curved cylinders, whose radii are separated by membrane thickness:

$$N_{Agg}^{Torus} = \frac{\pi 2[(r_1^2 - r_3^2) + (r_1^2 - r_3^2 - 2tr_1)]}{A_{Mol}}$$

Where $r_3=r_1-t$, when t equals the torus ring thickness. The membrane area ratio of the torus is calculated as follows:

$$MembraneAreaRatio^{Torus} = \frac{x}{2}\left[\frac{1}{tr_3 - tr_1}\right]$$

where $x = r_1^2-r_3^2$.

Estimating the area per copolymer (A_{mol}) to be 5.9 nm^2 and the membrane thickness and torus ring thickness to be 7.9 nm and 42 nm respectively we can see how these parameters scale with radius. A_{mol} was estimated from the density and the radius of the copolymer, conducted in previous studies,[34,47,48] while the membrane thickness and toroid ring thickness were averaged from multiple TEM measurements.

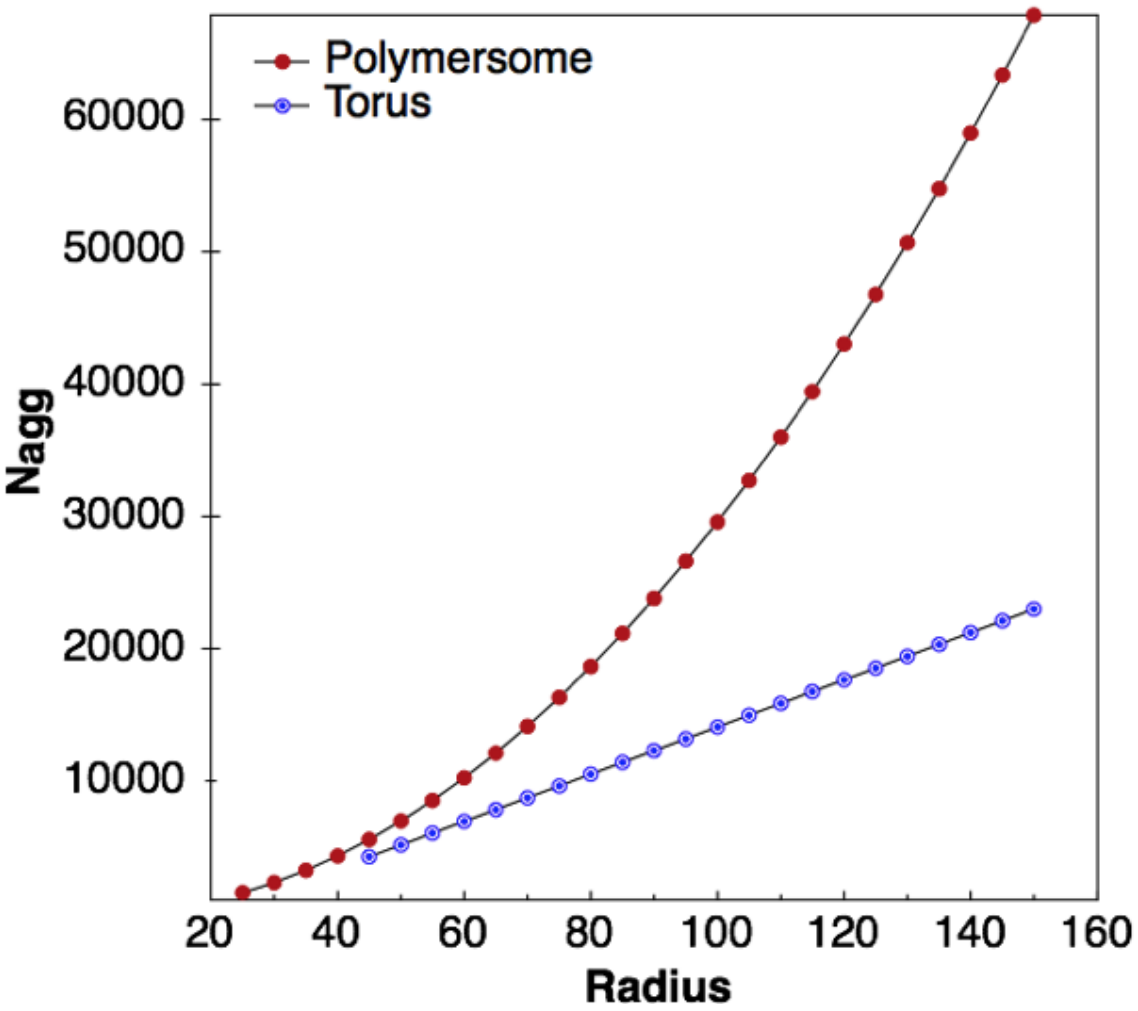

Figure 4.11: The total number of chains per aggregate for polymersomes and toroidal particles, assuming a constant membrane thickness and torus ring diameter. The torus requires consistently less material to form. This was calculated by taking the membrane volumes of polymersomes and toroidal vesicles and dividing them by a constant PDPA volume to reach the number of chains per aggregate. By conducting this calculation across a range of particle diameters and plotting the values as shown here, it can be seen that a toroidal vesicle of equal diameter requires less polymer to form when compared to its spherical counterpart. This difference becomes greater as the particle size increases.

Figure 4.12 shows that ratio of copolymer present in the outer and inner leaflets for polymersomes to tend towards unity with increasing particle radius. Assuming a constant molecular area for both the inner and outer membrane copolymers means that the inner membrane material must exhibit greater curvature per molecule. This become increasingly unfavourable for membrane forming copolymers as discussed in Chapter 1.

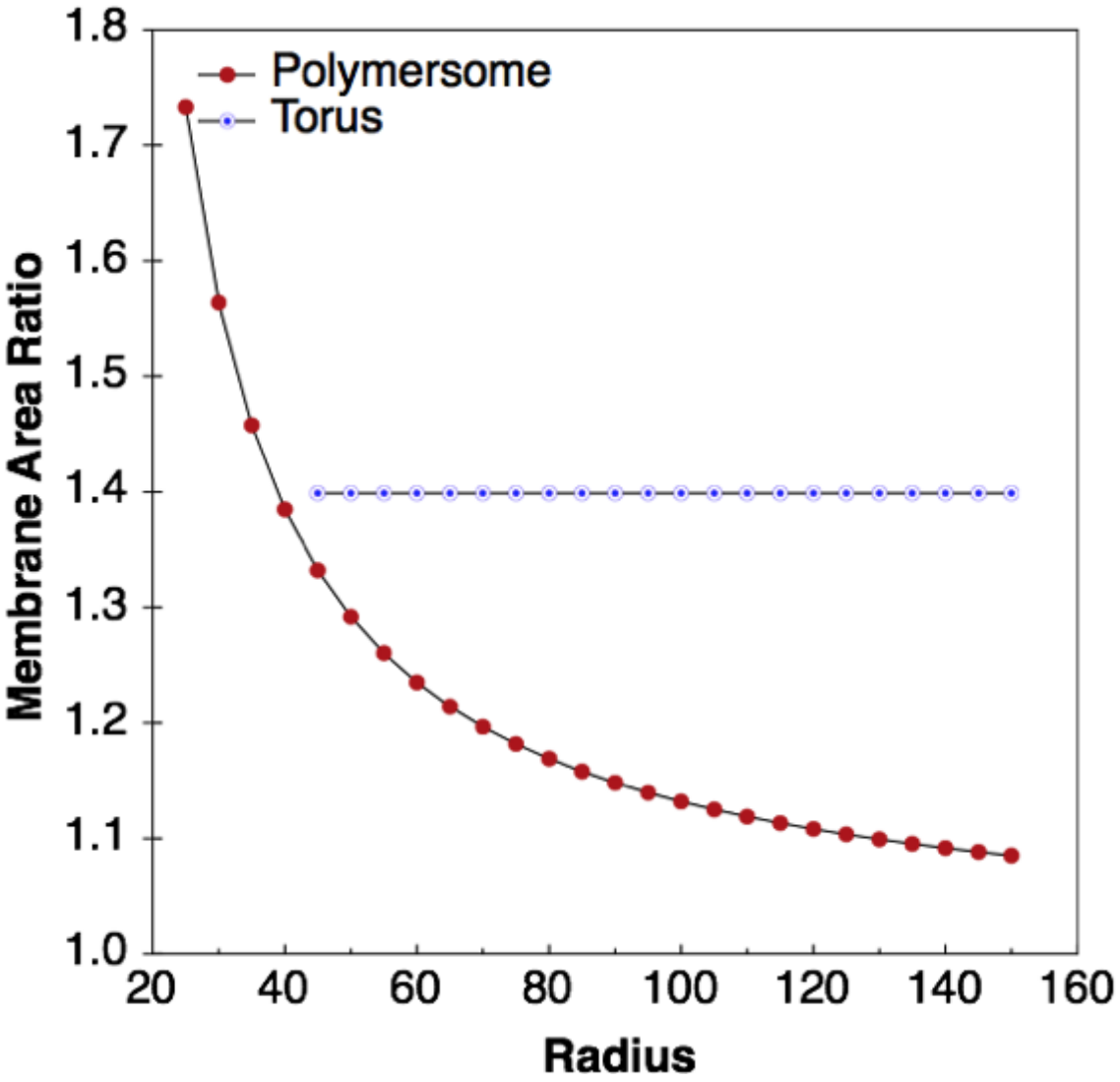

Figure 4.12: The membrane area ratios for torus particles remains constant with size. Whereas the polymersome radius ratio tends towards unity for larger vesicle sizes.

However, the leaflet ratio for the torus was maintained at 1.4:1 (outer:inner) above the critical radius of 40 nm, below which a torus with a ring thickness of 42 nm cannot be formed. Also, the mass of copolymer required to form a torus was consistently lower than that for polymersomes of equal size. This would suggest that growth via nucleation and a torus is more likely to form when less material is available. Therefore, these calculations present a potential situation where torus particles would form preferentially to spherical polymersomes, namely when there is an increased potential for bilayer mass asymmetry. Through this a hypothesis was developed; that a greater degree of PDPA ionisation leads to a higher probability of copolymer exchange, resulting in a larger amount of unimers between aggregates. As the formation process reaches an end (increase in pH), the equilibrium between aggregates and

unimers shifts towards forming aggregates, due to the reduction in copolymer ionisation. Any copolymer not already forming aggregates will either attempt to integrate with already formed structures, or it will nucleate together to form a new aggregate. The insertion of material into the outer section of the membrane creates a mismatch that drives spontaneous curvatures, resulting in genus aggregates. The extra material is unlikely to flip and transfer through the core, as the process is more energetically expensive than unimer expulsion. [37]

4.1.8 Unimer Addition

In order to test the theory of genus formation, unimers were added to pre-formed polymersomes under conditions of high copolymer ionisation. It has been observed that polymersomes and their contents are stable at refrigerated temperatures for long periods of time. [32,49] At this temperature the copolymer is partially ionised (see Chapter 3) but appears to remain assembled as per polymersomes (Figure 4.13).

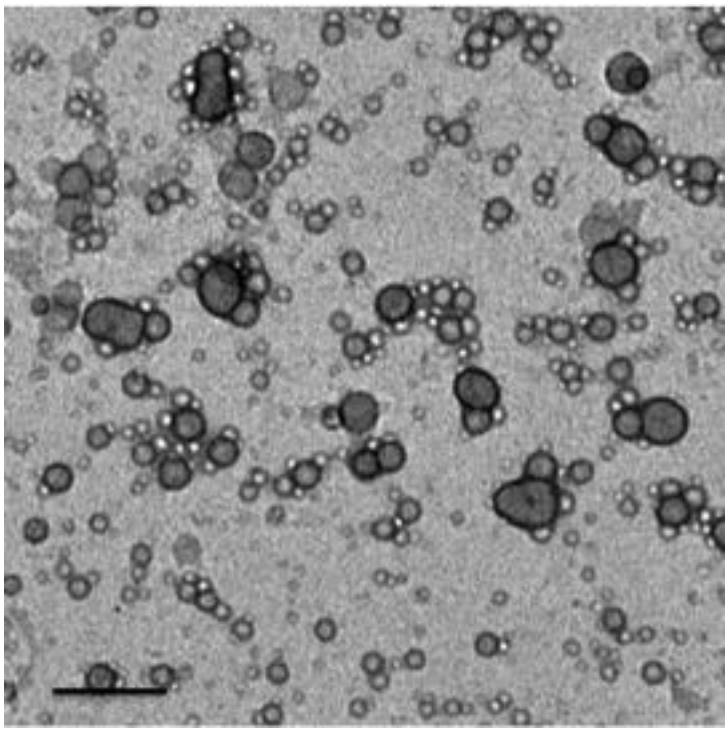

Figure 4.13: A TEM micrograph of polymersomes produced via the pH switch method and stored at refrigerated temperature for 1 month. Scale bar equals 200 nm.

Polymersomes in this study were produced by film rehydration and stirred for a minimum of one month to yield predominantly spherical polymersomes with almost no genus characteristics (Figure 4.14).

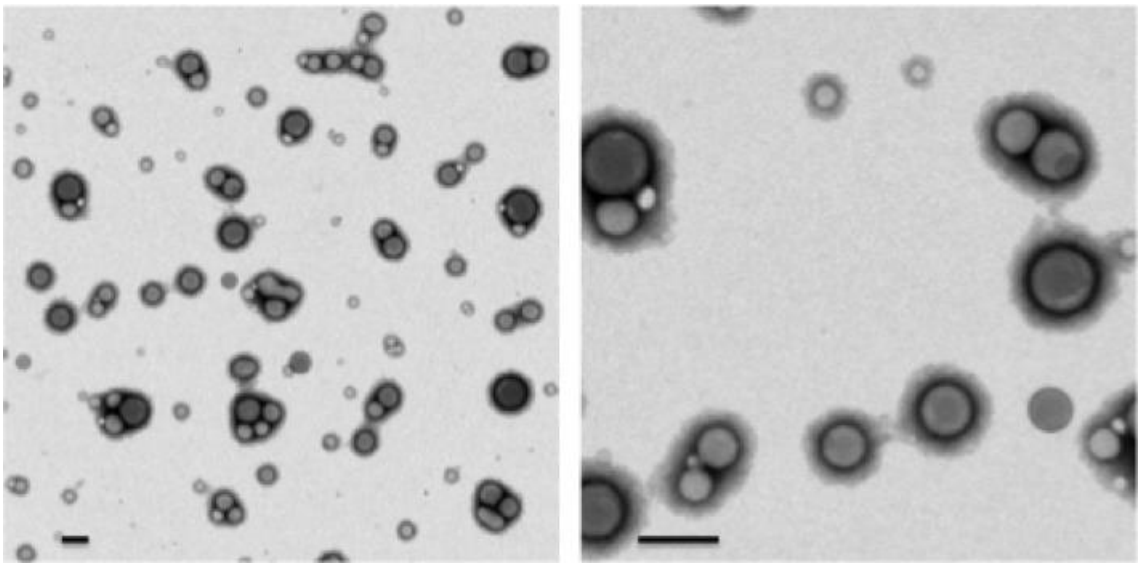

Figure 4.14: TEM micrographs of a film rehydration sample used for unimer addition experiments. A high yield of spherical polymersomes is observed. Scale bar = 200 nm.

A sample was then cooled to 1℃ and the pH adjusted to 7.2, left undisturbed for 30 minutes before returning the pH to 7.5 and heating to room temperature. No change in polymersome morphology was observed (Figure 4.15).

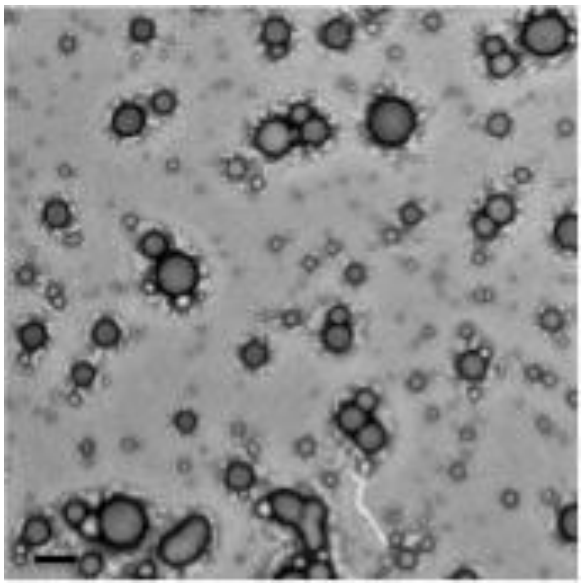

Figure 4.15: A TEM micrograph showing a sample taken down to 1°C and pH 7.2 before being corrected to pH 7.5 and ambient temperature. Very few genus features were observed. Scale bar = 200 nm.

A sample of pH 5 polymer unimers was cooled to 1℃ and brought to pH 7.2; under these conditions the polymer is still mostly ionised and the solution remains clear. Alongside this, a sample of genus free, pre-formed polymersomes (Figure 4.16 A) were cooled to 1℃ and their pH was slowly

dropped to 7.2. The polymersomes are stable under these conditions for a minimum of 30 minutes as shown in Figure 4.15.

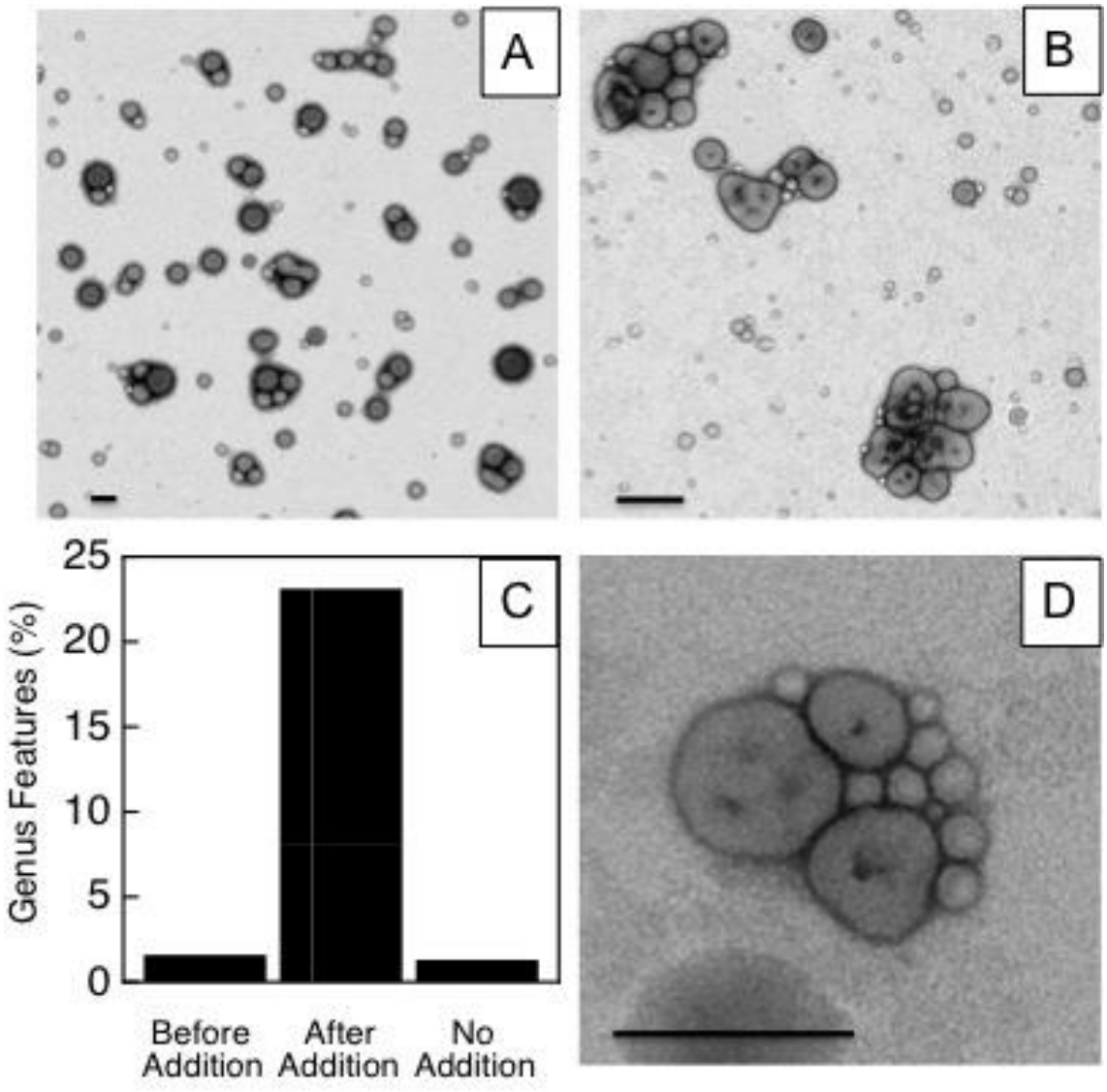

Figure 4.16: TEM micrographs show polymersomes before addition of unimers (A) and after the addition of 0.1 M ratio of unimers (B,D). The surface of some particles exhibit interesting topological features as indicated in micrograph (D). The percentage of particles demonstrating such features is shown (C), with >600 particles counted from each sample. Scale bar = 200nm.

At this point a 0.1 M ratio of unimer solution was transferred to polymersome sample. This sample was left to stir at 1℃ for 15 minutes before bringing the pH back to 7.5 and heated rapidly to reduce the polymer ionisation. The addition of extra polymer to the pre-formed polymersomes appeared to generate genus type features (Figure 4.16 B). Whilst few of the aggregates appeared to have achieved full perforation into a genus particle, many appeared to have interesting topological features such as indentations (Figure 4.16 D). Image analysis revealed that approximately 23% of particles displayed these

topological features, compared to approximately 1.5% before addition and 1.3% without unimer addition (Figure 4.16 C). The addition of extra material to the external environment of the polymersomes altered the topology of the aggregates.

These indentations resulted from an attempt to minimise the overall vesicle curvature after the generation of spontaneous curvature by a difference in bilayer mass. This spontaneous curvature is most likely formed from the insertion of unimer chains into the external leaflet of the polymersome membrane. However, these undulations do not appear to achieve full perforation of the structure, which would have resulted in a genus polymersome. The cross-sections of the particles seen in Figure 4.16 B and D more closely represent the shapes predicted by the ADE model, shown in Figure 4.4.

4.1.9 Chapter Summary

Herein, it has been shown that pH responsive copolymer PMPC-PDPA has the capacity to produce a range of intriguing structures with topological features known as genus events. There appeared to be a strong relationship between the degree of copolymer ionisation and both the size and number of genus events. The copolymer ionisation was controlled via temperature, as discussed in the previous chapter. Theoretical models for membrane systems revealed a range of shapes for enclosed membranes using the Area Difference Elasticity model. Whilst the Helfrich bending energy predicts that the torus is a minimal energy state for vesicular forming membranes, studies conducted on polymerisable lipids revealed torus vesicle formation upon heating and reassembly. Also, high genus polymersomes have been observed in a polymer system by altering the external chemical environment to induce spontaneous curvature.

The genus polymersomes produced from PMPC-PDPA more closely resemble those seen by Haluska *et al.* using a PBD-PEO system, [29] which indicate the generation of spontaneous curvature and a membrane mass imbalance. However, the addition of PMPC-PDPA unimers to the external environment of polymersomes to induce a larger mismatch in membrane leaflet mass failed to produce full genus polymersomes. This result indicates two possible hypotheses: firstly, there may be an additional factor influencing the

formation of genus events during the self-assembly process. Secondly, the structures formed from the addition of unimers may be precursors to full genus structures. Longer timescales and greater concentrations of unimers may therefore illicit full genus events.

4.2.0 References

1. Munkres, J. *Topology*. (Pearson, 2000).
2. McMahon, H. T. & Gallop, J. L. Membrane curvature and mechanisms of dynamic cell membrane remodelling. *Nature* 438, 590–596 (2005).
3. Deuling, H. J. & Helfrich, W. Red Blood-Cell Shapes as Explained on Basis of Curvature Elasticity. *Biophys. J.* 16, 861–868 (1976).
4. Massachusetts Institute of Technology. Principal curvatures of a surface. *Gallery of Minimal Surfaces* at <http://profs.scienze.univr.it/~baldo/tjs/principal_curvatures.html>
5. Catenoid. *Flickr - Photo Sharing!* at <https://www.flickr.com/photos/exploratorium/2421180181/>
6. Helfrich, W. Blocked Lipid Exchange in Bilayers and Its Possible Influence on Shape of Vesicles. *Z. Naturforschung C- J. Biosci.* C 29, 510–515 (1974).
7. Miao, L., Seifert, U., Wortis, M. & Dobereiner, H. G. Budding Transitions of Fluid-Bilayer Vesicles - the Effect of Area-Difference Elasticity. *Phys. Rev. E* 49, 5389–5407 (1994).
8. Dobereiner, H. G., Evans, E., Kraus, M., Seifert, U. & Wortis, M. Mapping vesicle shapes into the phase diagram: A comparison of experiment and theory. *Phys. Rev. E* 55, 4458–4474 (1997).
9. Dobereiner, H. G., Selchow, O. & Lipowsky, R. Spontaneous curvature of fluid vesicles induced by trans-bilayer sugar asymmetry. *Eur. Biophys. J. Biophys. Lett.* 28, 174–178 (1999).
10. Raphael, R. M. & Waugh, R. E. Accelerated interleaflet transport of phosphatidylcholine molecules in membranes under deformation. *Biophys. J.* 71, 1374–1388 (1996).
11. Mohandas, N. & Evans, E. Mechanical-Properties of the Red-Cell Membrane in Relation to Molecular-Structure and Genetic-Defects. *Annu. Rev. Biophys. Biomol. Struct.* 23, 787–818 (1994).
12. Kas, J. & Sackmann, E. Shape Transitions and Shape Stability of Giant Phospholipid-Vesicles in Pure Water Induced by Area-to-Volume Changes. *Biophys. J.* 60, 825–844 (1991).
13. Farge, E. & Devaux, P. F. Shape Changes of Giant Liposomes Induced by an Asymmetric Transmembrane Distribution of Phospholipids. *Biophys. J.* 61, 347–357 (1992).
14. Julicher, F., Seifert, U. & Lipowsky, R. Conformal Degeneracy and Conformal Diffusion of Vesicles. *Phys. Rev. Lett.* 71, 452–455 (1993).
15. Mui, B. L. S., Dobereiner, H. G., Madden, T. D. & Cullis, P. R. Influence of Transbilayer Area Asymmetry on the Morphology of Large Unilamellar Vesicles. *Biophys. J.* 69, 930–941 (1995).
16. Seifert, U. Vesicles of Toroidal Topology. *Phys. Rev. Lett.* 66, 2404–2407 (1991).
17. Willmore, T. J. & Hitchin, N. *Global Riemannian Geometry*. (Ellis Horwood, 1984).

18. Marques, F. C. & Neves, A. Min-Max Theory and the Willmore Conjecture. *Differ. Geom. Arxivorg ArXiv12026036* (2012).
19. Bauer, M. & Kuwert, E. Existence of minimizing Willmore surfaces of prescribed genus. *Int. Math. Res. Not.* 2003, 553–576 (2003).
20. Kusner, R. Estimates for the biharmonic energy on unbounded planar domains, and the existence of surfaces of every genus that minimize the squared-mean-curvature integral. *Elliptic Parabol. Methods Geom.* 67–72 (1996).
21. Ouyang, Z. C. Anchor Ring-Vesicle Membranes. *Phys. Rev. A* 41, 4517–4520 (1990).
22. Mutz, M. & Bensimon, D. Observation of Toroidal Vesicles. *Phys. Rev. A* 43, 4525–4527 (1991).
23. Yager, P., Schoen, P. E., Davies, C., Price, R. & Singh, A. Structure of Lipid Tubules Formed from a Polymerizable Lecithin. *Biophys. J.* 48, 899–906 (1985).
24. Fourcade, B., Mutz, M. & Bensimon, D. Experimental and Theoretical-Study of Toroidal Vesicles. *Phys. Rev. Lett.* 68, 2551–2554 (1992).
25. Pochan, D. J. *et al.* Toroidal triblock copolymer assemblies. *Science* 306, 94–97 (2004).
26. Zhu, J. T., Liao, Y. G. & Jiang, W. Ring-shaped morphology of 'Crew-Cut' aggregates from ABA amphiphilic triblock copolymer in a dilute solution. *Langmuir* 20, 3809–3812 (2004).
27. Huang, H., Chung, B., Jung, J., Park, H. W. & Chang, T. Toroidal Micelles of Uniform Size from Diblock Copolymers. *Angew. Chem.-Int. Ed.* 48, 4594–4597 (2009).
28. He, X. H. & Schmid, F. Spontaneous formation of complex micelles from a homogeneous solution. *Phys. Rev. Lett.* 100, (2008).
29. Haluska, C. K., Gozdz, W. T., Dobereiner, H. G., Forster, S. & Gompper, G. Giant hexagonal superstructures in diblock-copolymer membranes. *Phys. Rev. Lett.* 89, (2002).
30. Du, J. Z., Tang, Y. P., Lewis, A. L. & Armes, S. P. pH-sensitive vesicles based on a biocompatible zwitterionic diblock copolymer. *J. Am. Chem. Soc.* 127, 17982–17983 (2005).
31. Bories-Azeau, X., Armes, S. P. & van den Haak, H. J. W. Facile synthesis of zwitterionic diblock copolymers without protecting group chemistry. *Macromolecules* 37, 2348–2352 (2004).
32. Pearson, R. T., Warren, N. J., Lewis, A. L., Armes, S. P. & Battaglia, G. Effect of pH and Temperature on PMPC–PDPA Copolymer Self-Assembly. *Macromolecules* 46, 1400–1407 (2013).
33. Blanazs, A., Madsen, J., Battaglia, G., Ryan, A. J. & Armes, S. P. Mechanistic insights for block copolymer morphologies: how do worms form vesicles? *J Am Chem Soc* 133, 16581–7 (2011).
34. Battaglia, G. & Ryan, A. J. Bilayers and interdigitation in block copolymer vesicles. *J. Am. Chem. Soc.* 127, 8757–8764 (2005).
35. Shen, L., Du, J. Z., Armes, S. P. & Liu, S. Y. Kinetics of pH-induced formation and dissociation of polymeric vesicles assembled from a water-soluble zwitterionic diblock copolymer. *Langmuir* 24, 10019–10025 (2008).
36. Creutz, S., van Stam, J., De Schryver, F. C. & Jerome, R. Dynamics of poly((dimethylamino)alkyl methacrylate-block-sodium methacrylate) micelles. Influence of hydrophobicity and molecular architecture on the exchange rate of copolymer molecules. *Macromolecules* 31, 681–689 (1998).

37. Nakano, M. *et al.* Flip-Flop of Phospholipids in Vesicles: Kinetic Analysis with Time-Resolved Small-Angle Neutron Scattering. *J. Phys. Chem. B* 113, 6745–6748 (2009).
38. Nicolai, T., Colombani, O. & Chassenieux, C. Dynamic polymeric micelles versus frozen nanoparticles formed by block copolymers. *Soft Matter* 6, 3111–3118 (2010).
39. Nose, T. & Iyama, K. Micellization and relaxation kinetics of diblock copolymers in dilute solution based on A-W theory: I. Description of a model for core-corona type micelles. *Comput. Theor. Polym. Sci.* 10, 249–257 (2000).
40. Halperin, A. & Alexander, S. Polymeric Micelles - Their Relaxation Kinetics. *Macromolecules* 22, 2403–2412 (1989).
41. Underhill, R. S., Ding, J. F., Birss, V. I. & Liu, G. J. Chain exchange kinetics of polystyrene-block-poly(2-cinnamoylethyl methacrylate) micelles in THF/cyclopentane mixtures. *Macromolecules* 30, 8298–8303 (1997).
42. Van Stam, J., Creutz, S., De Schryver, F. C. & Jerome, R. Tuning of the exchange dynamics of unimers between block copolymer micelles with temperature, cosolvents, and cosurfactants. *Macromolecules* 33, 6388–6395 (2000).
43. Rager, T., Meyer, W. H. & Wegner, G. Micelle formation of poly(acrylic acid)-block-poly(methyl methacrylate) block copolymers in mixtures of water with organic solvents. *Macromol. Chem. Phys.* 200, 1672–1680 (1999).
44. Lund, R., Willner, L., Richter, D. & Dormidontova, E. E. Equilibrium chain exchange kinetics of diblock copolymer micelles: Tuning and logarithmic relaxation. *Macromolecules* 39, 4566–4575 (2006).
45. Lund, R., Willner, L., Stellbrink, J., Lindner, P. & Richter, D. Logarithmic chain-exchange kinetics of diblock copolymer micelles. *Phys. Rev. Lett.* 96, (2006).
46. Lund, R. *et al.* Structural Observation and Kinetic Pathway in the Formation of Polymeric Micelles. *Phys. Rev. Lett.* 102, (2009).
47. LoPresti, C. *et al.* Controlling Polymersome Surface Topology at the Nanoscale by Membrane Confined Polymer/Polymer Phase Separation. *Acs Nano* 5, 1775–1784 (2011).
48. Forster, S. *et al.* Lyotropic phase morphologies of amphiphilic block copolymers. *Macromolecules* 34, 4610–4623 (2001).
49. Lomas, H. *et al.* Non-cytotoxic polymer vesicles for rapid and efficient intracellular delivery. *Faraday Discuss.* 139, 143–159 (2008).

Chapter 5.1: Temperature-Induced PMPC-PDPA Polymersome Formation

Introduction

5.1.1 Objectives

As discussed in Chapter 3 there is a strong relationship between solution temperature and copolymer pK_a, which leads to the formation of unpredicted structures. The hypothesis developed in this report is that the total number of protonated amine groups in the PDPA block can be altered by adjusting the pH or the temperature. Chapter 3 mapped out the structures produced at different working temperatures, where the formation was driven by an increase in the pH. This next chapter covers an investigation into producing PMPC-PDPA polymersomes formed from a change in temperature by maintaining a constant pH during the formation process.

Results

5.1.2 Temperature/pH Relationship

To recap, temperature has a strong effect on the acid dissociation constant (pK_a) of PDPA. Specifically, the pK_a decreases on increasing the temperature. By modelling this behaviour using the Henderson-Hasselbach equation it is possible to estimate the degree of ionisation across the temperatures and pH values investigated. This approach loses its accuracy for pK_a values greater than two pH units from neutral and ignores shielding effects from being a polyelectrolyte.[1] These results are repeated for ease of reference in Figure 5.1. Please note, experimental work in this chapter was conducted using block lengths $PMPC_{25}$-$PDPA_{94}$ only.

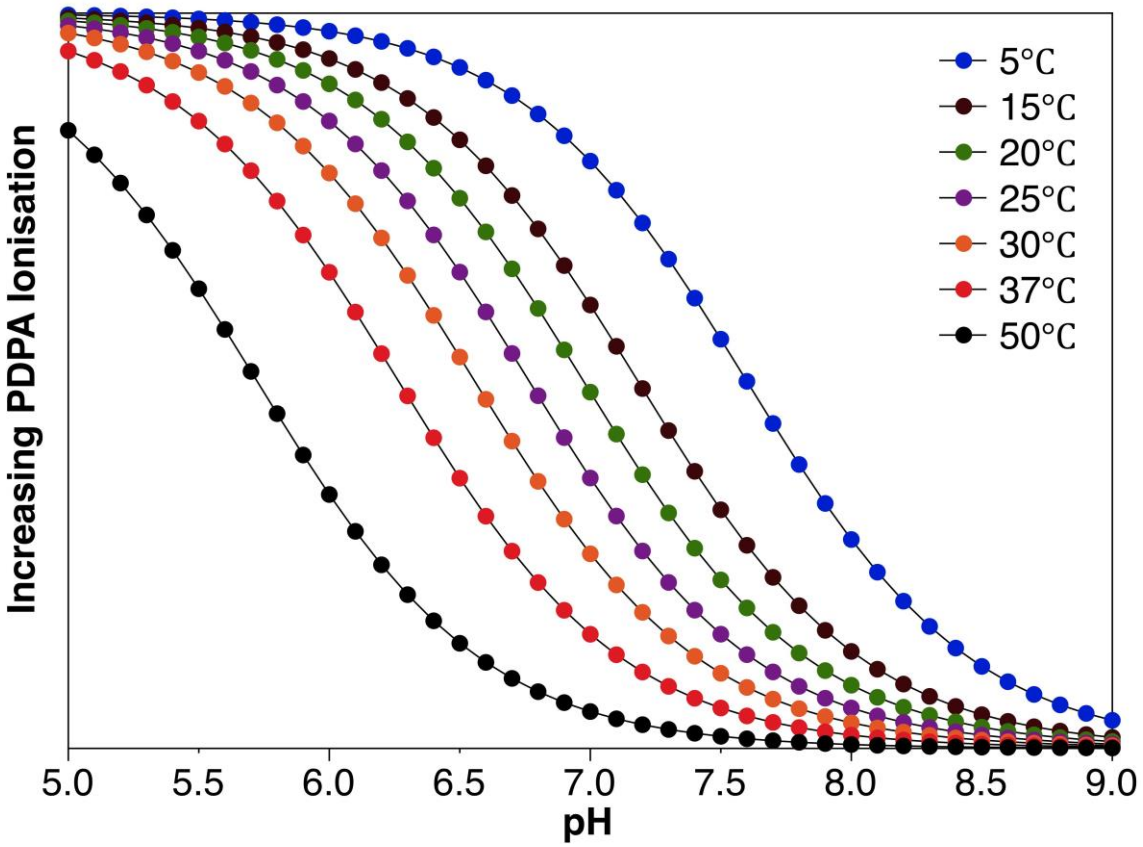

Figure 5.1: Outcomes of the Henderson-Hassalbach equation, showing the degree of copolymer ionisation as a degree of pH and temperature. There appears to be a general trend of increased copolymer ionisation at both lower sample temperatures and lower sample pH values.

As the degree of protonation is altered (either by the pH or the temperature) the DPA molecular volume changes, which results in a change in the molecular packing parameter. This idea is illustrated in figure 5.2 and supports the observations seen in Chapter 3 where polymersomes were produced at low temperatures (high PDPA ionisation and a swollen block length) by a copolymer which had been previously shown to be micelle forming.[2] The inverse was seen with the longest block length copolymer, which formed micelles at higher temperatures.

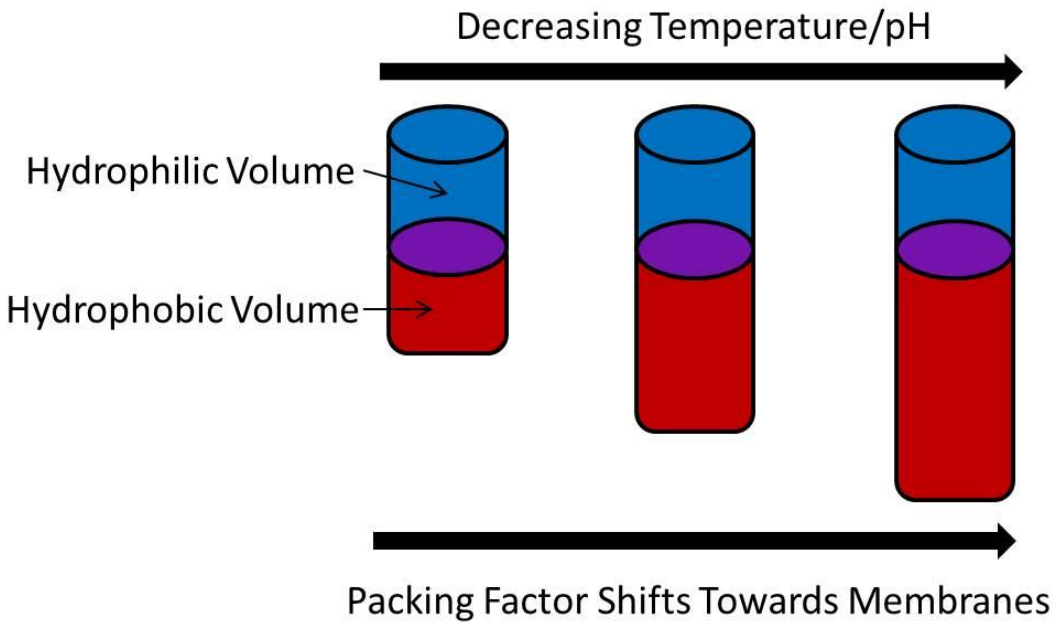

Figure 5.2: Illustration of the theory that the molecular volume is altered by the pH or temperature to produce different molecular packing factors. The change in molecular packing factor leads to the formation of different structures.

In order to explore the relationship between pH and temperature, further experiments were conducted where the pH was kept constant using a microprobe and the addition of small amounts of acid/base via a syringe driver, while the temperature was altered. Self-assembly was directly monitored using the temperature controlled Peltier device connected to a UV/Vis spectrophotometer.

5.1.3 Controlling Self-Assembly by Altering The Temperature

By cooling samples to 1°C at pH 5, it ensured that all the polymer chains existed as molecularly dissolved hydrophilic chains due to the pH being more than two units below the copolymer pK_a at this temperature. In the formation experiments covered in Chapter 3, self-assembly was accomplished by increasing the pH above the pK_a while keeping the temperature constant. For the experiments covered in this Chapter, the pH was kept constant while increasing the temperature. Increasing the temperature reduces the pK_a, thereby driving self-assembly. In order to simultaneously control the temperature and measure the assembly process, the relative absorbance of the sample was measured using a temperature controlled UV/Vis spectrophotometer. Figure 5.3 shows the baseline measurements of the PBS

and the copolymer at pH 6.6 measured at 1 °C to show the lack of scattering present at the start of the experiment.

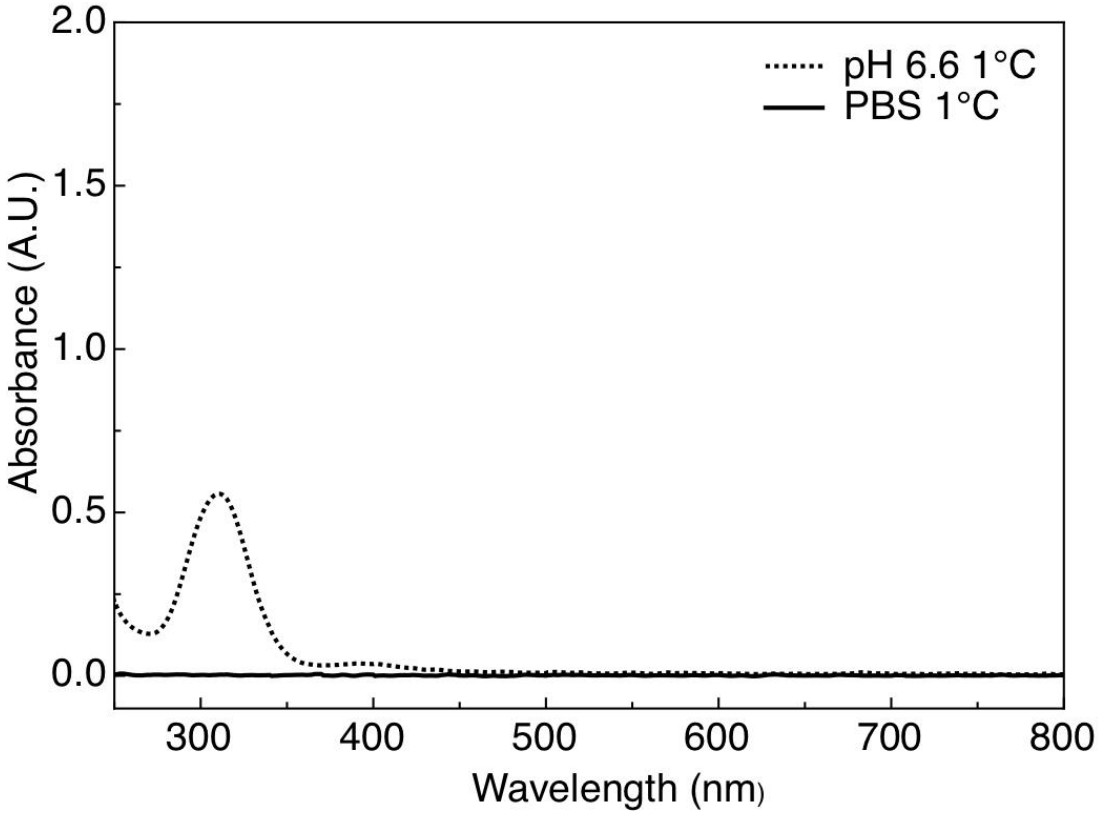

Figure 5.3: UV/Vis spectra showing the PBS baseline used and the copolymer ($PMPC_{25}$-$PDPA_{94}$) at pH 6.6 and 1 °C. The peak at 320 nm is absorbance from the copolymers' RAFT agent that remains attached after synthesis, whereas at longer wavelengths no absorption signals are observed for the background or the sample.

By increasing the temperature of the sample at a constant pH, the change in absorbance at increasing temperatures was measured. Figure 5.4 shows the spectra from 1°C to 75°C in 5°C intervals. Measurements taken between 1°C and 25°C show very similar spectra. This indicates that either the copolymer remains dispersed as copolymer chains, or that the aggregates forming are too small to produce sufficient scattering to measure via this method. Once the sample temperature reaches 30°C, an increase in absorbance is observed at longer wavelengths despite the lack of strongly absorbing functional groups in the $PMPC_{25}$-$PDPA_{94}$ copolymer. Therefore, any signal increase can be assigned to formation of structures in the sample capable of scattering the incident light. Also, the shape of the absorption spectrum is indicative of Rayleigh scattering, as Rayleigh scattering is dependent on size of structures causing the scattering and wavelength of the

incident light to inverse 4th power.[3] Scattering increases as the sample temperature is raised. Measurements were taken up to 75°C as an end point, where the spectra remained constant to the next spectra, a further two data points were taken but not shown as they were unchanged.

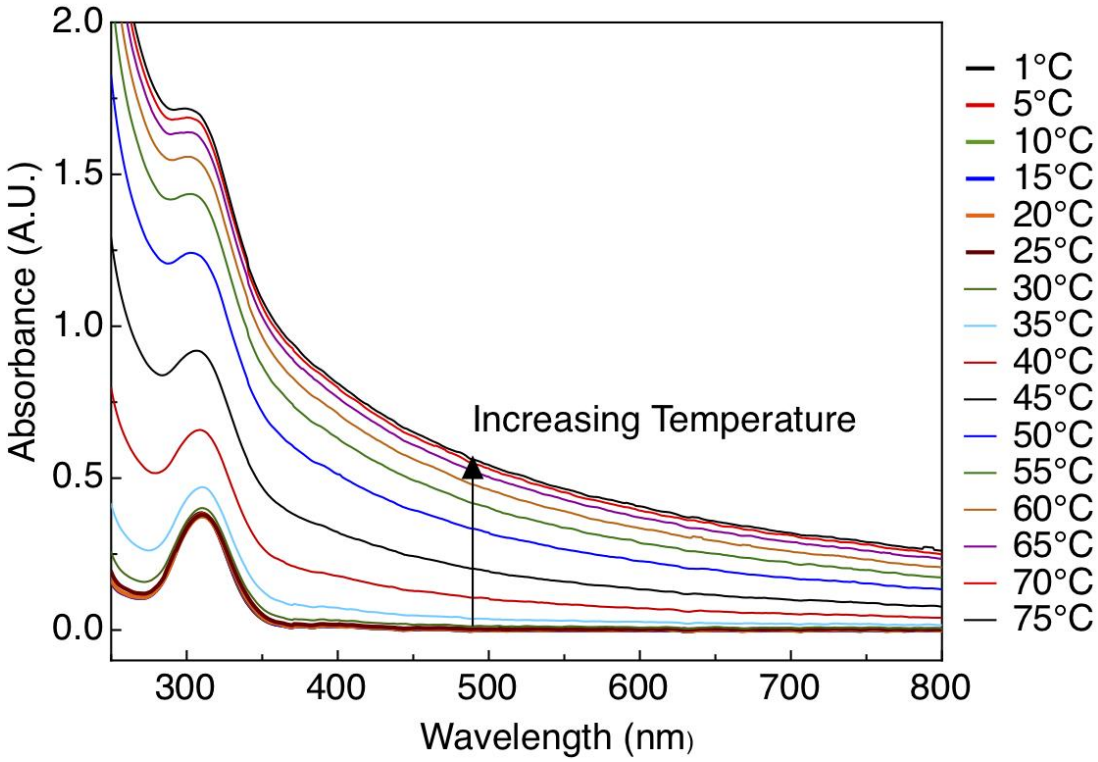

Figure 5.4: UV/Vis absorbance spectra from a pH 6.6 sample measured between 1°C and 75°C. The increase in temperature shows an increase in absorbance, which can be assigned to scattering due to the lack of chromophores and the shape of the spectra.

By taking the absorbance values at a given wavelength and plotting them against sample temperature it is possible to examine the trend in the scattering increase in more detail. Figure 5.5 plots the absorbance values at a wavelength of 550 nm, where measurements were taken at increasing temperatures up to 75°C and also for decreasing temperature to 1°C.

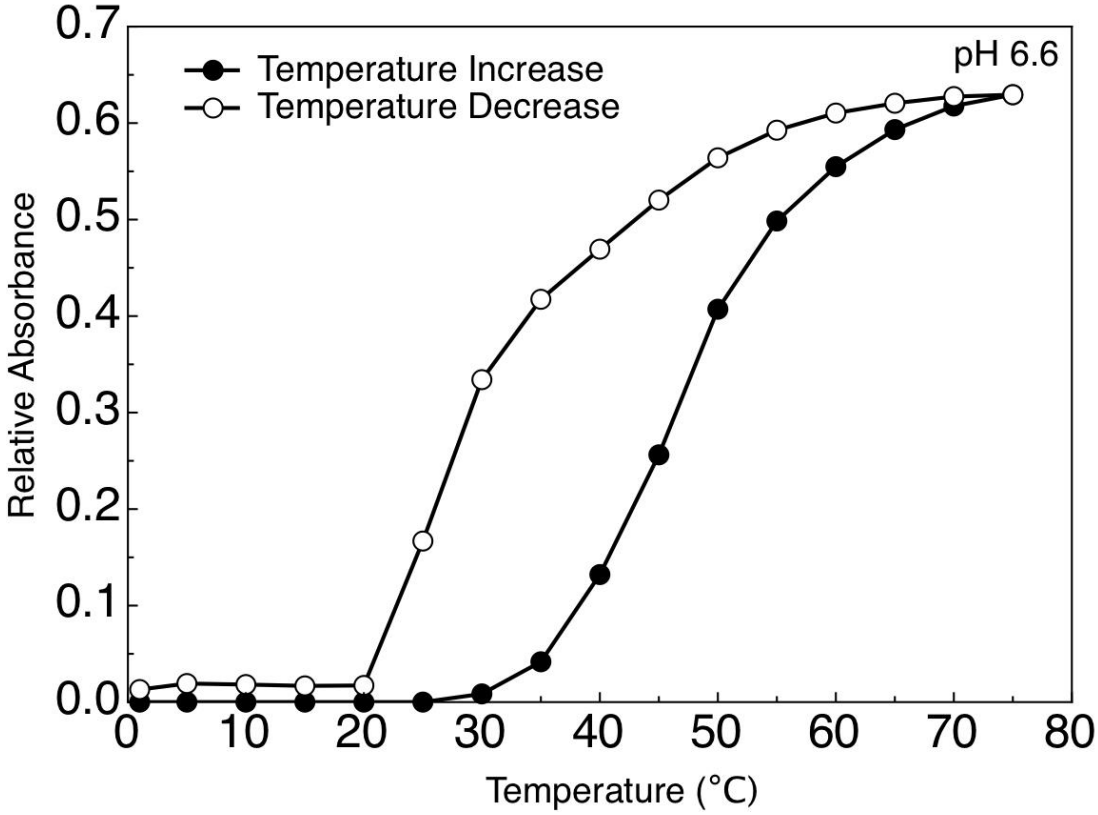

Figure 5.5: Absorbance values taken at 550nm and plotted as a function of sample temperature. At each point the sample was left to equilibrate to the temperature set for 5 minutes.

Figure 5.6 shows the relative scattering increase with temperature for samples at pH values of 6.6, 6.8, 6.9 and 7.0. Each measurement shows an increase in scattering as the sample temperature is raised and the scattering effects plateau at elevated temperatures. The point at which a measurable difference in absorbance is first observed occurs at 20°C for pH 7, 25°C for pH 6.9 and pH 6.8, and also at 30°C for pH 6.6. Additionally, the point at which a plateau is reached is different for each sample. The plateau starts at 75°C, 75°C, 60°C and 40°C for pH values of 6.6, 6.8, 6.9 and 7.0 respectively. Using the Henderson-Hasslebach equation and the pK_a estimations from Chapter 3, the degree of copolymer ionisation at these points has been roughly calculated. Taking the onset of aggregation as the increase of absorption and the corresponding plateau points as the end of aggregate formation, a rough trend showing aggregation occurring at higher temperatures for lower sample pH values can be observed.

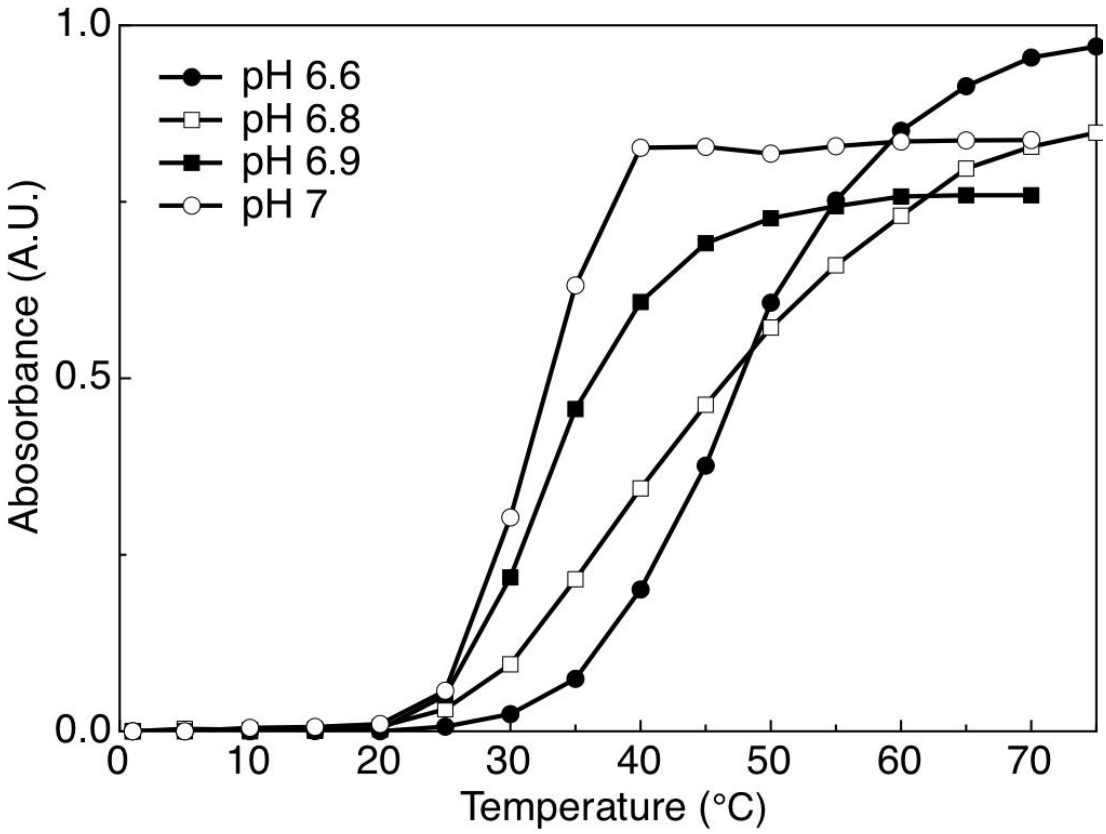

Figure 5.6: Absorbance measurements taken at 400nm for samples at pH 6.6, 6.8, 6.9 and 7.0. As the sample pH is increased the curves shift towards lower temperatures and appears to plateau at lower temperatures, as expected. Measurements were not taken when cooling for the non-pH 6.6 samples due to time constraints.

As mentioned, for the sample at pH 6.6, measurements were also taken as the temperature was taken back down to 1°C, shown in Figure 5.5. Absorbance values from the decreasing temperature measurements do not line up with the increasing temperature measurements. Decreasing temperature measurements remain at higher absorbance values than the corresponding measurements from increasing temperature samples. Absorbance values return to baseline values at 20°C, which is 10°C lower than the measurable aggregation point of 30°C. This would indicate that the individual assemblies remained larger or aggregated together over the course of the experiment, or that once formed, the polymersomes are stable at higher degrees of PDPA protonation. Without somehow sampling these points for morphological analysis it is difficult to determine the exact structures formed. Samples were not taken at different temperatures for imaging due to the inability to control the temperature for the staining and microscopy process.

However, the pH 6.6 sample was brought to pH 7.4 at 75°C after the spectra remained constant, in order to maintain any structures formed when the

sample was cooled to ambient temperatures for analysis by transmission electron microscopy. Figure 5.7 shows the presence of both vesicles and micelles, the agglomeration of the particles is mostly likely due to the less efficient stirring within the cuvette and may account for the discrepancy in absorbance values in the cooling measurements. The presence of polymersomes correlates well with the increased scattering and qualitatively there also appears to be a high amount of polymersomes compared to micelles. Unfortunately, I was unable to take sufficient images to provide quantitative data. However, from a single low magnification image it can be seen that there is a micelle to polymersome ratio of approximately 2.6:1.

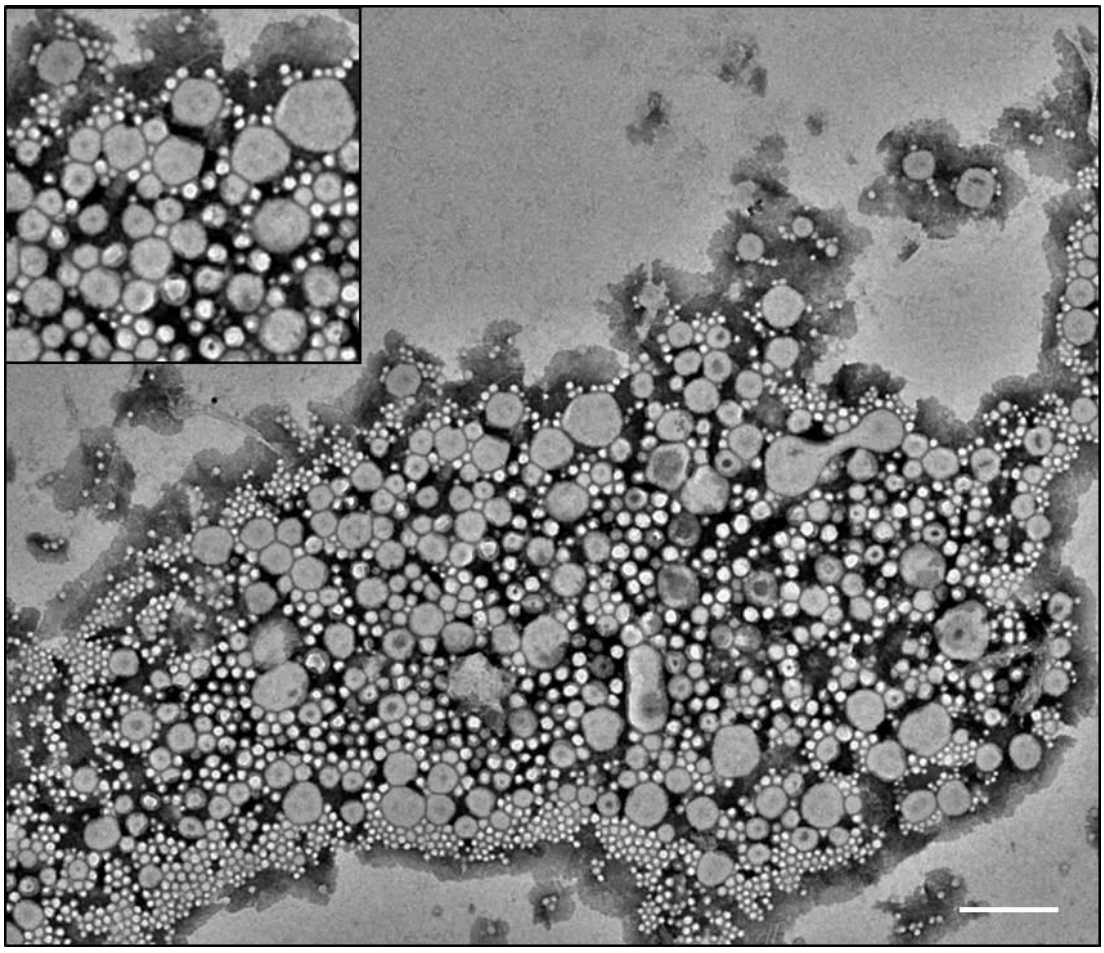

Figure 5.7: Transmission electron micrograph showing polymersomes and micelles formed by self-assembly driven by an increase in temperature at constant pH. Contrast was produced using PTA staining. Scale bar equals 200 nm.

As seen in Figure 5.7, it may be possible to form polymersomes by varying temperature, in contrast to the approach described in Chapter 3, where the formation was driven by adjusting pH. By maintaining a constant pH at low temperatures the copolymer remains ionised and therefore exists mostly as

molecularly-dissolved unimers. By raising the temperature, the pK_a decreases towards the sample pH, whereby the PDPA block becomes less protonated. Eventually the sample becomes sufficiently deprotonated for aggregation to become energetically favourable over dispersed unimers. This leads to an increase in absorbance due to scattering. The point at which scattering is first observed is between 0.415α and 0.477α for the four samples measured, indicating that between 50-60% of the polymer must be deprotonated in order for self-assembly to occur. The relatively low sensitivity of absorbance and the 5°C temperature intervals between measurements could account for some of the variation. It must also be reiterated that the Henderson-Hassalbach equation is a rough approximation of the charged behaviour of PDPA in 100 mM phosphate buffered saline. Nevertheless this is a relatively small window of copolymer ionisation.

The points at which the curves plateau are harder to accurately determine. However, the curves all appear to have begun to plateau after 0.116α. Taking these values as the boundaries, we can see that the majority of self-assembly occurs between 0.5α and 0.1α. These values provide a limit for the beginning and end points of PMPC-PDPA self-assembly in terms of copolymer ionisation. This ionisation can then be controlled by either temperature or pH to induce self- assembly. As expected, the higher the starting pH, the lower the plateau temperature, and the more shifted the curve is towards low temperatures. This is due to the sample pH starting closer to the pK_a, therefore, a smaller temperature increase is required to reach 0.1α. Figure 5.5 shows a discrepancy between the absorbance values when the sample temperature is increased (assembly) compared to a temperature decrease (disassembly). This hysteresis between assembly and the disassembly may indicate that there is an energy cost to disassembling the polymersomes. Previous work using pH jumps conducted by Shen *et al.* has shown that the disassembly process is much more rapid than the assembly.[4] This is due to the close proximity of the copolymer chains in the assembled state which causes rapid dispersion (complete in approximately 5 ms) due to repulsive forces on ionisation. On the other hand, during assembly where intermolecular attraction dominates, there is a complex reorganisation process which slows the progress from unimers to polymersomes.[4–6] Also, due to the large pH jump of pH 2 to pH 10 in the study by Shen *et al.*, the copolymer is rapidly taken between the two

environments, fully protonated at pH 2 and deprotonated at pH 10. Such a rapid pH jump drives the assembly to occur very quickly, over approximately 350 ms. Similarities in the shapes of the curves for both increasing and decreasing temperatures indicates that both processes go through the same pathways. This means that the disassembly process is not a rapid dissociation of polymer chains, as otherwise a sharp drop in absorbance would be expected. The steady nature of the curves indicates a gradual process in both directions. The hypothesis presented here is that the copolymer could have experienced the temperature change slowly, allowing for the sample to equilibrate to the ionisation at each data point.

5.1.4 Chapter Summary

In summary, it is possible to use a temperature change to drive the self-assembly of PMPC-PDPA polymersomes. This provides advantages for the encapsulation of pH sensitive cargo and provides an additional route of formation. Temperature changes may be easier to control experimentally than sample pH. In addition, scaling up the formation process would be simpler using a temperature formation process when compared to a pH change, due to problems with mixing at larger volumes. In addition temperature can be regulated externally, whilst pH requires the addition of acid/base, this is advantageous when maintaining a sterile sample environment for biomedical applications. Additional experiments involving differing DPA block lengths and pH values are needed to fully map the temperature driven self-assembly behaviour of PMPC-PDPA. However, the initial results in this chapter show a promising alternative formation process available.

5.1.5 References

1. Po, H. N. & Senozan, N. M. The Henderson-Hasselbalch equation: Its history and limitations. *J. Chem. Educ.* **78,** 1499–1503 (2001).
2. Giacomelli, C. *et al.* Phosphorylcholine-based pH-responsive diblock copolymer micelles as drug delivery vehicles: Light scattering, electron microscopy, and fluorescence experiments. *Biomacromolecules* **7,** 817–828 (2006).
3. Barnett, C. E. Some Applications of Wave-length Turbidimetry in the Infrared. *J. Phys. Chem.* **46,** 69–75 (1942).
4. Shen, L., Du, J. Z., Armes, S. P. & Liu, S. Y. Kinetics of pH-induced formation and dissociation of polymeric vesicles assembled from a water-soluble zwitterionic diblock copolymer. *Langmuir* **24,** 10019–10025 (2008).
5. Blanazs, A., Armes, S. P. & Ryan, A. J. Self-Assembled Block Copolymer Aggregates: From Micelles to Vesicles and their Biological Applications. *Macromol Rapid Commun* **30,** 267–77 (2009).
6. Blanazs, A., Madsen, J., Battaglia, G., Ryan, A. J. & Armes, S. P. Mechanistic insights for block copolymer morphologies: how do worms form vesicles? *J Am Chem Soc* **133,** 16581–7 (2011).

Chapter 6.1: Polymersome Calculations and Encapsulation

Introduction

6.1.1 Aims and Objectives

So far, this report has focused primarily on controlling the formation of PMPC-PDPA polymersomes for drug delivery purposes. As discussed in the Introduction Chapter, the size and shape of the DDS strongly impacts its effectiveness.[1] However, for DDS, encapsulation is another important variable to account for. Encapsulation is the term used to describe the entrapment of a substance inside a drug delivery system. This is desirable because the substance of interest (typically a therapeutic drug or biomolecule) is then segregated and protected from the external environment and can be delivered into a biological system. By subsequently protecting the cargo from the immune system of a particular biological system, greater delivery efficiency can be achieved.[2,3]

For polymersomes, hydrophilic molecules will reside within the aqueous lumen, whilst hydrophobic cargo will reside within the membrane. Amphiphilic molecules therefore locate themselves at either the internal or external interface between the membrane and aqueous corona. These sections of varying polarity within the same structure allow for a much wider range of molecules to be encapsulated within polymersomes than in micelles, where only hydrophobic cargo can be trapped without chemically bonding it to the copolymer. Polymersomes also offer the ability to co-encapsulate molecules of differing hydrophobicity/hydrophilicity, allowing for the simultaneous delivery of two or more compounds. To date, a range of molecules have been successfully encapsulated using polymersomes, many of which were covered in Chapter 1. Many published studies focus primarily on showing that a particular compound could be encapsulated and viably delivered to cells.[4–11]

This chapter aims to take a general approach by producing a model to assess the effectiveness of encapsulation experiments by comparing the theoretical amount of compound that could be encapsulated, with the encapsulation that was achieved experimentally. The rationale for this chapter was to improve the tools of the research group when encapsulating molecules. This approach could be of particular use for drug delivery experiments that are transitioning from a proof of concept stage to a more reproducible study.

Therefore, this chapter focuses on improving the accuracy of calculations that determine the number of polymersomes in a given sample and the amount of entrapped cargo per polymersome.

Results

6.1.2 Methods of Polymersome Loading

Prior to discussion of the probability of encapsulation, the stages of polymersome formation where encapsulation can occur should be explained. Encapsulation during polymersome formation is highly dependent on the chemistry of both the polymer and the molecule for encapsulation. For example, the thin film hydration route to polymersome formation allows for high vesicle loading of hydrophobic compounds due to them being combined with the copolymer prior to film formation. This is possible providing that the therapeutic molecules are soluble in the same solvents used to produce the copolymer film. The formation process then occurs as summarised in Chapter 1, due to the subsequent diffusion of water into the copolymer film. The hydrophobic cargo present will partition into the polymersome membrane during formation in order to avoid the incoming water. Inversely, there is a greater chance to encapsulate a hydrophilic compound when the formation process occurs from molecularly dispersed chains, especially during the final stages of formation between the formation of “octopi” or “jellyfish” and a sealed polymersome.[12,13]

The process of solvent switch formation (the replacement of organic solvent with water via dialysis) appears to generate a similar morphological route,[14,15] which would indicate that hydrophilic compounds would become trapped in the polymersome lumen as it forms. However, hydrophobic compounds may also achieve a high encapsulation efficiency using the solvent switch process, by remaining dispersed within the organic solvent which partitions into the membrane as more water is added to the system. As the solvent is removed the hydrophobic compounds would remain in the membrane. This route theoretically achieves high levels of encapsulation for both hydrophilic and hydrophobic species. Unfortunately, as mentioned previously, solvent switch production is unfavourable for biomedical applications due to the toxicity of the residual solvent.

6.1.3 Loading Efficiency

The efficiency with which a molecule is encapsulated depends on a number of variables that include concentration, solubility, charge, size, processing and stability. However, these can be split into two broad groups, variables that affect the number of polymersomes and those which modulate the chemical or physical interactions between the cargo and the polymer. Often, predicting the encapsulation efficiency is a complex procedure that requires large quantities of information about the copolymer and any molecules of interest. Herein, the general variables effecting encapsulation shall be described and a simple model for assessing encapsulation efficiency will be summarised.

In a single polymer system where all the chains form polymersomes, increasing the amount of polymer simply increases the number of polymersomes. This continues until the polymer concentration reaches a phase boundary such as packed polymersomes or interconnected tubes.[16–19] More specifically, the density of polymersomes reaches a level where they begin to impinge upon neighbouring polymersomes and pack together. At this point, polymersomes can no longer be counted as isotropically dispersed and the relationship between the number of particles and the probability of encapsulation changes. Therefore, for the sake of this discussion, only isotropically dispersed polymersomes will be taken into account. The greater the number of polymersomes that are produced, the more aqueous medium is present in the polymersome lumen.

In addition, the sizes of the polymersomes also dictate the total volume of trapped water. Simply, larger vesicles will contain greater amounts of water, for a constant membrane thickness. Calculating the internal volume of a polymersome and seeing how it scales with size and concentration allows us to visualise the optimum situation for encapsulation of a hydrophilic compound. The internal volume of a polymersome can simply be calculated as the volume of a sphere with the radius equal to the polymersome radius minus the membrane thickness. This calculation does not take into account the hydrophilic corona when using measured values for polymersome diameter.

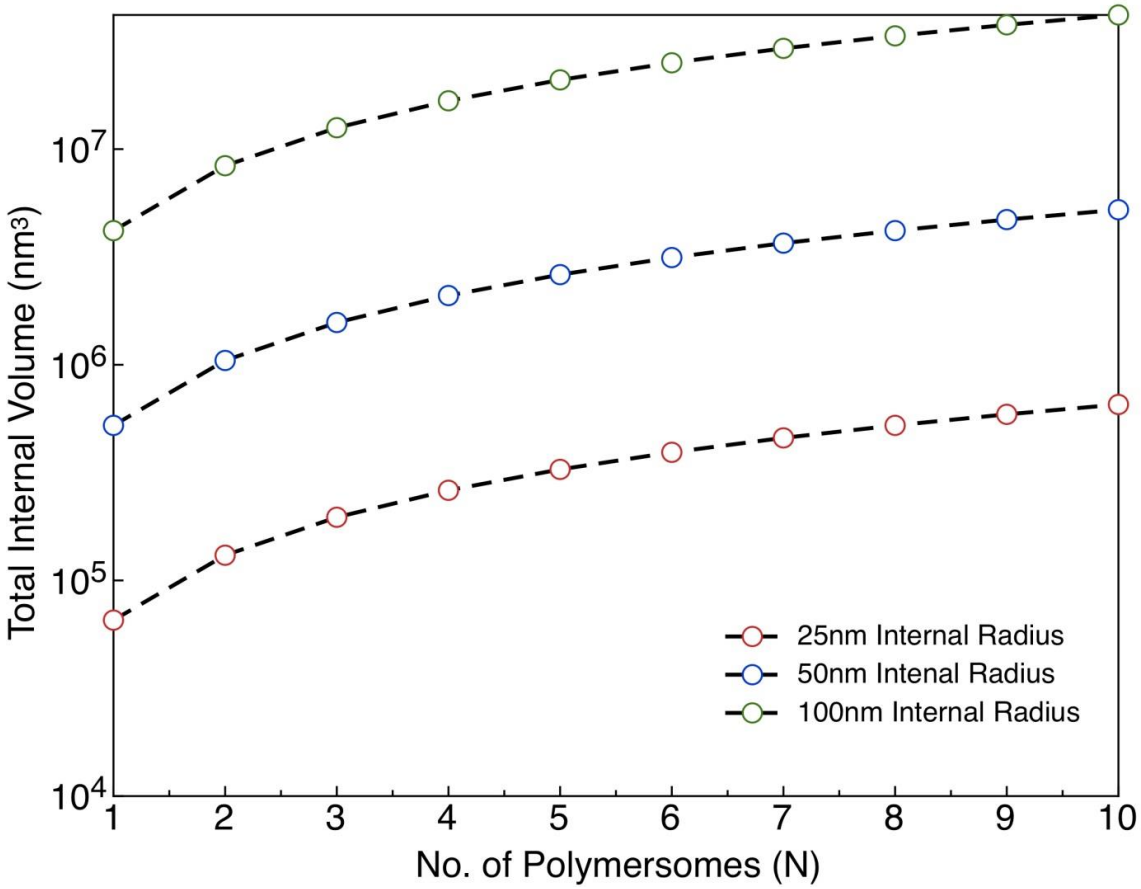

Figure 6.1: Scaling of the polymersome lumen with radius and number, illustrate that a single larger polymersome contains a greater volume of liquid in total than 10 polymersomes of half the size.

Figure 6.1 shows that larger and a greater number polymersomes result in a higher total lumen volume. Higher values for this volume contribute to more successful hydrophilic encapsulation events, assuming that the molecule for encapsulation has a much smaller hydrodynamic volume than the lumen itself. Similarly, the total amount of hydrophobic compound encapsulated would be improved by increasing the amount of polymer forming vesicles, as this increases the amount of membrane space present in the system. The volume of the membrane can be calculated as the total polymersome volume minus the lumen volume.

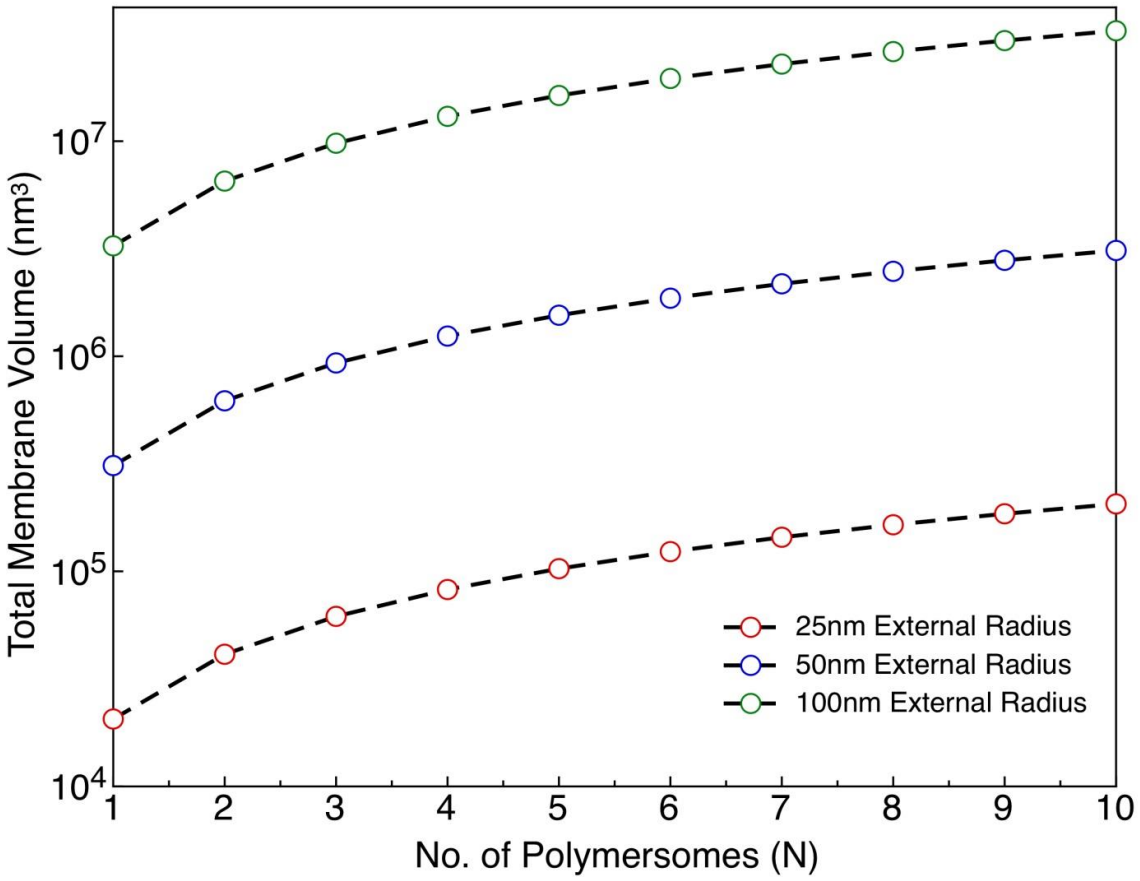

Figure 6.2: The total membrane volume follows the same relationship as lumen volume. A single larger polymersome has a greater total volume than 10 polymersomes of half the size. Overall, the membrane volume is smaller than the lumen volume.

From these calculations (at a constant membrane thickness of 8 nm as estimated from TEM measurements from previous experiments in Chapters 3 and 4) it is seen that larger polymersomes scale again more favourably for total membrane volume (Figure 6.2). Unlike hydrophilic encapsulation within the vesicle lumen, hydrophobic encapsulation may not simply scale with available volume. The hydrophobic membrane is a densely packed, entangled environment with very little space for large hydrophobic molecules to become entrapped. Also, there is likely to be an upper threshold on the amount of hydrophobe that can be stored per unit volume of membrane before disrupting the self-assembly. These limitations for both hydrophilic and hydrophobic cargos are highly dependent on the chemistry of both the polymersome and the cargo molecule. For the sake of simplicity, all molecules for encapsulation discussed here are assumed to be much smaller than the copolymer itself, i.e. << 20 kDa. Therefore, for encapsulation, larger polymersomes have a higher probability of entrapping cargo. However, for drug delivery applications it has

been observed that smaller particles with diameters between 50-100 nm are preferable. [1]

6.1.4 Calculating the Number of Polymersomes in a Sample

The previous section highlighted the impact that polymersome size has on encapsulation. However, in reality a polymersome sample will contain a range of sizes and other 'contaminating' structures such as micelles. Therefore, a more accurate approach to estimating encapsulation efficiency would be to calculate the number or percentage of polymersomes in a given sample and use this to calculate the lumen volume. This information then allows for prediction of the typical hydrophilic encapsulation. These results can then be compared to measured values to judge whether a particular processing method or compound has a positive impact on encapsulating. In order to calculate the number of polymersomes in a sample, a few pieces of information are required. Namely, the number of polymer chains present in the system, the number of polymer chains present in a polymersome of a given size and the size distribution of the sample. The number of polymer chains present in a polymersome can be calculated by dividing the membrane volume by the volume of a single PDPA block.

The molecular volume of the PDPA block was calculated by dividing the polymer molecular weight by the Avogadro constant, multiplied by the DPA density.[20,21] Using this value for PDPA, the number of chains per aggregate (polymersome/micelle/genus particle) (N_{Agg}), can be calculated for a given vesicle diameter, simply by dividing the membrane volume by the PDPA molecular volume. By applying this calculation to a size distribution of polymersomes formed by a known amount of polymer, the total number of polymersomes and therefore the total internal volume can be calculated. Dynamic light scattering (DLS) gives a gaussian distribution of particle sizes typically between 0.3 nm and 10 μm.[22] Often the results are presented as an intensity-averaged size distribution. However, the intensity of scattered light scales with particle radius to the power of 6.[23] This can cause problems with polydisperse samples, non-spherical samples or with samples of greatly differing size populations.

Due to the relationship between scattering intensity and size, samples suffering from polydisperse samples etc. give readings of a larger size

distributions than is actually the case. However, if the measurement is of a good standard, with typically two or less populations with narrow peaks, then the result can be mathematically converted into a number distribution. The Zetasizer Nano ZS DLS is able to convert the data automatically and give both the intensity and number distributions. Using a number-based distribution normalises the relative quantities of each particle population to its detector intensity. This gives a linear relationship between the numbers of particles present in each size population. For example, if the measured value for 100 nm is twice that for 50 nm then there are twice as many 100 nm polymersomes as there are 50 nm polymersomes.

The calculation to determine the number of polymersomes present can be applied to the data taken from normalised light scattering results, giving the number of vesicles at each size measurement. Using the standard conditions for the Zetasizer Nano ZS, the size distribution is split into seventy discrete size populations and the relative intensity for each size is given. Figure 6.3 shows a typical PMPC-PDPA polymersomes intensity distribution (black points) after purification, converting the measurement into a number distribution (white points) shows the relative amounts of each size population.

Using the approach described, the total polymersome internal volume of a sample can be measured. Using this volume the amount of hydrophilic compound that would ideally be encapsulated can be calculated from the compound concentration. By comparing the experimental values to the predicted ones, a measure of the effectiveness of the experimental set up is obtained. Due to time constraints, the experiment and estimations described here could not be fully validated. However, this calculation remains a tool to compare experimental set ups. For example, increasing the concentration of the drug to be encapsulated or adjusting the formation method by altering the temperature may produce different encapsulation results. This calculation provides a point of reference to measure the relative success of each encapsulation experiment, providing that the same cargo molecule is used each time.

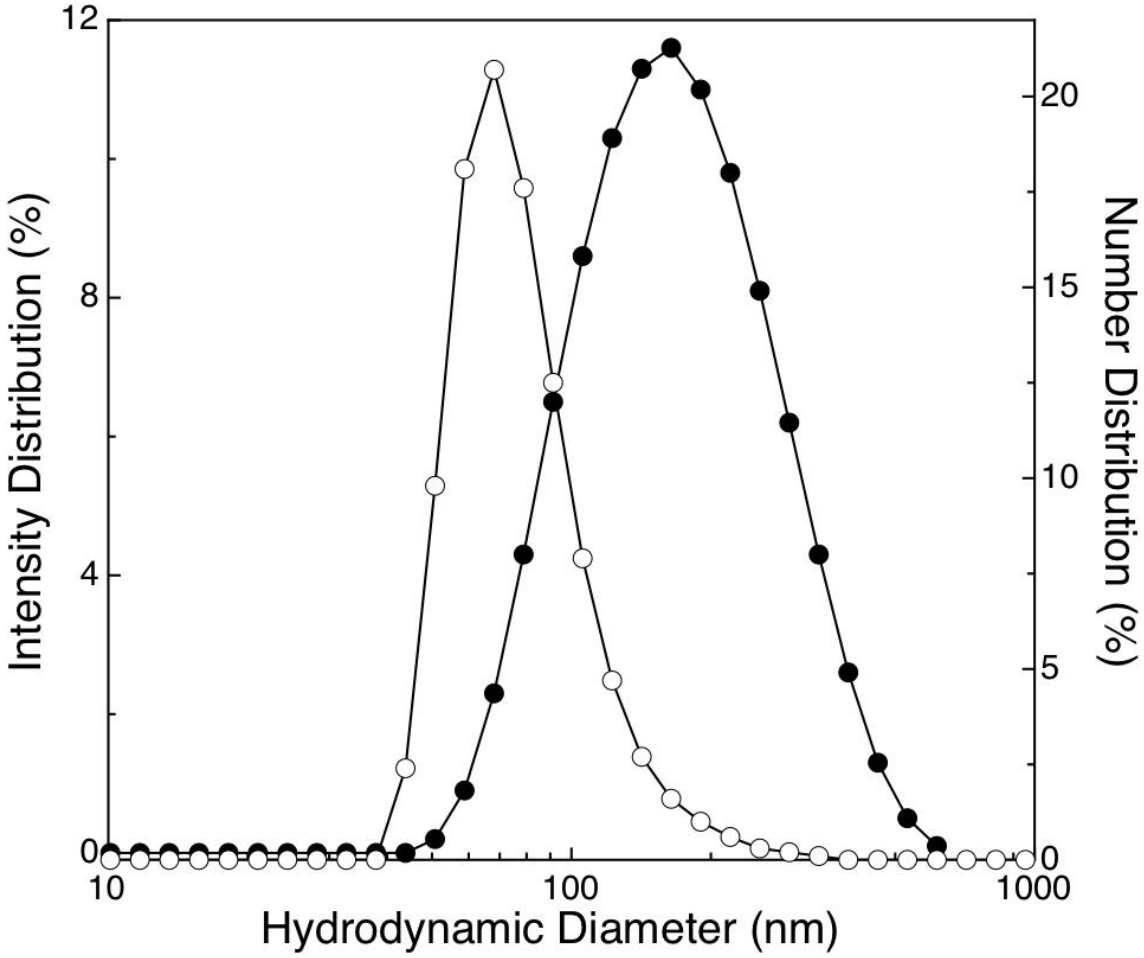

Figure 6.3: Light scattering data of PMPC-PDPA polymersomes after purification. The intensity distribution shows a single peak with a size range between 50nm and 400nm (black points). Converting the measurement into a number distributions shows the relative amounts of each sub-populations (white points). This process assumes that all aggregates are spherical.

To summarise the data so far, a calculation previously used to quantify the number of polymersomes of a set size [20,21] was applied to size distribution data to more accurately determine the number of polymersomes in a given sample. This information allows for the encapsulation efficiency to be assessed. Additionally, an estimation of the number of polymersomes in your sample, the average amount of cargo molecule per polymersome and the ratio of copolymer to cargo are all useful pieces of information for pharmaceutical studies and comparisons. The calculation makes assumptions that the molecular volume is constant and that all particles are spherical polymersomes. Therefore, the quality of the sample, in terms of being purely polymersomes, highly impacts the accuracy of the calculation. The next section focusses on improving the standard method used to purify polymersome samples in order to improve sample quality for calculation.

6.1.5 Polymersome Purification

The results shown in Figure 6.3 were purified so that any un-encapsulated cargo, micelles and large aggregates were removed. This is an essential step, as the calculations described here work on the assumption that there are no micelles present in the system and that the light scattering distribution data is representative of the particle population distribution. For the approach of producing polymersomes for drug delivery applications, the formation of a micelle is a waste of copolymer and also reduces the efficiency of the production process. In addition, as mentioned in the experimental section, light scattering measurements are biased towards larger particle diameters. Therefore, in a PMPC-PDPA sample with a combination of micelles (typical diameter ≈ 30 nm) and polymersomes (typical diameter range from 50-250 nm) the micelle fraction can be underestimated during the conversion from intensity distribution to number distribution. To correct for this potential problem when calculating the number of polymersomes, the micelles must be removed from the system.

In order to correct for the presence of micelles mathematically, many assumptions must be made and light scattering data across a large concentration range should be conducted for each sample. Another approach is to physically remove the micelle fraction of the sample prior to light scattering analysis. In order to achieve this, size exclusion chromatography (SEC) was used. Due to a greater number of routes through the stationary phase available to smaller particles, these have a longer path length compared with larger particles and will exit the chromatography column after the fraction of larger particles has been collected. SEC therefore allows for size distributions to be separated out by collecting fractions at different time points.

6.1.6 Size Exclusion Chromatography Methodology

Size exclusion chromatography was conducted using a stationary phase of sepharose 4B gel with a bed volume varying from 20 cm^3 to 25 cm^3. Originally, bench top columns with a flow rate dictated by gravity (approximately 0.5 ml/min collected dropwise) were used to assess separation, then later on a more refined system using a chromatography pump and fraction collector was used. The approach was utilised to assess the distribution of polymersomes and micelles, alongside the encapsulation of detectable molecules. For a typical

bench-top SEC column, the amount of sepharose that a sample is subjected to alters the total surface area for separation.[24] Varying degrees of sample separation can be achieved by altering the sample volume or the sepherose volume, within the limits of the set up. These limits are usually defined by positive or negative interactions between the sample and stationary phase, the size difference between the populations to be separated and the pore size of the sepharose used.

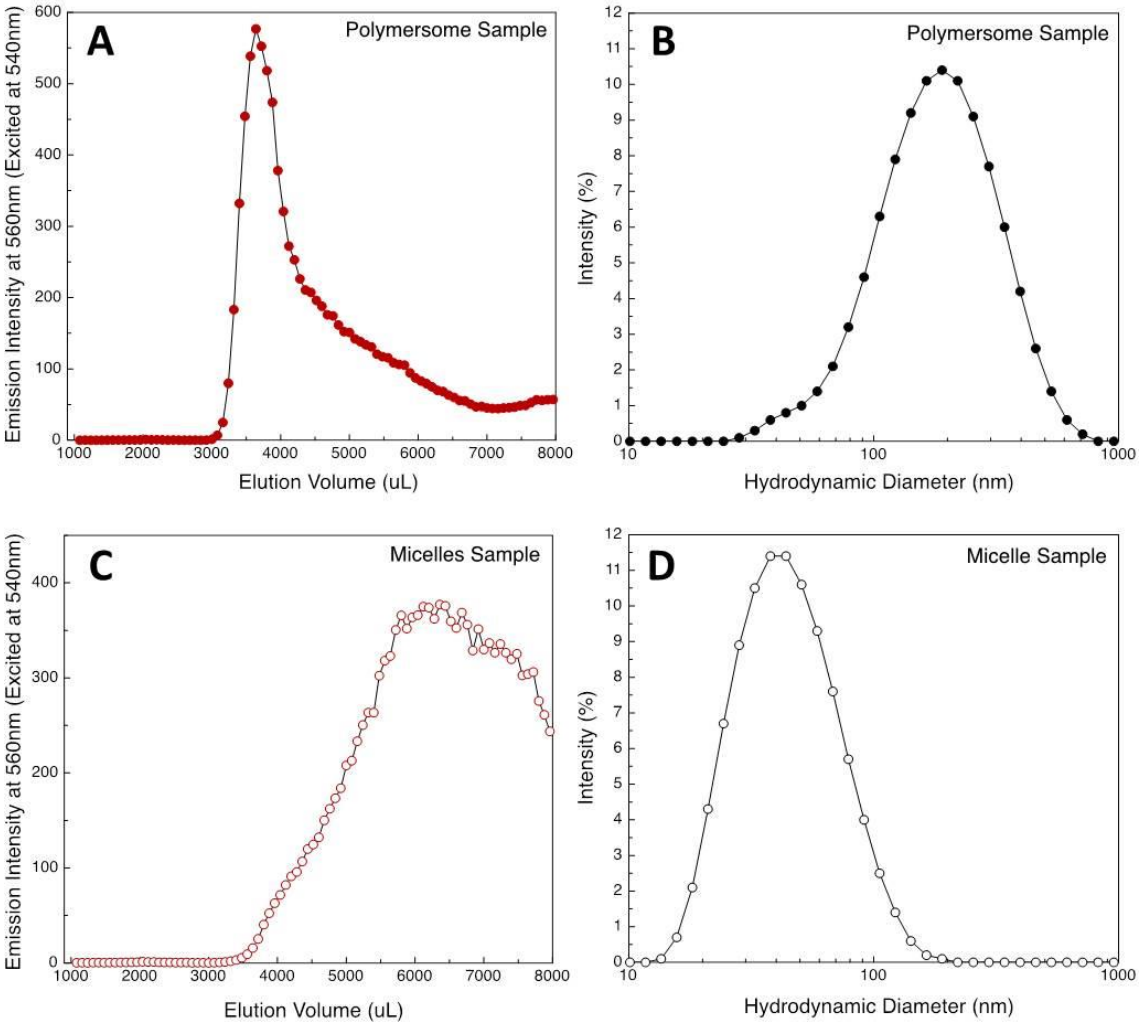

Figure 6.4: Samples were separated using a bench top size exclusion chromatography column with sepharose 4B stationary phase. A and B show the column separation and size distribution of a sample of polymersomes. C and D show the column separation and the size distribution of a sample of micelles. The majority of the polymersomes (>100 nm) leave the column between 3-5mL of elution volume, whilst the micelles (<50 nm) emerge between 5-7.5mL.

The use of these bench-top columns for polymersome purification has the advantages of being versatile to sample volume and easily sterilised. Therefore, depending on the sample volume, different columns can be produced to meet the individual requirements of the user, whether the

requirements are scaled up purification, or analysis of a preparation method or encapsulation procedure. However, these columns are susceptible to user errors and show only moderate separation resolution of micelles from polymersomes. In Figure 6.4, two samples were used to show the separation efficiency of the bench-top column, one was PMPC-PDPA polymersomes made under ambient conditions and the other was produced at 50°C to produce a micelle only sample. There is a clear separation of the two populations, however, as mentioned, this manual approach lacks reproducibility.

In order to gain more control and reproducibility, an automated SEC system was set up. As shown in Figure 6.5, a sealed column with a bed volume of 22 mL was attached to a chromatography pump for controlled flow rates (0.339 mL/min) to create a SEC using a High Pressure Liquid Chromatography system (HPLC-SEC). Online fluorescent and absorbance measurements were obtained and a fraction collector was utilised to isolate samples of interest (Figure 6.6). This approach generated a more efficient separation of micelles and polymersomes. The system was also used to separate genus structures from micelles, which would allow for biological studies to be conducted on genus only samples (Figure 6.7). However, only 50 µL of polymersomes at a polymer concentration of 0.25 mg/mL could be injected, meaning that purification of a typical sample (1-3 mL, at 1-10 mg/mL) would take a long time to process. In addition, maintaining sterility with the HPLC equipment is more challenging than the bench top columns, which fit easily into sterile flow cabinets.

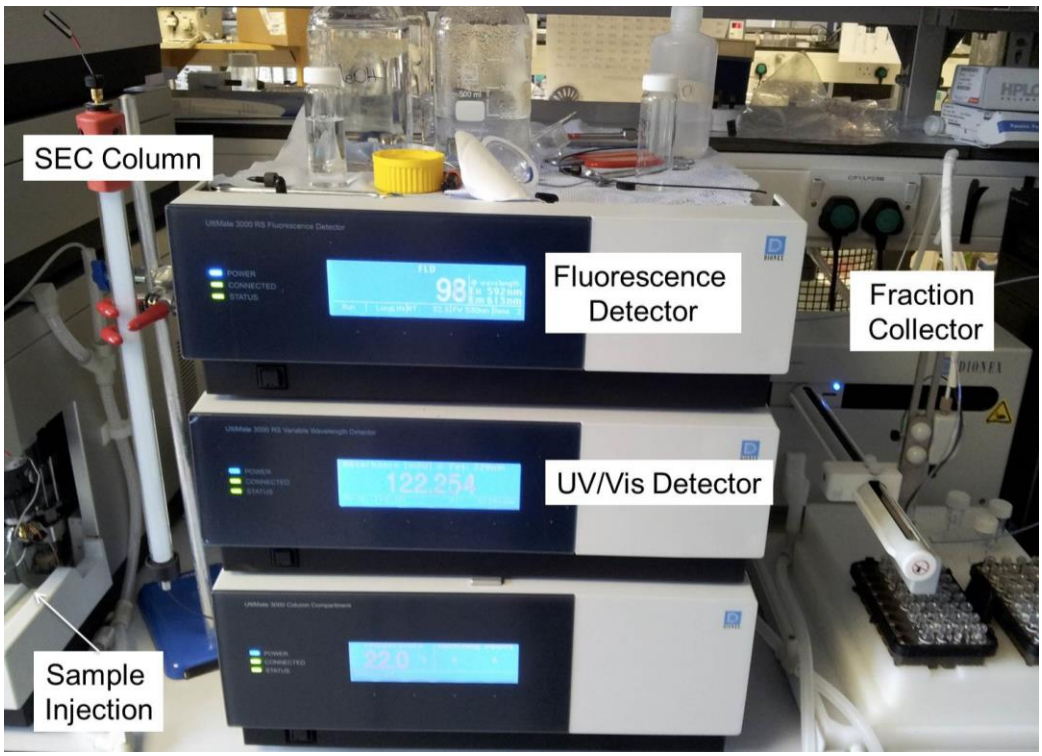

Figure 6.5: A packed SEC column was connected to the HPLC detectors and fraction collector as shown above. Measurement time was 70 min plus 30 min continuous phase between each run to ensure a flat baseline.

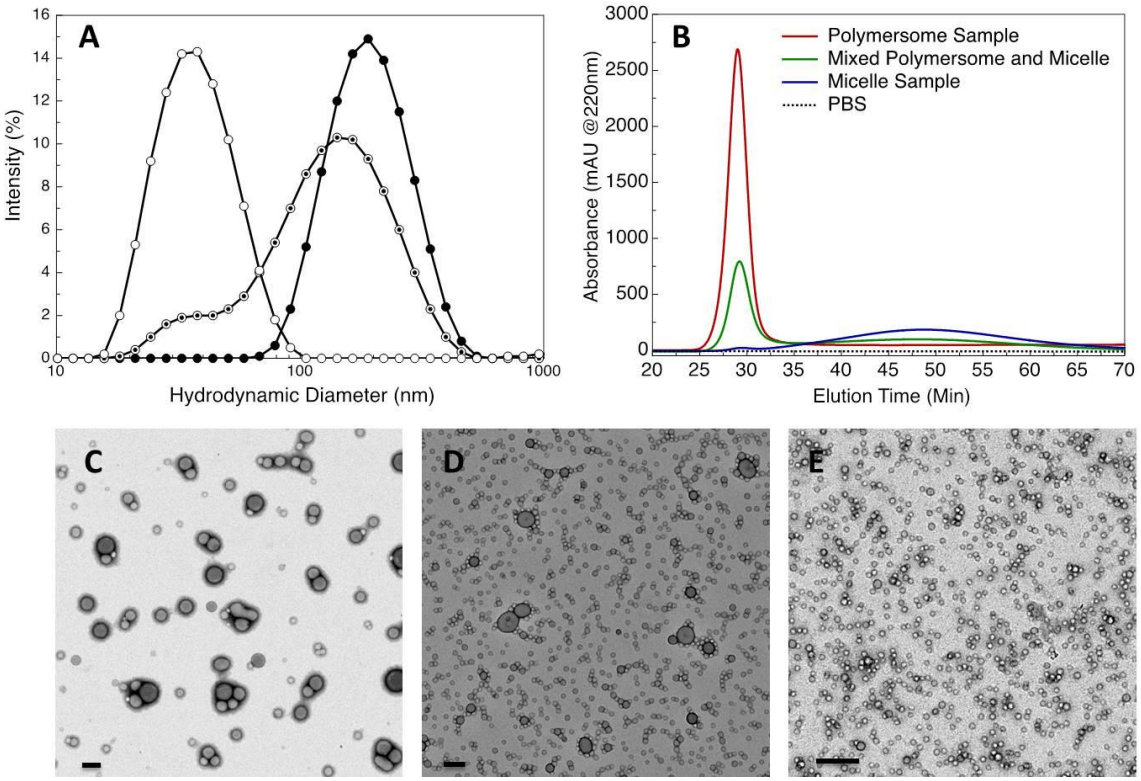

Figure 6.6: A) Light scattering measurements showing the size distributions of the three samples used to test the automated SEC system. The black points correspond to the polymersome sample and the white points correspond to the micelle sample. The mixed points show the distribution of a mixed polymersome and micelle sample. B) SEC traces using an absorbance detector. Two distinct populations can be seen with a good separation, the first between 25-32 minutes and the second between 35-65 minutes. C), D) and E) show the electron micrographs of the polymersome, mixed polymersome and micelle and micelle samples respectively prior to separation. Scale bar equals 200 nm.

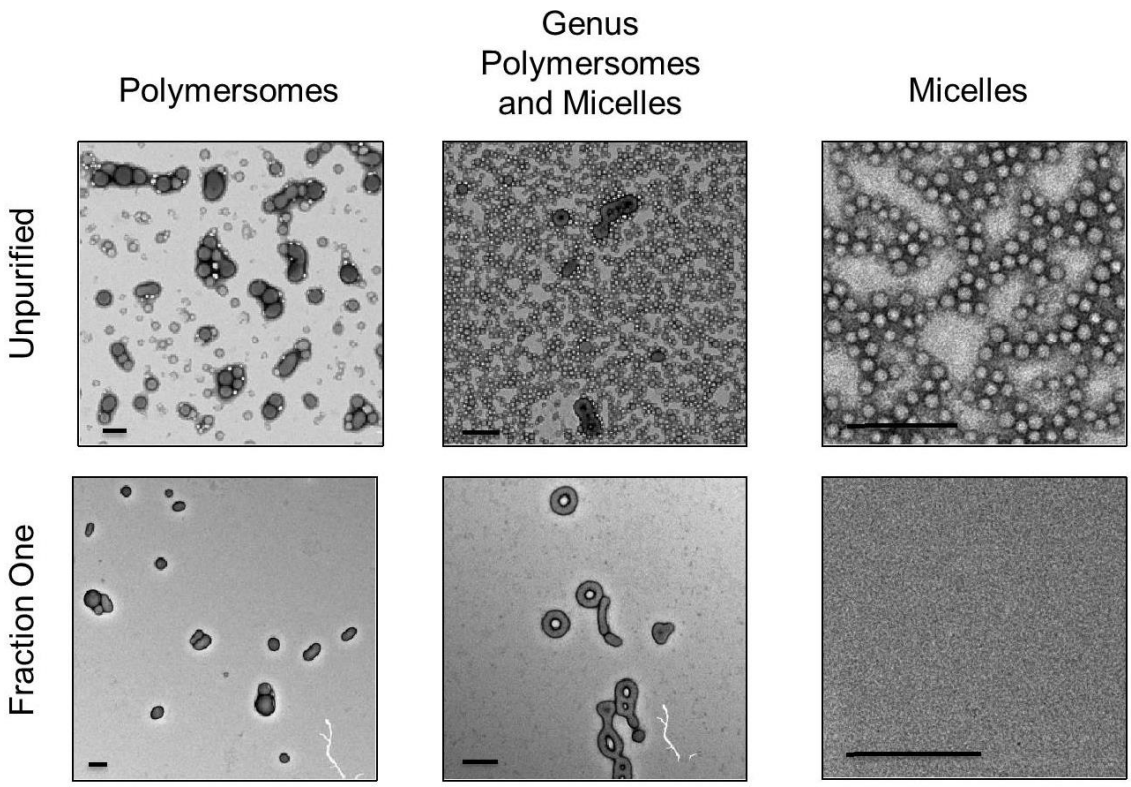

Figure 6.7: Transmission electron micrographs showing polymersome, genus particle and micelle samples before purification using the HPLC SEC set-up and after samples were gathered from the first peak using the fraction collector. No micelles are present in the samples collected from the first fraction, showing a high separation efficiency with this set up. Scale bar equals 200 nm.

As mentioned, the small sample volume and the long elution times of the HPLC-SEC system make automated purification unlikely with this set-up. However, larger columns and injection loops would allow for greater sample volumes to be processed. Also, separation efficiency could be reduced in favour of greater sample volumes or higher sample concentrations. Therefore, under the conditions used here, the HPLC-SEC functions more as an analytical tool than a purification processing tool, allowing for the qualitative analysis of the polymersome to micelle ratio to be observed (Figures 6.8 and 6.9). In addition, temperature formation samples were reproduced and analysed using the HPLC-SEC set up. Figure 6.8 shows the separation profiles of structures formed by $PMPC_{25}$-$PDPA_x$ (where x = 47, 77, 94 or 147) at temperatures between 5°C and 50°C. These profiles have a good correlation with the light scattering and electron microscopy results from the samples discussed in Chapter 3. The first peak (25-35 minutes) is generated by the larger polymersomes or genus particles, whilst the second peak (40-65 minutes) is formed by the micelles. Some measurements show detectable levels still

leaving the column at 90 minutes indicating the presence of even smaller objects. These are most likely individual polymer chains or fragments of polymer that have degraded.

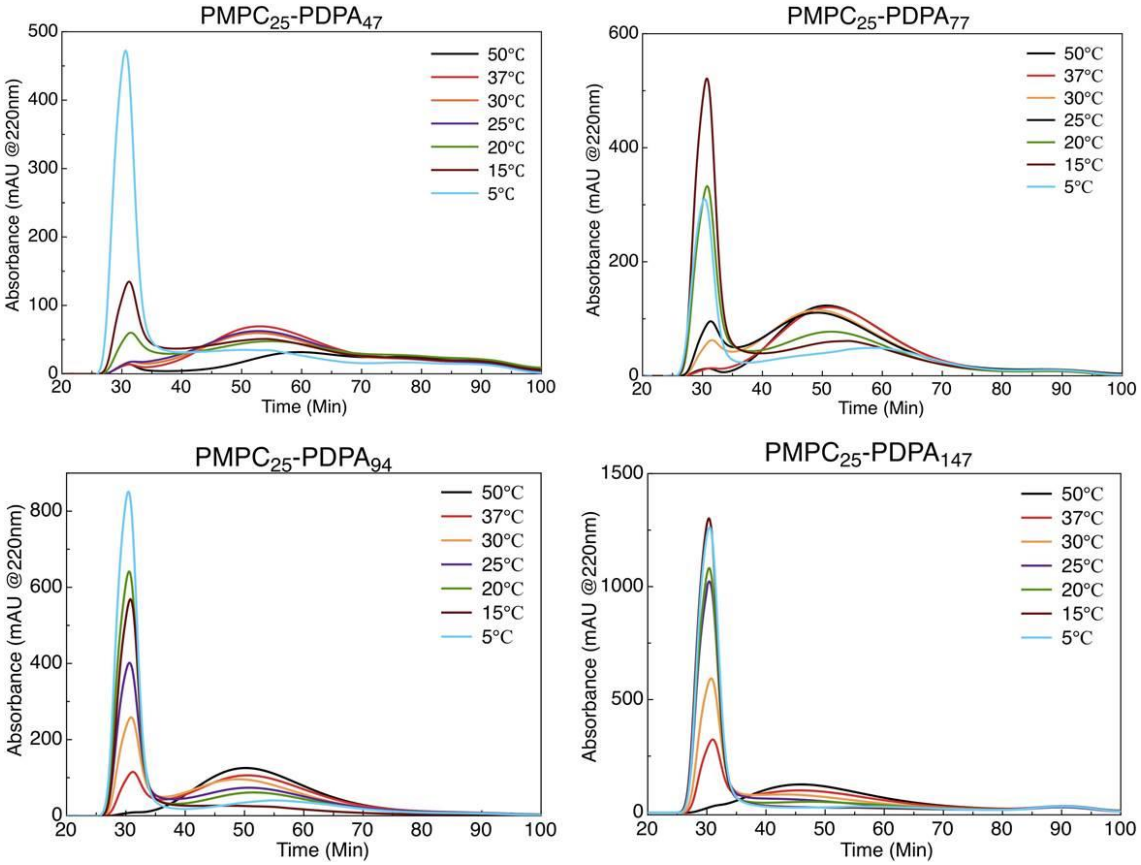

Figure 6.8: SEC traces of temperature controlled formation samples, as also discussed in Chapter 3. The results have a good correlation with the DLS and TEM data seen previously. There is an increase in the amount of larger aggregates at lower temperatures and longer PDPA block lengths. All samples measured are at the same concentration of 0.25 mg/mL.

Figure 6.9 shows the results of plotting the area ratios of the first and second peaks, which was not a quantitative measurement as the absorbance measurements taken by the HPLC-SEC were not corrected for scattering by the larger particles. However, qualitatively, a similar trend towards smaller particles as per the light scattering results (a larger peak 2 area) at higher temperatures and shorter PDPA block length can be seen.

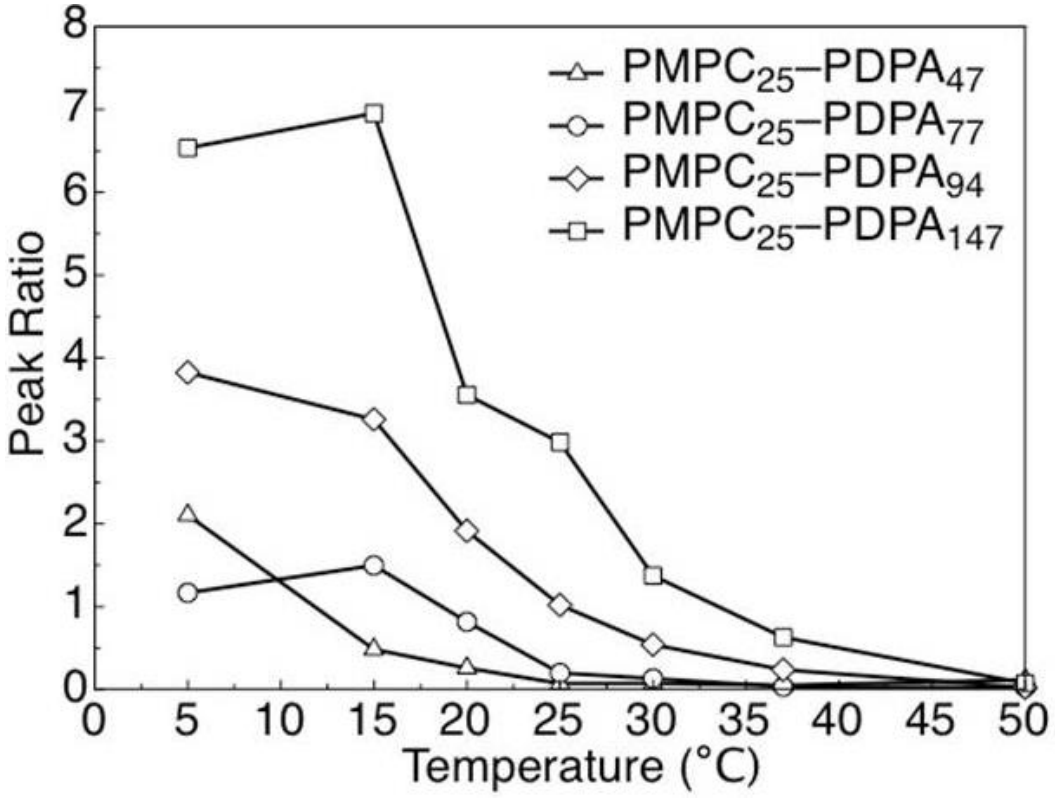

Figure 6.9: Plotting the first and second peak area ratios clearly shows the trend towards micelles at higher temperatures.

6.1.7 Encapsulation Efficiency

So far, it has been shown that the number of polymersomes in a sample can be estimated if the concentration of the polymer is known and the size distribution data can be used. This calculation makes a few assumptions of constant molecular volume and that all polymer in the system forms polymersomes and not micelles or genus particles. In order to reduce the errors of these assumptions, the samples can be purified using size exclusion chromatography (SEC), as shown previously an automated SEC set up using a High Pressure Liquid Chromatography (HPLC) system. The HPLC-SEC system removes micelles from the samples, which allows for highly accurate encapsulation data to be performed. This next section briefly discusses the methods for calculating encapsulation efficiency and its relevance for drug delivery systems.

For the work conducted here, the encapsulation efficiency of a sample can be calculated in a two different ways. Encapsulation efficiency can simply be the amount of cargo successfully entrapped within the polymersomes after purification, which can be given as a percentage of the original mass added. This approach is the most simple as it requires no information on the state of

the polymersomes themselves. Additionally, the method is quick and gives the success of the encapsulation process and an indication as to any interactions between the cargo and polymersomes. Values greater than 50% suggest that the cargo molecule is favourably interacting with the polymersomes or aggregating with itself.

With a purified sample and the information covered in this chapter, a more accurate calculation of encapsulation efficiency for hydrophilic cargoes can be determined that is based upon the number and size of the polymersomes present. This approach centres on comparing the total encapsulated volume and therefore the amount of cargo that would be molecularly dispersed in such volume, with the measured amount of encapsulated cargo. The total internal volume of polymersomes is calculated by the sum of the internal volumes for each polymersome size measured. Assuming an even distribution of hydrophilic cargo, the theoretical encapsulation is equal to the polymersome internal volume as a fraction of the sample volume multiplied by the mass of cargo that was added initially. The second encapsulation efficiency calculation is therefore the ratio of the theoretical mass encapsulated against the actual mass encapsulated.

The calculation presented here is much more versatile, as it provides the efficiency of the overall process, showing any potential interactions between the cargo molecule and the polymersomes. For example, 100% efficiency shows that the encapsulation was exactly as expected, whilst <100% indicates that the process was less efficient or that there is a negative interaction between the polymer and the cargo or between the cargo molecules. These negative interactions could be charge repulsion, steric hindrance or cargo aggregation, all of which would reduce the probability of being successfully encapsulated. For efficiency values >100% this shows a greater amount of cargo being entrapped than expected, indicating a positive interaction such as opposing charges. Unfortunately, this approach to encapsulation efficiency cannot be applied to hydrophobic cargo molecules. The hydrophobic effect is the main driving force in trapping cargo within the membrane, making it difficult to predict the amount of encapsulation.

6.1.8 Chapter Summary

In summary, there is a conflict between the desired size of polymersomes for biomedical delivery applications and encapsulation of hydrophilic therapeutic molecules. Larger polymersomes scale better for encapsulation than smaller polymersomes in terms of volume available to trap cargo. In addition, the number of molecules per polymersome is shown using simple geometric calculations, taken from papers by Battaglia *et al.*[21,25] This equation is then applied to light scattering data to improve the accuracy in calculating the number of polymersomes present in a sample. The limiting factor in such a calculation is the requirement of a "micelle free" sample, in order to treat all scattering objects as spherical polymersomes.

Size exclusion chromatography (SEC) was used to remove the micelle fraction; two approaches were shown, a bench-top column and a column attached to a HPLC system. The bench-top approach was less accurate at removing the micelles but is able to handle a variety of sample volumes more successfully. In addition, it is easily sterilised and can be kept RNAse and DNAse free for biological work. The disadvantage of this set-up is that it is completely manual and very user dependent, which makes it prone to errors and reproducibility issues. The HPLC SEC system is a fully automated system complete with absorbance and fluorescence detectors, which provided excellent separation resolution. However, the sample volume was limited by the injection volume and the long separation times resulted in a slow sample throughput. For reference, the samples in Figure 6.8 took a total of 60 hours to analyse, not including preparation of the column, which takes 24 hours to switch between standard HPLC mode and HPLC SEC. The poor throughput speed is offset by the high degree of separation and the ability to automatically collect fractions. While this set up is probably not ideal for frequent use, the option to produce high purity samples has been made available in a scalable manner.

Finally, two approaches to calculating encapsulation efficiency are outlined. The first requires little to be known about the sample and gives the encapsulation as a percentage of the original cargo added. The second approach requires a greater amount of sample knowledge and utilises the calculations and techniques discussed in this chapter to give a predicted encapsulation to compare against the measured value. These calculations are

essential in order to move polymersomes into marketable medical products and ensure that correct and consisted doses are achieved.

6.1.9 References

1. Canton, I. & Battaglia, G. Endocytosis at the nanoscale. *Chem. Soc. Rev.* **41,** 2718–2739 (2012).
2. Lasic, D. D. Doxorubicin in sterically stabilized liposomes (vol 380, pg 562, 1996). *Nature* **381,** 630–630 (1996).
3. Lasic, D. D. Recent developments in medical applications of liposomes: sterically stabilized liposomes in cancer therapy and gene delivery in vivo. *J. Controlled Release* **48,** 203–222 (1997).
4. Chierico, L., Joseph, A. S., Lewis, A. L. & Battaglia, G. Live cell imaging of membrane / cytoskeleton interactions and membrane topology. *Sci. Rep.* **4,** (2014).
5. Colley, H. E. *et al.* Polymersome-Mediated Delivery of Combination Anticancer Therapy to Head and Neck Cancer Cells: 2D and 3D in Vitro Evaluation. *Mol. Pharm.* **11,** 1176–1188 (2014).
6. Gill, M. R., Derrat, H., Smythe, C. G. W., Battaglia, G. & Thomas, J. A. Ruthenium(II) Metallo-intercalators: DNA Imaging and Cytotoxicity. *Chembiochem* **12,** 877–880 (2011).
7. Korobko, A. V., Jesse, W. & van der Maarel, J. R. C. Encapsulation of DNA by cationic diblock copolymer vesicles. *Langmuir* **21,** 34–42 (2005).
8. Korobko, A. V., Backendorf, C. & van der Maarel, J. R. C. Plasmid DNA encapsulation within cationic diblock copolymer vesicles for gene delivery. *J. Phys. Chem. B* **110,** 14550–14556 (2006).
9. Discher, D. E. Polymersome delivery of siRNA and antisense oligonucleotides. *Abstr. Pap. Am. Chem. Soc.* **237,** (2009).
10. Patikarnmonthon, N. PMPC-PDPA polymersomes-mediated siRNA delivery. (University of Sheffield, 2014). at <http://etheses.whiterose.ac.uk/5476/>
11. Giacomelli, C. *et al.* Phosphorylcholine-based pH-responsive diblock copolymer micelles as drug delivery vehicles: Light scattering, electron microscopy, and fluorescence experiments. *Biomacromolecules* **7,** 817–828 (2006).
12. Blanazs, A., Madsen, J., Battaglia, G., Ryan, A. J. & Armes, S. P. Mechanistic insights for block copolymer morphologies: how do worms form vesicles? *J Am Chem Soc* **133,** 16581–7 (2011).
13. Blanazs, A., Armes, S. P. & Ryan, A. J. Self-Assembled Block Copolymer Aggregates: From Micelles to Vesicles and their Biological Applications. *Macromol Rapid Commun* **30,** 267–77 (2009).
14. Jain, S. & Bates, F. S. Consequences of nonergodicity in aqueous binary PEO-PB micellar dispersions. *Macromolecules* **37,** 1511–1523 (2004).
15. Jain, J. P. & Kumar, N. Self Assembly of Amphiphilic (PEG)(3)-PLA Copolymer as Polymersomes: Preparation, Characterization, and Their Evaluation As Drug Carrier. *Biomacromolecules* **11,** 1027–1035 (2010).
16. Battaglia, G. & Ryan, A. J. The evolution of vesicles from bulk lamellar gels. *Nat. Mater.* **4,** 869–876 (2005).
17. Battaglia, G. & Ryan, A. J. Effect of amphiphile size on the transformation from a lyotropic gel to a vesicular dispersion. *Macromolecules* **39,** 798–805 (2006).

18. Battaglia, G. & Ryan, A. J. Pathways of polymeric vesicle formation. *J. Phys. Chem. B* **110,** 10272–10279 (2006).
19. Battaglia, G. & Ryan, A. J. Neuron-like tubular membranes made of diblock copolymer amphiphiles. *Angew. Chem.-Int. Ed.* **45,** 2052–2056 (2006).
20. LoPresti, C., Lomas, H., Massignani, M., Smart, T. & Battaglia, G. Polymersomes: nature inspired nanometer sized compartments. *J. Mater. Chem.* **19,** 3576–3590 (2009).
21. LoPresti, C. *et al.* Controlling Polymersome Surface Topology at the Nanoscale by Membrane Confined Polymer/Polymer Phase Separation. *Acs Nano* **5,** 1775–1784 (2011).
22. Malvern Instruments Ltd. *Dynamic Light Scattering an Introduction in 30 minutes*. (Malvern Instruments Ltd). at <http://www.malvern.com/en/support/resource-center/technical-notes/TN101104DynamicLightScatteringIntroduction.aspx>
23. Berne, B. J. P., R. *Dynamic Light Scattering, With applications to Chemistry, Biology and Physics*. (Dover Publications, 2000).
24. Mori, S., Barth, H.G. *Size Exclusion Chromatography*. (Springer, 1999).
25. Battaglia, G. & Ryan, A. J. Bilayers and interdigitation in block copolymer vesicles. *J. Am. Chem. Soc.* **127,** 8757–8764 (2005).

Chapter 7.1 – Discussion

Background

7.1.1 Introduction

Understanding of lipid vesicles' biological importance has grown rapidly since its discovery in the 1960s, and both the structural characteristics of lipid vesicles as well as applications in signaling and compartmentalisation are of interest to the physical and biological sciences.[1,2] Co-polymers have enhanced the study of synthetic vesicles from a bottom-up approach, by using the spontaneous arrangement of the copolymers to assess the physical characteristics and self-assembly/disassembly of polymersomes. The fully synthetic nature of polymersomes allows for physicochemical control over the building blocks due to advances in controlled radical polymerisation. As our understanding deepens, polymersomes are starting to emerge as therapeutic agents, capable of entrapping, protecting and delivering a cargo under biological environments.[3] As a drug delivery system (DDS), polymersomes offer a more durable, adjustable and responsive alternative to fully lipid, and hybrid lipid/polymer counterparts.[4–6]

The scope of this thesis was to enhance the self-assembly of polymersome forming amphiphilic copolymer poly(2-[methacryloyloxy]ethyl phosphorylcholine)−poly(2- [diisopropylamino]ethyl methacrylate) [PMPC-PDPA] for biomedical applications. The biocompatible nature of PMPC and the pH-responsiveness of PDPA allow this copolymer to be a prime candidate for biomedical applications such as intracellular drug delivery.[3,7] Ideally the polymersomes would match the requirements of a DDS, namely to form polymersomes of a correct size for internalisation, avoid clearance by the immune system (approximately 50–100 nm)[2,8] stealthy chemistry, protection of the cargo and a release mechanism. The latter three points are covered by the PMPC-PDPA chemistry and the entangled polymer membrane, resulting in biocompatibility and relatively high mechanical strength for vesicular structures.[9] One of the toughest obstacles for producing polymersomes is controlling their dimensions, this is important as the size and shape of the vesicles greatly alters their interactions with biology.

Of the two broader methods for producing vesicles, "top-down" and "bottom-up", the top-down approach is experimentally simpler in terms of

scientific understanding and implementation. However, the top-down approach requires the membrane to be broken apart, then to reform into smaller vesicles or aggregates. Micropipette aspiration measurements conducted on lipid and polymer vesicles by Bermudez *et al.* showed that polymer membranes have much greater mechanical strength.[4–6,10] This approach can be beneficial for drug delivery applications by ensuring that the cargo is protected and the vesicle can withstand biological forces. Although "tougher" vesicles are more suitable for drug delivery it can create problems during production, as polymersomes can be difficult to break when using a top-down approach. Additionally, the high molecular weight of PMPC-PDPA does not lend the copolymer to extrusion methods in order to control the size of structures formed.[7] Therefore, the main aim of the work in this thesis was to control the polymersome size using a bottom-up approach, through controlling self-assembly.

Understanding of amphiphilic self-assembly has progressed rapidly over the last decade.[11–13] In theory, polymersomes are produced when the balance of amphiphilic forces favor the formation of a membrane. For PMPC-PDPA, previous studies had shown this to be true for PDPA values greater than 70 degrees of polymerisation at a constant PMPC block length of 25 units. Using 4 copolymers of differing PDPA block lengths (3 membrane-producing formulations and 1 micelle-forming), the aim was to optimise the self-assembly process in order to produce polymersomes of an ideal size for a DDS.

7.1.2 Temperature Effects on PMPC-PDPA Polymersome Formation

The approach used to influence the formation of polymersomes was altering the temperature during the self-assembly process. My hypothesis was that higher molecular energy and collisions at elevated temperatures would increase the rate of self-assembly for PMPC-PDPA in order to reduce the size of the polymersomes formed. The initial results were promising, as samples formed at low temperatures showed higher turbidity and hydrodynamic values (200-400nm) by dynamic light scattering (DLS), whilst the opposite was true for samples produced at elevated temperatures as shown in Figure 3.6. However, morphological data obtained using transmission electron microscopy (TEM) (Figure 3.7) revealed that certain samples were adopting non-spherical

conformations with interesting topological features (see samples at 5°C in figure 3.7) , whilst others contained only micelles (50°C samples).

A clear trend with both temperature and PDPA block length emerged from the light scattering and electron microscopy data. The lower the temperature and the longer the block length, the larger the aggregate produced (Figure 3.6), with a greater number of topographical aberrations on average (Figure 4.9). This trend of greater polymersome size with increasing block length was believed to be a result of the polymer attempting to form more planar membranes as the packing factor shifted towards 1 at longer DPA block lengths. However, experiments observing the effects of temperature on copolymer titrations revealed that the pK_a increased to 7.5 at 5°C (Figure 3.3). Therefore, under the standard pH switch process from pH 5 to pH 7.4, the copolymer experienced vastly differing degrees of protonation depending on the sample temperature. Specifically, at 5°C this equated to a shift in total PDPA ionisation from >95% at pH 5 to around 55% at pH 7.4, whilst at 50°C this shift altered from around 85% at pH 5 down to 5% at pH 7.4, as predicted using the Henderson-Hasslebach equation (Figure 3.4). The higher degree of protonation leads to the PDPA block swelling and occupying a larger effective volume than expected, this in turn pushes the amphiphile to more planar packing factor values at lower temperatures (Figure 5.2). The formation of polymersomes at 5°C using the micelle-forming polymer ($PMPC_{25}$-$PDPA_{47}$: Figure 3.7) supports this theory of a swollen PDPA block.

The formation of micelles only in the $PMPC_{25}$-$PDPA_{77/94}$ samples made at 50°C (Figure 3.7) also supports the idea that the PDPA volume is changing. At the elevated temperatures the block would collapse to reduce its interaction with water and push the packing factor towards micelles. However, this result alone is less convincing than the formation of polymersomes at 5°C using $PMPC_{25}$-$PDPA_{47}$. This is because the generation of micelles at higher temperatures may be due to the structures being kinetically trapped into forming the simplest structure available. Figure 3.9 showed that the diameter scaling of the micelles formed fits a scaling power of 1/3 as opposed to the expected 2/3. This indicates that the copolymer is more coiled up than expected and that the formed micelles are molecularly frustrated, kinetically trapped structures.[14,15] Therefore, there may be a combination of the packing factor being altered with

temperature with an increase in kinetically trapped structures at the more elevated temperatures tested.

This effect of solution temperature has been seen previously in polymersome systems, Förster et al studied the effects of temperature on the morphology of PEO-PVP (poly (ethyleneoxide)- block – poly (vinylpyridine)).[16] In this study they observed the reversible transformation from polymersomes to cylindrical and then spherical micelles as the solution temperature decreased. They conclude this to be due to a swelling of the PEO corona as the solubility increases at lower temperatures, generating an increased curvature. Chapter 3 supports the theory that the copolymer packing factor alters with temperature for these two copolymer systems. For the PEO-PVP system the corona forming block alters, whilst for the PMPC-PDPA system used in this thesis, the core forming block adjusts.

7.1.3 Topology and Genus Formation

As discussed, the formation of large, oddly shaped particles by membrane forming copolymers (PDPA block lengths of 77-147) was observed in Figure 3.7. There was a trend of larger particles and a greater number of topological features with decreasing temperature (increasing DPA ionisation) as seen in Figure 4.6 and 4.9. Chapter 4 focused on these formations using $PMPC_{25}$-$PDPA_{94}$. These complex topological features are simple to identify, they appear as hole or perforations through the particles, these “hole” are known as Genus events and therefore the particle is named a genus particle.

The theory behind the formation of non-spherical particles shows that changes in difference of the outer and inner membrane area or changes in the lumen volume result in a range of non-spherical particles being formed, which is shown in Figure 4.4. The addition of a genus event to any of these structures has been calculated to be a constant energy cost.[17] The driving force for the production of genus particles appears to be spontaneous curvature, which is a force generated due to a change in the chemistry or the mass of the outer and inner surfaces of a vesicle.[18–20] As the ionisation of PDPA is increased at lower temperatures (Figure 3.4), it could be theorised that there is an increase in chain exchange between polymersome. While the probability of this occurring is minimal for such a large molecular weight amphiphile (~23,000 Da), this probability increases as the hydrophobicity of the molecule decreases.[21,22]

Therefore, the amount of mass in exchange at any given time would be higher at lower temperatures. The externally located unimers may only integrate themselves into the outer leaflet of the copolymer membrane; this therefore creates a mismatch in the membrane leaflet mass ratio, leading to spontaneous curvature. The amount of chain incorporation would in theory increase with DPA ionisation and would lead to larger particles with more genus events.

Figures 4.6 and 4.9 show that both the particle size and number of genus events increase with decreasing sample temperature. This theory was tested by taking polymersomes with no genus characteristics (Figure 4.14) and cooling them to 1°C before dropping the pH to 7.2 and leaving to stir for 30 minutes. After raising the pH to 7.5 and the temperature to ambient conditions, TEM showed no evidence of genus features (Figure 4.15). The experiment was then repeated and at pH 7.2 and 1°C, 0.1M of a dissolved sample that had been raised to pH 7.2 from pH 5 at 1°C was added and left to stir. Under these conditions the added sample remained clear throughout the experiment, indicating little or no self-assembly. Figure 5.5 supports this observation, indicating that a lower temperature (or higher ionisation) is needed to disassemble formed particles compared to the initial onset of self-assembly.

After raising the pH and the temperature the sample was analysed using TEM. Figure 4.16 shows the sample after addition of extra polymer chains. There has been an increase in the amount of topological features, however, no full genus events were observed. Future work is required to determine whether full genus events can be generated via the addition of more polymer chains or longer experimental times. To my knowledge, this is the first experiment to observe a change in the topology of polymersomes via the addition of copolymer to the external surface. Previously, high genus polymer structures have been produced via the addition of sugar to the outside surface to drive asymmetry and spontaneous curvature.[18] To my knowledge, the work covered in Chapters 3 and 4 is the first reproducible formation of genus particles using a pH responsive polymersome system.

7.1.4 Temperature Driven Polymersome Formation

Due to the strong relationship between temperature and the pK_a of PDPA (Figure 3.3), a hypothesis developed that an alternative formation process would be viable. By maintaining a constant pH and altering the temperature of

the sample, the degree of copolymer ionisation can be altered (Figure 5.1). By starting the formation process at low temperatures (1-5°C) it is possible to reach pH values around 7 without observing aggregation (Figures 5.3 and 5.6). By raising the temperature the pK_a is lowered, resulting in self-assembly, as seen in Figure 5.4) due to an increase in the percentage of hydrophobic DPA present in the system. By conducting multiple samples using turbidimetry measurements, it was shown that between 50–60% of the DPA functional groups had to be deionised in order for self-assembly to occur to a measurable degree (Figure 5.6). The self-assembly process appears to finish at around 90% deionisation as calculated using Figure 5.1, demonstrating that a small number of charged DPA groups can exist without disrupting the self-assembly. Figure 5.7 shows that the formation of polymersomes using a temperature increase is possible. This proof of concept experiment may lead to alternative production processes for PMPC-PDPA. Temperature responsive polymers have been used to form polymersomes, such as poly (ethylene oxide) – poly (N-isopropylacrylamide) (PEO-PNIPAM).[23] Studies using PNIPAM are mostly focused on using the temperature responsiveness as a release mechanism.

The control over PMPC-PDPA using both pH and temperature make for a versatile tool in the study of molecular self-assembly. As the copolymer is biocompatible, biological interactions can also be assessed. Relationships between vesicle curvature and biological interactions are a highly researched area in both scaffold development for tissue engineering and intracellular drug delivery.[24] The formation of genus particles for delivery would be an exciting variation on the use of spherical nano-devices.

7.1.5 Purification and Encapsulation Theory

Controlling polymersome size using temperature, pH or degree of polymerisation has shown some limited success with PMPC-PDPA, as described in Chapters 3, 4 and 5. It is possible to create samples with size distributions as narrow as a few hundred nanometers using the film hydration (Figure 6.6A) and pH switch (Figure 6.4B) methods as discussed in this thesis. However, in addition to the polymersomes, samples are invariably contaminated with smaller micelle structures or larger polymer aggregates and occasionally genus structures (Figure 6.7). For biomedical applications it is crucial to be able to purify samples from these contaminants and ideally reduce the range of sizes

produced. With the temperature-controlled study, smaller polymersomes were formed at higher temperatures (Figure 3.6) ; however, these samples contained high numbers of micelles. Inversely, lower temperature samples produced larger polymersomes and less micelles, but also contained larger genus aggregates. For biological applications samples must be purified in order to remove the copolymer that has failed to form polymersomes. To date, Size Exclusion Chromatography (SEC) has been widely used in the purification of vesicles,[25] PMPC-PDPA polymersomes included.[7] However, the use of SEC for PMPC-PDPA primarily focused on removing un-encapsulated compounds from formed aggregates, rather than for the removal of micelles alongside small molecules.[26]

Previous work by Battaglia *et al.*[9,13] calculated the number of polymersomes in a sample by assuming that the sample contained only polymersomes of a set diameter. This thesis has improved upon these calculations, firstly by converting light scattering data to linearly scaling volume distribution values (Figure 6.3) and applying the calculation to each data point. Secondly, the standardisation of the chromatography process for both an analytical process and a production scale purification process has been evaluated. The accuracy of the calculation correlations with the purity of the sample due to the assumption that all particles measured are polymersomes. The best separation was achieved using a sepherose 4B column attached to a HPLC pump, UV/Vis and Fluorescence detectors and a fraction collector (Figure 6.5 and 6.6). This allowed for all of the micelles to be removed and only the polymersomes to remain (Figure 6.7), which maximised the quality of the light scattering data and the calculations conducted afterwards. However, this accuracy could only be achieved by adding 50μL of diluted (0.25mg/mL) polymersomes to the column and this resulted in poor sample throughput, despite the automated approach. Inversely, manual, bench-top SEC columns (Figure 6.4) were able to process larger sample volumes of 0.5mL. However, the collection of fractions was conducted manually and separation suffered from the larger sample volumes and higher sample concentration (1mg/mL).

The appropriate purification approach should be therefore determined according to the experimental requirements. For basic toxicity testing and initial project work, the bench-top approach was faster and more user-friendly. For more advanced work, the quality of a HPLC purified sample is desirable. The

next logical step would be to increase the volume and the number of columns attached to the HPLC system in order to process larger quantities of polymersomes at a higher standard. Also, transportation of the HPLC system to a laminar flow cabinet or a clean room would be essential for preparation of sterile polymersomes.

7.1.6 Future Work

Genus Particles

This work has shown that PMPC-PDPA is capable of producing particles with genus events or "holes" through their structures. The hypothesis developed here is that these structures formed when a sphere is not the most energetically favourable configuration due to the addition of copolymer to the outer leaflet of formed polymersomes. There are very few examples of block copolymer genus vesicles, i.e. genus structure with an aqueous lumen. Therefore, a large amount of future work could be conducted using genus polymersomes. Firstly, I would characterise their morphology using alternative methods such as cryogenic transmission electron microscopy (Cryo TEM) and atomic force microscopy (AFM). Cryo TEM would allow for the 3D structure of the particle to be imaged and the volume to be measured, as opposed to the dried and collapsed structure seen in ambient TEM. AFM would give more detailed information on the surface characteristics and perhaps some mechanical information. Another experiment would be to encapsulate hydrophilic compounds to evaluate if an aqueous lumen is present. Currently, the size of these particles suggest that this is the case, but further validation would be beneficial. It would also be interesting to compare the uptake kinetics of genus particles against polymersomes and micelles, both spherical and cylindrical.

Temperature Effects

The relationship between PDPA's acid dissociation constant (pK_a) and temperature has opened up a several avenues for future research. Firstly, investigations would further explore whether smaller temperature intervals and different copolymer concentrations could lead to a greater control over the size and type of structures produced. A more complex model than the Henderson-Hasslebach equation for predicting the degree of PDPA ionisation would be a

logical step in future works. Once this is determined I would map the structures and the ionisation of more copolymer block lengths at different concentrations to explore the boundary conditions. For example, assessing the formation of genus particles and polymersomes at the higher temperatures where micelles are predominantly formed would be interesting. By then relating the work back to the degree of copolymer ionisation, it may be possible to predict the required temperature and concentration to produce polymersomes of a given size for any synthesized block length of PDPA. Another experiment would be to investigate the effects of temperature on the formation via film hydration to see whether any similar results to the pH switch process are seen.

Future work could also expand on the use of increased temperature to drive self-assembly. There are examples of temperature based systems where different structures were produced by altering the copolymer packing factor.[16] However, in general, temperature is an easier variable to control than mixing of two or more liquids, which is the case for the pH switch method. Therefore, a temperature-based formation system may be a more efficient approach for scaling up the production of PMPC-PDPA polymersomes. Scaling up the formation and purification of polymersomes and making the process as automated as possible would reduce the current issues with high sample variability, which are largely due to human errors.

X-Ray Experiments

Over the course of my PhD I visited two synchrotrons to characterise the concentration related phases of PMCP-PDPA and to analyse the structure of the solid copolymer film prior to hydration. These experiments were not fully completed; initial results can be seen in Appendix. Nevertheless, the structure of the solid film when formed in different solvents may lead to a change in rate or pathway of polymersomes formation when using film hydration as a production method. Small angle x-ray scattering (SAXS) experiments on the formation process are complicated by two main factors.

1. The formation process is very rapid, meaning that any data from intermediate steps would be of very low signal to noise ratio, unless the concentration could be increased.
2. Driving the formation via the addition of base to the sample increases the electron density due to the addition of salt ions. This complicates the

production of the appropriate background samples to subtract from the raw data.

By using a temperature formation process, data points could be taken at set temperature intervals similar to the Figure 5.4 in Chapter 5. This would also simplify the problems with produce accurate background samples.

Encapsulation and Purification

The work covered in this thesis on encapsulation provides a model to evaluate the efficiency of a hydrophilic encapsulation experiment, compared to a theoretical value. Future work could test the model using a variety of hydrophilic compounds and formation methods to build up a dataset of the encapsulation process.

The automated purification system described in Chapter 6 shows that high degrees of size separation can be achieved for analytical purposes. However, for scalable purification, this process is currently too time consuming for the typical volumes used in drug delivery experiments. Therefore, one area for further work would be to explore options for purifying larger volume samples without the reproducibility issues of manual size exclusion chromatography columns. One such approach would be to use inflow dialysis membranes, with defined molecular weight cut-offs in order to remove micelles. A few initial experiments were conducted using a hollow fibre dialysis machine to purify then concentrate a 500 mL sample of polymersomes. The early results look promising; this approach is scalable and could easily be conducted in sterile conditions.

7.1.7 Thesis Conclusions

The main objective of this report was to evaluate and improve the production of polymersomes for biological applications, namely drug delivery systems; this was conducted by controlling the temperature during formation. The main conclusions are:

1. Temperature appears to have an effect on the acid dissociation constant (pK_a) of PDPA as estimated by potentiometry; the pK_a increased as the sample temperature was reduced. This resulted in altered formation processes as the pH was increased from pH 5 to pH 7.5, possibly due to changes in the pK_a. A range of structures were produced from this formation method that included micelles, polymersomes and complex assemblies called genus particles. The hypothesis for these unpredicted structures is that the shift in the pK_a leads to varying degrees of charge present in the PDPA block during formation. This leads in turn to a change in the packing factor of the amphiphile which alters the structures formed. More work is required to see whether the size of polymersomes can be reproducibly controlled using smaller temperature intervals. However, this work showed that several structures of interest could be produced using a range of copolymer block lengths.
2. Temperature can be used to drive the formation of PMPC-PDPA polymersomes, which was measured in situ using turbidometry and a formed sample was imaged using electron microscopy.
3. A greater proportion of genus particles were observed when formation was conducted at low temperatures (higher PDPA charge density). However, due to experimental constraints it would not be feasible to sample the required number of micrographs for statistical analysis. Based on results published here and other works, a working theory that genus structures are formed due to the addition of copolymer to the outside leaflet of already-formed polymersomes was developed. This was tested and while full genus particles were not observed, the topologies produced could be precursor genus structures.
4. An automated purification rig was developed to remove all micelles and unencapsulated cargo from samples. A high degree of purification was

achieved, which took longer than standard procedures and could not be conducted under sterile conditions.

5. As well as the production of polymersomes, it is important to standardise the encapsulation process for comparative purposes. Currently this is a simplified process due to a lack of sample information and reliable purification tools. An improvement on the currently used method of calculating the number of polymersomes in a sample was developed using specific light scattering data, which allowed for a more accurate predication of the number of polymersomes present in a sample and the total encapsulated volume.

7.1.8 References

1. Alberts, B. J., A. Lewis, J. Raff, M. Roberts, K. Walter, P. *Molecular Biology of the Cell*. (2007).
2. Canton, I. & Battaglia, G. Endocytosis at the nanoscale. *Chem. Soc. Rev.* **41,** 2718–2739 (2012).
3. Lomas, H. *et al.* Non-cytotoxic polymer vesicles for rapid and efficient intracellular delivery. *Faraday Discuss.* **139,** 143–159 (2008).
4. Discher, B. M. *et al.* Polymersomes: Tough vesicles made from diblock copolymers. *Science* **284,** 1143–1146 (1999).
5. Bermudez, H., Brannan, A. K., Hammer, D. A., Bates, F. S. & Discher, D. E. Molecular weight dependence of polymersome membrane structure, elasticity, and stability. *Macromolecules* **35,** 8203–8208 (2002).
6. Bermudez, H., Hammer, D. A. & Discher, D. E. Effect of bilayer thickness on membrane bending rigidity. *Langmuir* **20,** 540–543 (2004).
7. LoPresti, C., Lomas, H., Massignani, M., Smart, T. & Battaglia, G. Polymersomes: nature inspired nanometer sized compartments. *J. Mater. Chem.* **19,** 3576–3590 (2009).
8. Decuzzi, P. & Ferrari, M. The receptor-mediated endocytosis of nonspherical particles. *Biophys. J.* **94,** 3790–3797 (2008).
9. Battaglia, G. & Ryan, A. J. Bilayers and interdigitation in block copolymer vesicles. *J. Am. Chem. Soc.* **127,** 8757–8764 (2005).
10. Discher, D. *et al.* Polymersome membrane dynamics: From lateral diffusion to electroporation. *Abstr. Pap. Am. Chem. Soc.* **221,** U315–U315 (2001).
11. Magin, R. L., Wright, S. M., Niesman, M. R., Chan, H. C. & Swartz, H. M. Liposome Delivery of NMR Contrast Agents for Improved Tissue Imaging. *Magn. Reson. Med.* **3,** 440–447 (1986).
12. McMahon, H. T. & Gallop, J. L. Membrane curvature and mechanisms of dynamic cell membrane remodelling. *Nature* **438,** 590–596 (2005).
13. Massignani, M. *et al.* Controlling Cellular Uptake by Surface Chemistry, Size, and Surface Topology at the Nanoscale. *Small* **5,** 2424–2432 (2009).
14. Jain, S. & Bates, F. S. On the origins of morphological complexity in block copolymer surfactants. *Science* **300,** 460–464 (2003).
15. Jain, S. & Bates, F. S. Consequences of nonergodicity in aqueous binary PEO-PB micellar dispersions. *Macromolecules* **37,** 1511–1523 (2004).
16. Rank, A., Hauschild, S., Forster, S. & Schubert, R. Preparation of Monodisperse Block Copolymer Vesicles via a Thermotropic Cylinder-Vesicle Transition. *Langmuir* **25,** 1337–1344 (2009).
17. Seifert, U. Vesicles of Toroidal Topology. *Phys. Rev. Lett.* **66,** 2404–2407 (1991).
18. Haluska, C. K., Gozdz, W. T., Dobereiner, H. G., Forster, S. & Gompper, G. Giant hexagonal superstructures in diblock-copolymer membranes. *Phys. Rev. Lett.* **89,** (2002).
19. Dobereiner, H. G., Selchow, O. & Lipowsky, R. Spontaneous curvature of fluid vesicles induced by trans-bilayer sugar asymmetry. *Eur. Biophys. J. Biophys. Lett.* **28,** 174–178 (1999).
20. Dobereiner, H. G., Lehmann, A., Goedel, W., Selchow, O. & Lipowsky, R. Membrane curvature induced by sugar and polymer solutions. *Mater. Sci. Cell* **489,** 101–106 (1998).
21. Creutz, S., vanStam, J., Antoun, S., DeSchryver, F. C. & Jerome, R. Exchange of polymer molecules between block copolymer micelles studied by emission spectroscopy. A method for the quantification of unimer exchange rates. *Macromolecules* **30,** 4078–4083 (1997).

22. Van Stam, J., Creutz, S., De Schryver, F. C. & Jerome, R. Tuning of the exchange dynamics of unimers between block copolymer micelles with temperature, cosolvents, and cosurfactants. *Macromolecules* **33,** 6388–6395 (2000).
23. Qin, S., Geng, Y., Discher, D. E. & Yang, S. Temperature-Controlled Assembly and Release from Polymer Vesicles of Poly(ethylene oxide)-block- poly(N-isopropylacrylamide). *Adv. Mater.* **18,** 2905–2909 (2006).
24. Discher, D. E. & Ahmed, F. Polymersomes. *Annu. Rev. Biomed. Eng.* **8,** 323–341 (2006).
25. Holzer, M., Barnert, S., Momm, J. & Schubert, R. Preparative size exclusion chromatography combined with detergent removal as a versatile tool to prepare unilamellar and spherical liposomes of highly uniform size distribution. *J. Chromatogr. A* **1216,** 5838–5848 (2009).
26. Canton, I. *et al.* Fully synthetic polymer vesicles for intracellular delivery of antibodies in live cells. *Faseb J.* **27,** 98–108 (2013).

Appendix

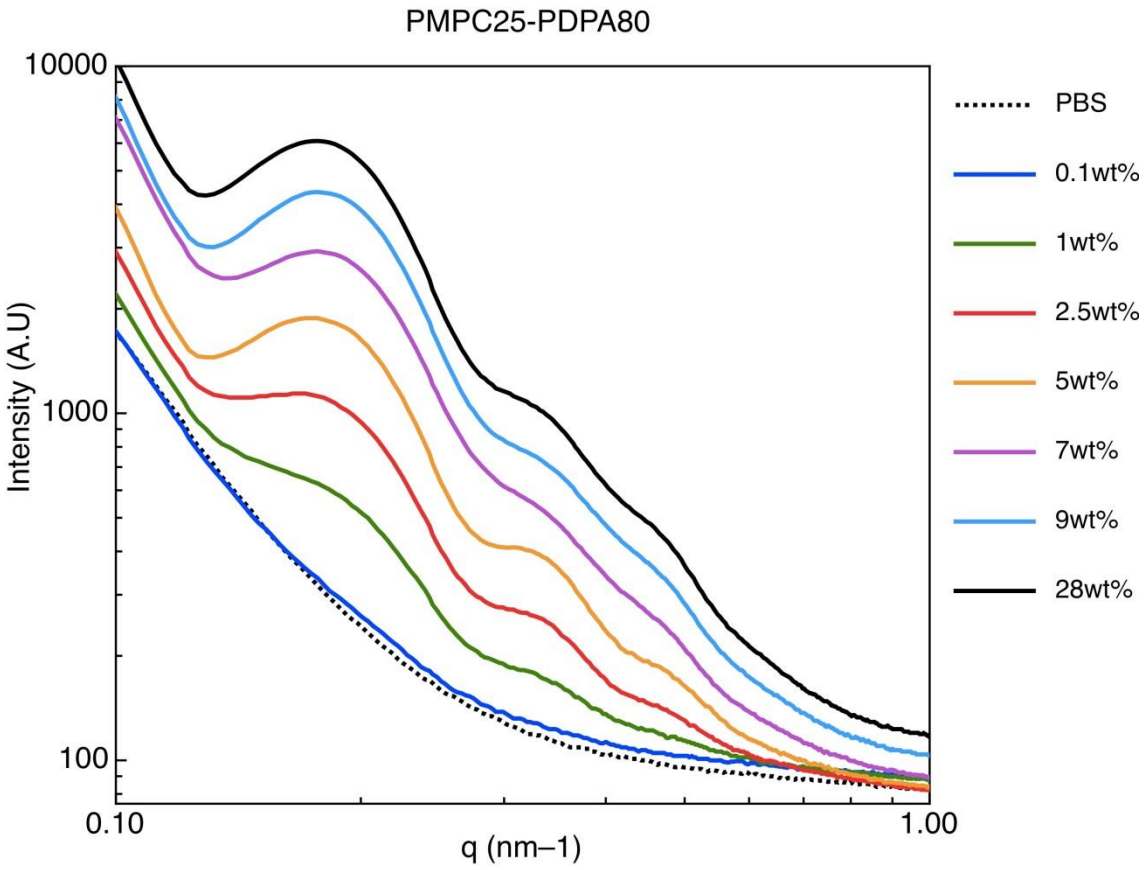

Figure A1 - SAXS data of $PMPC_{25}$-$PDPA_{80}$ copolymer at varying concentrations. These samples were created by forming polymersomes at 2.5mg/mL and either diluting or concentrating (by dialysis) as required. Samples were exposed for 3 minutes each at a camera length of 2 meters and a beam size of 1.5 x 1 mm. The appropriate air and PBS background samples have been removed. However, a polymersome model was not applied to analyse the data. However, it can be seen that the form factor is shifting towards lower q values which indicates aggregation. Generating a phase diagram for PMPC25-PDPA80 is an area of interest for future work. Identifying the lamellar phase and measuring the electron distribution can allow us to measure the molecular volume directly

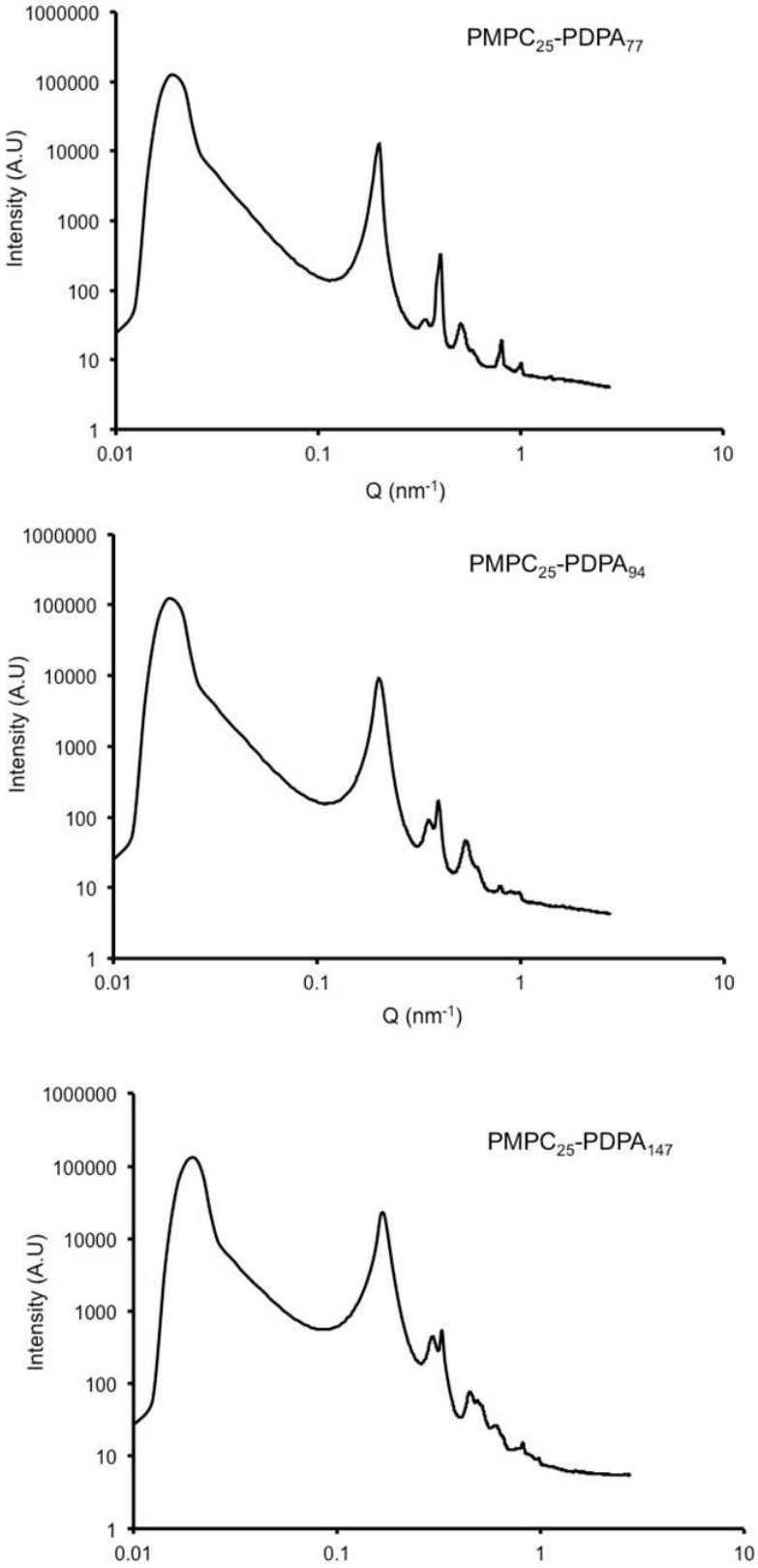

Figure A2 - SAXS data of solid films for $PMPC_{25}$-$PDPA_{77,94}$ and $_{147}$. These films were cast in a 2:1 volume ratio of $ChCl_3$:MeOH and then solvent annealed using the same solvent ratio for 48 hours. A ruby mica background has been subtracted from the data. The films were not indexed; however, the structures looks similar across these 3 polymer block lengths. $PMPC_{25}$-$PDPA_{47}$ was not available for measurement at the time of the experiment. This would be a particular area of interest for future work, as the structure of the films may affect the hydration kinetics and pathways.

Macromolecules

Article

pubs.acs.org/Macromolecules

Effect of pH and Temperature on PMPC–PDPA Copolymer Self-Assembly

Russell T. Pearson,[†,‡,§,∥,⊥] Nicholas J. Warren,[∥,#] Andrew L. Lewis,[%] Steven P. Armes,[#] and Giuseppe Battaglia*[,†,‡,§,∥]

[†]The Krebs Institute, [‡]The Centre for Membrane Interaction and Dynamics, [§]The Sheffield Cancer Research Centre, [∥]The Department of Biomedical Science, [⊥]Department of Materials Science and Engineering, and [#]The Department of Chemistry, The University of Sheffield, Firth Court, Western Bank, Sheffield, South Yorkshire, United Kingdom S10 2TN

[%]Biocompatibles UK Ltd., Farnham, Surrey, United Kingdom GU9 8QL

Supporting Information

ABSTRACT: The effect of temperature on a pH-responsive amphiphilic diblock copolymer, namely poly(2-(methacryloyloxy)ethyl phosphorylcholine)–poly(2-(diisopropylamino)ethyl methacrylate) (PMPC–PDPA), has been studied using dynamic light scattering (DLS), transmission electron microscopy (TEM), and potentiometry. The dissociation constant (pK_a) for the conjugate acid form of the PDPA block was determined for four PMPC–PDPA copolymers with varying volume fractions of DPA over a wide range of temperatures. The pH-modulated amphiphilic character of PMPC–PDPA drives its self-assembly in aqueous solution. Both the solution temperature and PDPA degree of polymerization have a dramatic effect on the size and morphology of the various copolymer nanostructures formed between pH 5 and pH 7.5, as judged by DLS and TEM studies. Copolymer morphologies include spherical micelles, vesicles (also known as "polymersomes"), and high genus assemblies. Interestingly, polymersomes were formed by each of the four diblock copolymers. Perhaps more surprisingly, polymersomes were obtained at 5 °C for the shortest DPA block length and at 50 °C for the longest DPA block length. Potentiometric titrations confirmed that the pK_a of the PDPA block had a strong temperature dependence, with a maximum value of 7.60 at 5 °C and of a minimum value of 5.75 at 50 °C. However, no difference in pK_a was observed across the four copolymers, suggesting no dependence on the mean degree of polymerization.

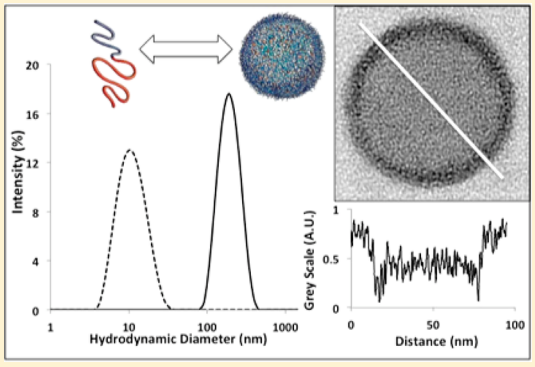

INTRODUCTION

Over the past few decades there has been significant interest in supramolecular structures formed from amphiphilic macromolecules.[1,2] Spontaneous assembly occurs in selective solvents to form a range of aggregates, including spherical micelles, cylindrical micelles, and vesicles. Vesicles, in particular, are commonplace in biology, compartmentalization, and movement between both intra- and extracellular environments often occurs via trafficking vesicles composed of naturally occurring phospholipids.[3] This ability to protect and transport a payload between cells means that vesicle-forming amphiphiles have received particular attention in the field of nanomedicine as potential delivery vectors for both hydrophilic and hydrophobic payloads. Lipid-based vesicles or liposomes have also been utilized with some success in this field.[4,5] However, the enhanced mechanical properties[6−8] and greater payload retention[9] of polymer vesicles (also known as polymersomes) offer significant advantages over liposomes for this approach to drug delivery.

Advances in controlled "living" polymerization techniques[10] have aided the synthesis of a wide range of well-defined diblock copolymers with relatively low polydispersities (M_w/M_n < 1.30). This has facilitated the design of fully synthetic "superamphiphiles" that are capable of forming either vesicles or micelles in aqueous solution.[2] In principle, block copolymers offer several advantages over lipid or hybrid lipid/polymer systems. The macromolecular nature of copolymers leads to an entropically favorable entangled membrane conformation,[11] which results in enhanced colloidal stability.[6,7,12] Such parameters can be altered by tuning the polymer chemistry (i.e., monomer type and molecular weight), and several moieties can be conjugated to either the hydrophilic or hydrophobic domains to tune bioactivity.[13−15]

The dimensionless molecular packing parameter $p = v/a_0l$ describes the relationship between a given amphiphile and the molecular curvature that two or more such amphiphiles would ideally adopt,[16] where a_0 equals the optimal interfacial area between the hydrophilic and hydrophobic fractions and v and l are the molecular volume and length of the hydrophobic segment, respectively. By maintaining a constant hydrophilic

Received: October 26, 2012
Revised: January 28, 2013
Published: February 14, 2013

volume fraction and either increasing or decreasing the relative hydrophobic volume fraction, the intermolecular curvature is altered, allowing a range of supramolecular aggregates to be formed. For values of $p \leq {}^1/_3$, the high curvature favors the formation of spherical aggregates known as micelles; at intermediate curvatures where ${}^1/_3 < p \leq {}^1/_2$ a cylindrical architecture is the preferred conformation. This generates long tubular structures known as cylindrical micelles: at the cylinder termini, the formation of highly curved end-caps avoids the exposure of the hydrophobic core to the aqueous solvent. The formation of molecularly frustrated end-caps is allowed due to its lower energy penalty compared to exposing the hydrophobic cores.[16] At low curvature, where the ratio of hydrophilic/hydrophobic volume fractions approaches unity (${}^1/_2 < p \leq 1$), amphiphiles will preferentially generate membranes. The membrane then wraps up, forming a hollow sphere known as a vesicle or, when formed from polymeric amphiphiles, a polymersome. Curving to evenly distribute the molecular frustration over the entire surface of the structure is more energetically favorable than creating highly curved edges.[16] Experimentally, an extensive range of assemblies have been reported, along with various transient species such as "jellyfish" or "octopi".[17,18]

Poly(2-(methacryloyloxy)ethyl phosphorylcholine)−poly(2-(diisopropylamino)ethyl methacrylate) (PMPC−PDPA) is a pH-responsive diblock copolymer that can self-assemble to form supramolecular aggregates (Figure 1) such as polymersomes and micelles. Previous studies have shown that $PMPC_x$−$PDPA_y$ with x = 25−30 and y = 70−160 form polymersomes, whereas shorter PDPA block lengths (y < 60) produce micelles.[19−21] The pH-responsive nature of the PDPA block means that these chains protonate, becoming cationic and water-soluble below its pK_a, but deprotonate, becoming hydrophobic and water-insoluble above its pK_a.[22,23] In contrast, the zwitterionic PMPC block remains highly hydrophilic over a wide range of aqueous solution conditions. Thus, the amphiphilic character of this copolymer can be switched on or off via pH modulation.

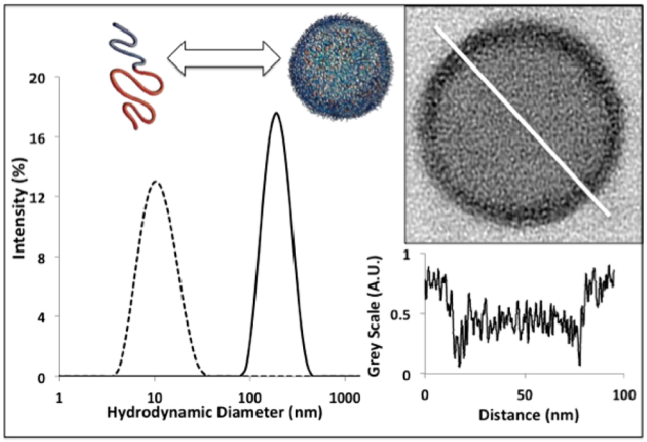

Figure 1. Dynamic light scattering studies confirm the formation of molecularly dissolved copolymer chains at low pH and self-assembled polymersomes at neutral pH. The transmission electron micrograph image is of a single polymersome positively stained with phosphotungstic acid. Membrane thicknesses are estimated as shown by the gray scale profile of the white line.

For many biomedical applications, the ability to control the polymersome dimensions is highly desirable.[24−26] This can be achieved by two different approaches. A "top-down" method reduces the average diameter by subjecting the polymersomes to sufficient force to rupture the membrane, producing two or more smaller polymersomes from the original parent polymersome dispersion. Methods traditionally associated with liposome production such as sonication, freeze−thaw cycles, and extrusion are commonly used to control polymersomes size.[1,27] However, these processing routes also rely on how efficiently the membrane can be broken, an event which is significantly harder to achieve in polymersomes compared to liposomes,[8] and can potentially reduce the amount of encapsulated cargo. In contrast, "bottom-up" approaches rely on altering the molecular structure or environment to control the formation process and resulting self-assembled nanostructures. This is frequently achieved by adjusting the mean degree of polymerization or by using organic solvent/water mixtures.[28] Recently, we have shown that polymersomes can be loaded after their formation using electroporation.[29] This enables us to separate the polymersome formation process from cargo encapsulation.

A study into the pH-responsive vesicle-forming copolymer poly(2-vinylpyridine−poly(ethylene oxide)) (P2VP−PEO) by Förster et al. reveals a morphological transformation based on solution temperature.[30] They show a reversible process wherein polymer vesicles degenerate initially to cylindrical micelles and then to spherical micelles as the solution temperature is decreased. The proposed mechanism relates the increased solubility of the corona forming PEO block due to decreased solution temperature, with an alteration of the molecular packing parameter. Specifically, the swelling of the PEO block generates increased curvature via intermolecular repulsion, resulting in a shift toward micelle assemblies. However, the effects of temperature on the pK_a of pH-responsive core forming P2VP block were not included within the scope of this investigation. In addition, Lecommandoux et al. conducted a study into the pH- and temperature-driven self-assembly behavior of double hydrophilic block copolymer poly[2-(dimethylamino)ethyl methacrylate]poly(glutamic acid) (PDMAEMA-PGA).[31] They show that the process of self-assembly into polymersomes and micelles can be tuned via altering electrostatic and/or hydrophobic interactions based on pH and temperature.

In this study, we investigate the ability to control the aqueous self-assembly of a series of four biocompatible PMPC−PDPA diblock copolymers simply by manipulating the solution temperature.

MATERIALS AND METHODS

Unless otherwise stated, all materials were purchased from Sigma-Aldrich (UK) at the highest purity grade and used without further purification. 4-Cyano-4-(2-phenylethane sulfanylthiocarbonyl)-sulfanylpentanoic acid chain transfer agent (PETTC) was synthesized according to a previously reported method.[32] Deuterated methanol (CDOD, 99.96 atom %) was purchased from Goss Scientific (UK). Solvents were obtained from Fisher Scientific (Loughborough, UK) and were used as received. Hydrochloric acid (HCl, 32%, general purpose grade) was purchased from Fisher Scientific (Loughborough, UK) and was used as received. 2-(Methacryloyloxy)ethyl phosphorylcholine monomer (MPC, 99.9% purity) was donated by Biocompatibles UK Ltd. (Farnham, UK) and was used as received. 2-(Diisopropylamino)ethyl methacrylate was purchased from Scientific Polymer Products, Inc. (Ontario, NY), and passed through a basic alumina column to remove its inhibitor prior to use. Phosphate-

dx.doi.org/10.1021/ma302228m | Macromolecules 2013, 46, 1400−1407

buffered saline (PBS) was prepared from tablets obtained from Oxoid (Basingstoke, UK). Regenerated cellulose dialysis membrane (1000 MWCO) was purchased from Spectra/Por.

Synthesis of Various PMPC Macro-CTAs. MPC (10.32 g, 34.92 mmol, target DP 25) and PETTC (0.474 g, 1.40 mmol) were dissolved in ethanol (9.0 mL). After purging with nitrogen for 20 min in an ice bath, ACVA (V501) initiator (0.098 g, 0.35 mmol, 0.25 equiv) was added, and the mixture was purged for a further 5 min. At this point the flask was immersed in an oil bath at 75 °C. After 1 h, the reduction in the vinyl proton signal in the ^{1}H NMR spectrum indicated 97% monomer conversion. The reaction flask was removed from the oil bath and opened to the air, and the reaction solution was diluted with ethanol. The PMPC macro-CTA was precipitated into THF to remove any unreacted PETTC and subsequently dialyzed against methanol for 24 h, changing the methanol every 2 h for the first 8 h. After solvent removal via rotary evaporation, a glassy yellow solid was obtained, which was placed in a vacuum oven overnight at 50 °C to remove residual methanol. The final PMPC macro-CTA was characterized by both ^{1}H NMR spectroscopy (CD_3OD) and aqueous GPC using a series of near-monodisperse poly(ethylene oxide) calibration standards. Final composition: PMPC25 M_n = 9800; M_w/M_n = 1.19.

Alcoholic Solution Synthesis of PMPC-*b*-PDPA by RAFT Using a PMPC Macro-CTA. As a representative example, $PMPC_{25}$–$PDPA_{147}$ diblock copolymer was prepared by placing $PMPC_{25}$ macro-CTA (0.50 g, 0.068 mmol, 1 equiv) and DPA (2.02 g, 4.74 mmol, target DP for PDPA block = 140) into a 25 mL round-bottomed flask containing a magnetic stirrer bar. Dissolution in ethanol was achieved with the aid of sonication, followed by stirring and purging with nitrogen for 20 min in an ice bath. ACVA initiator was added (4.6 mg, 0.017 mmol, 0.25 equiv), and the mixture was purged for a further 5 min. At this point, the flask was immersed in an oil bath at 75 °C. After 18 h, ^{1}H NMR indicated 95% DPA conversion. The reaction was removed from the oil bath, opened to the air, and diluted with ethanol. Purification was achieved by dialysis against ethanol overnight followed by 1 week against water with twice-daily water changes. After freeze-drying from water overnight, the pure product was isolated as a light yellow powder. The final polymer was characterized by both ^{1}H NMR spectroscopy in CD3OD and GPC (3:1 chloroform/methanol eluent) (Figure S1). Final composition: $PMPC_{25}$–$PDPA_{147}$; M_n = 31 400, M_w/M_n = 1.27.

Polymersome Self-Assembly Using a pH Switch. Copolymer self-assembly was performed by increasing the solution pH from mildly acidic to approximately neutral pH; this was achieved by the addition of sodium hydroxide (NaOH). Copolymer solutions in phosphate-buffered saline (100 mM PBS) were made up at a concentration of 5 mg/mL (0.05 wt %) and adjusted to pH 5. This ensured that the copolymer chains were molecularly dissolved, generating a homogeneous initial solution. Equal volumes of copolymer solution and various aqueous NaOH solutions were mixed and stirred for 15 min prior to measuring the solution pH. This process was repeated until the concentration required to induce a pH jump from pH 5.0 to pH 7.5 was obtained for all four copolymers used in this study, typically 0.012–0.0155 M for $PMPC_{25}$–$PDPA_{47}$ to $PMPC_{25}$–$PDPA_{147}$. This equates to less than a 5% variation in sample ionic strength overall. Because of PMPC–PDPA being a polyelectrolyte, the ionic strength and type of ions present are expected to influence copolymer volume. This may be the case for more dilute molarities; however, no noticeable effect has been observed around 100 mM. Studies conducted by Mahon et al. on PMPC elution times in various aqueous solutions saw no difference with ionic strength but large differences in elution time in the presence of divalent anions.[33] For temperature-controlled pH adjustments, 500 μL of copolymer solution was immersed in a water bath set at the desired temperature and allowed to equilibrate for 15 min. In the same water bath, the required NaOH solution was also allowed to reach the same temperature. Then 500 μL of NaOH was added to the copolymer solution before stirring for 1 h at constant temperature. Samples were then removed from the water bath and allowed to reach room temperature, prior to sonication and subsequent analysis by DLS and TEM.

Dynamic Light Scattering. Dynamic light scattering studies were performed using a Zetasizer Nano ZS instrument (Malvern) at a copolymer concentration of 0.25 mg/mL. Measurements consisted of 12–14 subruns each of 10 s duration; a total of three measurements were conducted and then averaged to give intensity-average particle size distributions. Samples were analyzed at 25 °C at a scattering angle of 173° using a 633 nm HeNe laser.

Transmission Electron Microscopy. Phosphotungstic acid (PTA) was dissolved in boiling distilled water to produce a 0.75 wt % solution. 5 M NaOH was added dropwise while stirring, until the solution pH reached pH 7.5. After allowing to cool, this staining solution was passed through a 0.20 μm sterile filter and kept in the fridge prior to use. A small volume (5 μL) of the copolymer solution was added to a freshly glow-discharged, carbon-coated copper/palladium square mesh grid (Agar Scientific) and allowed to adsorb for 1 min. The grid was then blotted dry, before immersing it in a droplet of PTA stain for 5 s; afterward, the grid was blotted dry for a second time, and any excess liquid was removed under vacuum. This resulted in positively stained samples suspended on a thin carbon film. Imaging was conducted using a FEI Tecnai G2 Spirit electron microscope. Micrographs were recorded at 120 keV and analyzed using Gatan Digital Micrograph and Image J64 software packages.

Potentiometric Titration. Titrations were conducted using a custom-built rig, consisting of a heated water bath, a magnetic stirrer, a syringe driver, and a pH meter. First, 500 μL of copolymer solution at a concentration of 2.0 mg/mL was allowed to equilibrate at the required temperature for 30 min. Then 2.0 mL of 5×10^{-3} M NaOH was added to the copolymer solution at a flow rate of 0.17 mL/min, under constant sample agitation. Microprobe pH measurements were taken at 5 second intervals and exported to a computer automatically.

RESULTS AND DISCUSSION

A series of four pH-responsive amphiphilic diblock copolymers, $PMPC_{25}$–$PDPA_n$, were synthesized by reversible addition–fragmentation chain transfer (RAFT) polymerization using a single batch of $PMPC_{25}$ macro-CTA. This strategy allowed a series of copolymers to be prepared with an identical PMPC block and varying PDPA block lengths. Characterization of the resulting four copolymers by ^{1}H NMR spectroscopy indicated mean degrees of polymerization (DP) of the PDPA block of 47, 77, 94, and 147 units. GPC studies (3:1 chloroform/methanol eluent) indicated that the M_n values increased systematically with target DP, as expected. Moreover, narrow molecular weight distributions were achieved for all the diblock copolymers (M_w/M_n = 1.24–1.27).

Potentiometric titration curves were produced for copolymers by plotting the solution pH against the volume of added NaOH. Acid dissociation constants (pK_a) were measured as the midpoint of the plateau region of each curve. Because of the highly hydrophobic nature of unprotonated DPA, it is unfeasible to conduct such titrations upon the homopolymer. Upon reaching the polymer's pK_a, the material is forced out of solution via the hydrophobic effect. Figure S2 shows an increase in copolymer pK_a as the solution temperature is lowered. Plotting the experimental pK_a values (Figure 2) against solution temperature reveals a linear relationship regardless of the mean DP of the PDPA block, with minimum and maximum values of 5.74 ± 0.008 and 7.59 ± 0.028 being obtained at 50 and 5 °C, respectively. Therefore, at 5 °C and pH 7.5 the ratio of protonated to deprotonated tertiary amine groups is approximately equal. Figure 3 shows the estimated degree of copolymer ionization as predicted using the Henderson–Hasselbach equation. Modeling the ionization physics of polyelectrolytes is a highly complex process. However, the

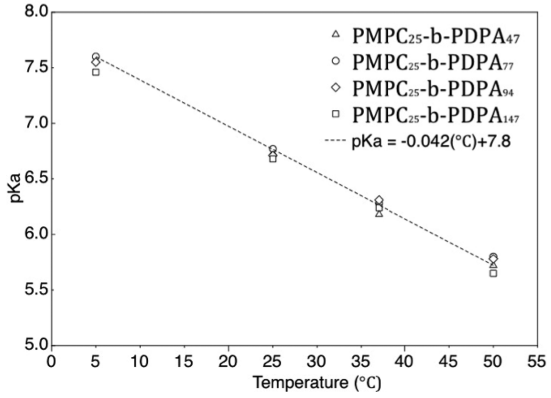

Figure 2. pK_a values obtained from potentiometric titration curves for each PMPC$_{25}$–PDPA$_n$ diblock copolymer at various temperatures. Note the linear temperature dependence and the lack of any dependence on the mean degree of polymerization of the PDPA block (n).

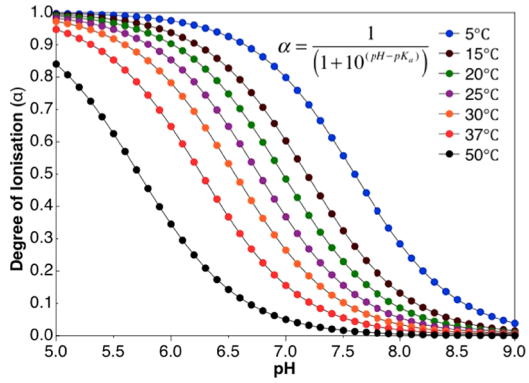

Figure 3. Degree of copolymer ionization as a function of solution pH and temperature. Data were calculated using the pK_a values obtained from potentiometric titrations.

simpler Henderson–Hasselbach approach allows us to visualize the graduated ionization behavior of the weak polycation PDPA, specifically that the ratio of protonated to deprotonated groups shifts logarithmically toward the deprotonated state for pH values greater than the pK_a. There appears to be no difference in pK_a values observed for the four PDPA block lengths, suggesting that the degree of polymerization has essentially no effect on pK_a, at least above the minimum mean DP tested (DP = 47).

In order to assess the effect of temperature on the polymersome dimensions, samples were analyzed by dynamic light scattering, which reports intensity-average size distributions (see Figure S3). Interestingly, there is no more than a 5% variation in size for PMPC$_{25}$–PDPA$_{47}$ micelles (mean diameter = 37 nm) formed at 30, 37, and 50 °C. At 25 °C, the average assembly diameter increases from 37 to 48 nm. A further significant size increase is observed lower temperatures, with copolymer aggregates produced at 5 °C having an average diameter of 160 nm. DLS size distributions for PMPC$_{25}$–PDPA$_{77}$ and PMPC$_{25}$–PDPA$_{94}$ show the same trend: much larger particles are formed at 37, 30, or 25 °C compared to that at 50 °C. For pH adjustment of copolymer solutions at 20 or 15 °C, there is relatively little difference in size. Similarly, PMPC$_{25}$–PDPA$_{147}$ forms larger nanostructures relative to the other copolymers between 50 and 30 °C, while below 30 °C there is rather little size variation. Lower temperatures also produce higher particle polydispersities, suggesting a range of particle sizes and/or shapes. Strangely, 5 °C solutions of PMPC$_{25}$–PDPA$_{94}$ and PMPC$_{25}$–PDPA$_{147}$ produce smaller particles than copolymer solutions prepared at higher temperatures. However, these solutions contain large amounts of sedimented copolymer, indicating the formation of large aggregates that do not remain suspended long enough for a meaningful light scattering measurement. Therefore, these particular results represent the minor fraction of copolymer aggregates that remain in solution for the 15 min required for a

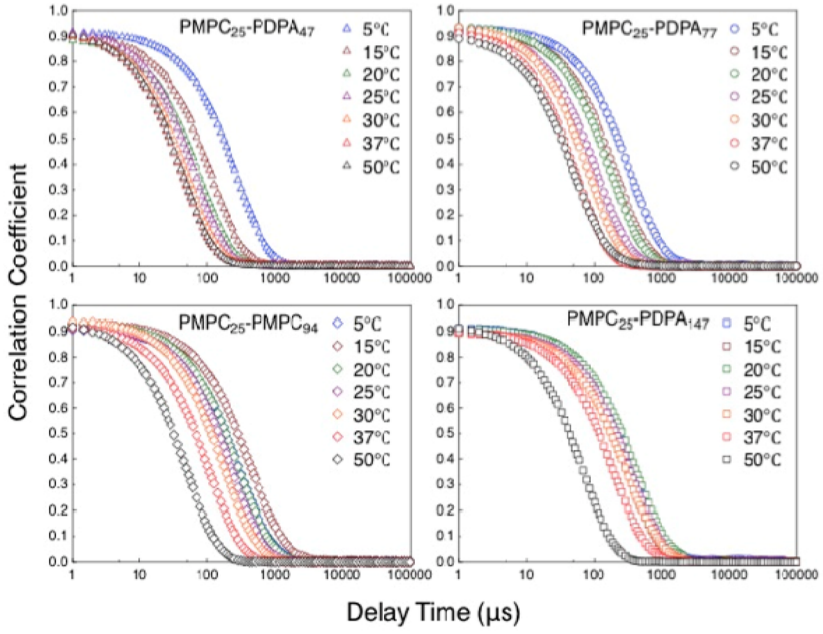

Figure 4. Decaying correlation functions. A shift to longer delay times for lower temperature samples indicates the formation of larger particles. A smooth baseline and a single-exponential decay indicate that accurate measurements have been achieved. For intensity-averaged distribution data see the Supporting Information.

dx.doi.org/10.1021/ma302228m | *Macromolecules* 2013, 46, 1400–1407

DLS measurement. Figure 4 displays the decaying correlation functions for the samples discussed above. There is clearly a shift toward longer decay times, which is indicative of the presence of larger particles.

Intensity-average hydrodynamic diameters were calculated and plotted as a function of temperature for the four diblock copolymers used in this study (Figure 5). At 50 °C, each copolymer formed its smallest aggregate with hydrodynamic diameters of 37 ± 6, 35 ± 3, 37 ± 4, and 48 ± 3 nm for PDPA block lengths of 47, 77, 94, and 147, respectively. DLS measurements recorded between 50 and 20 °C indicate an increase in average hydrodynamic diameter, with values of 53 ± 6, 116 ± 7, 185 ± 11, and 295 ± 34 nm at 20 °C for PDPA block lengths of 47, 77, 94, and 147, respectively. Measurements conducted on 15 and 5 °C samples show a similar trend of increasing diameter between these temperatures: 85.8 ± 7.2 nm to 166.6 ± 9.2 nm and 138.5 ± 13.7 nm to 251.1 ± 58.3 nm for $PMPC_{25}$–$PDPA_{47}$ and $PMPC_{25}$–$PDPA_{77}$, respectively. For $PMPC_{25}$–$PDPA_{94}$ and $PMPC_{25}$–$PDPA_{147}$, copolymer aggregates produced at 5 and 15 °C possessed high polydispersities and inconsistent mean diameters, suggesting that sedimentation of large aggregates occurs during the DLS measurements.

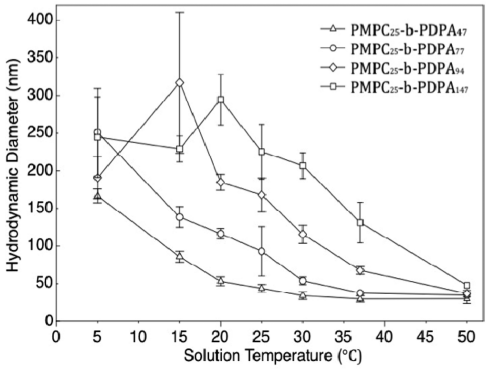

Figure 5. Average hydrodynamic particle diameters gained from intensity-averaged dynamic light scattering measurements. A trend of increasing particle size with decreasing solution temperature and greater mean degree of polymerization is seen. Error bars represent the standard deviation (N = 3).

As mentioned above, increasing the PDPA volume fraction reduces the molecular curvature, which favors the formation of polymersomes. This is consistent with the light scattering measurements, since copolymers with longer PDPA blocks consistently form larger aggregates. Figure 6 displays the aggregate morphologies formed by the $PMPC_{25}$–$PDPA_n$ copolymers across a range of temperatures and PDPA block lengths. At 50 °C, all four copolymers produce relatively small aggregates, as shown in Figure 5. TEM images indicate the formation of micelles for $PMPC_{25}$–$PDPA_{47}$, $PMPC_{25}$–$PDPA_{77}$, and $PMPC_{25}$–$PDPA_{94}$ and a mixture of micelles and small polymersomes for $PMPC_{25}$–$PDPA_{147}$. Analysis of the TEM images indicate mean particle dimensions of 32 ± 4 and 52 ± 14 nm, respectively. At 37 °C, $PMPC_{25}$–$PDPA_{47}$ and $PMPC_{25}$–$PDPA_{77}$ form spherical micelles with relatively narrow size distributions. However, both $PMPC_{25}$–$PDPA_{94}$ and $PMPC_{25}$–$PDPA_{147}$ form a mixture of polymersomes and micelles at this temperature. $PMPC_{25}$–$PDPA_{47}$ also forms micelles at 30 °C, while a mixture of polymersomes and micelles are observed for $PMPC_{25}$–$PDPA_{77}$ and $PMPC_{25}$–$PDPA_{94}$. However, $PMPC_{25}$–$PDPA_{147}$ begins to form particles with genus "events". $PMPC_{25}$–$PDPA_{47}$ forms micelles, and $PMPC_{25}$–$PDPA_{77}$ produces both micelles and polymersomes at 25 °C. In addition, there are also some nonspherical particles present with diameters greater than 50 nm, possibly indicating tubular polymersomes. So-called genus particles are produced at 25 °C for $PMPC_{25}$–$PDPA_{94}$ and $PMPC_{25}$–$PDPA_{147}$, with larger and more complex genus assemblies being produced by $PMPC_{25}$–$PDPA_{147}$. $PMPC_{25}$–$PDPA_{47}$ contains a mixture of micelles and polymersomes at 20 °C, which is in contrast to that observed at higher temperatures. For $PMPC_{25}$–$PDPA_{77}$, TEM indicates the presence of polymersomes and larger nonspherical nanostructures, indicating the onset of genus assemblies. $PMPC_{25}$–$PDPA_{94}$ and $PMPC_{25}$–$PDPA_{147}$ continue to produce larger and more complex genus particles at 20 °C. The three higher molecular weight diblock copolymers also form genus structures at both 15 and 5 °C; DLS studies

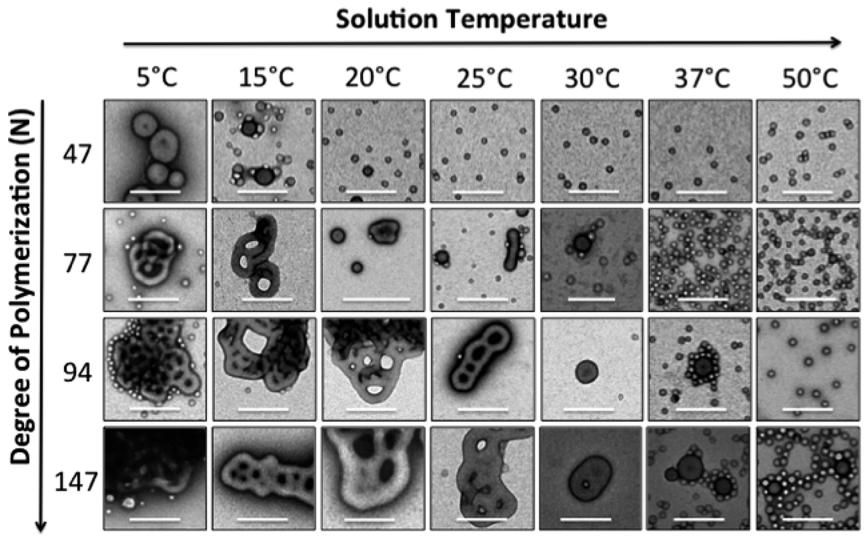

Figure 6. Transmission electron micrographs showing typical macromolecular assemblies formed by each copolymer across the solution temperature range tested. Particle contrast was achieved by positive staining using phosphotungstic acid. Scale bar = 200 nm.

dx.doi.org/10.1021/ma302228m | *Macromolecules* 2013, 46, 1400–1407

support this interpretation, showing the production of larger particles. Interestingly, $PMPC_{25}$–$PDPA_{47}$ also produces polymersomes at 15 and 5 °C, which is unexpected for the relatively short PDPA block length. However, it may be worth noting that the samples looked sparser under TEM observation. The comparable DLS scattering intensity between equal concentration samples at 5 and 50 °C indicates fewer, larger structures produced (see Figure S3).

The mean polymersome membrane thickness and micelle diameter were estimated from TEM images for all four copolymers. Figure 7 shows the average membrane thickness

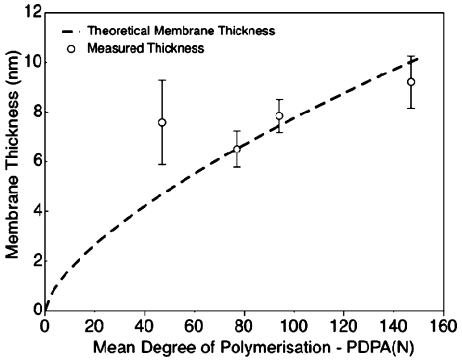

Figure 7. Membrane thickness measurements taken from TEM micrographs then plotted against the mean degree of DPA polymerization. The three longest block lengths follow the predicted scaling for membrane thickness of vesicle forming copolymers. The shortest copolymer with a DPA block length of 47 produces membranes much thicker than those predicted.

plotted against the mean degree of polymerization, N, of the core-forming PDPA block. For the three longest copolymers, the membrane thickness scales with $N^{2/3}$, which is expected for entangled polymeric membranes and micelles.[11,34] However, the polymersomes formed by $PMPC_{25}$–$PDPA_{47}$ display membranes that are around 8 nm, which is ~3 nm thicker than the theoretical estimation. As previously stated, this particular copolymer is not expected to form polymersomes. Despite this, polymersome morphologies are observed at subambient temperatures (5 or 15 °C) (see Figure 6) In this case, the membrane thicknesses are comparable to that expected for a core-forming block of twice the length. This suggests that the copolymer adopts a relatively extended (uncoiled) conformation within the membrane. This is most likely due to the solution pH lying close to the pK_a, resulting in a relatively swollen PDPA block. However, micelle diameters scale with $N^{1/3}$ (Figure 8) rather than the expected $N^{2/3}$ as predicted by Birshtein and Zhulina model for block copolymer spherical micelles.[35] This would suggest that for PDPA blocks with N larger than 47 micelles are frustrated and formed with less copolymers than the theoretical micelle. This ultimately indicated that these micelles are rather kinetically trapped assembly nuclei that would evolve into a more thermodynamically stable vesicles given time and unimer exchange.

As predicted from the molecular packing parameter, increasing the relative hydrophobic volume fraction is sufficient to drive the formation of nanostructures with lower curvatures. Traditionally, this can be achieved by targeting a higher degree of polymerization for the hydrophobic block. However, the pH-responsive nature of PDPA allows additional fine control over its effective pervaded volume. At pH 7.5 and 50 °C, the

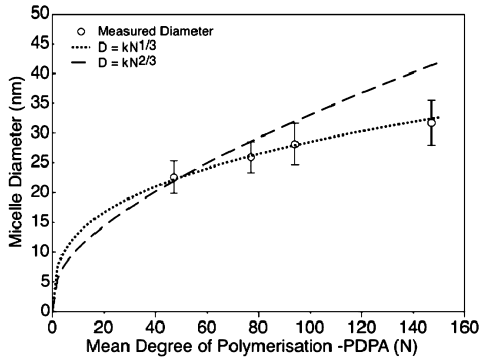

Figure 8. Micelle diameters estimated from TEM images of $PMPC_{25}$–$PDPA_n$ copolymers prepared at 50 °C plotted against the mean degree of polymerization of the PDPA. The data scale better with $N^{1/3}$ than $N^{2/3}$, indicating a highly coiled conformation for this core-forming block.

copolymer is 1.7 pH units above its pK_a (Figure 2), and its mean degree of protonation is less than 1% (Figure 3). In this near-neutral hydrophobic state, the PDPA block collapses to reduce its effective volume since water is a bad solvent. Its scaling follows the typical power law for strongly segregated systems, where $R_g \propto N^{2/3}$. Given the strong temperature dependence of the pK_a value for the PDPA block, the degree of protonation increases as the solution temperature is lowered. As the PDPA chains become more protonated (cationic), water gradually becomes a good solvent, thus increasing its effective volume in solution. When the PDPA block is fully protonated, it is extended to its maximum volume and can be modeled as a charged polyelectrolyte. Its scaling is controlled by the balance between the charge density and the presence of counterions in solution which, for a long flexible polyelectrolyte,[36] scales as $R_g \propto N^{3/5}$. However, under these conditions PMPC–PDPA is no longer amphiphilic, and thus there is no hydrophobic driving force for self-assembly. Therefore, at a certain critical degree of protonation (which is both pH- and temperature-dependent), self-assembly occurs to produce copolymer morphologies that are dictated by the molecular packing factor. Between this minimum degree of protonation and full deprotonation, the effective volume fraction of the PDPA block alters. This in turn generates a range of molecular packing parameters, in addition to those dictated by the mean degree of polymerization. Furthermore, once these assembly nuclei are produced, they are stable within the temperature range studied for at least 4 months. Figure S4 shows the DLS intensity-average diameters determined for $PMPC_{25}$–$PDPA_{147}$ copolymer aggregates initially produced at 50 °C and then stored at room temperature. This suggests that there is not unimer exchange at pH above the pK_a; hence, all the copolymers are assembled.

Adjusting the solution temperature for the self-assembly of $PMPC_{25}$–$PDPA_n$ drastically changes the aggregate morphology. The pK_a of the PDPA block is rather sensitive to temperature, causing the copolymer to exhibit varying degrees of protonation at a constant pH value. This generates a range of molecular volumes as the PDPA block swells or collapses, therefore producing significant variation in the molecular packing parameter. This parameter dictates the preferred geometric packing between two or more amphiphiles, and in turn, the nanostructures formed during self-assembly. However, the amphiphilic character of the copolymer chains generated by the increase in pH simultaneously leads to spontaneous

dx.doi.org/10.1021/ma302228m | Macromolecules 2013, 46, 1400–1407

nucleation driven by the hydrophobic effect. Once nucleation occurs, the aggregated copolymer chains undergo internal rearrangement so to adopt the most energetically favorable conformation dictated by the molecular packing factor.[17] For all but the highest molecular weight copolymer, only micelle formation is observed at higher temperatures. This indicates that these micelles are kinetically trapped nanostructures formed by a combination of relatively fast nucleation kinetics and limited unimer exchange. Conversely, the formation of polymersomes with thick membranes by the shortest block copolymer indicates a change in the packing parameter. Greater ionization of the PDPA chains at lower temperatures is expected to favor unimer exchange. However, an increase in the rate of unimer exchange does not explain polymersome formation by $PMPC_{25}$–$PDPA_{47}$, which has been previously shown to produce micelles. The formation of membranes approximately twice as thick as predicted from scaling theory indicates that the copolymer chains adopt highly extended conformation. This suggests that the increase in volume by the PDPA block in response to its ionization is somewhat greater than the concomitant increases in area and length. This produces a higher packing parameter, which favors membrane (and hence polymersome) formation. The formation of genus structures is due to the generation of spontaneous curvature by the copolymer membrane. This curvature is caused by the reduced probability of the copolymer membrane to undergo molecular reorganization via mechanisms such as "flip-flopping". These genus structures are explored in more detail elsewhere (paper under revision). The increased entropic penalty of exposing the hydrophobic PDPA block to water and the hydrophilic PMPC block to the nonpolar membrane causes high molecular weight copolymer membrane flipping to become energetically unfavorable.[37−39] Similarly, unimer exchange is also more unfavorable for longer copolymer chains. However, an increase in hydrophilic character of the membrane-forming block reduces this energetic penalty.[40,41]

CONCLUSIONS

In this study, we have shown that a pH-sensitive diblock copolymer, PMPC–PDPA, is capable of forming a range of colloidal aggregates in aqueous solution via a pH switch. This can be achieved either by varying the degree of polymerization or by controlling the solution temperature. In particular, the relationship between temperature and pK_a allows the degree of copolymer ionization to be conveniently modulated. This temperature-controlled approach may allow novel mechanisms for the formation of PMPC–PDPA polymersomes to be explored.

ASSOCIATED CONTENT

Supporting Information

Figures S1–S4. This material is available free of charge via the Internet at http://pubs.acs.org.

AUTHOR INFORMATION

Corresponding Author

*E-mail g.battaglia@sheffield.ac.uk.

Notes

The authors declare no competing financial interest.

ACKNOWLEDGMENTS

The authors thank Miss Silvia Bianco for the design of the cartoons. This work was funded by the EPSRC (EP/I0011697/1 and EP/G062137/1) and Biocompatibles. The R.T.P. studentship was funded by the EPSRC Doctoral Training Account allocated to the Dept. of Materials Sci. and Eng. G.B. acknowledges the contribution of the ERC STG award.

REFERENCES

(1) LoPresti, C.; Lomas, H.; Massignani, M.; Smart, T.; Battaglia, G. Polymersomes: Nature Inspired Nanometer Sized Compartments. *J. Mater. Chem.* **2009**, *19*, 3576–3590.
(2) Smart, T.; et al. Block Copolymer Nanostructures. *Nano Today* **2008**, *3*, 38–46.
(3) Rothman, J. E. Mechanism of Intracellular Protein-Transport. *Nature* **1994**, *372*, 55–63.
(4) Song, G.; Wu, H. L.; Yoshino, K.; Zamboni, W. C. Factors Affecting the Pharmacokinetics and Pharmacodynamics of Liposomal Drugs. *J. Liposome Res.* **2012**, *22*, 177–192.
(5) Felgner, P. L.; et al. Lipofection - A Highly Efficient, Lipid-Mediated DNA-Transfection Procedure. *Proc. Natl. Acad. Sci. U. S. A.* **1987**, *84*, 7413–7417.
(6) Bermudez, H.; Hammer, D. A.; Discher, D. E. Effect of Bilayer Thickness on Membrane Bending Rigidity. *Langmuir* **2004**, *20*, 540–543.
(7) Bermudez, H.; Brannan, A. K.; Hammer, D. A.; Bates, F. S.; Discher, D. E. Molecular Weight Dependence of Polymersome Membrane Structure, Elasticity, and Stability. *Macromolecules* **2002**, *35*, 8203–8208.
(8) Discher, B. M.; et al. Polymersomes: Tough Vesicles Made from Diblock Copolymers. *Science* **1999**, *284*, 1143–1146.
(9) Battaglia, G.; Ryan, A. J.; Tomas, S. Polymeric Vesicle Permeability: A Facile Chemical Assay. *Langmuir* **2006**, *22*, 4910–4913.
(10) Wang, J. S.; Greszta, D.; Matyjaszewski, K. Atom-Transfer Radical Polymerization (Atrp) - a New Approach Towards Well-Defined (Co)Polymers. *Abstr. Pap. Am. Chem. Soc.* **1995**, *210*, 227-PMSE.
(11) Battaglia, G.; Ryan, A. J. Bilayers and Interdigitation in Block Copolymer Vesicles. *J. Am. Chem. Soc.* **2005**, *127*, 8757–8764.
(12) Discher, B. M.; et al. Cross-Linked Polymersome Membranes: Vesicles with Broadly Adjustable Properties. *J. Phys. Chem. B* **2002**, *106*, 2848–2854.
(13) Blanazs, A.; Massignani, M.; Battaglia, G.; Armes, S. P.; Ryan, A. J. Tailoring Macromolecular Expression at Polymersome Surfaces. *Adv. Funct. Mater.* **2009**, *19*, 2906–2914.
(14) Massignani, M.; et al. Controlling Cellular Uptake by Surface Chemistry, Size, and Surface Topology at the Nanoscale. *Small* **2009**, *5*, 2424–2432.
(15) LoPresti, C.; et al. Controlling Polymersome Surface Topology at the Nanoscale by Membrane Confined Polymer/Polymer Phase Separation. *ACS Nano* **2011**, *5*, 1775–1784.
(16) Israelachvili, J. N.; Mitchell, D. J.; Ninham, B. W. Theory of Self-Assembly of Hydrocarbon Amphiphiles into Micelles and Bilayers. *J. Chem. Soc., Faraday Trans. 2* **1976**, *72*, 1525–1568.
(17) Blanazs, A.; Madsen, J.; Battaglia, G.; Ryan, A. J.; Armes, S. P. Mechanistic Insights for Block Copolymer Morphologies: How Do Worms Form Vesicles? *J. Am. Chem. Soc.* **2011**, *133*, 16581–16587.
(18) Fernyhough, C.; Ryan, A. J.; Battaglia, G. pH Controlled Assembly of a Polybutadiene-Poly(methacrylic acid) Copolymer in Water: Packing Considerations and Kinetic Limitations. *Soft Matter* **2009**, *5*, 1674–1682.
(19) Lomas, H.; et al. Efficient Encapsulation of Plasmid DNA in pH-Sensitive PMPC-PDPA Polymersomes: Study of the Effect of PDPA Block Length on Copolymer-DNA Binding Affinity. *Macromol. Biosci.* **2010**, *10*, 513–530.

(20) Du, J. Z.; Tang, Y. P.; Lewis, A. L.; Armes, S. P. pH-Sensitive Vesicles Based on a Biocompatible Zwitterionic Diblock Copolymer. *J. Am. Chem. Soc.* **2005**, *127*, 17982−17983.
(21) Giacomelli, C.; et al. Phosphorylcholine-Based pH-Responsive Diblock Copolymer Micelles As Drug Delivery Vehicles: Light Scattering, Electron Microscopy, and Fluorescence Experiments. *Biomacromolecules* **2006**, *7*, 817−828.
(22) Butun, V.; Armes, S. P.; Billingham, N. C. Synthesis and Aqueous Solution Properties of near-Monodisperse Tertiary Amine Methacrylate Homopolymers and Diblock Copolymers. *Polymer* **2001**, *42*, 5993−6008.
(23) Lomas, H.; et al. Biomimetic pH Sensitive Polymersomes for Efficient DNA Encapsulation and Delivery. *Adv. Mater.* **2007**, *19*, 4238.
(24) Johnston, A. P. R.; Such, G. K.; Ng, S. L.; Caruso, F. Challenges Facing Colloidal Delivery Systems: From Synthesis to the Clinic. *Curr. Opin. Colloid Interface Sci.* **2011**, *16*, 171−181.
(25) Best, J. P.; Yan, Y.; Caruso, F. The Role of Particle Geometry and Mechanics in the Biological Domain. *Adv. Healthcare Mater.* **2012**, in press.
(26) Canton, I.; Battaglia, G. Endocytosis at the Nanoscale. *Chem. Soc. Rev.* **2012**, *41*, 2718−2739.
(27) Massignani, M.; Lomas, H.; Battaglia, G. Polymersomes: A Synthetic Biological Approach to Encapsulation and Delivery. *Mod. Tech. Nano- Microreact./-React.* **2010**, *229*, 115−154.
(28) Sanson, C.; et al. Biocompatible and Biodegradable Poly(trimethylene carbonate)-b-poly(L-glutamic acid) Polymersomes: Size Control and Stability. *Langmuir* **2010**, *26*, 2751−2760.
(29) Wang, L.; et al. Encapsulation of Biomacromolecules within Polymersomes by Electroporation. *Angew. Chem.* **2012**, DOI: 10.1002/anie.201204169.
(30) Rank, A.; Hauschild, S.; Forster, S.; Schubert, R. Preparation of Monodisperse Block Copolymer Vesicles via a Thermotropic Cylinder-Vesicle Transition. *Langmuir* **2009**, *25*, 1337−1344.
(31) Agut, W.; Brulet, A.; Schatz, C.; Taton, D.; Lecommandoux, S. pH and Temperature Responsive Polymeric Micelles and Polymersomes by Self-Assembly of Poly[2-(dimethylamino)ethyl methacrylate]-b-Poly(glutamic acid) Double Hydrophilic Block Copolymers. *Langmuir* **2010**, *26*, 10546−10554.
(32) Semsarilar, M.; Ladmiral, V.; Blanazs, A.; Armes, S. P. Anionic Polyelectrolyte-Stabilized Nanoparticles via RAFT Aqueous Dispersion Polymerization. *Langmuir* **2011**, *28*, 914−922.
(33) Mahon, J.; Zhu, S. Interactions of Poly(2-methacryloyloxyethyl phosphorylcholine) with Various Salts Studied by Size Exclusion Chromatography. *Colloid Polym. Sci.* **2008**, *286*, 1443−1454.
(34) Jain, S.; Bates, F. S. Consequences of Nonergodicity in Aqueous Binary PEO-PB Micellar Dispersions. *Macromolecules* **2004**, *37*, 1511−1523.
(35) Birshtein, T. M.; Zhulina, E. B. Scaling Theory of Supermolecular Structures in Block Copolymer Solvent Systems 0.1. Model of Micellar Structures. *Polymer* **1989**, *30*, 170−177.
(36) Netz, R. R.; Andelman, D. Neutral and Charged Polymers at Interfaces. *Phys. Rep.* **2003**, *380*, 1−95.
(37) Shen, L.; Du, J. Z.; Armes, S. P.; Liu, S. Y. Kinetics of pH-Induced Formation and Dissociation of Polymeric Vesicles Assembled from a Water-Soluble Zwitterionic Diblock Copolymer. *Langmuir* **2008**, *24*, 10019−10025.
(38) Nakano, M.; et al. Flip-Flop of Phospholipids in Vesicles: Kinetic Analysis with Time-Resolved Small-Angle Neutron Scattering. *J. Phys. Chem. B* **2009**, *113*, 6745−6748.
(39) Anglin, T. C.; Conboy, J. C. Kinetics and Thermodynamics of Flip-Flop in Binary Phospholipid Membranes Measured by Sum-Frequency Vibrational Spectroscopy. *Biochemistry* **2009**, *48*, 10220−10234.
(40) Creutz, S.; van Stam, J.; De Schryver, F. C.; Jerome, R. Dynamics of Poly((dimethylamino)alkyl methacrylate-block-sodium methacrylate) Micelles. Influence of Hydrophobicity and Molecular Architecture on the Exchange Rate of Copolymer Molecules. *Macromolecules* **1998**, *31*, 681−689.
(41) Creutz, S.; vanStam, J.; Antoun, S.; DeSchryver, F. C.; Jerome, R. Exchange of Polymer Molecules between Block Copolymer Micelles Studied by Emission Spectroscopy. A Method for the Quantification of Unimer Exchange Rates. *Macromolecules* **1997**, *30*, 4078−4083.